1998

The effect of biodiesel oxidation on engine performance and emissions

Abdul Monyem
Iowa State University

INFORMATION TO USERS

This manuscript has been reproduced from the microfilm master. UMI films the text directly from the original or copy submitted. Thus, some thesis and dissertation copies are in typewriter face, while others may be from any type of computer printer.

The quality of this reproduction is dependent upon the quality of the copy submitted. Broken or indistinct print, colored or poor quality illustrations and photographs, print bleedthrough, substandard margins, and improper alignment can adversely affect reproduction.

In the unlikely event that the author did not send UMI a complete manuscript and there are missing pages, these will be noted. Also, if unauthorized copyright material had to be removed, a note will indicate the deletion.

Oversize materials (e.g., maps, drawings, charts) are reproduced by sectioning the original, beginning at the upper left-hand corner and continuing from left to right in equal sections with small overlaps. Each original is also photographed in one exposure and is included in reduced form at the back of the book.

Photographs included in the original manuscript have been reproduced xerographically in this copy. Higher quality 6" x 9" black and white photographic prints are available for any photographs or illustrations appearing in this copy for an additional charge. Contact UMI directly to order.

UMI

A Bell & Howell Information Company
300 North Zeeb Road, Ann Arbor MI 48106-1346 USA
313/761-4700 800/521-0600

The effect of biodiesel oxidation on engine performance and emissions

by

Abdul Monyem

A dissertation submitted to the graduate faculty

in partial fulfillment of the requirements for the degree of

DOCTOR OF PHILOSOPHY

Major: Mechanical Engineering

Major Professor: Jon H. Van Gerpen

Iowa State University

Ames, Iowa

1998

Graduate College

Iowa State University

This is to certify that the Doctoral dissertation of

Abdul Monyem

has met the dissertation requirements of Iowa State University

Signature was redacted for privacy.

Major Professor

Signature was redacted for privacy.

For the Major Program

Signature was redacted for privacy.

For the Graduate College

TABLE OF CONTENTS

LIST OF FIGURES

LIST OF TABLES

ABSTRACT

Biodiesel is a fuel consisting of the alkyl monoesters of vegetable oils or animal fats. Biodiesel is nontoxic, renewable, and biodegradable. Biodiesel-fueled engines produce less carbon monoxide, unburned hydrocarbon, and particulate emissions than diesel fueled engines. One drawback of biodiesel is that it is susceptible to oxidation which can induce polymerization of the esters and can form insoluble gums and sediments which are known to cause fuel filter plugging. However, no research has been conducted to determine the impact of oxidized biodiesel on engine emissions and fuel system performance.

The objective of this study was to relate the chemical and physical processes associated with biodiesel oxidation to the conditions that affect engine performance and emissions. In addition, a relationship was sought between ASTM D2274, a diesel fuel-based stability test and AOCS Cd 8-53 and Cd 3a-63 which characterize the chemical changes in the fuel.

It was expected that the fuel filters would plug as the vegetable oil esters oxidized but no filter plugging was observed in this study even when the fuel oxidized beyond the level that would be encountered in practice. Recent research by others has suggested that the filter plugging may be associated with reactions between the diesel fuel additives and biodiesel.

The engine performance of the oxidized biodiesel was similar to that of No. 2 diesel fuel with nearly the same thermal efficiency, and slightly higher fuel consumption.

Oxidized biodiesels produced between 14% and 16% lower CO and HC emissions and smoke number compared to unoxidized biodiesel. No statistically significant difference was found between the NO_x emissions from oxidized biodiesel and unoxidized biodiesel. Oxidized biodiesel experienced a one degree shorter ignition delay than unoxidized biodiesel. The ignition delay was almost linearly correlated to CO and HC emissions. A common linear relationship was found between the start of combustion and the NO_x emissions. When the NO_x was plotted against the start of combustion timing, the neat biodiesel produced lower NO_x emissions than the No. 2 diesel fuel.

1. INTRODUCTION

History records that Rudolph Diesel, a German engineer, introduced the diesel engine over a century ago. Since then, a great deal of research and development has taken place not only in the design area but also in finding an appropriate fuel. Diesel engines are widely used as power sources for medium and heavy-duty applications because of their lower fuel consumption and lower emissions of carbon monoxide (CO) and unburned hydrocarbons (HC) compared with gasoline engines.

For many years, the ready availability of inexpensive middle-distillate petroleum fuels provided little incentive for experimenting with alternative, renewable fuels for diesel engines. However, since the oil crisis of the 1970s, research interest has expanded in the area of alternative fuels. Since then, many proposals have been made regarding the availability and productivity of an environmentally sound fuel that could be domestically sourced. Many alternative fuels have been suggested including methanol, ethanol, compressed natural gas (CNG), liquefied petroleum gas (LPG), liquid natural gas (LNG), vegetable oils, reformulated gasoline, and reformulated diesel fuel. Of these alternative fuels, only ethanol and vegetable oils are non-fossil fuels.

While alcohol fuels can be burned very cleanly and represent a feasible transportation fuel, they have several disadvantages. Although it is possible to burn alcohols in conventional engines with efficient combustion and very low emission levels, they are not generally considered to be a good choice because of their low energy content compared with petroleum. Ethanol's heating value is only about 65% that of diesel fuel.

Ethanol also has a very low cetane number, which renders it unsuitable for use in diesel engines.

In Europe, vegetable oil-based fuels have been widely considered as a potential fuel source. Only recently has the United States considered these types of fuels to be a reasonable source of alternative fuel. The properties of vegetable oils render them best suited for use in diesel engines [1-3].

Many researchers have concluded that vegetable oils hold promise as alternative fuels for diesel engines [4-10]. However, using raw vegetable oils for diesel engines can cause numerous engine-related problems [11-13]. The increased viscosity, low volatility, and poor cold flow properties of vegetable oils lead to severe engine deposits, injector coking, and piston ring sticking [14-17]. However, these effects can be reduced or eliminated through transesterification of the vegetable oil to form a mono ester [14, 18]. The process of transesterification removes glycerol from the triglycerides and replaces it with radicals from the alcohol used for the conversion process [19]. This process decreases the viscosity but maintains the cetane number and the heating value.

Increasingly strict emissions regulations have forced researchers to look for ways to achieve emission reductions through fuel modifications. It has been found that oxygen addition to the fuel can reduce exhaust emissions from motor vehicles [20-21]. Especially for direct injected(DI) engines, there is general agreement that some fraction of vegetable oil esters in No. 2 diesel fuel can provide a substantial reduction in HC, CO, and particulate emissions, although at the cost of an increase in NO_x emissions [16, 21-23].

Biodiesel is a fuel consisting of the alkyl monoesters of vegetable oils or animal

fats. The most common form of biodiesel in the United States is made with methanol and soybean oil and is known as soy methyl ester, or methyl soyate. One drawback of biodiesel is that there is a tradeoff between biodiesel's tendency to oxidize and its cold flow properties. Saturated compounds have higher cetane numbers and are less prone to oxidation than unsaturated compounds but they tend to crystallize at unacceptably high temperatures. Biodiesel from soybean oil is highly unsaturated so its cold flow properties are acceptable, however it is very prone to oxidation. The impact of this oxidation on the engine's performance and emissions is not currently understood. A recent study [24] showed that the cetane number of biodiesel increased as the biodiesel oxidized up to a peroxide value of 80. Higher cetane number means that the fuel autoignites more easily in the engine cylinder. This is an advantage but there are also some disadvantages related to oxidation. Hydroperoxides are the initial products of oxidation at ordinary temperatures. They are very unstable and have a tendency to attack elastomers. In addition, the hydroperoxides can induce polymerization of the esters and form insoluble gums and sediments. Recent research has shown that the oxidation products, sediment and gum, caused fuel filter plugging [16]. However, no research has yet been conducted to determine the maximum degree of oxidation allowable for the fuel to be used in diesel engines.

A number of diesel emissions studies have been conducted with blends of esters of vegetable oils with diesel fuel. Also, a significant number of research projects have been conducted with other oxygenated fuels. It has been seen that the oxygenated fuels tend to reduce some emissions. However, no research has been conducted to determine

the impact of oxidized vegetable oil esters on engine emissions and fuel system performance.

The overall objective of this study was to relate the chemical and physical processes associated with biodiesel oxidation to the conditions that affect engine performance and emissions.

The specific objectives of this study were to:

1. understand the changes that occur in the fuel when it oxidizes.
2. establish a connection between ASTM fuel stability tests and AOCS tests. ASTM D2274 is a diesel fuel-based test which measures sediment and gum formation and AOCS Cd 8-53 and Cd 3a-63 are tests which measure the chemical changes the fuel undergoes during oxidation.
3. evaluate the impact of oxidized fuel on engine performance and exhaust emissions.
4. compare the calculated fuel burning rate for oxidized biodiesel with the burning rate for unoxidized fuel and a baseline diesel fuel.

This dissertation contains six chapters. The first chapter has provided a general introduction and statement of objectives. The second chapter provides a literature review. The third chapter discusses the experimental apparatus and procedures to be used for the tests. The fourth chapter discusses the data collection and analysis including the burning rate (heat release) model. The fifth chapter discusses the exhaust emissions for oxidized biodiesel and the results of the heat release analysis. The final chapter summarizes the conclusions related to this study.

2. REVIEW OF LITERATURE

In this chapter, background information on biodiesel and the processes related to its oxidation and stability are discussed. This is followed by a discussion of the emissions of vegetable oil esters.

2.1 Vegetable Oils

Since the invention of the compression ignition engine, researchers have been investigating alternative fuels. Rudolph Diesel used vegetable oils as diesel fuel [35]. However, the limitations of his engine design and the high cost of vegetable oils caused him to favor petroleum-based fuels. Before the OPEC oil embargo of the 1970s, there was little incentive for experimenting with vegetable oil-based fuels. Since then, a number of researchers have investigated vegetable oil based fuels [25-32]. Many of them have concluded that vegetable oils can be safely burned for short periods of time in a diesel engine. However, as noted earlier, using raw vegetable oil in a diesel engine for extended periods of time may result in severe engine deposits, piston ring sticking, injector coking, and thickening of the lubricating oil [25, 27, 33-37]

Most of the properties of vegetable oil are similar to diesel fuel, but the viscosity of vegetable oil is 11 to 17 times higher than diesel fuel. The high viscosity is due primarily to the high molecular weight of the triglyceride molecules which typically consist of three 18-carbon chains attached to a single glycerin backbone. Higher viscosity reduces fuel atomization and increases the fuel injection spray penetration. Higher spray penetration is thought to be at least in part responsible for the difficulties experienced

with engine deposits and thickening of the lubrication oil [25, 29, 38].

Hemmerlein et al. [33] used six modern DI diesel engines to evaluate the effects of rapeseed oil on engine performance and emissions. Their results showed that there were no significant effects of rapeseed oil on engine performance compared with diesel fuel. Carbon monoxide (CO) emissions were up to 100% higher over the whole engine operating range with rapeseed oil compared to diesel fuel. An increase in HC emissions was measured for most of the engines. The increase depended on the operating range of the engines and could amount to an increase of 290% compared to diesel fuel. Emissions of nitrogen oxides were up to 25% lower with rapeseed oil. Also, soot emissions were lower over the whole operating range with rapeseed oil. The particulate emissions were reduced around 30 to 50% with rapeseed oil in divided combustion chamber engines. Direct injection engines showed 90 to 140% higher particulate emissions with rapeseed oil compared to diesel fuel.

A significant factor in reducing carbon buildup in the engine is the level of saturation of the vegetable oil. Oils with higher levels of saturation are more desirable for fuels. Petroleum-based diesel fuels have higher levels of saturation than vegetable oils. The double bonds that are typical of unsaturated molecules are very susceptible to oxidation.

Petroleum-based diesel fuel contain carbon and hydrogen atoms, arranged in straight-chain and branched-chain structures as well as aromatic configurations. The straight-chain structure is preferred for better diesel ignition quality. Diesel fuel can contain both saturated (having no C-C double bonds) and unsaturated (having one or

more C-C double bonds) hydrocarbons, but the unsaturated hydrocarbons are not present in large enough amounts to make fuel oxidation a problem. The aromatics, although unsaturated, are oxidation-resistant and their presence does not cause a fuel oxidation problem.

Vegetable oils are fatty esters of glycerol (triglycerides) and have the chemical structure as shown in Figure 2.1 [25].

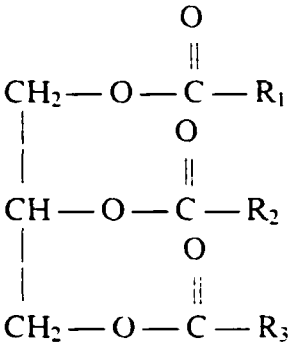

Figure 2.1 Vegetable oil's structural notation

where R_1, R_2, and R_3 represent the hydrocarbon chain of the fatty acids. R_1, R_2, and R_3 may be the same, depending upon the particular oil, but generally are different in chain length and in the number of double bonds present.

2.2 Transesterification

The viscosity of the fuel is a prime concern because of its effects on the injected fuel spray pattern. Diesel fuel injectors are designed for fuels with viscosity similar to No. 2 diesel fuel. If the viscosity of vegetable oil could be reduced, it would reduce

engine operation problems.

Transesterification is the process of reacting a triglyceride, such as one of the vegetable oils, with an alcohol in the presence of a catalyst to produce free glycerol and fatty acid esters. Transesterification reduces the viscosity of vegetable oils without significantly affecting the heating value of the fuel and has been found to overcome some of the drawbacks of 100% vegetable oils. The molecular weight of a typical ester molecule is roughly one third that of a straight vegetable oil molecule and has a viscosity only 50% higher than that of diesel fuel. Figure 2.2 illustrates the reaction using methanol and potassium hydroxide. Other alcohols such as ethyl, isopropyl, and butyl alcohol could also be used. Similarly, other alkaline catalysts besides potassium hydroxide can be used such as sodium hydroxide and sodium methoxide. Acid catalyzed transesterification is also possible.

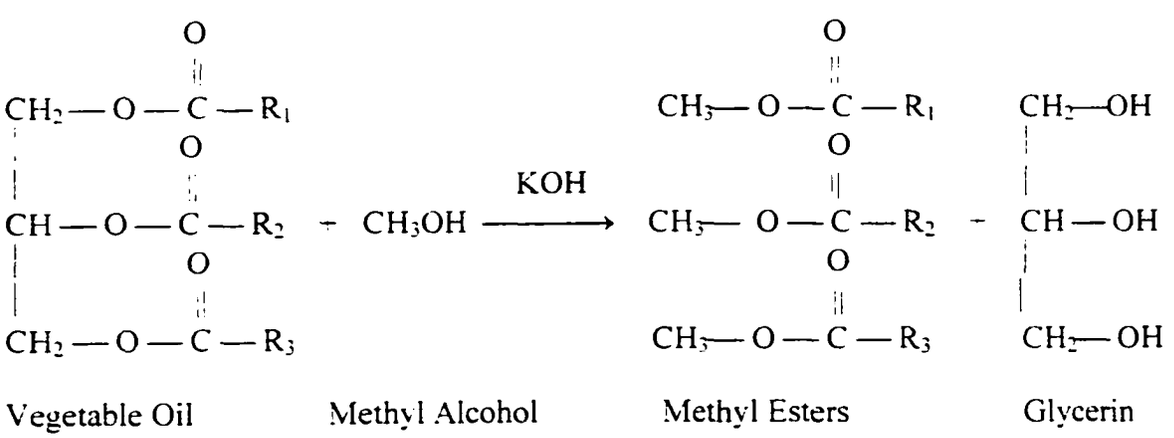

Figure 2.2. Transesterfication of vegetable oil using methanol and potassium hydroxide catalyst.

2.3 Oxidation

Because of their unsaturated nature, vegetable oils are very prone to oxidation. Vegetable oils are oxidized through contact with molecular oxygen in the air. Oxidation reactions that occur without any outside influence are called *autoxidation*. As defined in Stauffer's Fats and Oils Handbook [39], autoxidation is a series of free radical reactions, initiated and propagated by free radicals reacting with methylene -CH2- groups that are adjacent to double bonds. This is why the rate of oxidation is so strongly affected by the degree of saturation of the oil. A free radical having an unpaired electron is a very reactive species. A typical autoxidation reaction mechanism is shown in Figure 2.3. At the beginning of the autoxidation process, a hydrogen radical is extracted, and one of the double bonds shifts, moving the radical site to the outer carbon (reaction 1). Dissolved oxygen adds to this site, generating a peroxyl radical (reaction 2); this abstracts a

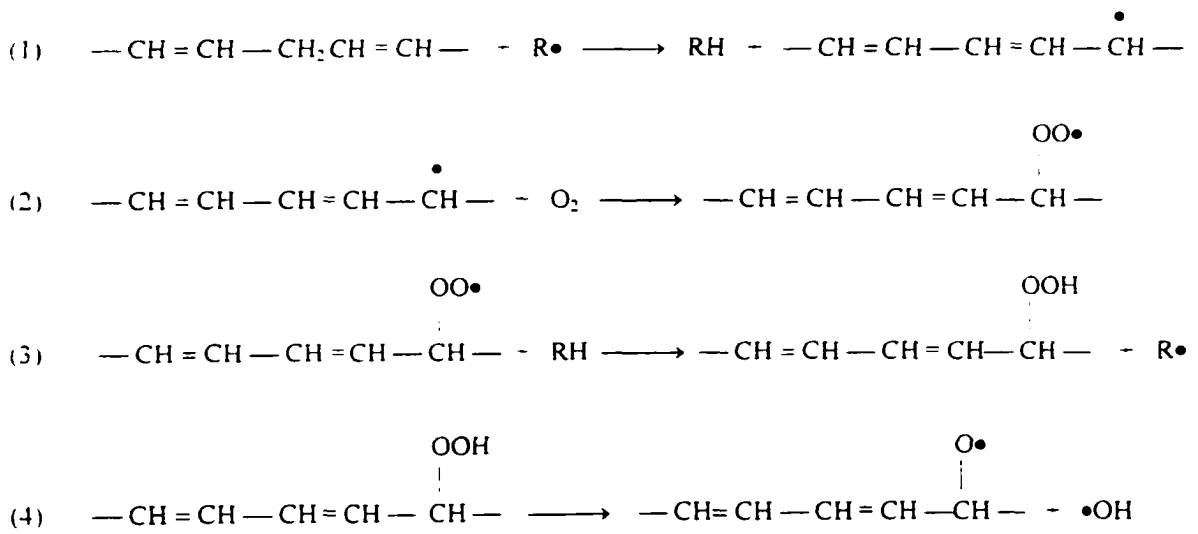

Figure 2.3 Reactions occurring during autoxidation of fat [39].

hydrogen from a donor-perhaps another methylene group making a hydroperoxide (reaction 3). The hydroperoxide splits to generate two free radicals, a hydroxyl and an alkoxyl radical (reaction 4). This reaction is catalyzed by traces of metal ions such as iron and copper. Each free radical in this reaction can initiate another chain of reactions. The radicals involved in autoxidation can also participate in polymerization reactions such as:

$$R^{\bullet} + R^{\bullet} \rightarrow R\text{—}R$$

or

$$R^{\bullet} + ROO^{\bullet} \rightarrow ROOR$$

These reactions produce high molecular weight insoluble sediments and gums.

Most vegetable oils contain natural antioxidants, such as vitamin E (tocopherol). These antioxidants react with the active free radicals and transfer them to the antioxidant. The radical of the antioxidant has a low reactivity and does not initiate new reaction chains. However, as free radicals continue to form, eventually all the antioxidant will be consumed, and the oxidation will then proceed rapidly.

2.4 Fuel Stability

With or without any external initiation biodiesel fuel will oxidize when it is in contact with oxygen. External initiation may be heat, light, metals, and chemicals. When oxygen comes in contact with biodiesel, the double bond reacts with oxygen to produce a variety of chemical products, and this can alter the properties of biodiesel. When this process occurs at ordinary temperatures, the initial products are hydroperoxides. The extent of this level of oxidation can be characterized by the peroxide value as measured

with the American Oil Chemists' Society (AOCS) official method Cd 8-53. As the oxidation continues, the peroxides may split and form aldehydes, ketones, and short chain acids that cause an unpleasant odor. Also, sediment and gum formations are the products of oxidation through polymerization of the peroxides. These changes in the fuel's chemical properties are identified as a fuel stability problem.

Fuel stability can be classified as storage stability, thermal stability, and oxidative stability. Storage stability is associated with any fuel changes while the fuel is in storage for a long time. The fuel may be exposed to the air. Thermal stability is associated with any fuel changes as the fuel is heated. Again, the fuel may be in contact with air. Oxidative stability is associated with fuel changes through the oxidation process when the fuel is in contact with oxygen from air.

There are two categories of test methods for fuel stability. One category consists of standard tests specified by the American Society for Testing and Materials (ASTM), and the other category is the AOCS tests. The ASTM thermal stability test for diesel fuel (D2274) consists of heating the fuel to 95 °C while bubbling oxygen through it for 16 hours, and then measuring the amount of gum and sediment produced in the process [40].

The AOCS tests quantify the level of peroxides in the fuel that have developed as a result of oxidation [41, 42]. Peroxides are considered intermediates in the lipid oxidation reaction scheme. The peroxide value is expressed as milliequivalents of peroxide per 1000 grams of sample. The Oil Stability Index (OSI) method, AOCS Official Method Cd 12b-92 [43], may be used as an alternate method for characterizing oxidation. This method measures the time required for the sample to pass through its

induction period. This is the point when the antioxidants have been exhausted and oxidation begins rapidly. In this method a stream of purified air is passed through a sample of oil or fat which is held in a temperature controlled bath. The effluent air from the sample is bubbled through deionized water. The conductivity of the water is then monitored continually. The effluent air contains volatile organic acids, swept from the oxidized sample, that increase the conductivity of water as oxidation proceeds. The Oil Stability Index (OSI) is defined as the point where the rate of change of oxidation is a maximum. The acid and peroxide value tests are explained in Appendices A and B.

Duplessis et al. [44] conducted stability studies on methyl and ethyl fatty acid esters of sunflower seed oil. Storage tests on the methyl and ethyl fatty acid esters were conducted for 90 days with six different experimental treatments at three different temperature levels (20 °C, 30 °C, and fluctuating around 50 °C). Storage of esters in contact with air, especially at temperatures above 30 °C, resulted in significant increases in peroxide value, ultraviolet absorption, free fatty acids, viscosity, and anisidine values. The anisidine value is a measure of the aldehyde and ketone content of the ester. Retarded oxidation for all temperature levels was found when contact with oxygen was limited. Viscosity increased at all three temperature levels, but the rate of viscosity change at higher temperature was higher than at the lower temperature. A direct relationship was found between the viscosity increase and the oxidation parameters (acid, peroxide, and anisidine value). Exposure to light resulted in a small increase in the oxidation parameters of esters stored at the highest temperature level. An antioxidant, tertiary butylhydroquinone (TBHQ), prevented oxidation of samples stored under

moderate conditions, but they found it was not effective if the samples were stored under high temperature (50 C). Mild steel had little catalytic effect on the oxidation parameters. Methyl esters oxidized slightly slower than ethyl esters during the storage test.

Van Gerpen et al. [24] oxidized two fuels, freshly prepared methyl esters and distilled methyl esters, under fluorescent light with continuous stirring at room temperature. AOCS official method Cd 8-53 was used to measure the peroxide value. The peroxide value of the freshly prepared, undistilled esters increased almost linearly with increasing time. For these esters, it took 24 days to reach a peroxide value of 80. However, the distilled methyl esters, which had their natural antioxidant Vitamin E removed, oxidized much faster. It took only 6 days to reach a peroxide value of 96. Later measurements of the cetane number showed that it increased as the oxidation continued to increase until a peroxide value of 80 was reached. The cetane number for both undistilled and distilled esters were the same when they had the same peroxide value.

2.5 Diesel Engine Emissions Fueled with Vegetable Oil Esters

Although vegetable oils have been used in a limited way in the past, most current attention has focused on transesterified vegetable oils that have proven successful in many ways. Several researchers have observed that the exhaust emissions are affected by the use of vegetable oil esters. Chang et al. [21] used a four-cylinder turbocharged DI diesel engine fueled with blends of methyl and isopropyl esters of soybean oil in No. 2 diesel fuel to test the engine's performance and emissions. The results indicated that engine performance for all the fuel blends was similar to No. 2 diesel fuel. The CO

emissions of all fuel blends were significantly lower than for No. 2 diesel fuel and the greatest CO emissions reduction (25.3%) was found with 50% blends with methyl esters. All ester blends lowered HC emissions except for the 20% methyl ester blends with low-sulfur diesel. However, a slight increase of HC emissions compared to No. 2 diesel fuel was not statistically significant. The NO_x emissions for all fuel blends were higher than for No. 2 diesel fuel. A significant NO_x emissions increase was found for 20% and 50 % isopropyl and winterized methyl esters blends with No. 2 diesel fuel. The winterized blend was produced by cooling ordinary methyl esters of soybean oil until some of the saturated components started to crystallize. These were removed to produce a product with improved cold flow characteristics. The 50% isopropyl ester blend had 12.1% higher NO_x emissions. The blends with methyl esters had the lowest increase in NO_x emissions, which was below 4%. All fuel blends had significantly improved particulate emissions. The 50% ester blends decreased particulate emissions by at least 17.4%, and the largest reduction in particulate emissions was found for the 50% isopropyl esters with low-sulfur No. 2 diesel fuel, which gave a 28% reduction.

Schmidt [45] studied the emission and performance characteristics of the individual fatty esters found in soybean-based biodiesel. A John Deere 4276T four cylinder, turbocharged direct injection diesel engine was fueled with pure methyl esters of all of the fatty acids found in soybean oil (methyl soyate, methyl palmitate, methyl stearate, methyl oleate, methyl ester of safflower oil, and methyl ester of linseed oil) and isopropyl esters of two fatty acids at 20% and 50% blends in No. 2 diesel fuel. The safflower and linseed oils were chosen because they are high in linoleic and linolenic

acids, respectively. Particulate emissions reduction was found for some of the esters. Methyl palmitate reduced the particulate emissions more than all of the other fatty esters. The largest particulate reduction of 30% was found for the 50% blend of methyl palmitate. The CO emissions reduction was not significant. However, methyl stearate and methyl palmitate appeared to reduce CO the most when blended with diesel fuel. The HC emissions decreased as the percent ester increased for all of the esters. The most significant reduction in HC emissions was found for methyl stearate and methyl palmitate esters, which gave reductions of about 30%. The NO_x emissions did not change significantly for any of the esters. The BSFC increased as the amount of ester in the fuel increased, due to the lower energy content of the ester fuels.

Geyer et al. [46] used a single cylinder 0.36 L direct injection diesel engine to provide a comparison of performance and emissions data when operating on neat vegetable oils, transesterified vegetable oils, and diesel fuel. The results indicated that the thermal efficiencies of the vegetable oils were slightly better than No. 2 diesel fuel and higher exhaust gas temperatures were found. The unburned hydrocarbons and carbon monoxide emissions generally decreased with increased load. However, the methyl esters of sunflowerseed oil had higher carbon monoxide (CO) emissions at the full load setting. The NO_x emission was significantly higher for the methyl esters at all rack settings.

Scholl and Sorenson [1] fueled a direct injection diesel engine with soybean oil methyl ester and diesel fuel to investigate the combustion of the methyl ester. The results indicated that the soybean oil methyl ester behaved comparably to diesel fuel in terms of performance and rate of heat release. Lower HC emissions and smoke number were

found for the methyl ester. The CO emissions results were mixed. The NO_x emissions were strongly related to the cylinder pressure. The variation of injection timing had a pronounced effect on performance and emissions for both fuels. The test also included two injection nozzle diameters. For a small nozzle diameter at the two timings investigated, standard and 5^o retarded, the CO emissions were slightly lower for the methyl ester. For a large nozzle diameter, the CO emissions were the same for diesel fuel and the methyl soyate at the standard timing. The CO emissions for the methyl soyate were higher at all but the highest load for the retarded timing. The HC emissions from the methyl ester were about one half of those from the diesel fuel.

Graboski et al. [47] used a 1991 DDC Series 60 engine to study the effect of blending biodiesel (methyl soyester) with diesel on the engine's exhaust emissions. The study showed that as the percent biodiesel increased, the NO_x emission increased, while the HC, CO, and particulate matter decreased. For a 35% biodiesel blend with diesel fuel, the NO_x emission increased by only 1% while the particulate emission decreased by 26%. For 100% biodiesel, the NO_x emission increased by 11% while the particulate matter (PM) decreased by 66%. The carbon monoxide (CO) was reduced by 47% and the total HC by 44%.

Alfuso et al. [48] reported on a test that had been carried out on a DI, turbocharged diesel engine. The study found that the methyl ester of rapeseed oil caused an increase in NO_x emissions, a decrease in HC and CO emissions, as well as a strong reduction of smoke. However, the particulate matter produced by the methyl ester in transient cycles was higher than that of diesel fuel. The discrepancy between smoke level

and particulate matter was indicative of high soluble organic fraction in the particulate when fueling with biodiesel.

Last et al. [22] investigated the potential for improving emissions from a DI diesel engine using different blends of methyl soyate. Substantial emissions improvements were found with a relatively small methyl ester fraction. At the standard injection timing calibration, reductions in HC, CO, and particulate emissions at 10, 20, 30, 50, and 100% blends were found compared to 100% diesel fuel. The NO_x emission increased linearly with the methyl ester fraction. Fuel consumption increased over the full load range as the fraction of soybean methyl ester became larger.

Clark et al. [16] experienced fuel filter plugging with both methyl and ethyl esters, while they were using a John Deere 4239 TF direct-injection, 4-cylinder, turbocharged diesel engine. Inspection of the filter revealed a gummy substance on the "dirty" side of the filter. They suspected the gum formation took place after the fuel drum was opened to be used. During subsequent tests, the fuel was filtered as it was removed from the barrel using a cannister filter. This procedure eliminated the plugging problem in the engine filter. They found that engine performance was not the same for soybean ester fuels and diesel fuel. A slight power loss combined with an increase in fuel consumption were experienced with the soybean esters, because the lower heating value of the esters is less than for diesel fuel. It was also found that no notable difference in emissions occurred among the esters and the No. 2 diesel fuel except for an increase in NO_x emissions for the esters. No wear was found on the cylinder walls (liners) and piston, and no piston rings were found to be stuck. However, piston deposits were

significantly greater for the methyl ester.

Generally, transesterified vegetable oil and its blends with diesel fuel reduce CO, HC, smoke, and particulate emissions, but usually increase NO_x emissions slightly relative to No. 2 diesel fuel. The magnitudes of the emission changes appear to be engine dependent. The engine performance and durability of these fuels is also comparable to diesel fuel.

2.6 Diesel Engine Emissions for Other Oxygenated Diesel Fuels

Fatty acid esters contain oxygen atoms in their molecules while a hydrocarbon fuel like diesel fuel does not. The addition of oxygen atoms in the fuel means that the fuel will burn leaner in the central core of the fuel spray which reduces the formation of solid carbon and allows the unburned hydrocarbon and particulate to burn more completely before the combustion products leave the combustion chamber.

The success of oxygenated gasoline has sparked interest in the use of oxygenated compounds in diesel fuel. Oxygenates were first used over fifty years ago to produce clean burning diesel fuels. Since that time many research projects have been conducted to determine the effect that oxygenated fuels will have on diesel engine performance and emissions. Liotta et al. [49, 50] investigated the effect of several different oxygenated fuel additives on emissions. Two reference diesel fuels were also used for their investigation. One was a low sulfur fuel with about 31% aromatics and the other was a low sulfur and low aromatic fuel. The oxygenated compounds were selected on the basis of toxicity, economic viability as fuel additives, and fuel blending properties. The fuel

blending properties included: additive solubility, flash point, viscosity, solubility of water, and the water partitioning of the additive. Three glycol ethers, an aromatic alcohol, an aliphatic alcohol, and a polyether polyol were selected for evaluation. Diglyme and methyl soyate were also included to allow comparisons to previous results. Most of the oxygenated additives used in the study did not affect the cetane number in the base fuel. Based on the EPA heavy-duty transient emissions test cycle, CO was generally reduced, a varying effect was found on the total hydrocarbon emissions, and NO_x emission showed a small increase for all oxygenated additives. The particulate matter emissions were reduced with the oxygenated fuels and this reduction appeared to be related to the amount of oxygen in the fuel. The oxygenated fuels also reduced the total aldehyde and ketone emissions.

McCormick et al. [20] also investigated the effect of several oxygenates on emissions. The transient emissions testing was performed on two heavy-duty DI diesel engines: a Detroit Diesel 6V92 and a Detroit Diesel Series 60. Ethanol, 1-octanol, decanoic acid, and soybean oil methyl ester were selected for evaluation and blended at the 1 and 2 wt % oxygen levels. Octanol, decanoic acid, and methyl soyate were tested in the 6V92 engine at the 1 wt % level. The 1 wt % level corresponded to blends of 8.5 vol % octanol , 5.2 vol % decanoic acid, and 8.9 vol % methyl soyate in No. 2 diesel fuel, respectively. Ethanol, octanol, and methyl soyate were tested in the Series 60 engine at the 2 wt % level. Two wt % oxygen corresponded to blends of 6.5 vol % ethanol, 16.6 vol % octanol and 17.7 vol % methyl soyate in No. 2 diesel fuel. All of the oxygenates tested in the 6V92, 2-stroke engine produced a significant reduction in particulate matter

(PM) emissions in the range of 12-17%. For octanol at the 1 wt % level of oxygen, hydrocarbon (HC) emissions were increased 4%, carbon monoxide (CO) emissions were decreased 2.8%, NO_x emissions were decreased 1.1%, and the PM emissions were decreased 17.2%. For octanol at the 2 wt % level of oxygen, hydrocarbon (HC) emissions were increased 24.9%, carbon monoxide (CO) emissions were decreased 2.1%, NO_x emissions were decreased 3%, and PM emissions were decreased 37.6%. For methyl soyate at the 1 wt % level of oxygen, hydrocarbon (HC) emissions were increased 0.8%, carbon monoxide (CO) emissions were decreased 7%, NO_x emissions were increased 2.3%, and PM emissions were decreased 15.4%. For methyl soyate at the 2 wt % level of oxygen, hydrocarbon (HC) emissions were decreased 10.2%, carbon monoxide (CO) emissions were decreased 13.9%, NO_x emissions were increased 2.5%, and PM emissions were decreased 19.5%. Methyl soyate produced significantly less CO emissions at the 2 wt % level of oxygen than at the 1 wt % level of oxygen. Octanol also produced less CO emissions for both oxygen levels. In the Series 60 engine, ethanol generally produced very poor engine operation.

Schmidt [45] compared the emissions from biodiesel with emissions when the air oxygen content was increased, and when long chain hydrocarbons and cetane improver were added. The oxygen content of the intake air was controlled by adding oxygen and nitrogen, respectively, to the intake air system. The solid portion of the particulate emissions decreased by 33% as the intake oxygen content increased from 20.5% to 22%. However, the soluble portion of the particulate emissions remained relatively constant. The NO_x emissions increased as the oxygen content in the intake system increased. The

CO emissions decreased slightly and the HC emissions remained fairly constant as the oxygen content of the intake air was increased. The ethylhexyl nitrate cetane improver increased the cetane number by 10.3 points. This cetane improver reduced the particulate emissions by 6% but no effect was found on the oxides of nitrogen (NO_x) emissions. Normal-octadecane, a long chain hydrocarbon, decreased the particulate and unburned hydrocarbon emissions but did not change the oxides of nitrogen (NO_x) emissions. Particulate and hydrocarbon emissions decreased by 21% and 22% respectively, for a 50/50 blend of n-octadecane and diesel fuel.

In general, oxygenated fuels produce a significant reduction in particulate emissions from diesel engines but in most cases also cause the nitrogen oxide emissions to increase.

3. EQUIPMENT AND PROCEDURE

A primary objective of this study was to relate the chemical and physical processes associated with biodiesel oxidation to the conditions that affect engine performance and emissions. In this chapter, the equipment that was used to accomplish the objectives will be discussed. To establish the connection between the chemical and physical processes associated with biodiesel, a fuel filter test setup was constructed. The first section discusses this biodiesel fuel filter test setup. The second section describes the engine test setup. The third section describes the emissions equipment and the data acquisition system is presented in the last section. These last three sections are to evaluate the impact of oxidized fuel on engine performance and exhaust emissions.

3.1 Biodiesel Fuel Filter Test Apparatus

3.1.1 Fuel filter test apparatus setup

Recent research has indicated that biodiesel may be subject to fuel filter plugging problems caused by sediment and gum formation [16]. Due to the unsaturated nature of biodiesel, the fuel changes chemically to form these compounds. Gum and sediment are the end products of polymerization reactions that can occur during oxidation. The ASTM D2274 test measures sediment and gum formation and the AOCS tests Cd 8-53 and Cd 3a-63 measure fuel oxidation. To establish the relation between these two tests, a fuel filter test stand was built.

The SAE J905 standard for fuel filter testing was followed to construct the test

stand. A schematic of the test stand is shown in Figure 3.1. Three eighths of an inch stainless steel tubing was used for the entire test rig. A Holley model 12-802 electric fuel pump followed by a Fleetguard model FS1001 fuel filter in a horizontal line was firmly attached with a strut to the top of a 55-gallon barrel. The biodiesel fuel was pumped from the 55-gallon barrel and pushed through the fuel filter before returning to the 55-gallon barrel. A Validyne model P305D differential pressure transducer was used to take the differential pressure across the fuel filter. A four-way valve was used to take fuel samples at a point down stream of the filter. A four-way fitting at the beginning of the flow was used to install two K-type thermocouples. One of the thermocouples was connected to an Omega Model CN9000A temperature controller to control the temperature of the fuel in the barrel and the other was connected to the data acquisition system to record the temperature. A flexible electric heating tape was wrapped around the barrel to heat the fuel.

In this part of the experiment, a total of four test rigs using 55 gallon barrels and a test rig with a 5-gallon stainless steel container were used. Two of the barrels were maintained at a controlled temperature at 60 °C and the other two were at room temperature. The 5-gallon test rig was maintained at 60 °C. The temperature of 60°C was chosen because this is a reasonable value for fuel circulating through a diesel engine fuel system. The flow rate was kept constant for all the tests.

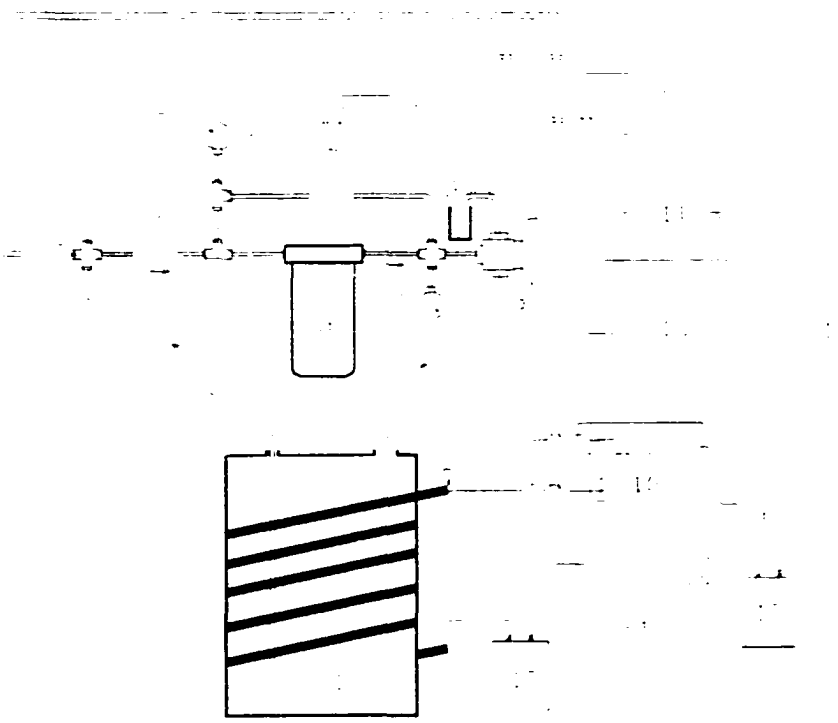

1. 55-gallon barrel 2. K-type thermocouples 3. Holley model 12-802 electric fuel pump 4. 12 Volt DC supply 5. Pressure gauge 6. Fleetguard model FS1001 fuel filter 7. Differential pressure transducer 8. Three-way valve 9. Sample container 10. Scanner 11. Ice point 12. Volt meter 13. Computer 14. Omega Model CN9000A temperature controller 15. 110 Volt AC supply 16. Relay 17. Flexible electric heating tape

Figure 3.1 Schematic diagram of the fuel filter rig

3.1.2 Data acquisition system for filter rig

A Quick Basic program was used to collect data from all five test rigs. A computer was used to measure the time, temperature, and differential pressure across the filter, for each test rig. Eleven channels were needed for all five test rigs. A scan of the eleven data channels was taken every five minutes and was stored in the computer.

The electronic data acquisition system was only used for the initial portion of the testing. When it was found that the filters were not plugging, most of the test data were logged manually.

3.1.3 Pressure drop and chemical properties of biodiesel data collection procedure

The main variables in this test were time, initial oxidation level (peroxide value) of the biodiesel, percent of biodiesel blended with No. 2 diesel fuel, viscosity, acid value, and temperature. The blends of 20% and 50% biodiesel with No. 2 diesel fuel were tested at 60 ^{o}C and at room temperature. These four tests were conducted in the 55-gallon barrels. In each test, 33 gallons of fuel were used. Only a single 100 % biodiesel test at 60 ^{o}C was conducted in the stainless steel container. This test was conducted with 5000 grams of pure biodiesel.

The fuel blend was circulated through the filter during the test and as the test proceeded, the fuel blend oxidized. Initially, the oxidation rate was slow because of its antioxidant content. This slow oxidation period is called the induction period. After the induction period, the fuel oxidized rapidly. One product of the fuel oxidation was the production of sediment and gum. This sediment and gum were collected by the filter and

the pressure drop across the filter began to rise. Although it was never reached during the test, eight inches of mercury pressure drop across the filter was considered to be a plugged fuel filter.

The pressure drop across the filter was initially taken every five minutes and fuel samples for the properties were taken every day. However, after a few days, the samples were taken every other day and the fuel filter pressure drop was monitored at this frequency as well. The fuel flow rate was kept constant by adjusting the voltage across the pump. A graduation cylinder was used to measure the flow rate.

3.1.4 ASTM D2274-94, standard test method for oxidation stability of distillate fuel oil

ASTM test method D2274 is the most commonly used method for characterizing the thermal and oxidative stability of diesel fuel. It was found during the course of this project that D2274 has significant problems when used to measure the stability of biodiesel. Since the procedures used to perform D2274 must be understood to explain its shortcomings, it will be described in detail below. Similar descriptions of the procedures used to measure the acid value and peroxide value are provided in Appendices A and B, respectively.

Oxidation is a chemical process that can cause insoluble material to form in the fuel. Any substance that catalyzes oxidation reactions will cause greater quantities of insolubles to form. For example, copper and chromium catalyze the oxidation reaction. It is important that any residues that could contain these metals be eliminated from the

apparatus.

It is necessary to define a few terms used in the ASTM method such as adherent insolubles, filterable insolubles, total insolubles, and trisolvent. Material which is produced in the course of stressing distillate fuel under the conditions of this test and which adheres to the glassware after rinsing the fuel from the system can be defined as adherent insolubles. Filterable insolubles is the material which is produced in the course of stressing distillate fuel under the conditions of this test that can be removed from the fuel by filtration. Total insolubles is the sum of the adherent and filterable insolubles. Trisolvent is a solution of equal volumes of toluene, acetone, and methanol.

The test method used for ASTM D2274 is described below:

A 300 ml sample of middle distillate fuel is aged at 95 °C for 16 hr while pure oxygen is bubbled through the sample at a rate of 3 L/h. After aging, the sample is cooled to approximately room temperature before filtering to get the filterable insoluble quantity. Adherent insolubles are then removed from the oxidation cell and associated glassware with trisolvent. The trisolvent is then evaporated to obtain the quantity of adherent insolubles. The sum of the filterable and adherent insolubles is the total insolubles. The result is expressed as milligrams per 100 ml of fuel.

An oxidation cell of borosilicate glass as shown in Figure 3.2, a temperature controlled heating bath, a flowmeter, a filter drying oven, a filter media of 47 mm diameter cellulose ester membrane with pore size of 0.8 micrometer, a borosilicate glass beaker, and a hot plate are needed for these tests. Also, isooctane of 99.75% purity, oxygen of 99.5% purity, and trisolvent are needed for this test.

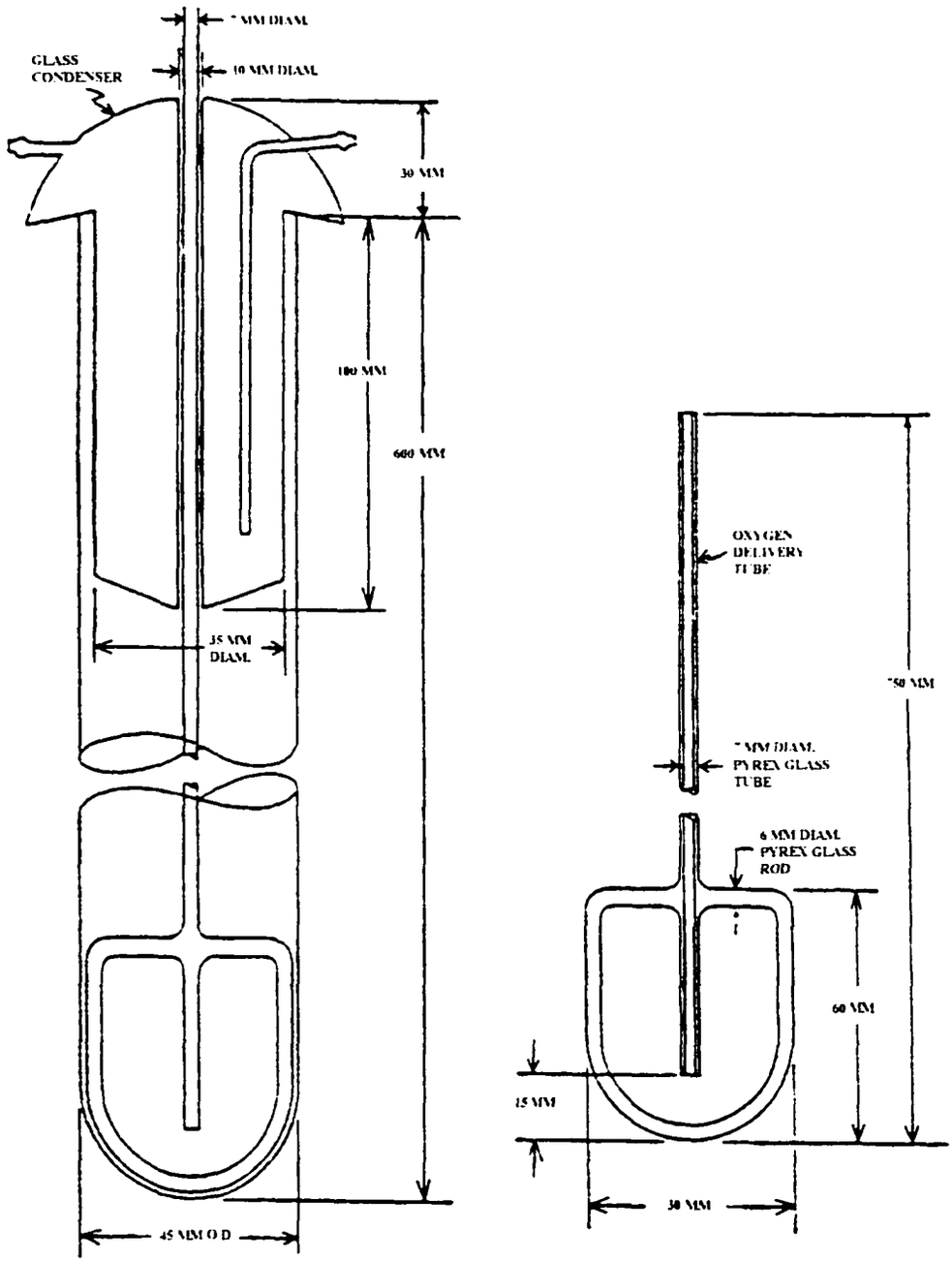

Figure 3.2 Oxidation cell of borosilicate glass [40]

Procedure:

1. Preparing the sample: Before using the sample in the oxidation cell, the sample must be filtered. About 400 ml of sample is poured through the filter while applying 80 kPa (12 psi) of suction. The same filter can never be used twice.
2. Assembling the oxidation apparatus: place an oxygen delivery tube into a clean oxidation cell and pour 300 +/-5 ml of filtered sample into the cell. Immerse the test cell into the controlled temperature of a 95 °C heating bath. Place the cell in a dark place. Maintain the oxygen flow into the sample at 3 L/h for 16 hours.
3. Cooling the sample: Remove the sample from the heating bath and place in a dark place at room temperature until the room temperature is attained or no longer than 4 hours.
4. Determining filterable insolubles: Use one pair of matched filters with one filter on top of the other. Place these filters on top of a membrane filter support. A clamp holds firmly the filter support and the filter funnel. Pour the cooled sample through the filters while applying suction of about 80 kPa (12 psi). On completion of filtration, completely rinse the oxidation cell and oxygen delivery tube by pouring 50 ml of isooctane through the filter assembly three times. After filtration is complete, disconnect the top part of the filter assembly, and wash down the rim of the filter media and the adjacent part of the filter media with an additional 50 ml of isooctane. Dry the two filter media at 80 °C for 30 min. Then, cool them for 30 min. and weigh the upper and lower filter separately to the nearest 0.1 mg.
5. Determining the adherent insoluble: After final rinsing of the oxidation cell and the

oxygen delivery tube with isooctane. remove the adherent insolubles from the surface of the oxidation cell and the oxygen delivery tube with three equal volumes of 25 ml of trisolvent. Collect the rinsings and evaporate the trisolvent at 135 °C under a hood. To measure the impurities in the trisolvent. an equal volume of trisolvent is used to get the adherent insoluble blank. Weigh the cooled and dry sample to the nearest 0.1 mg.

Calculation:

Calculate the filterable insolubles weight (A) in mg per 100 ml of sample. Subtract the weight of the blank (bottom) filter (W_1) from the sample (top) filter (W_2) and divide by 3.0 to express the result as mg per 100 ml.

$$A = (W_2-W_1)/3$$

Calculate the adherent insolubles weight (B) in mg per 100 ml.

$$B = ((W_6-W_4)-(W_5-W_3)) / 3$$

Where:

W_6 = final weight of the sample beaker. mg

W_4 = tare weight of the sample beaker. mg

W_5 = final weight of the blank beaker. mg

W_3 = tare weight of the blank beaker. mg

The sum of A+B is the total insolubles.

The use of this test method in an attempt to measure the gum and sediment formation with biodiesel is described in the Results and Discussion chapter.

3.2 Engine Test Setup

The main purpose of this part of the experiment was to determine the performance and oxides of nitrogen (NO_x) emissions of oxidized biodiesel compared with non-oxidized biodiesel and No. 2 diesel fuel. To accomplish this purpose, a John Deere 4276T four-cylinder, four-stroke, turbocharged DI diesel engine was connected to a 150 HP General Electric model TLC2544 DC electric dynamometer. The engine in which the fuel is injected into a chamber directly above the piston crown is called DI diesel engine while in indirect-injection (IDI) engine the fuel is injected into an auxiliary combustion chamber which is separated from the main combustion chamber by a flow restriction or nozzle. The basic engine specifications are provided in Table 3.1. A GE Siltron dynamometer controller controls the dynamometer. The dynamometer controls the speed of the engine and the rack position of the fuel injection pump controls the output torque.

The atmospheric pressure was measured with a Datametric Barocel pressure sensor. Boost pressure, exhaust pressure, and engine lubricating oil pressure were measured with bourdon pressure gages.

Table 3.1 John Deere 4276T diesel engine specification

Bore	106.5 mm
Stroke	127.0 mm
Connecting rod length	202.9 mm
Compression ratio	16.8:1
Maximum power	57.1 kW @ 2100 rpm
Peak torque	305.0 Nm @ 1300 rpm
Firing order	1-3-4-2

Kistler model 6061B and model 6230M1 pressure transducers were installed in the engine. The model 6061B was installed in the engine cylinder head to measure the cylinder pressure. The model 6230M1 was installed in the injection line to measure the fuel injection pressure. These pressure transducers were used to measure the pressures at every quarter degree of crankshaft rotation for 50 engine cycles. The average of 50 cycles data was saved in the computer for later analysis. The calibration of the pressure transducers is presented in Appendix C.

A PCB model 462A charge amplifier was used to amplify the pressure signal and a computer collected the pressure data. The pressure signal was recorded by a computer through a National Instruments ATMIO-16 data acquisition board.

A Meriam laminar flow element was used to measure the volume flow rate of air into the engine. An electronic scale and a stopwatch were used to measure the fuel flow rate.

3.3 Emission Measurement Equipment

3.3.1 Gaseous emissions equipment

A schematic of the gaseous emission measurement system is shown in Figure 3.3. A portion of the exhaust gas was drawn directly from the exhaust pipe with a vacuum pump located in a temperature-controlled oven. After necessary filtering, a portion of the sample passed through the HC analyzer. The rest of the sample gas passed through a condenser to remove the water. The dry sample was then distributed to the analyzers. Two Beckman model 864 infrared analyzers measured the concentrations of carbon

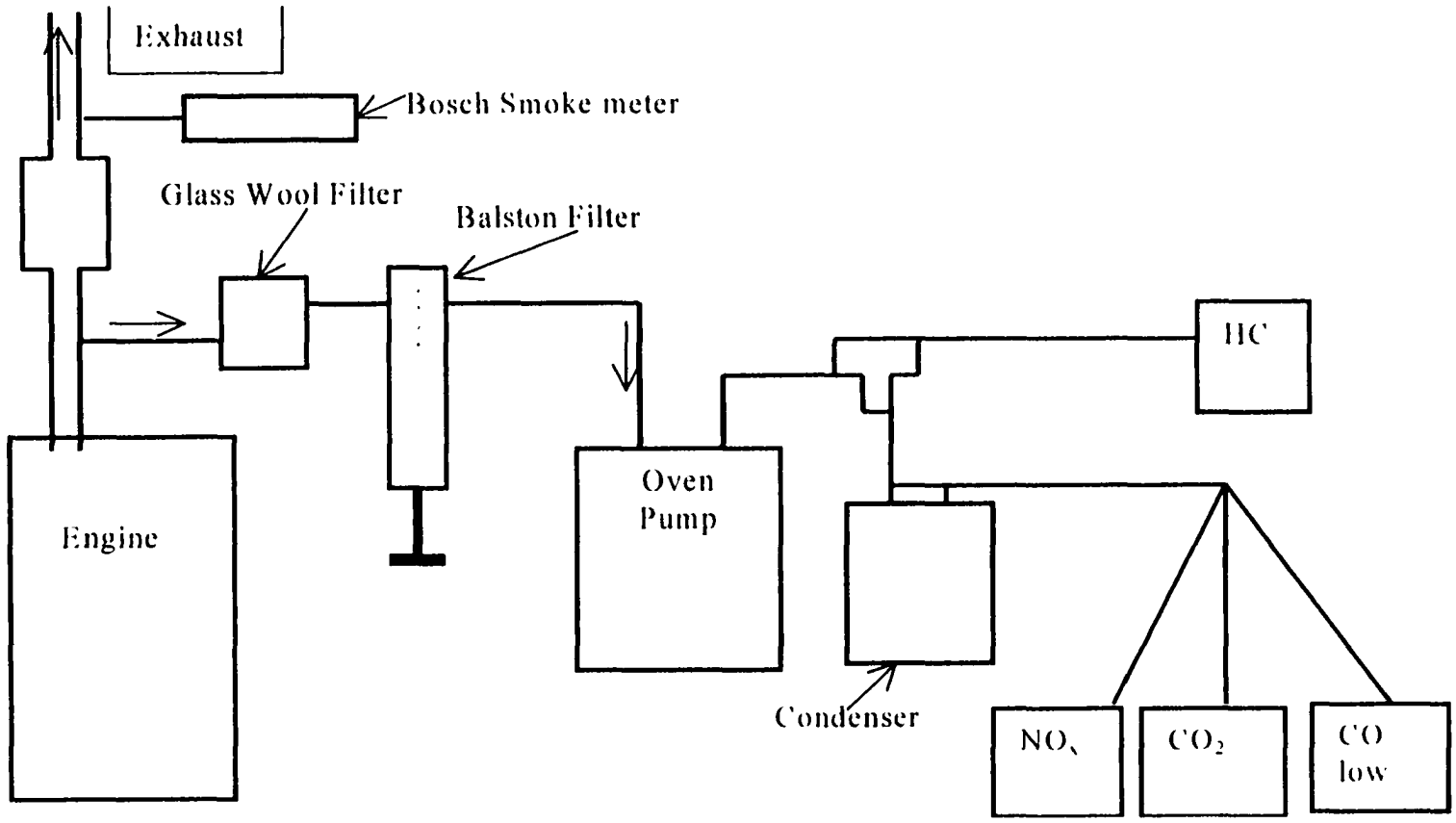

Figure 3.3 Schematic diagram for gaseous emissions measurement system

monoxide (CO) and carbon dioxide (CO_2) in the engine exhaust. A Thermo Environmental Instruments Inc. Model 42H chemiluminescent NO-NO_2-NO_x analyzer and a Thermo Environmental Instruments Inc. Model 350 chemiluminescent NO-NO_2-NO_x analyzer were used to measure the concentrations of NO and NO_x. Three other NO/NO_x analyzers were used for comparisons to make sure the collected data were correct.

The sampling lines were maintained at positive pressure after the oven pump. The reason for maintaining the positive pressure was so that if leaks develop, they will leave the system without contaminating the sample. As an additional confirming test, sometimes the calibration was performed by supplying the calibration gas at the near end of the analyzer and then supplying the same calibration gas at the far end of the analyzer to make sure that the concentrations were the same.

The sample for the hydrocarbon analyzer passed through a 190°C heated sampling line. The oven also maintained the vacuum pump at a 190°C temperature throughout the test. A Beckman model 402 heated flame ionization detector hydrocarbon analyzer and a Beckman model 7003 polarigraphic oxygen monitor were used to measure the concentrations of unburned hydrocarbon (HC) and the oxygen in the exhaust gas. A Bosch smoke meter was used to measure the smoke level.

3.3.2 Biodiesel oxidation process

To establish the effect of oxidized biodiesel on the exhaust emissions it was necessary to oxidize the biodiesel. The oxidation of the biodiesel required approximately

one day. The oxidation process involved a 55-gallon barrel, a heating tape, a temperature controller, an oxygen cylinder, and a flow meter. The schematic diagram is shown in Figure 3.4. Hourly sampling was necessary to get the correct upper level of the oxidation range. It was desired to elevate the fuel peroxide value quickly without allowing the fuel viscosity to increase excessively. A total of three batches of 22 gallons of biodiesel each were oxidized to prepare the fuel. Each batch of biodiesel was sufficient for one three-day test sequence.

Three eighths of an inch stainless steel tubing was used to supply oxygen into the barrel. A thermocouple was connected to an Omega Model CN9000A temperature controller to control the temperature in the barrel. A flexible electric heating tape was used to heat the fuel in the barrel. Once the fuel temperature reached 60 °C, pure oxygen was bubbled into the biodiesel. The temperature was selected to be 60 °C, because it was found earlier that the biodiesel oxidized faster at this higher temperature. Samples were collected each hour and their peroxide value were measured. Sampling was continued until the peroxide value of the fuel reached 340 meq O_2/kg. At this point the oxidation process was stopped and the fuel was allowed to cool down to room temperature. Figure 3.5 shows the typical increase in peroxide value as the fuel was oxidized.

3.3.3 Emissions data collection procedure

Fuel with two different oxidation levels, unoxidized (PV = 28 meq O_2/kg) and oxidized (PV = 340 meq O_2/kg) biodiesel fuel were blended with No. 2 diesel fuel to make blends of 20% biodiesel and 80% diesel fuel. The neat biodiesels (100%HPV and

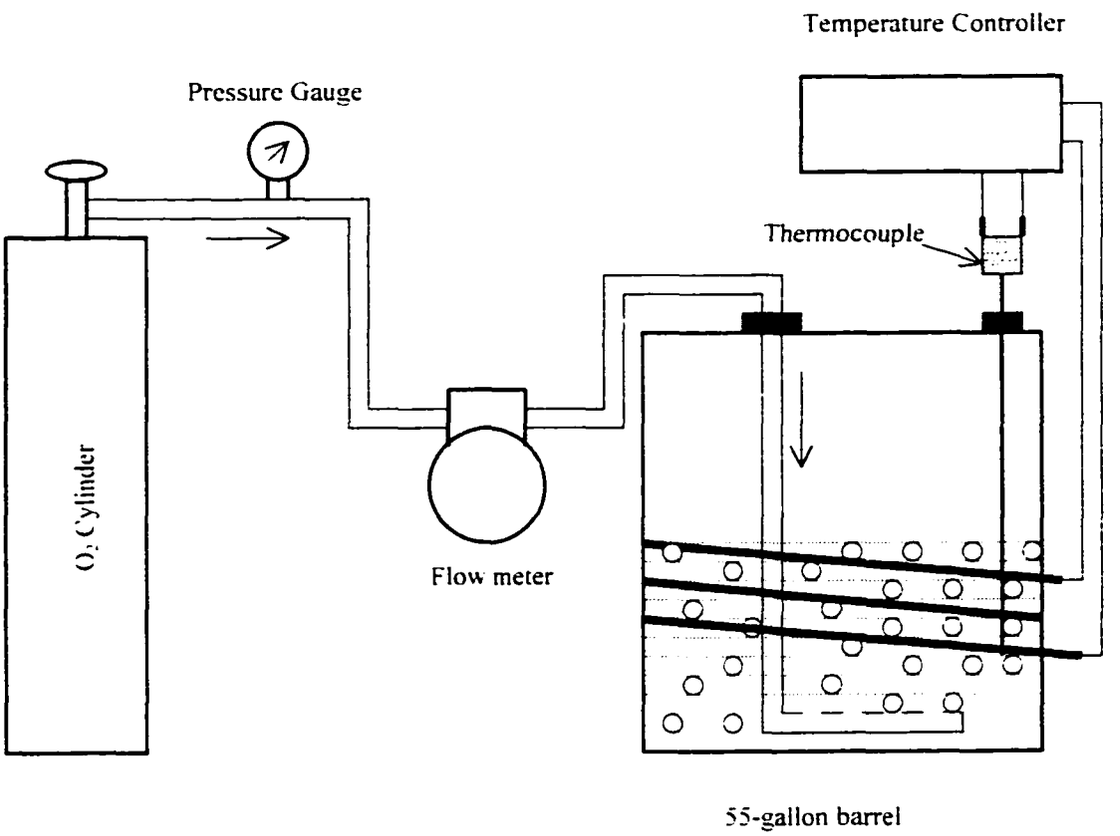

Figure 3.4 Schematic diagram for biodiesel oxidation rig

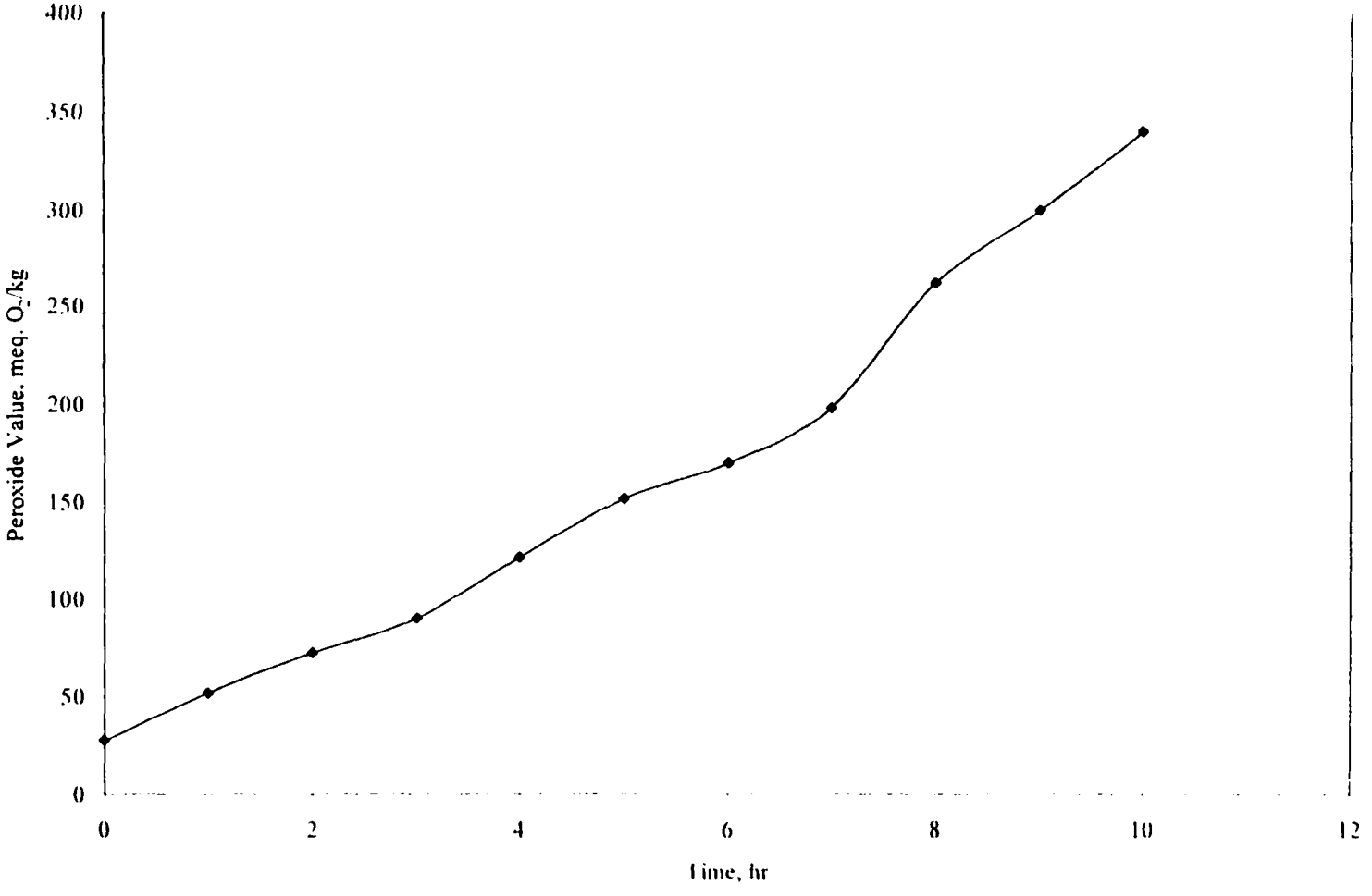

Figure 3.5 Biodiesel oxidation at 60° C

100%LPV), 20% blends (20%HPV and 20%LPV), and the base fuel (No. 2 diesel) were tested at different loads (100% and 20%) and timings (3° advanced, standard, 3° retarded). The tests were performed at steady state conditions at a single engine speed of 1400 rpm. The fuels and the test schedule are shown in Table 3.2.

3.4 Data Acquisition System

The cylinder and injection pressure data were measured using the Labview program with a 486 computer and a National Instruments Model ATMIO-16 data acquisition system. This system and related equipment are described in this section. The section is divided into three parts. The first part describes the shaft encoder. The second part describes the pressure transducers and the final part describes the charge amplifier.

3.4.1 Shaft encoder

A BEI Electronics, Inc. Incremental Optical Encoder (Model H-25) was used as an external pacer for the data acquisition process. The encoder was directly coupled to the engine shaft. The encoder consists of a transparent rotating disc with very fine lines etched onto it. These etched lines provide alternating dark and transparent spaces. A light source illuminates the disc while it rotates, and an alternating signal is produced when the etched lines block the light. An optical sensor measures the alternating signal. The disc has two sets of etched lines. The outer circle has only one etched line and the inner circle has 1440 etched lines (one for every quarter of a degree). A reference pulse is given when the single fine line (outer circle) blocks the light once per revolution. The other output

Table 3.2 Engine test conditions and fuels

	1400 RPM. Standard injection timing	
	100% of full load	20% of full load
Low peroxide value biodiesel (LPVB)	2D 20%LPVB 100%LPVB	2D 20%LPVB 100%LPVB
High peroxide value 340 biodiesel (HPVB)	2D 20%HPVB 100%HPVB	2D 20%HPVB 100%HPVB

	1400 RPM. 3° advanced injection timing	
	100% of full load	20% of full load
Low peroxide value biodiesel (LPVB)	2D 20%LPVB 100%LPVB	2D 20%LPVB 100%LPVB
High peroxide value 340 biodiesel (HPVB)	2D 20%HPVB 100%HPVB	2D 20%HPVB 100%HPVB

	1400 RPM. 3° retarded injection timing	
	100% of full load	20% of full load
Low peroxide value biodiesel (LPVB)	2D 20%LPVB 100%LPVB	2D 20%LPVB 100%LPVB
High peroxide value 340 biodiesel (HPVB)	2D 20%HPVB 100%HPVB	2D 20%HPVB 100%HPVB

2D: No.2 diesel fuel

gives 1440 pulses per revolution. An electronic circuit inside the encoder converts the signal from the optical sensor to a clean, sharp square wave.

The one pulse per revolution (ppr) signal is called the 'Z' signal, and the 1440 ppr signal is called the 'A' signal. The 'Z' signal is timed to occur precisely when the piston of the engine is at the bottom of the stroke. The 'Z' pulse will then be used to start the data acquisition system so that it begins to take data at the bottom of the stroke. The 'A' pulse will be used to trigger the data taking process. Once the 'Z' pulse starts the data taking process, the 'A' pulse tells the data acquisition system when to take the pressure data. The system takes the pressure data when the 'A' pulse undergoes a low-to-high transition. When the process is started by the 'Z' pulse, the data acquisition system will take the pressure data every quarter of a degree (1440 data points) for each revolution, and the process will continue for 50 cycles. The data acquisition system outputs a single cycle, which is the average of pressure measurements for 50 cycles.

3.4.2 Pressure transducer

Technical specifications and calibrations of the Kistler Model 6061A and Model 6230M1 pressure transducers are described in Appendix C. The operating principle of the pressure transducer is that when a quartz crystal is mechanically stressed it produces an amount of electric charge that is proportional to the magnitude of the stress. The transducer has a thin diaphragm welded to its body. When subjected to pressure this thin diaphragm deflects inward and pushes the crystal. When pressure develops, the electric charge produced by the sensor is converted into a proportional voltage in the charge

amplifier. Highly insulating and low-noise connecting cables are used with these transducers.

One difficulty arises with piezoelectric transducers during use. They do not hold a constant baseline output. The output voltage corresponding to a fixed pressure changes slowly with time. Piezoelectric measuring systems are suited primarily for measuring rapidly changing phenomena. Static measurement over any length of time is impossible. In principle, only pressure changes are measured, usually relative to atmospheric pressure.

3.4.3 Charge amplifier

A basic laboratory charge amplifier, the PCB Piezotronics Model 462A was used to convert the electrostatic charge signals from the piezoelectric transducer into proportional output voltage signals. This voltage signal can be read in equivalent pressure units by properly setting the charge amplifier sensitivity and range selector switch.

Before taking pressure data, the "OPERATE-GND" switch is always switched to the GND position. This operation discharges accumulated static charge which might contribute false pressure to the data.

4. DATA COLLECTION AND ANALYSIS

4.1 Statistical Analysis

As was mentioned before, biodiesel is a biodegradable fuel. That is, when it comes into contact with air it oxidizes. This oxidation is a function of time, light, heat etc. Currently there is no technology available to stop this oxidation process but it can be delayed by taking out some of the sources of oxidation. In practice, there will always be some sources available to oxidize the biodiesel. In this experiment, two different levels of oxidized fuel were investigated. Since time is a factor that affects oxidation, the age (day) effect is important to consider.

The highly oxidized biodiesel was prepared in the laboratory where working with large amounts of fuel can pose a safety problem. Also, on-going oxidation was another reason not to prepare a single large volume of fuel. Instead, three smaller batches of fuel were prepared. The variation of batch to batch oxidation was a variable that needed to be considered. The injection timing change also was a big factor to consider. Considering all these factors, the split-plot was the most appropriate design for this experiment. It is called the split-plot design because it had its origin in agricultural experimentation.

The engine emission measurement experiment was designed in such a way that the objectives of this project could be accomplished. Initially, different statistical designs were considered for this project. The factorial design was the first one suggested. Because of some limitations like injection timing setup, day to day variation, fuel preparation, and the age of fuel, the complete factorial design was not appropriate for this

project. Instead, a split plot design seemed to be the most appropriate for this kind of project. In factorial design, a variable like the injection timing needed to change several times in a single day test which was not practically possible. This can be considered as a limitation.

The split plot design consists of two stages. The first stage is related to the whole plot and the second stage is related to a subplot. This design is thus could be named a split plot design with a day as a "whole plot" and each of the ten runs within a day as a "sub-plot". This split plot design is shown in Table 4.1. The whole plot is a 3×3 Latin square and within each whole day plot is a 2×5 factorial experiment. A 3×3 Latin square design contains 3 rows and 3 columns. The three treatments (injection timings) are randomly assigned to experimental units within the rows and columns so that each treatment appears in every row and in every column. A factorial experiment is an experiment in which the response of dependent variables (emissions, fuel consumption etc.) is observed at all factor-level combinations of the independent variables. More extensive explanation of these topics is provided in Ott [51] and Neter et al. [52].

A SAS program was used to analyze the collected data. The program output was then tabulated in the analysis of variance (ANOVA) table which is presented in the Results and Discussion chapter. Also, another form of statistical analysis data called Tukey's grouping table was computed and is shown in Appendix D

Table 4.1 Split plot design

(a) Whole plot (3×3 Latin square)

Age / Batch	1	2	3
1	standard (day 1)	3° advanced (day 2)	3° retarded (day 3)
2	3° retarded (day 4)	Standard (day 5)	3° advanced (day 6)
3	3° advanced (day 7)	3° retarded (day 8)	Standard (day9)

(b) Randomly assigned subplot within each whole plot (2×5 factorial experiment)

Fuel / Load	100%HPVB	100%LPVB	20%HPVB	20%LPVB	NO.2D
100% load	10^{th}	5th	9th	3rd	1st
20% load	4th	8th	7th	6th	2nd

4.2 Data Analysis

The emissions data calculation process is presented in this section. All data were reported on a brake specific basis. Brake specific emissions are the mass flow rate of emissions divided by the brake power. Representing the data on a brake specific basis allows comparisons to be made between different sizes of engines. The first section

describes the calculation process for the gaseous emissions. The second section presents the humidity correction process for the oxides of nitrogen.

4.2.1 Gaseous emissions

The emissions data were taken for each fuel at one-second intervals for two separate five minute periods intervals. The first set of data was taken with the NO_x/NO meter set for NO_x emissions and the second set of data was taken for NO emissions. The data were then averaged to obtain the emissions data. It is general practice to express the emissions data on a "brake specific" basis. Brake specific emissions are the mass flow rate of the pollutant divided by the engine power.

A chemical equation for the combustion of the fuel was necessary to calculate the brake specific emissions from the measured exhaust concentration. The equation below is the balanced chemical equation for diesel fuel, assuming complete combustion.

$$C_xH_yO_z + (A/F)\,(0.21\,O_2 + 0.79\,N_2) = B\,(y_{co2,dry}\,CO_2 + y_{o2,dry}\,O_2 + y_{N2,dry}\,N_2) + C\;\;H_2O \quad (4\text{-}1)$$

where x = number of carbon atoms in an average fuel molecule

y = number of hydrogen atoms in an average fuel molecule

z = number of oxygen atoms in an average fuel molecule

$y_{i,dry}$ = mole fraction of chemical species on a dry basis

A/F = molar air/fuel ratio

B = number of moles of dry products per mole of fuel

C = number of moles of water per mole of fuel

This chemical equation can be solved by atom balance for B and C. Expressions for B and C are shown below.

$$B = (A/F) \div z/2 - y/4 \quad (4\text{-}2)$$

$$C = y/2 \quad (4\text{-}3)$$

Using the measured emissions data the above equations were solved on a brake specific (BS) emissions basis. The brake specific equations are as follows.

$$BSCO_2 = [\text{kmol } CO_2/\text{kmol dpg}] \times [\text{kmol dpg/kmol fuel}] \times [\text{kmol fuel/kg fuel}] \times [\text{kg fuel/hr}] \times [\text{kg } CO_2/\text{kmol } CO_2] \times [1/\text{kW}] \quad (4\text{-}4)$$

$$= [y_{co2}] \times [B] \times [1/MW_{fuel}] \times [m_{fuel}/1] \times [MW_{co2}/1] \times [1/\text{kW}]$$

$$= \text{kg/kW-hr}$$

$$BSCO = [\text{kmol CO/kmol dpg}] \times [\text{kmol dpg/kmol fuel}] \times [\text{kmol fuel/kg fuel}] \times [\text{kg fuel/hr}] \times [\text{kg CO/kmole CO}] \times [1/\text{kW}] \quad (4\text{-}5)$$

$$BSNO = [\text{kmol NO/kmol dpg}] \times [\text{kmol dpg/kmol fuel}] \times [\text{kmol fuel/kg fuel}] \times [\text{kg fuel/hr}] \times [\text{kg NO/kmol NO}] \times [1/\text{kW}] \quad (4\text{-}6)$$

$$BSNO_x = [\text{kmol } NO_x/\text{kmol dpg}] \times [\text{kmol dpg/kmol fuel}] \times [\text{kmol fuel/kg fuel}]$$

$\times$ [kg fuel/hr] $\times$ [kg NO_x/kmol NO_x] $\times$ [1/kW] (4-7)

BSHC = [kmol HC/kmol wpg] $\times$ [kmol wpg/kmol fuel] $\times$ [kmol fuel/kg fuel]

$\times$ [kg fuel/hr] $\times$ [kg HC/kmol HC] $\times$ [1/kW] (4-8)

where dpg = dry product gas

wpg = wet product gas

MW = molecular weight

M = mass flow rate, kg/hr

kW = brake power, kW

kmol = killo mole

4.2.2 Humidity correction factor for oxides of nitrogen

The correction of the oxides of nitrogen emission for the effects of humidity followed the procedure recommended by the Society of Automotive Engineers [53]. The specific humidity of the engine intake air, h, is computed from the following equation.

$$h = 621.10 \times P_v / (P_b - P_v) \quad (4\text{-}9)$$

where h = specific humidity, g H_2O/kg dry air

P_b= observed barometric pressure, kpa

P_v= partial pressure of water vapor, kpa

Ferrel's equation [54] listed below provides the partial pressure of water vapor, P_v, calculation.

$$P_v = P_w - 1.80\ A \times P_b\ (T_d - T_w) \qquad (4\text{-}10)$$

where P_w = saturation pressure of water vapor at the wet bulb temperature, kpa

T_d= dry bulb temperature, °C

T_w= wet bulb temperature, °C

A= experimentally derived constant = $3.67 \times 10^{-4}\ (1 + 0.001152\ T_w)$

The saturation pressure of water vapor at the wet bulb temperature is a least square fit to Keenan and Keye's steam table [55], which is shown below.

$$P_w = 0.6048346 + 4.59058\times10^{-2}\ T_w + 1.2444\times10^{-3}\ T_w^2 + 3.52248\times10^{-5}\ T_w^3 + 9.32206\times10^{-8}\ T_w^4 + 4.18128\times10^{-9}\ T_w^5 \qquad (4\text{-}11)$$

where P_w= saturation pressure of water vapor, kpa

T_w= wet bulb temperature, °C

The corrected oxides of nitrogen concentration can be calculated as the Society of Automotive Engineers recommends [53].

$$NO_{corr} = NO_{wet} \times 1/K \qquad (4\text{-}12)$$

Where NO_{corr} = corrected NO concentration, ppm

NO_{wet} = measured NO concentration on a wet basis, ppm

$K = 1 - 7A (h - 10.714) + 1.8 B (T - 29.444)$

$A = 0.044 (F/A) - 0.0038$

$B = -0.116 (F/A) - 0.0053$

T= intake air temperature, °C

F/A= fuel-air ratio (dry basis)

h= specific humidity, g H_2O/kg dry air

4.3 Analysis of Cylinder Pressure

Two sets of cylinder pressure data were taken at each operating condition. Both sets consisted of 50 cycles of averaged data taken every quarter in a degree. The large number of cycles were collected to cancel out the random noise. These data were intended for use in calculating heat release rates.

The voltage levels provided by the data acquisition system were converted to pressures following procedures recommended by Lancaster, et al. [56]. The sensitivity of the transducer measured calculated using a dead weight tester. The piezoelectric transducers do not hold an absolute pressure so it was necessary in this experiment to establish an absolute reference pressure. It was assumed that the pressure at the bottom dead center (BDC) before compression was equal to the intake manifold pressure.

4.4 Analysis of Injection Pressure

The injection pressure data taking procedure is the same as the cylinder pressure data collection. The two sets of injection pressure data were taken at each operation condition. Both sets of data consisted of 50 cycles of averaged data taken at 0.25° intervals. These injection pressure data were taken immediately after the cylinder pressure data. The same data acquisition system was used to collect both. To eliminate the random noise, fifty cycles of data were necessary. These data were intended for use in estimating the fuel injection timing.

The data acquisition system provided the voltage levels. These voltage levels were then converted to pressures. The sensitivity of the transducer was collected from its manufacturer-supplied calibration certificate. The specifications for this transducer are shown in Appendix C.

The data triggering technique is the same as for the cylinder pressure data. Sample injection pressure profiles are shown in Figure 4.1. These pressure profiles reveal the presence of large amplitude pressure waves in the injection pressure. These pressure waves may not be the characteristic of the actual injection pressure. Tadakazu et al. [57] describe how the pressure wave moves back and forth in the injection line. According to the authors, when the fuel is subjected to high pressure, a positive pressure zone moves forward inside the tube. At the end of the injection nozzle, this positive pressure inverts to a negative pressure zone and moves backward. These positive and negative pressures are responsible for the large amplitude waves in the injection pressure profiles.

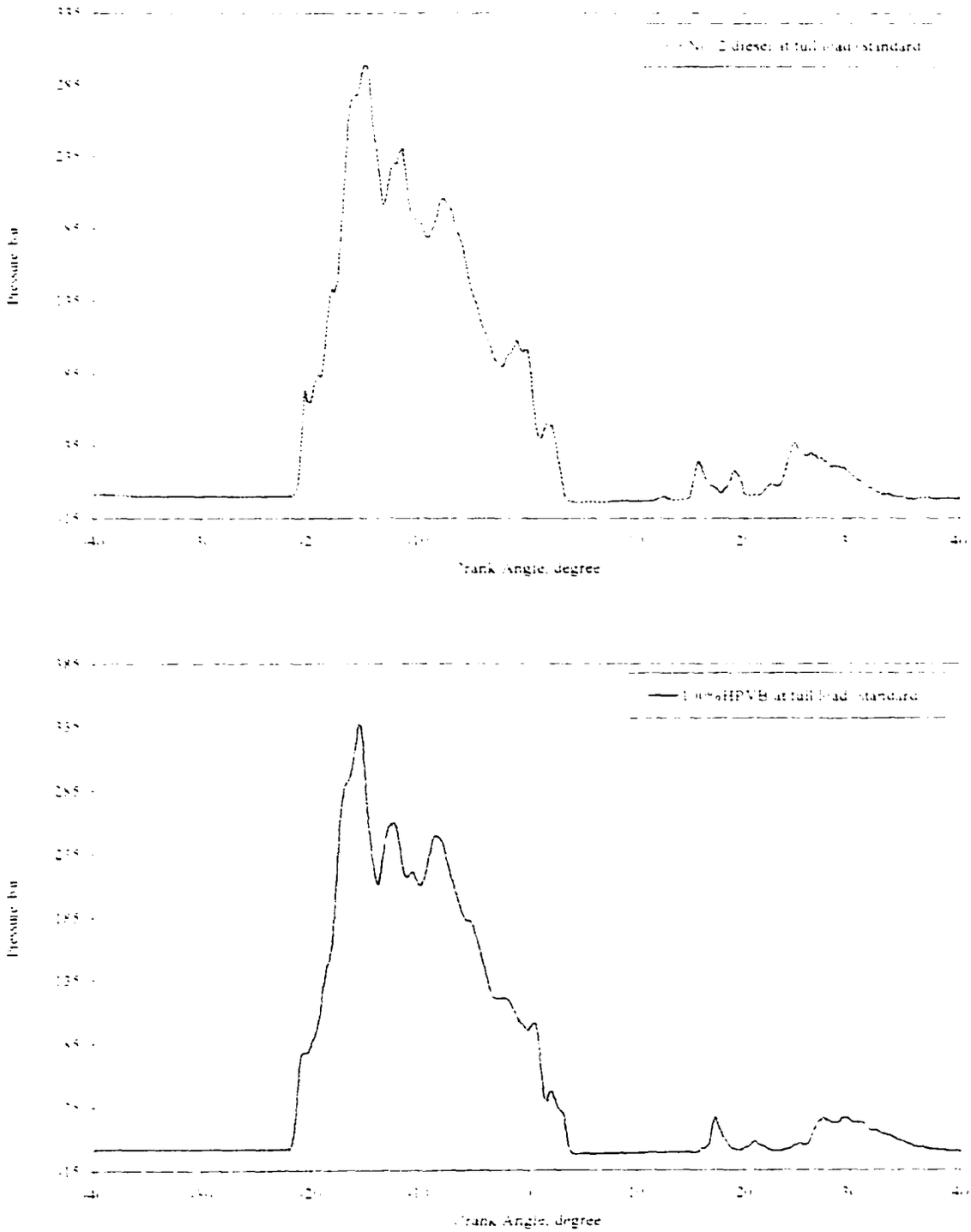

Figure 4.1 Injection pressure

4.5 Calculation of Ignition Delay

The ignition delay in a diesel engine was defined as the time (or crank angle) between the start of fuel injection into the combustion chamber and the start of combustion. The start of injection is usually taken as the time when the injector needle lifts off its seat (determined from the injection pressure data). The start of combustion is more difficult to determine precisely. Henein and Bolt [58] define three possible definitions of ignition delay. The first is the illumination delay, the second is the temperature rise delay and the last is the pressure rise delay. The illumination delay is defined as the time between the start of injection to the start of the luminous flame in the engine. Temperature rise delay is the time from the start of injection to a specified cylinder-averaged temperature rise due to combustion. Similarly, the pressure rise delay is the time between the start of injection and a specified pressure rise due to combustion. An alternative to these three definitions of ignition delay is to calculate the heat release rate and use it as the basis of the start of combustion as suggested by Van Gerpen [59]. In this study, the start of combustion was defined in terms of the change in slope of the heat-release rate which occurs at ignition. The definition of ignition delay used in this study was the time between when the injection line pressure had reached 207 bar and when the slope of the heat release rate determined from the cylinder pressure data, had started to rise rapidly. Measurements of the injection's nozzle-opening-pressure had shown that the fuel injected into the cylinder at an injection line pressure of 207 bar. The next section more completely describes the techniques used to determine the start of combustion from the heat release rate.

4.6 Heat Release Analysis

4.6.1 Calculation procedure

Heat release rate calculation is a useful tool for investigating diesel engine combustion. The most basic model for this heat release rate begins with the first law of thermodynamics. The basic heat release rate calculation was extended by Krieger and Borman [60] to obtain an apparent fuel mass burning rate. Walson, Pilley, and Marzouk [61] proposed an empirical correlation for the mass burning rate. Many other researchers have also investigated, and extended the work related to heat release rate calculation [62, 63]. All these advanced methods use sophisticated methods for calculating the gas properties. One of the more sophisticated models for calculating the gas properties was presented by Olikara and Borman [64]. These sophisticated techniques make the heat release calculation very complex. For simple determination of the start of combustion a more simple heat release rate calculation is adequate.

Simple methods of analysis which yield the rate of release of the fuel's chemical energy (often-called heat release), through the diesel engine combustion process are described in this chapter. The method of analysis begins with the first law of thermodynamics and three basic assumptions. The first assumption is that the trapped charge is contained in a uniform single zone of constant composition from intake valve closing to exhaust valve opening. The second assumption is that the charge inside the cylinder behaves as an ideal gas. The third assumption is that the energy released by combustion can be modeled as a heat addition to the cylinder. Based on these

assumptions the heat release rate can be derived. This heat release rate is lumped together with the heat loss. From the first law:

$$\frac{dU}{dt} = \dot{Q} - \dot{W} \tag{4-13}$$

$$mC_v \frac{dT}{dt} = \dot{Q} - P\frac{dv}{dt} \tag{4-14}$$

Where: $\dot{Q}$ is the combination of the heat release rate and the heat-transfer rate across the cylinder wall.

$\dot{W}$ is the rate of work done by the system due to system boundary displacement.

The ideal gas assumption can be used to simplify the equation (4-14).

$$PV = mRT \tag{4-15}$$

Which can be differentiated to give:

$$\frac{dT}{dt} = \frac{1}{mR}\left(P\frac{dV}{dt} + V\frac{dP}{dt} \right) \tag{4-16}$$

After combining these two equations, the heat release rate equation becomes.

$$\dot{Q} = \left(\frac{C_v}{R} + 1 \right) P\frac{dV}{dt} + \frac{C_v}{R} V\frac{dP}{dt} \tag{4-17}$$

Replacing time (t) with crank angle θ, the above equation becomes

$$\dot{Q} = \frac{\gamma}{\gamma + 1} P \frac{dV}{d\theta} + \frac{1}{\gamma - 1} V \frac{dP}{d\theta} \tag{4-18}$$

Where γ is the ratio of specific heats, C_p/C_v. An appropriate range for γ for diesel heat-release analysis is 1.3 to 1.35. Equation (4-18) is often used with a constant value of γ within this range [65]. The appropriate value of γ during combustion which will give the most accurate heat-release information is not well defined [66, 67], but the equation is more than adequate for predicting the start of combustion.

4.6.2 Heat release vs. crank angle profiles

A sample heat release rate profile, calculated from experimentally obtained cylinder pressure data according to the above procedure, is shown in Figure 4.2. The injection timing for the particular case shown was 17° BTDC and the start of combustion was about 9.1° BTDC. So the difference between these two is the ignition delay of 7.9° BTDC. It can be observed that the heat release rate is slightly negative during the delay period. This is due to heat loss from the cylinder and the cooling effect of the fuel vaporizing as the fuel is injected to the cylinder. The initial phase of combustion is observed to be very rapid. This is because of the combustion of the fuel which has mixed with air during the ignition delay period occurs rapidly in a few degrees of crank angle and when this burning mixture is added to the fuel, the fuel burns very rapidly. This is characterized as the premixed or rapid combustion phase.

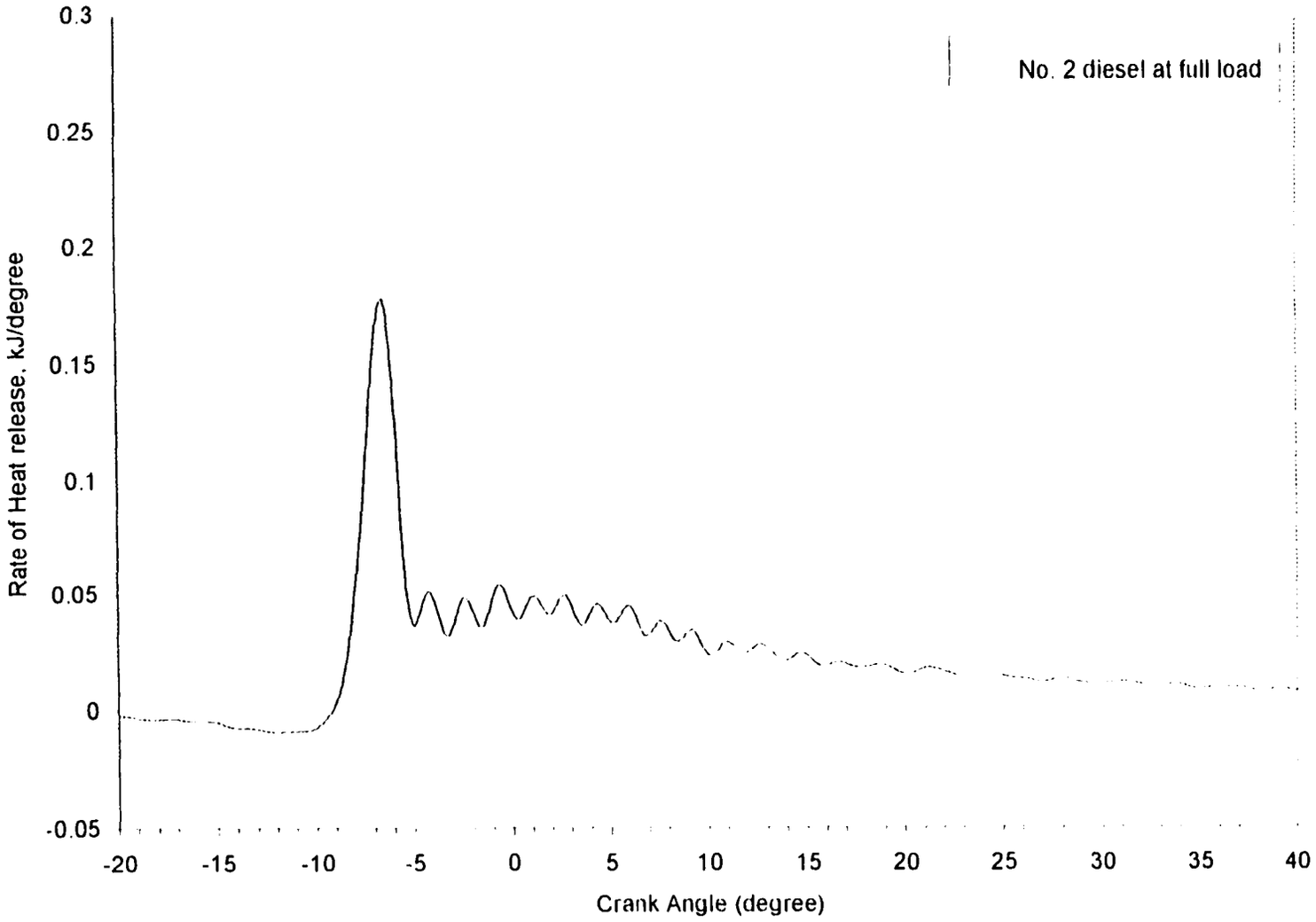

Figure 4.2 Heat release profile at full load

The duration of the premixed combustion for the case shown is about 4.1°. Following the premixed combustion is the slow phase of combustion which continues until most of the fuel is burned. This phase of combustion is called the mixing-controlled combustion phase. The final phase of combustion that occurs from about 30°ATDC to the end of the expansion stroke is characterized as the late combustion phase

4.6.3 Cylinder pressure smoothing technique

The heat release rate equation (4-18) has two derivative terms. One is the time derivative of volume which is an easily calculated quantity. The other is the time derivative of pressure which may contain some oscillations. In the burning rate equation, the pressure and the time derivative of pressure are important quantities. The pressure data collection technique was explained in the experimental section and the derivatives of pressure data can be obtained by differentiating the pressure data. Error in the pressure data or in the differentiation process will cause corresponding errors in the heat release rate. Austin and Lyn [68] pointed out that a 1° error in the pressure measurement can cause a 50% error in the heat release rate. Van Gerpen [59] also showed that small oscillations in the pressure data can cause errors in the heat release rate curve. So, the extremely sensitive heat release rate calculation requires not only accurate pressure data but also requires a robust technique for the numerical differentiation. A four point difference approximation was used to differentiate the pressure data. In the fluid mechanics and heat transfer area, most of the partial differential equations which involve first and second-partial derivatives use values at only two or three grid points. Using

these two or three data points, the most frequently used first-derivative approximations on a grid are the forward, backward, and central difference representations. All three of these representations for the first derivative were tested and failed to provide better results. Instead they provided very noisy pressure derivatives. At this stage, a four point difference representation was taken in consideration and successfully provided the better result. The first-derivative approximation using four points was:

$$(du/dx)_i = (-u_{i-2} - 8\,u_{i-1} - 8\,u_{i-1} + u_{i-2})/(12 \times \Delta\theta) \qquad (4\text{-}19)$$

where i = data locations in x, y directions.

u_i = pressure at the location of i.

$\Delta\theta$ = crank angle interval between i and i+1.

Also, the pressure data required some smoothing to reduce the unwanted noise, particularly from oscillations in the pressure data.

Van Gerpen [59] observed that the cases of worst oscillation correspond to cases of high initial rate of heat release. Based on his observation, it was concluded that the oscillations in the pressure data that manifested themselves in large oscillations in the heat release were probably local fluctuations due to pressure waves induced by the rapid rate of pressure rise at the start of combustion. He also mentioned that the pressure integrated over the piston face, which is the important quantity for calculating the work output of the engine, is probably relatively smooth and not affected by the local fluctuations. Since the cylinder pressure is the most important quantity required for the burning rate calculation, he suggested removing the pressure fluctuations. The removal of

the pressure fluctuations was necessary in order to calculate an acceptable heat release rate. Figure 4.3 shows the typical heat release rate before and after smoothing. The upper figure shows the unacceptable oscillation in the heat release rate calculation caused by oscillations in the pressure data. Smoothing is necessary to get some meaningful information from this heat release curve.

A smoothing technique suggested by Hamming [69, 70] called "Digital Filtering" reduces the noise dramatically. Van Gerpen [59] also found that this technique was reasonable. Digital filtering is the numerical process in which a new set of data is produced which has different frequency characteristics. The techniques used for this study are as follows:

$$g_i = 1/2\ (f_{i-1} + f_{i-1}) \qquad (4\text{-}20)$$

$$h_i = 1/3\ (g_{i-1} + g_I + g_{i-1}) \qquad (4\text{-}21)$$

Where f_i = the original data

g_i = intermediate value

h_i = the filtered data

Figure 4.4 shows the unsmoothed and smoothed pressure vs. crank angle curve. The changes in pressure derivatives are shown in Figure 4.5. The large amplitude oscillations in the derivative curves are mostly gone while the large peak due to the rapid combustion is reduced somewhat but still prominent.

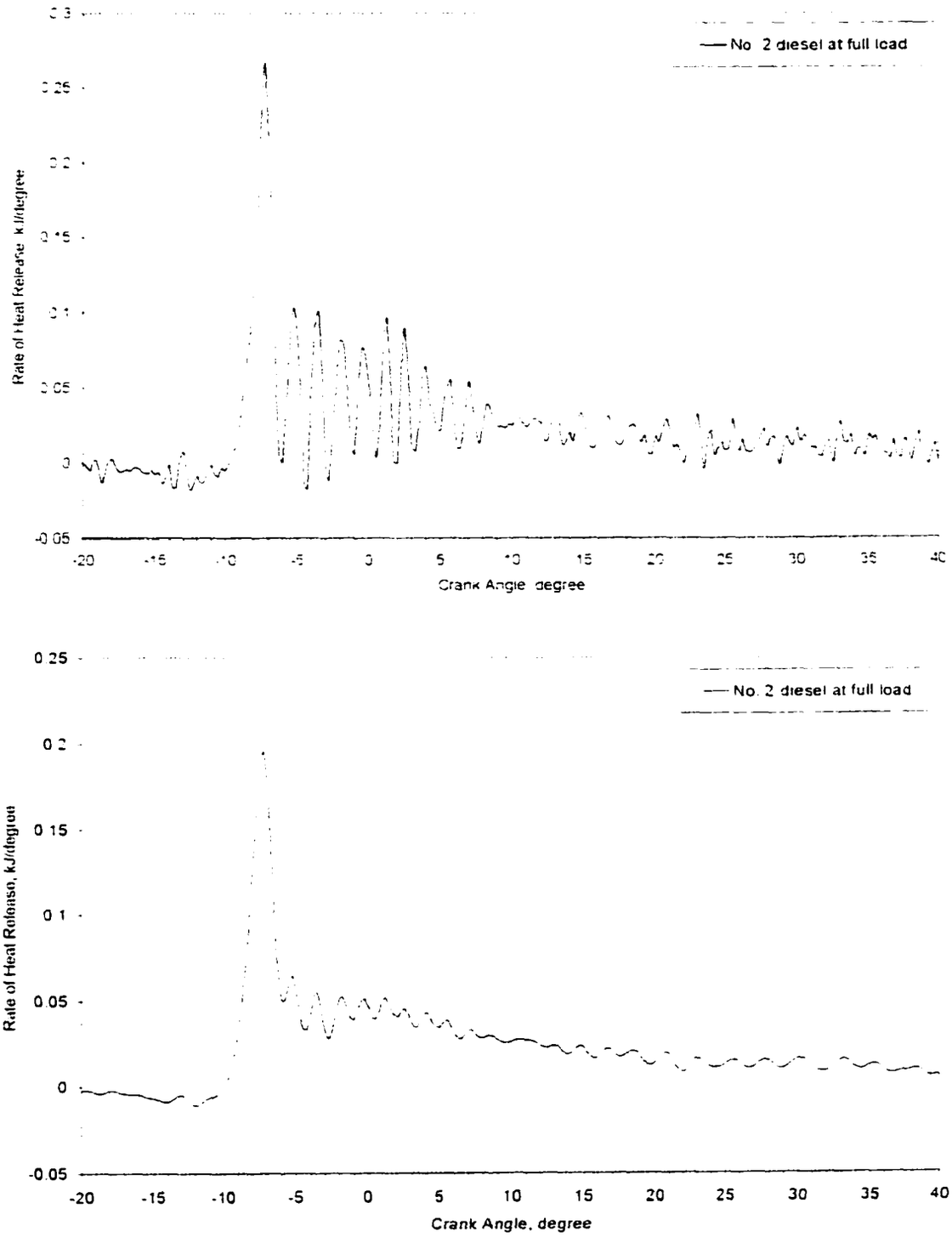

Figure 4.3 Heat release profile before and after smoothing

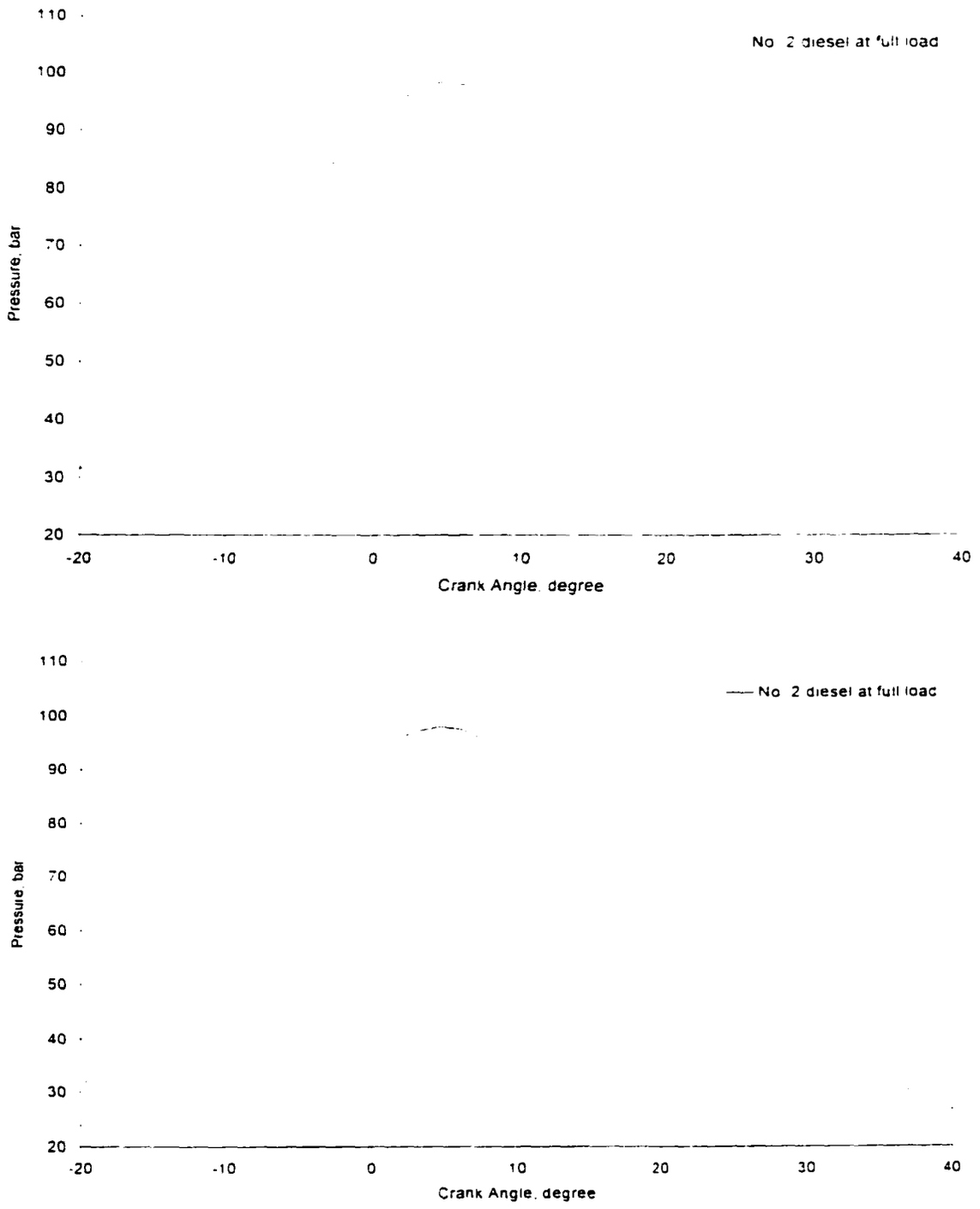

Figure 4.4 Cylinder pressure vs. crank angle curve before and after filtering

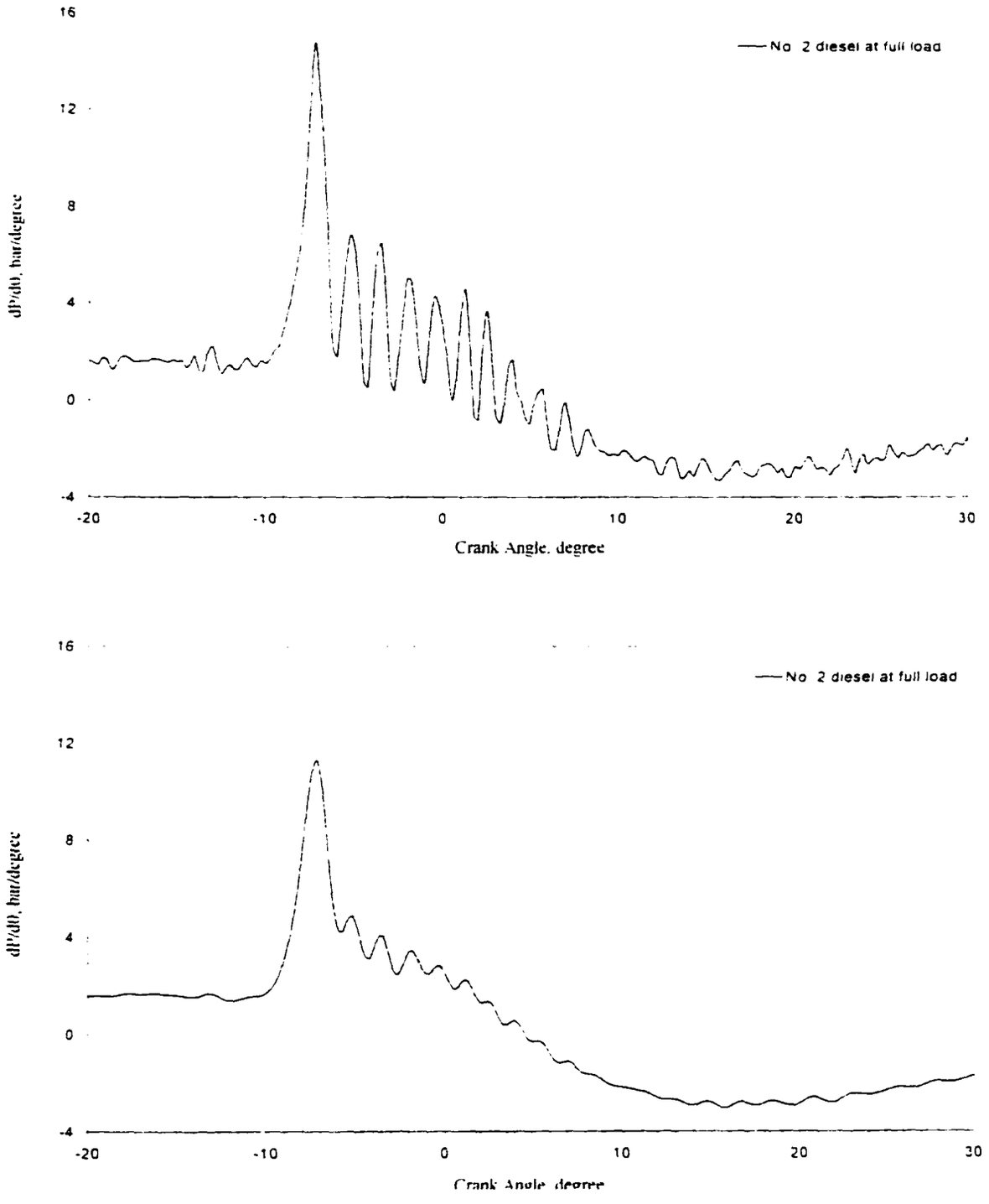

Figure 4.5 Cylinder pressure derivative vs. crank angle curve before and after filtering

5. RESULTS AND DISCUSSION

In this chapter, the effect of oxidized biodiesel on peroxide value, acid value, and viscosity are presented in the first section. These properties characterize the oxidative stability of biodiesel. The diesel engine performance when the engine is fueled with oxidized and unoxidized biodiesel and their blends at three different injection timings are discussed in the second section. The second section also includes the emissions of CO_2, CO, HC, NO_x, and smoke level for oxidized and unoxidized biodiesel and their blends at different injection timings. The injection pressure, start of combustion, and ignition delay for oxidized and unoxidized biodiesel and their blends at three different injection timings are discussed in third section. The last section presents the effects of ignition delay and start of combustion on engine emissions.

5.1 Effect of Aging on Oxidation of Biodiesel

Biodiesel oxidizes with time when it contacts oxygen. This oxidation does not need any external initiation, but external initiators such as heat, light, and metals help biodiesel to oxidize faster. This oxidation may be defined as biodiesel aging. The biodiesel aging effect on fuel chemistry and fuel properties are discussed in the next four sub-sections. More specifically, the first, second, and third sub-sections discuss the effect of biodiesel oxidation on the peroxide value, acid value, and the viscosity respectively. The fourth sub-section describes the interrelationships between peroxide value, acid value, and viscosity. The oxidative stability of biodiesel is discussed in the last section.

5.1.1 Effect of oxidation on the peroxide value of biodiesel

Hydroperoxides are the initial product of the oxidation of biodiesel. The level of this initial product is characterized by the peroxide value. These peroxides split and form aldehydes, ketones, and finally short chain acids. The level of these short chain acids is called the acid value. Sediment and gum formation are also associated with produced by oxidation. The level of peroxide value and acid values are measured by AOCS tests. The gum and sediment are measured by ASTM tests. Since the peroxide value, acid value, and gum and sediment are all oxidation products, there must be same relation between these properties. To establish a connection between the ASTM tests and the AOCS tests, the peroxide value, acid value, and viscosity were measured for a set of accelerated oxidative stability tests.

In order to understand the effect of oxidation on the properties of biodiesel fuel, five tests were conducted using the fuel filter test apparatus described in Section 3.1. Two of them were with 20% and 50% biodiesel in No. 2 diesel fuel at 60 °C. The blend of 20% biodiesel at 60 °C was tested for 60 days. At the end of 60 days the fuel pump failed which terminated the test. The blend of 50% biodiesel at 60 °C was tested for 74 days before the fuel pump failed. Two other tests were conducted with 20% and 50% biodiesel in No. 2 diesel fuel at room temperature (23 °C). The 20% biodiesel at room temperature test was conducted for 190 days. At the end of this test the pump had not failed completely but it had started to show signs of impending failure, such as increased noise level. The test of 50% biodiesel at room temperature was conducted for 87 days before the fuel pump failed. The final test was 100% biodiesel at 60 °C that ran for 38 days. At

the end of this test the fuel pump failed and the test was concluded. The failure of these pumps should not be interpreted as an indication of the quality of the pumps or any incompatibility between the pumps and biodiesel. During the test the flow rate was monitored and as it dropped due to increased fuel viscosity, the voltage applied to the pump was raised to compensate. Generally, by the end of the test, the voltage applied to the pump was above the manufacturers recommendations and this was the probable cause of failure.

The peroxide values are shown in Figure 5.1. It can be seen that all five tests demonstrated similar behavior. The peroxide value (PV) rises to a level between 300 and 400 meq. O_2/kg and then drops off. The three cases at 60 °C went through this process of rise and fall of PV within the first 1000 hours. The 100% biodiesel went through the cycle in the least time and the 20% biodiesel was the slowest. The two runs at room temperature were similar but much slower, both for the initial rise in PV and the subsequent return.

The initial PV for 100% and 50% biodiesel at 60 °C were 41.4 and 34.1 meq. O_2/kg. But the initial peroxide value for 20% biodiesel at 60 °C was only 3.1 meq. O_2/kg. This is primarily due to dilution of the biodiesel with diesel fuel since the diesel fuel does not readily form peroxides. The oxidation rate is known to be proportional to the peroxide value [74]. Fuel that already has a high peroxide value will oxidize more rapidly. The 20% blend has less biodiesel so the peroxide value will automatically be reduced by a factor of 5 from the neat biodiesel. If the initial peroxide value is low, then the induction period will be longer. The rate of decrease of peroxide value of 100%

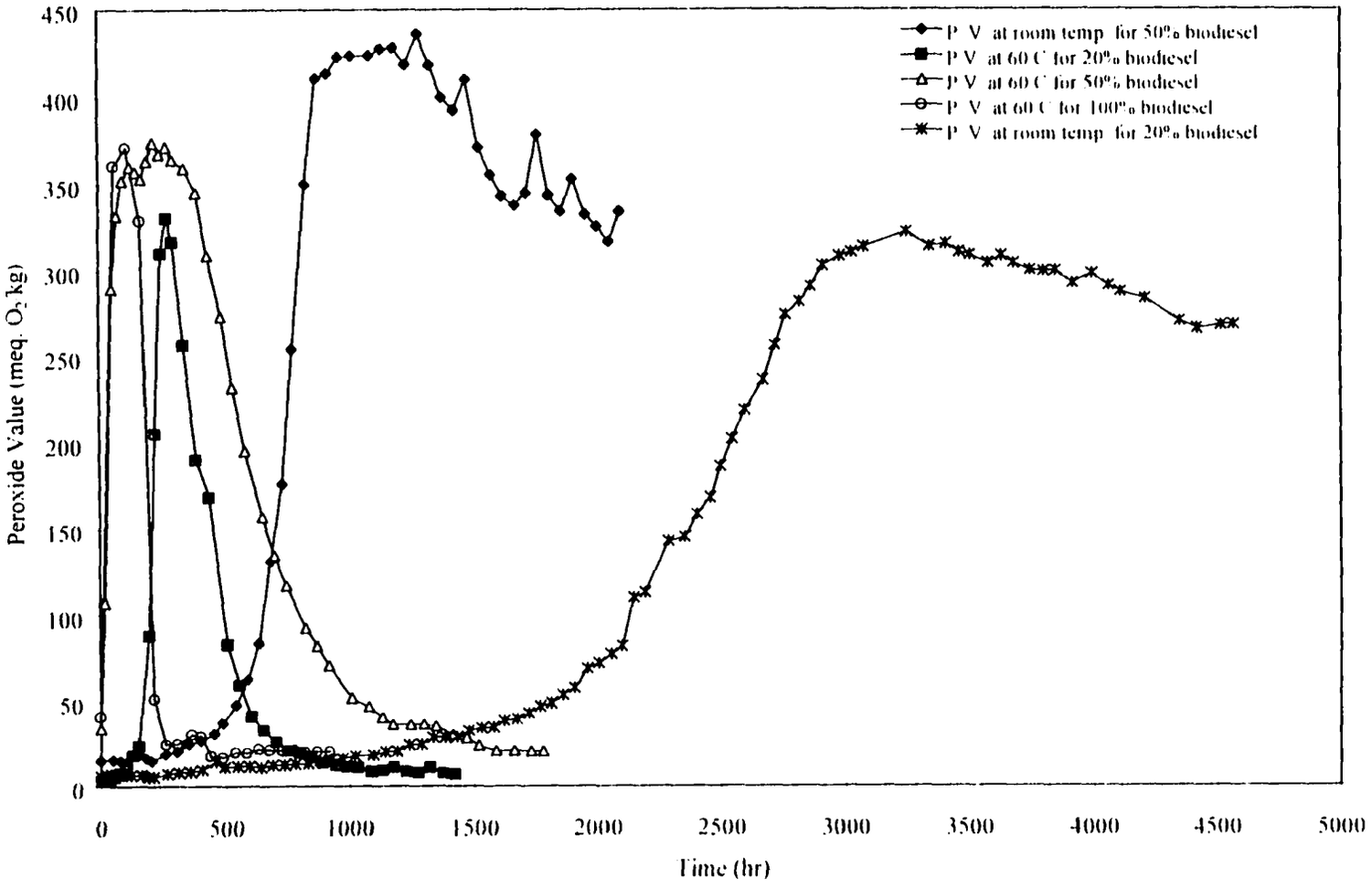

Figure 5.1 Effect of fuel aging on peroxide value of biodiesel

biodiesel at 60 °C is larger than the other blends. The drop in peroxide value for the 20% biodiesel at 60 °C occurred sooner than for the 50% biodiesel at 60 °C. The rate of decrease of peroxide value of 20% and 50% biodiesel at room temperature is much less than the 20% and 50% biodiesel at 60 °C. The peak peroxide values for the 100% and 50% biodiesel at 60 °C are 371 meq. O_2/kg at the 110th hour and 373 meq. O_2/kg at the 216th hour respectively. The peak peroxide values of the two blends, 20% biodiesel at 60 °C and 20% biodiesel at room temperature, are 331 meq. O_2/kg at 268th hour and 323 meq. O_2/kg at the 3249th hour respectively. These four peak peroxide values are close but the peak peroxide value for 50% biodiesel at room temperature was 436 meq. O_2/kg which is somewhat higher than the other blends. The rise of peroxide value for any blend of biodiesel at any temperature is somewhat constant and lies between 320 meq O_2/kg to 450 meq O_2/kg.

Miyashita et al. [71] investigated the autoxidation rates of various esters of safflower oil and linoleic acid. They found that the peroxide value increased rapidly after the induction period of autoxidation, but then decreased. The maximum peroxide value was recorded to be about 2000 meq O_2/kg for the methyl ester. They used the Calorimetric Iodine method [72] to measure the peroxide value. Gan et al. [73] investigated the effects of epoxidation on the thermal oxidative stabilities of fatty acid esters derived from palm oline. The fuel tested in their research was methyl ester of palm olein. They recorded the maximum peroxide value to be about 300 meq O_2/kg at the 288^{th} hour. This result was close to that observed in this experiment.

The PV reaches a maximum and then drops off probably because of the solubility

of O_2 in the ester. Once the induction period is over the oxidation proceeds rapidly to consume all the oxygen that is dissolved in the ester. When this oxygen is consumed, the rate drops off to the rate that can be sustained by diffusion of O_2 into the ester from the air surface.

5.1.2 Effect of oxidation on the acid value of biodiesel

To further understand the effect of oxidation on biodiesel, the acid values of the fuel samples described above were also measured. The results of the acid value tests are shown in Figure 5.2. The acid value for all the blends increased with time, but the rate of increase of acid value was different for the different fuel blends. It is clear from Figures 5.1 and 5.2 that the acid value starts to increase at a slightly later time from where the peroxide value starts to increase. The rate of increase of acid value is higher until the point where the peroxide value returns to a low value. Beyond this point the acid value increases slowly which indicates a slower rate of oxidation. For example, for 20% biodiesel at 60 °C, the peroxide value started to increase faster at the 192nd hour and returned to a low value at about the 500th hour. In between these two points the rate of change of acid value was 0.01 mg KOH/g per hour higher than the point after the 500th hour. A similar effect was observed for the 50% biodiesel at 60 °C, where the peroxide value started to increase faster at about the 19th hour and returned to a low value at about the 823rd hour. In between these two points the rate of change of acid value was 0.03 mg KOH/g per hour higher than after the 823rd hour. After the 823rd hour the slope decreased. For 100% biodiesel at 60 °C, the peroxide value increased rapidly right at

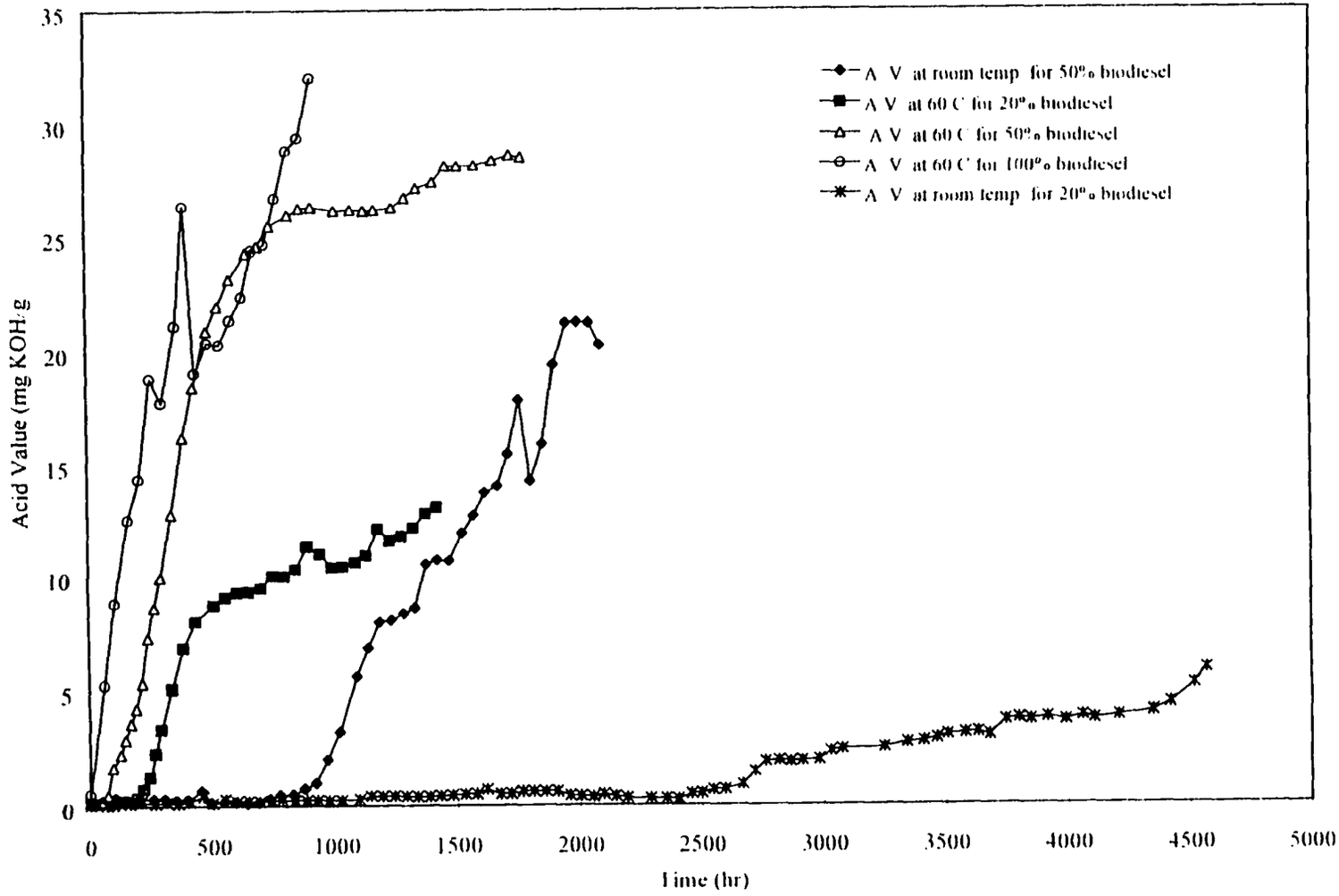

Figure 5.2. The effect of fuel aging on the acid value of biodiesel

beginning and returned to a low value at about the 258th hour. The rate of increase of acid value between these two points was higher. On this curve one of the acid value data points appears to be considerably off the curve. This could be a measurement mistake.

The peroxide value starts to increase faster at about the 640th hour for the 50% biodiesel at room temperature, but the rate of change of acid value starts to increase at about the 900th hour and the acid value continued to increase. A similar effect is observed for the 20% biodiesel at room temperature.

5.1.3 Effect of oxidation on the viscosity of biodiesel

The viscosities of the test samples are shown in Figure 5.3. The viscosity of all the blends increased with time. The rate of change of viscosity increased rapidly at the beginning of the test for all blends that were at 60 °C. This rapid increase in viscosity continued until the time where the rate of increase of acid value was a maximum. After this the rate of change of viscosity increased more slowly than at the beginning. A higher percent blend of biodiesel has a higher viscosity and rate of increase of viscosity than the lower percent of biodiesel. The temperature also has an effect on viscosity. The blends at 60 °C have a higher increase of viscosity than the blends at room temperature. The start of increase of viscosity is earlier for higher temperature fuel than for lower temperature fuel. The viscosity of 100% biodiesel at 60 °C increased more rapidly at the beginning of the test than later. The rate of increase of the viscosity up to about the 109th hour was higher which was also the time when the rate of increase of the acid value was a maximum also, and the highest peroxide value was observed. The viscosity for this 100%

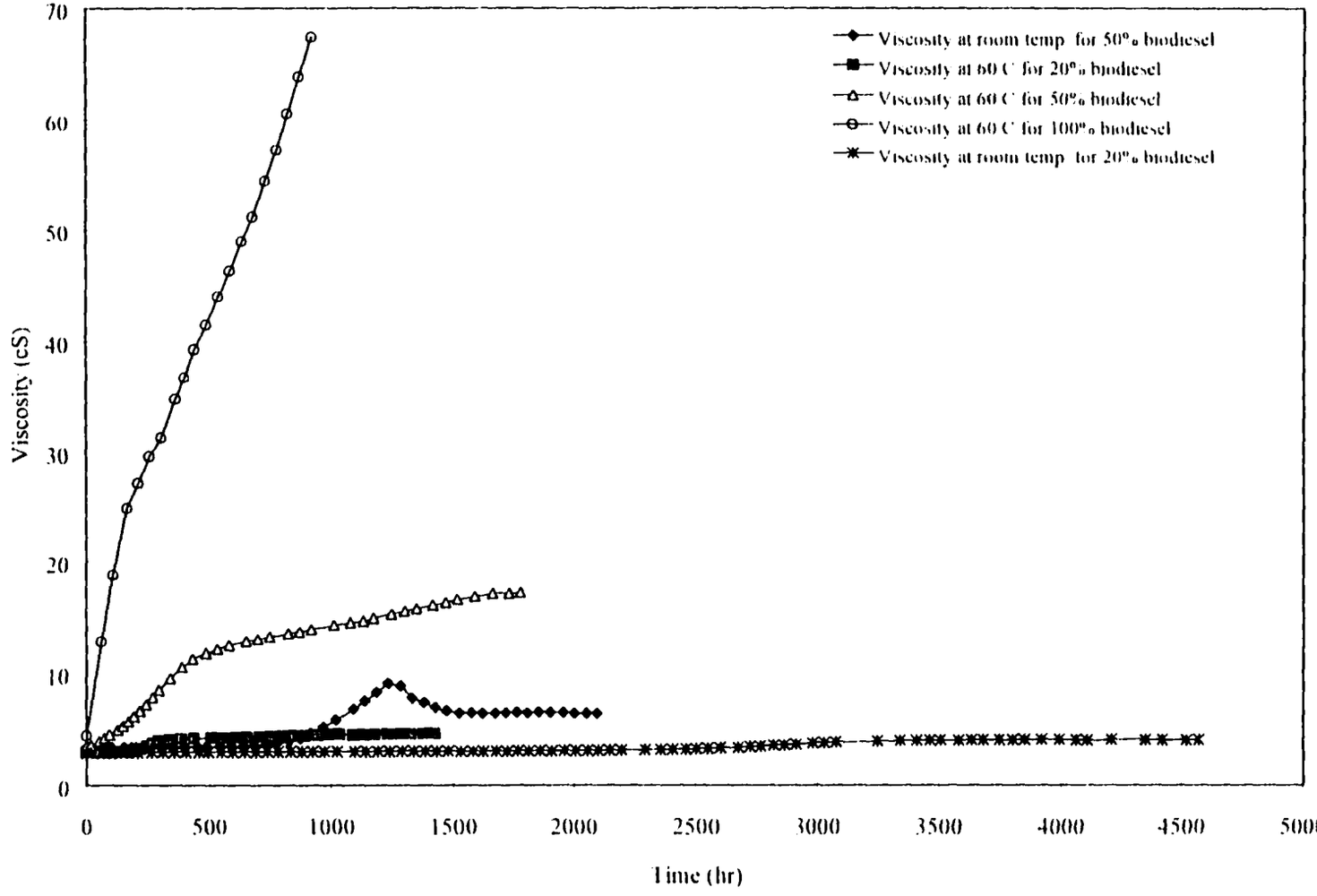

Figure 5.3. The effect of fuel aging on the viscosity of biodiesel

biodiesel started at 4.44 cS and ended at 67.43 cS. The final viscosities for the 50% biodiesel and 20% biodiesel at 60 °C were 17.22 cS and 4.62 cS, respectively. The blend of 50% biodiesel at room temperature behaved differently from the other blends. The viscosity for this blend started to increase at the 825th hour and continued to increase until the 1234th hour where it decreased until the 1574th hour and then it stayed relatively constant.

5.1.4 Interrelationships between peroxide value, acid value, and viscosity

Figures 5.4 and 5.5 show the relationship between viscosity and acid value, and viscosity and peroxide value, respectively. A linear relationship was found between the viscosity and the acid value. For all blends at all temperatures, viscosity increased as the acid value went up. For the 20% biodiesel at 60 °C and at room temperature, the viscosity vs. acid value curves fall in top of each other, but the acid value did not increase to as high a value for the room temperature case. The viscosity vs. peroxide value curves shown in Figure 5.5 for the 20% biodiesel at 60 °C and at room temperature also fall on top of each other, but the peroxide value did not decrease to as low a value at room temperature. For the 50% biodiesel at both 60 °C and at room temperature, the viscosity vs. acid value curve shown in Figure 5.4, shows the same trend as the 20% blends until the viscosity reaches 8 cS and the acid value reaches 7 mg KOH/g, then the viscosity and acid value for the 50% blend at 60 °C continues to increase while the viscosity for the 50% biodiesel at room temperature stayed constant as the acid value increased.

Figure 5.6 shows the acid value vs. peroxide value curve. From this figure it can

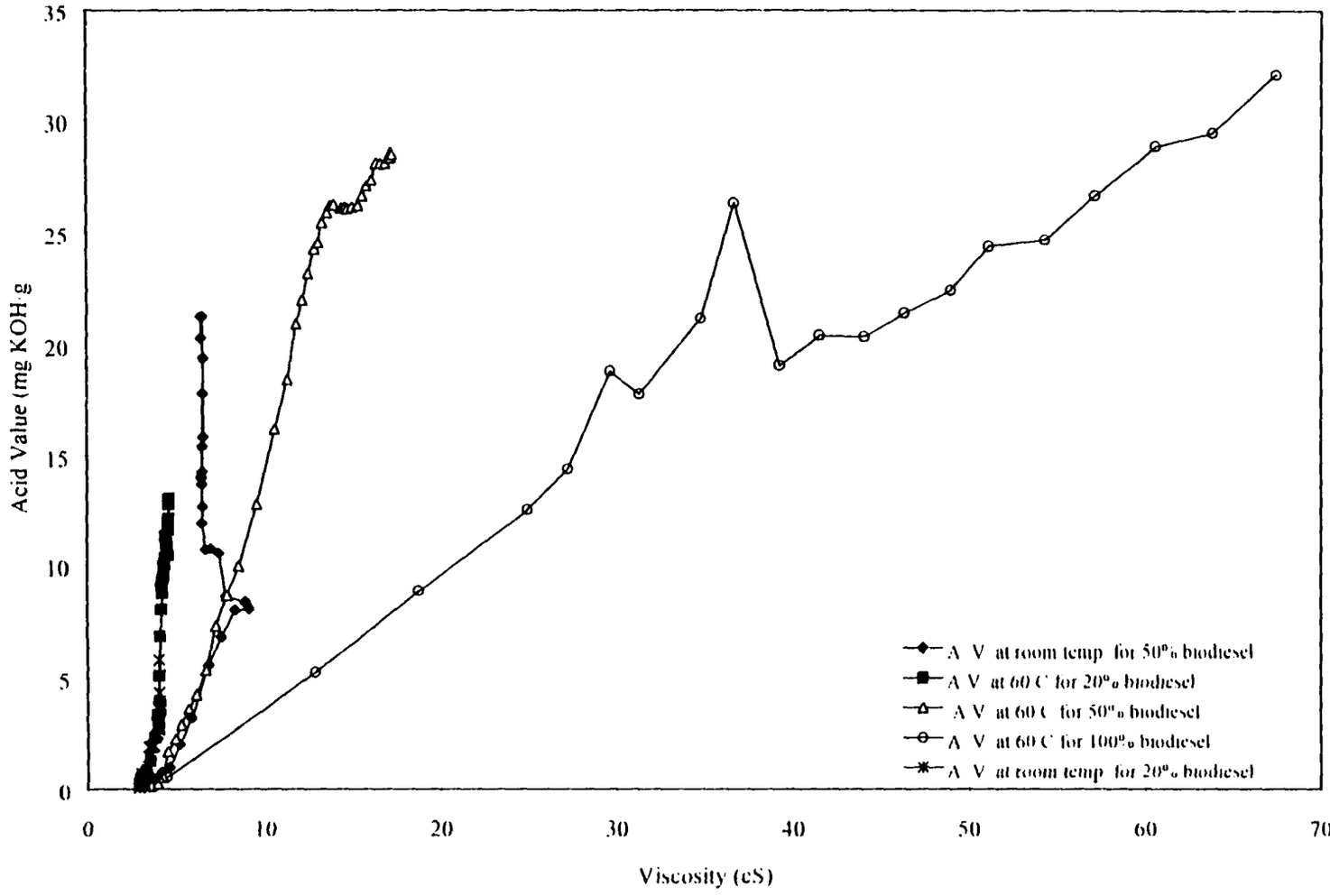

Figure 5.4. Viscosity vs. acid value for biodiesel blends

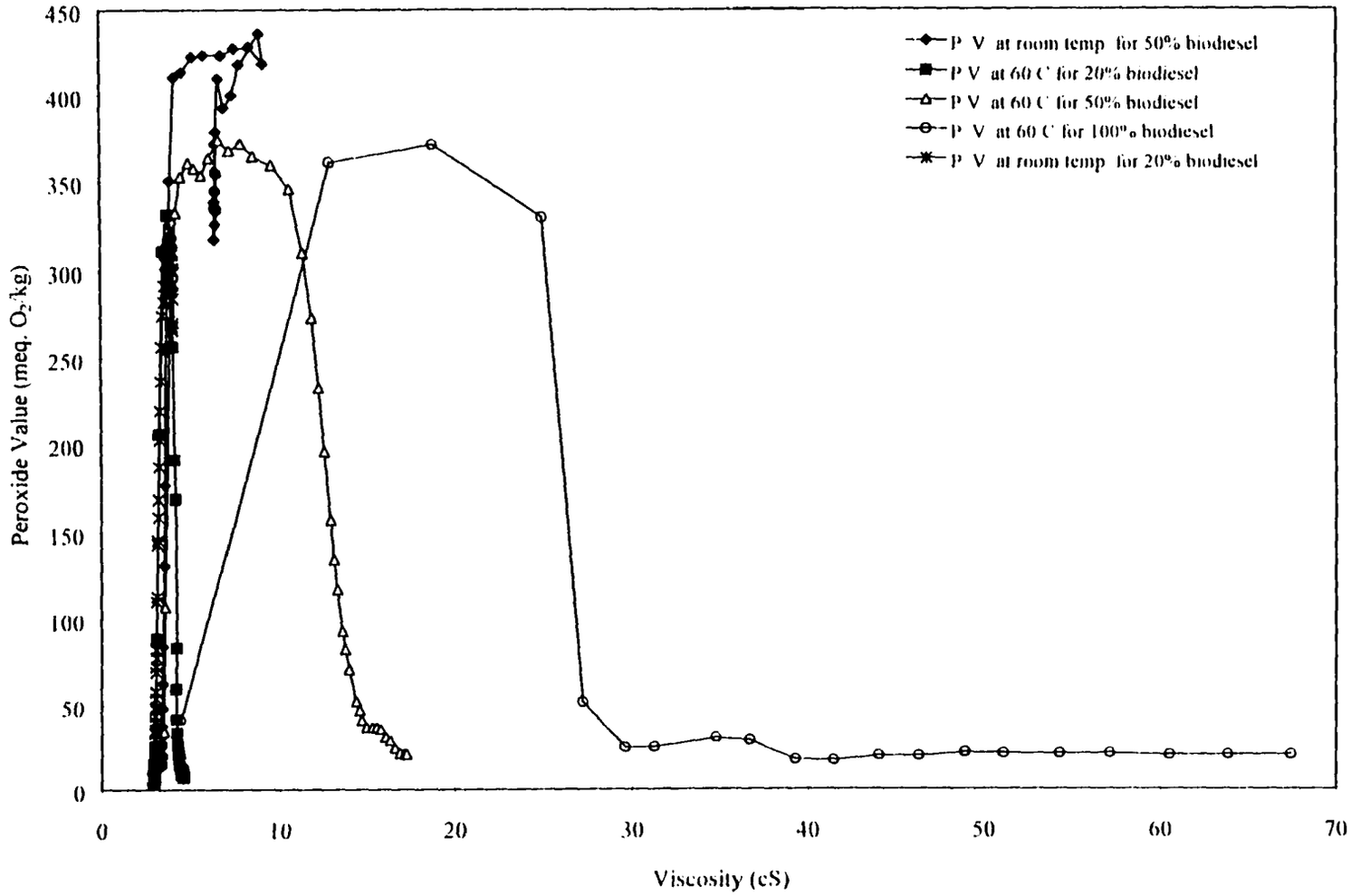

Figure 5.5. Viscosity vs. peroxide value for biodiesel blends

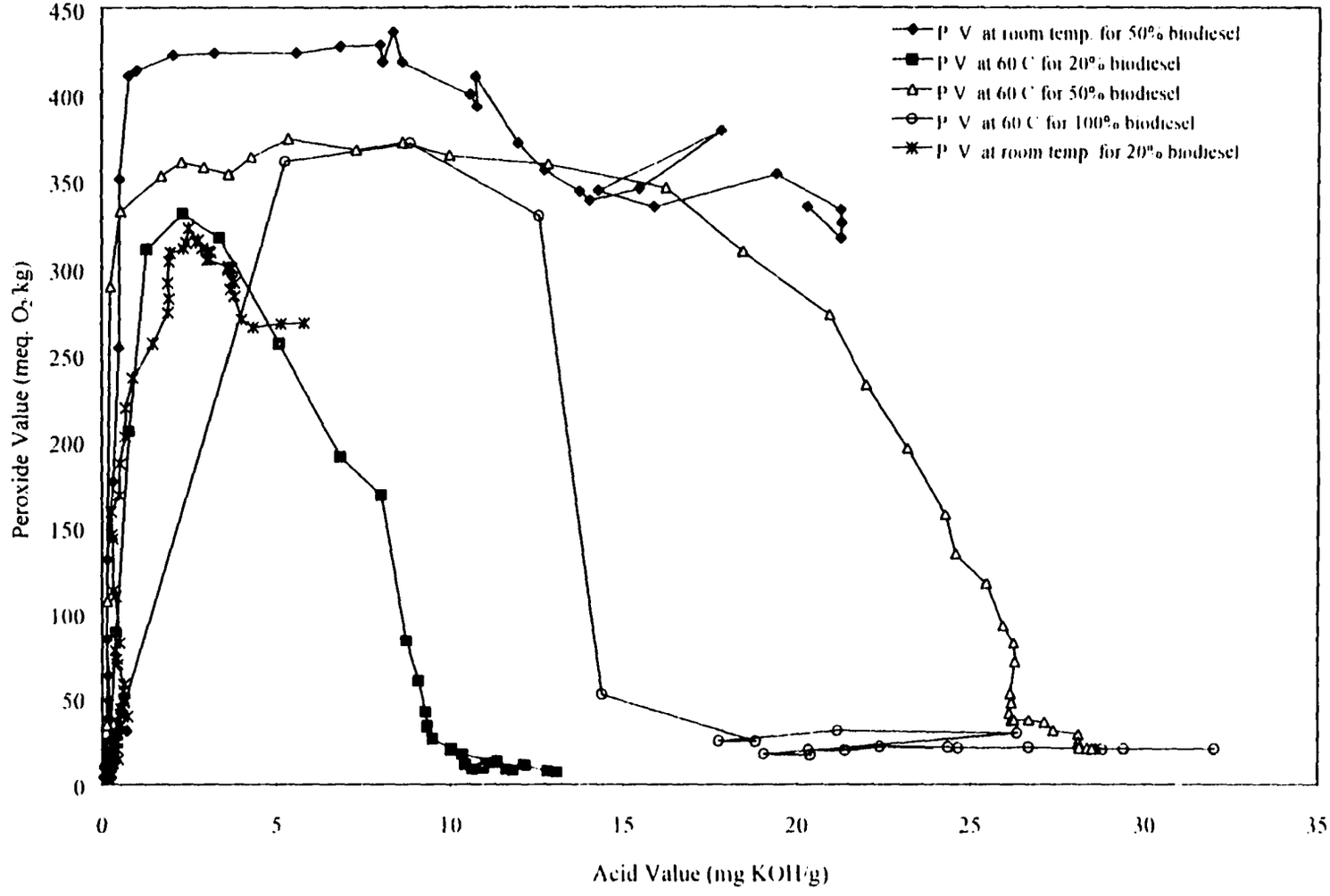

Figure 5.6. Acid value vs. peroxide value curves for biodiesel blends

be seen that the biodiesel blends can have high peroxide values while maintaining low acid value. However, when the peroxide value stays constant at a high value or starts to decrease, the acid value starts to increase rapidly.

5.1.5 Oxidative Stability of Biodiesel

The ASTM D2274 oxidative stability test method will be described in this section. The results of preliminary tests with this method are also presented. This test was performed as part of an unsuccessful attempt to establish the relationship between the AOCS (American Oil Chemists' Society) and the ASTM (American Society for Testing and Materials) tests.

5.1.5.1 ASTM D2274-94 test method for oxidative stability test

The standard way to measure the oxidative stability of diesel fuels is with the test method described in ASTM (American Society for Testing and Materials) D2274. The method uses accelerated oxidizing conditions to determine the mass of insoluble material formed by the fuel oxidation. A 300 ml sample of fuel is oxidized at 95 °C for 16 hr while pure oxygen is bubbled through the sample at the rate of 3 L/hr. In the ASTM test method, one set of matched pair filters are used. Matched filter pairs are necessary because the bottom filter is used as a blank and the difference between the top and bottom filters is the gum and filterable insoluble. Finding a matched pair of filters is very difficult, so it was necessary to modify the ASTM method. In the modified method used here, any two filters can used instead of a matched pair. Both the top (sample) and bottom

(blank) filter weights are measured before and after filtration of the sample. The filterable insolubles weight per 100 ml of sample (although the sample size is 300ml) can be expressed as follows:

$$A=((W_{ta}-W_{tb})-(W_{ba}-W_{bb}))/3 \quad (5\text{-}1)$$

Where A = filterable insoluble weight per 100 ml of sample, g/100 ml

W_{ta} = Top filter weight after filtration, g/300 ml

W_{tb} = Top filter weight before filtration, g/300 ml

W_{ba} = bottom filter weight after filtration, g/300 ml

W_{bb} = bottom filter weight before filtration, g/300 ml

To determine the filterable insoluble in the biodiesel fuel, several tests were performed by following the ASTM test method except for the calculation process described above. For all tests, 300 ml of biodiesel from a newly opened barrel of methyl soyate was used. Before performing the test all samples were filtered through two filters. For the actual test, 300 ml of pure filtered biodiesel was poured through the filter while applying a suction pressure of 80 kPa (12 psi). On completion of the filtration, three separate 50 ml volumes of isooctane were used to rinse the filter assembly. The two filters were then dried at 80 °C for 30 minutes, then cooled at room temperature for another 30 minutes before weighing. This procedure was followed for all tests. The results are shown in Table 5.1.

For the first test, the top and bottom filter weight differences were 0.01478 g and

Table 5.1. Filterable insoluble for different fuels

Test No.	Fuel	Amount of Fuel Filtered (ml)	Washing Fluid	No. of Washing Time (each time 50 ml)	Vacuum Pressure (psi)	Top Filter Weight (g)			Bottom Filter Weight (g)			Total Filterable Insoluble (g)	Filterable Insoluble (A) (g/100ml)
						After (Wta)	Before (Wtb)	Difference (Wta-Wtb)	After (Wba)	Before (Wbb)	Difference (Wba-Wbb)		
1	Biodiesel	300	Isooctane	3	12	1 09388	1 07910	0 01478	1 09335	1 07834	0 01501	-0 00023	-0 00008
2	No 2 Diesel	300	Isooctane	3	12	1 07566	1 07617	-0 00051	1 08359	1 08382	-0 00023	-0 00028	-0 00009
3	Isooctane	150	Isooctane	3	12	1 09678	1 09830	-0 00152	1 09573	1 09698	-0 00125	-0 00027	-0 00018
4	Biodiesel	50	Isooctane	3	12	1 08064	1 07988	0 00076	1 08342	1 08297	0 00045	0 00031	0 00062
5	Biodiesel	5	Isooctane	3	12	1 10497	1 08690	0 01807	1 10035	1 08436	0 01599	0 00208	0 01040
6	Biodiesel *	100	Isooctane	3	1	1 08425	1 07279	0 01146	1 09461	1 08201	0 01260	-0 00114	-0 00114
7	Biodiesel	300	Isooctane	10	12	1 06770	1 06747	0 00023	1 07310	1 07265	0 00045	-0 00022	-0 00007
8	Biodiesel	300	Isooctane	3	0	1 07814	1 07452	0 00362	1 06770	1 06551	0 00219	0 00143	0 00048
9	Biodiesel	300	Isooctane	3	1	1 08491	1 07442	0 01049	1 08504	1 07463	0 01041	0 00008	0 00003
10	Biodiesel	300	Isooctane	3	1	1 07767	1 07030	0 00737	1 07404	1 06790	0 00614	0 00123	0 00041
11	Biodiesel	300	Hexane	3	12	1 10316	1 08953	0 01363	1 11372	1 09622	0 01750	-0 00387	-0 00129
12	Biodiesel	300	Toluene	3	12	1 09094	1 07471	0 01623	1 08883	1 07573	0 01310	0 00313	0 00104
13	Bio +Isooct (1 1)	200	Isooctane	3	1	1 10781	1 09682	0 01099	1 10962	1 09958	0 01004	0 00095	0 00048
14	Biodiesel**	50	Isooctane	3	3	1 19566	1 08771	0 10795	1 21645	1 08722	0 12923	-0 02128	-0 0426

Biodiesel* 3:1 hexane and biodiesel mixture were poured through a silica gel column and separated by evaporation
Biodiesel** Highly oxidized biodiesel

0.01501 g. respectively. The large increase in weight for the blank filter was suspicious because it indicated that the biodiesel may not have been removed from the filter. The total filterable insoluble for this test is the difference between these two weights and was –0.00023 g. The sample for this test was 300 ml and the normal procedure is to report the insoluble weight per 100 ml of sample. After dividing by 3. the insolubles were –0.00008 g which is a low value. This would indicate a low level of gum and sediment even though the filters were found to have gained considerable weight. For the second test. the same procedure was used except that the sample was No. 2 diesel fuel and the test result was as expected. Instead of gaining weight as occurred during the methyl soyate test. both the top and bottom filters lost a small amount of weight. This expected result is generally believed to be caused by the isooctane removing a small amount of organic binder from the filter medium. It is the primary purpose for including the blank. The weight change of the top filter was -0.00051g and for the bottom was -0.00023 g. The total filterable insoluble was –0.00028 g/300 ml. and the filterable insoluble per 100 ml of sample was –0.00009 g. These results indicated that while the isooctane washing procedure was effective in removing the diesel fuel from the filters. it was not effective in removing the biodiesel.

In the third test. 150 ml of isooctane was used as a sample to determine whether it had any contamination that might have caused the weight increase observed during the first test. It was found that both the top and bottom filters lost weight. So the isooctane was not contaminated.

In tests 4 and 5. smaller amounts of biodiesel were used to determine whether the

biodiesel had some contamination or whether the washing process was not removing biodiesel. It was supposed that if the biodiesel contained gums and sediments that were responsible for the increases in weight observed in both filters, then using smaller amounts of biodiesel should give smaller weight increases. For test 5, where 5 ml of biodiesel was used, the top and bottom filters both gained weight. These weight gains were even larger than test 4 where 50 ml of biodiesel was used. So it was clear that the weight gain was not caused by contamination in the biodiesel.

As a final check on whether there might be polymers produced by fuel oxidation already present in the biodiesel an attempt was made to produce a "clean" sample of biodiesel. To make a low peroxide and low acid value biodiesel, a mixture of 3 parts hexane, and 1 part biodiesel was poured through a silica gel column. Before passing through the column, the peroxide and acid value for this biodiesel were 40.4 meq. O_2/kg and 1.904 mg KOH/g respectively. The mixture was then evaporated under vacuum at 74 ^{o}C to remove the hexane. Left over was the biodiesel with low peroxide and acid value. The peroxide and the acid value for this biodiesel were 2.2 meq. O_2/kg and 0.56 mg KOH/g. The highly polar silica gel should also have removed the gums and sediments. This low peroxide biodiesel was then used as a sample. The test results for this sample are shown as Test No. 6. The results for the test did not improve. Both top and bottom filters still gained weight. It appeared that the washing process did not work well.

To solve the washing problem three approaches were tried. The first approach was to increase the number of times the filters were washed with 50 ml of isooctane. The second approach was to apply different amounts of suction pressure. And the third

approach was to use different washing fluids. In Test no. 7 the number of times the filters were washed with isooctane was increased from 3 to 10. The weight change of the filters was much smaller, although it was still positive. This confirmed that inadequate filter washing was the problem. Washing the filters with this much isooctane was not considered to be an acceptable method because it was a significant departure from the ASTM procedure and this amount of isooctane may dissolve some of the gums and sediments that were being measured.

The next approach was to slow down the filtration process by reducing the vacuum used to draw the isooctane through the filters during the washing process. It was speculated that this might increase the contact between the isooctane and the biodiesel and improve the efficiency of its removal. The vacuum was reduced from 12 psi to 0 or 1 psi which greatly increased the time required for the sample to pass through the filter. The results of these tests are shown as Tests no. 8, 9, and 10. It was found that the efficiency of biodiesel removal could be improved by this technique but the amount of biodiesel remaining on the filter was still unacceptable.

Other solvents were also tried to see if they might be more effective at removing the biodiesel. The results of using hexane and toluene are shown as Tests no. 11 and 12, respectively. These solvents did not appear to be any more effective than isooctane. Other, more polar, solvents might be more effective at removing the biodiesel but they would also tend to remove the gums and sediments the test was trying to measure.

To investigate whether the higher viscosity of the biodiesel was a problem, a biodiesel and isooctane mixture was used as a sample for the test and the result is shown

as Test No.13. The results for this test did not improve either. Finally, to see if the technique was sensitive to the products of biodiesel oxidation, a very high acid value and viscosity fuel was used as a sample. The acid value for this sample was 32.03 mg KOH/g, the peroxide value was 20.5 meq. O_2/kg, and the viscosity was 67.43 cS. The test with this highly oxidized biodiesel is shown as Test No. 14. The top filter gained 0.10795 g and the bottom filter gained 0.12923 g for 50 ml of sample. The bottom filter gained more than the top filter, which should not happen if the filters were capturing insoluble material. The appearance of these filters after filtering looked like the gum material had collected at the outer edge of both filters as illustrated in Figure 5.7. It appears that all the gum material did not collect on the top filter but that some of the gum material passed through the top filter and collected on the bottom filter too. The gum material produced by biodiesel may consist of highly viscous material that can still pass through a filter. It was likely that all the gum material was not collected by the filters. Some may pass through both filters. At this point it was clear that the ASTM D2274 method was not going to work for biodiesel and further testing was terminated.

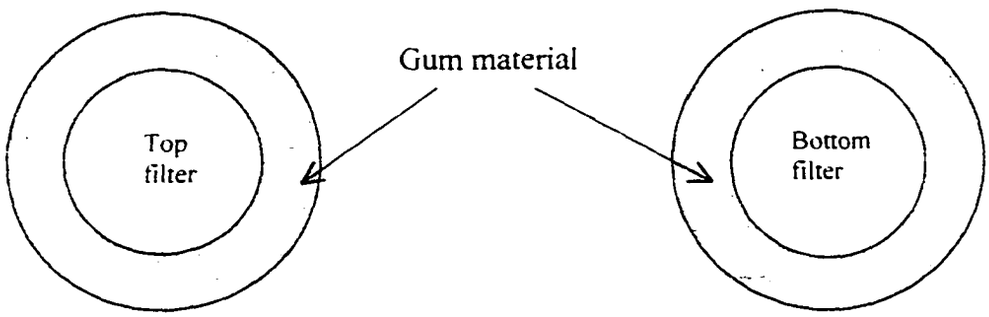

Figure 5.7 Collected gum and sediment on top and bottom filters

5.2 Diesel Engine Performance and Emissions

In this section, the performance and emissions of a diesel engine fueled with biodiesel are presented. The diesel engine performance results are presented in the first section. The second section investigates the effect of timing and fuel oxidation on the exhaust emissions. All raw data collected in the study are included in Appendix E.

5.2.1 Engine Performance

This section will discuss the engine power and the fuel consumption while the diesel engine was fueled with oxidized and nonoxidized soybean oil methyl esters (biodiesel). Three batches of highly oxidized biodiesel were used in this experiment. All batches of oxidized biodiesel had a peroxide value of 340 meq. O_2/kg.

In this experiment, three values of injection timing (3° advanced, standard, and 3° retarded) and five fuel blends were used. These blends were 100% highly oxidized biodiesel (100%HPV), 100% unoxidized biodiesel (100%LPV), 20% highly oxidized biodiesel blend with No. 2 diesel fuel (20%HPV), 20% unoxidized biodiesel blend with No. 2 diesel fuel (20%LPV), and the baseline No. 2 diesel fuel. All data were taken at 1400 rpm and at two load conditions. The load conditions were full-load (100% load) and light-load (20% load). The full-load was 190 ft-lb_f and the light load was 38 ft-lb_f.

In order to understand the effect of oxidized fuel and variable timing injection on engine performance and emissions, a statistical analysis was performed. This analysis can identify not only the effect of oxidized fuel and injection timing on emissions but also the effect of fuel batch, age of batch, the interaction between load and fuel, load and blend,

load and timing, timing and fuel, and the interaction among timing, load, and fuel. The results of the analysis for one parameter, the brake specific fuel consumption (BSFC), are shown in Table 5.2. In the table DF represent the degrees of freedom, SS represents the sum of squares and the probability distribution in repeated sampling (referred to as an F distribution) is given in the fifth (F Value) column. The significant factors can be identified from this analysis of variance (ANOVA) table. The factors which contain the star (*) symbol are the statistically significant factors. The following factors are significant for BSFC: timing (injection timing), fuel, load, and the interaction between fuel and load. The other factors, batch, age (batch age), the interactions between timing and fuel, timing and load, and the interaction between timing, fuel, and load did not have a statistically significant effect on the BSFC. The weight of the significance level, given

Table 5.2 Analysis of variance (ANOVA) for BSFC

Source	DF	Type I SS	Mean Square	F Value	Pr > F
Model*	38	770831.017	20023.743	2850.82	0.0001
BATCH	2	66.207	33.1037	10.19	0.1010
AGE	2	15.794	7.8972	2.41	0.0935
TIMING*	2	307.265	153.6325	46.84	0.0209
WHOLE PLOT ERROR	2	6.560	3.2800		
FUEL*	4	39511.632	9877.9080	1144.07	0.0001
LOAD*	1	727096.793	727096.7931	84212.05	0.0001
FUEL×LOAD*	4	3605.312	901.3280	104.40	0.0001
TIMING×FUEL	8	127.615	15.9520	1.85	0.0881
TIMING×LOAD	2	3.730	1.8650	1.22	0.9064
TIMING×FUEL×LOAD	8	99.686	12.4660	1.45	0.1991
Error	54	466.236	8.6340		
Corrected Total	88	771297.253			

R-Square=0.9994
BSFC Mean=332.7670

in terms of a probability, is called the level of significance (or P-value) of the statistical test and is shown in the column with the heading Pr > F. The smaller the value of this probability, the heavier the weight of the significance level. For all analyses conducted for this project, a 95% confidence interval was used. Since the level of significance for the factors, fuel, load, and the interaction between fuel and load are very small, these factors are highly significant for BSFC. The timing has a higher level of significance than the fuel, load, and the interaction between fuel and load. The confidence level for the timing is 98%. The Tukey's grouping, shown in Table 5.3, shows that variables with the same letter in the Tukey grouping column are not significantly different. From this table the BSFC for 3° advanced injection timing was significantly different than that at standard and 3° retarded injections. The difference between the standard and the 3° retarded injection timings was statistically insignificant. The minimum significant difference between the two injection timings was 2.755 g/kW-hr of fuel consumption. The 3° advanced injection timing had a higher BSFC than the other two injection timings. All fuels tested in this experiment, except for the 20% blends, were significantly different. The 100%HPV biodiesel had a higher BSFC then the 100%LPV biodiesel and the 100%LPV biodiesel was significantly different than the base fuel (No. 2 diesel).

Since the torque and the RPM in this experiment were kept constant, the brake power was constant throughout the test. Figures 5.8 and 5.9 show the brake specific fuel consumption (BSFC) vs. fuel type and timing for full (100%) and low (20%) load engine conditions, respectively. Both figures illustrate that the BSFC for biodiesel was higher than for the No. 2 diesel fuel. Since the energy per unit mass of biodiesel was lower than

Table 5.3 Tukey's Studentized Range (HSD) test for BSFC

Effect of Timing

Tukey Grouping	Mean	N	TIMING
A	335.3754	30	3deg_advanced
B	331.6928	30	3deg_retarded
B			
B	331.3316	30	Standard

Minimum Significant Difference= 2.7547

Effect of Fuel

Tukey Grouping	Mean	N	FUEL
A	359.8831	18	100%HPV
B	356.6013	18	100%LPV
C	317.9084	18	20%LPV
C			
C	317.8479	18	20%HPV
D	311.5921	18	2D

Minimum Significant Difference= 2.7641

Effect of Load

Tukey Grouping	Mean	N	LOAD
A	422.6484	45	20%
B	242.8848	45	100%

Minimum Significant Difference= 1.242

No. 2 diesel fuel, the fuel consumption increased to maintain the same brake power. The energy per unit mass of biodiesel was 37165 kJ/kg while for No 2 diesel fuel the energy per unit mass was 42578 kJ/kg. The heating value for the oxidized and non-oxidized biodiesel was considered to be the same. Oxidized biodiesel also had a higher BSFC than non-oxidized biodiesel. One reason could be when the biodiesel oxidized its energy content reduced and the other reason may be the combustion timing. Thompson et al. [74] found that the heat of combustion decreased as the peroxide value of the biodiesel increased. They found that the heating value decreased about 1.4% over 24 months

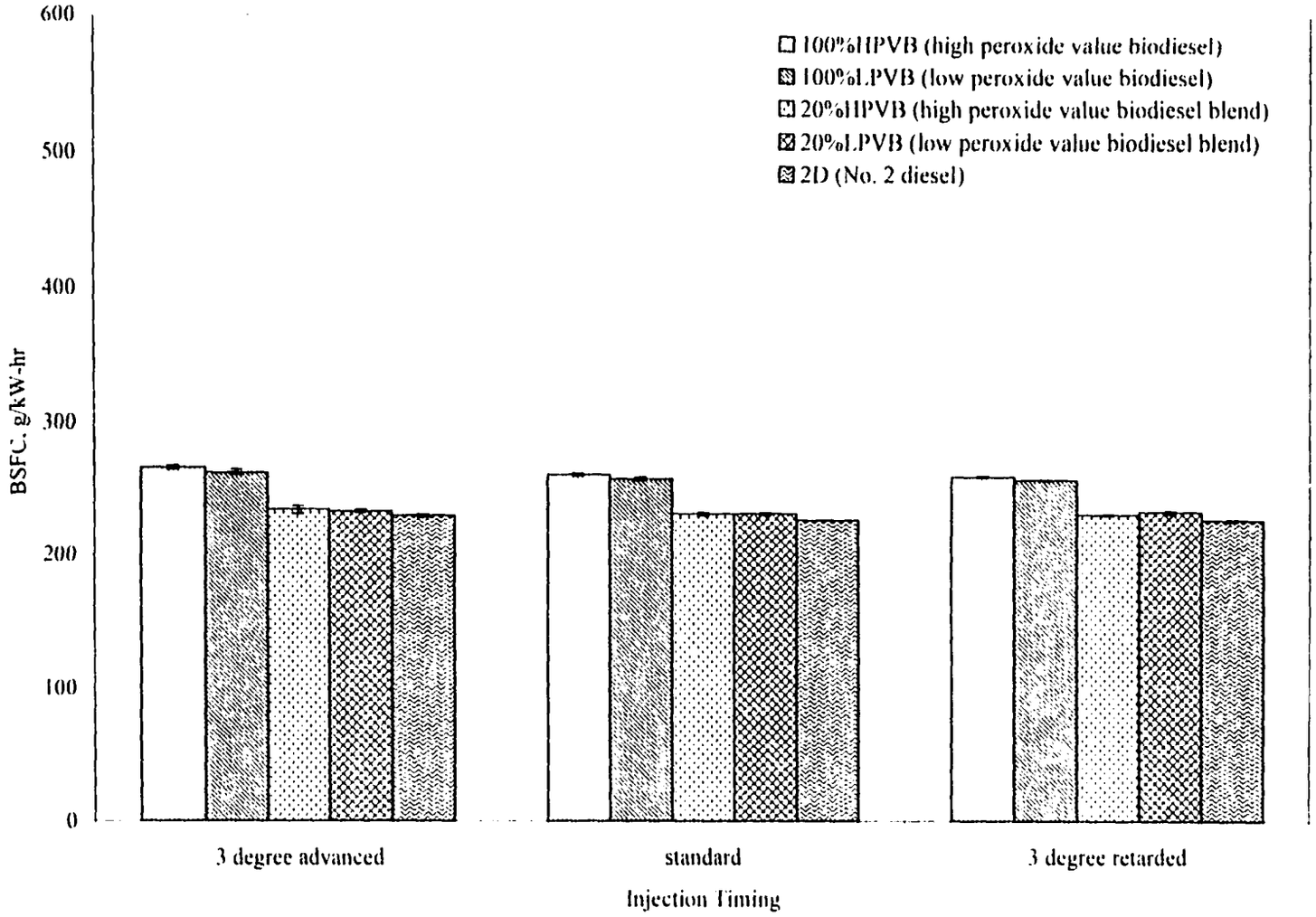

Figure 5.8 Brake specific fuel consumption (BSFC) at full-load engine condition

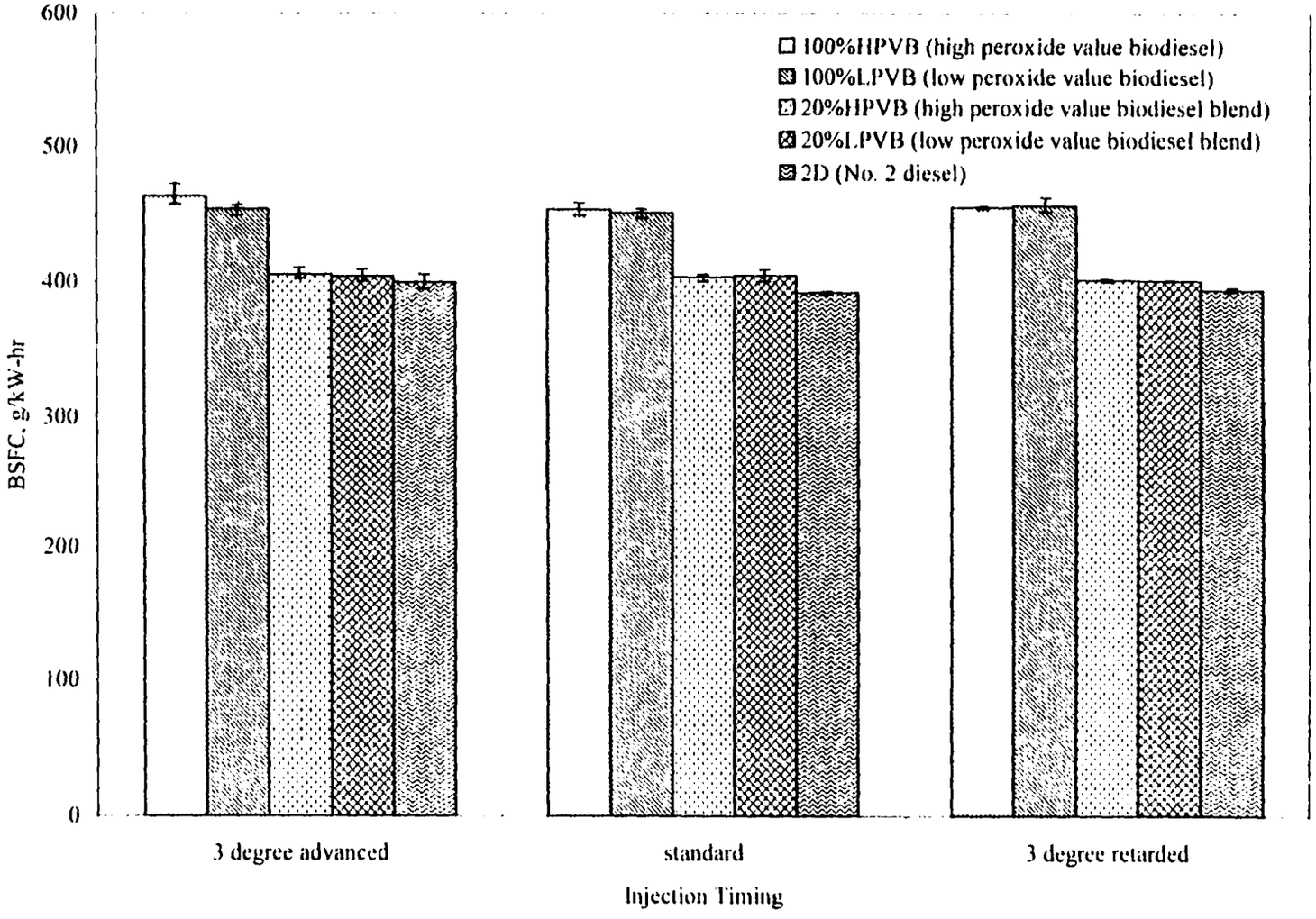

Figure 5.9 Brake specific fuel consumption (BSFC) at light-load engine condition

of storage. In accord with the results of this study, they found that the PV increased over this 24 months of storage. At the end of the storage, they found that the PV of the biodiesel had reached about 340 meq O_2/kg.

Figures 5.10 and 5.11 show the thermal efficiency of the engine for full and light loads. For the purposes of this calculation, the lower heating value (LHV) for the neat oxidized and unoxidized biodiesels were considered to be the same. The LHV for both oxidized and unoxidized biodiesels were assumed to be 37165 kJ/kg, while the LHV for the No. 2 diesel fuel was assumed to be 42578 kJ/kg. Figures 5.10 and 5.11 show that the thermal efficiency of the biodiesel and its blends is the same as for diesel fuel. This indicates that the engine converts the same amount of chemical energy to mechanical energy for all five fuel blends. The thermal efficiency for all five fuel blends was about 37% at the full load engine condition, while at the light load engine condition the thermal efficiency for all five fuel blends was about 21%.

A similar effect was found by Schumacher et al. [75]. In their investigation a 1991 Dodge pickup was fueled with methyl-ester of soybean oil and diesel fuel. Both fuels showed the same thermal efficiency. Chang et al. [76] fueled a John Deere 4276T four-cylinder, four-stroke, turbocharged DI diesel engine with biodiesel fuels and a diesel fuel. Chang found that the thermal efficiency of the ester blends was the same as for No. 2 diesel fuel, which was about 37%. This thermal efficiency matched the results of this experiment.

Figure 5.12 illustrates the BSFC on a percent basis above the baseline diesel fuel. The 100%HPV biodiesel at 3° advanced injection timing has a 15.7% increase in BSFC

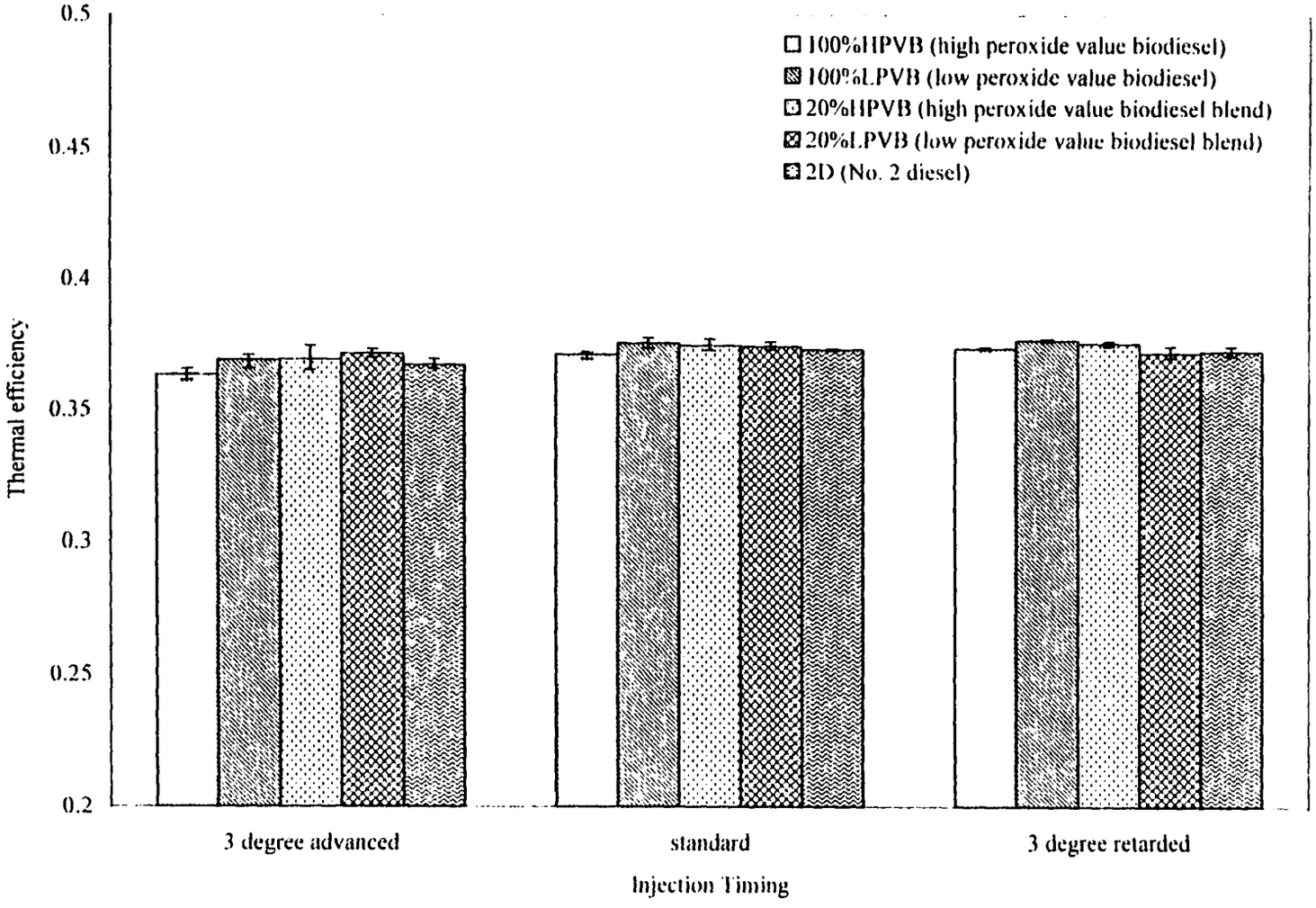

Figure 5.10 Thermal efficiency at full-load engine condition

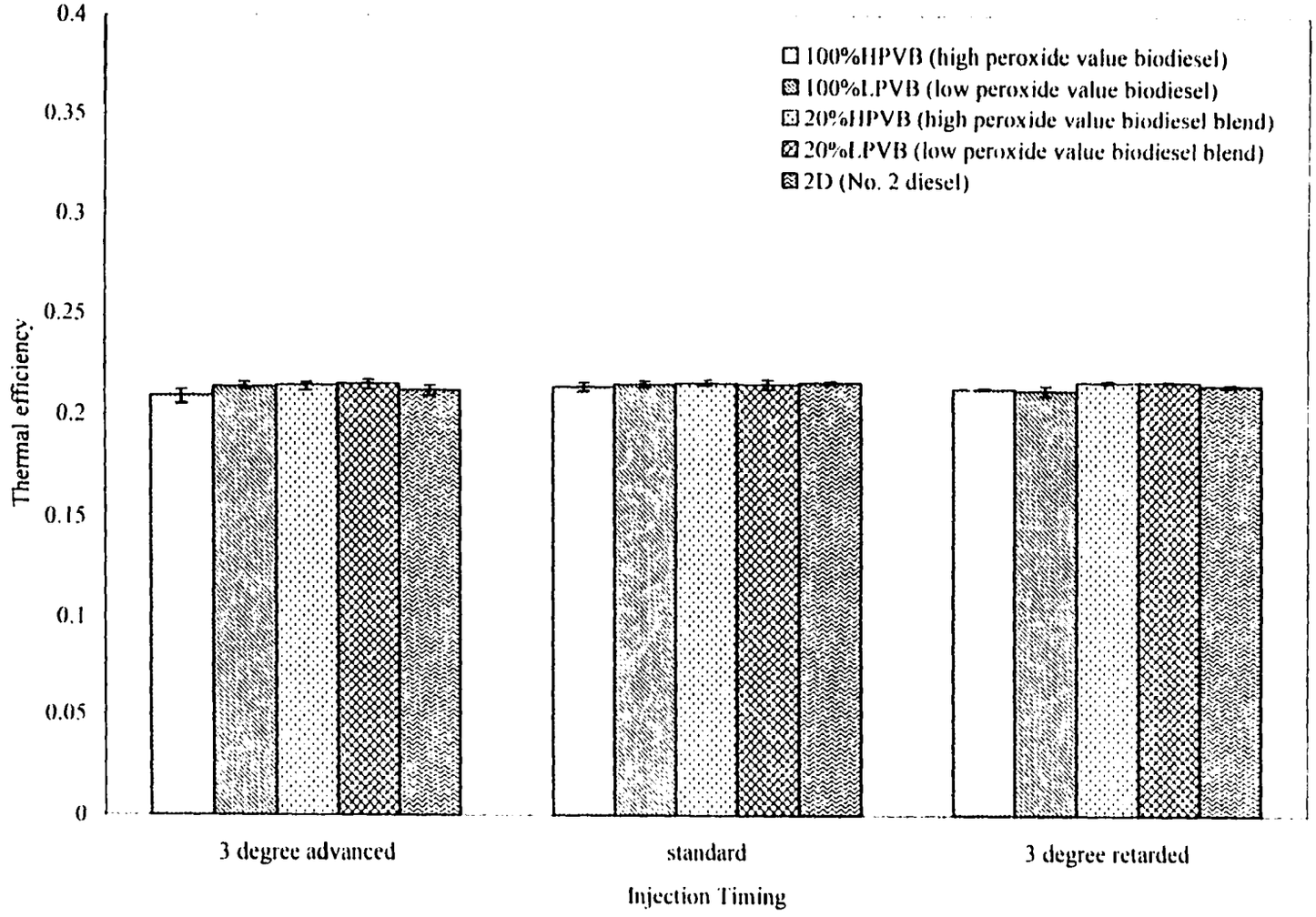

Figure 5.11 Thermal efficiency at light-load engine condition

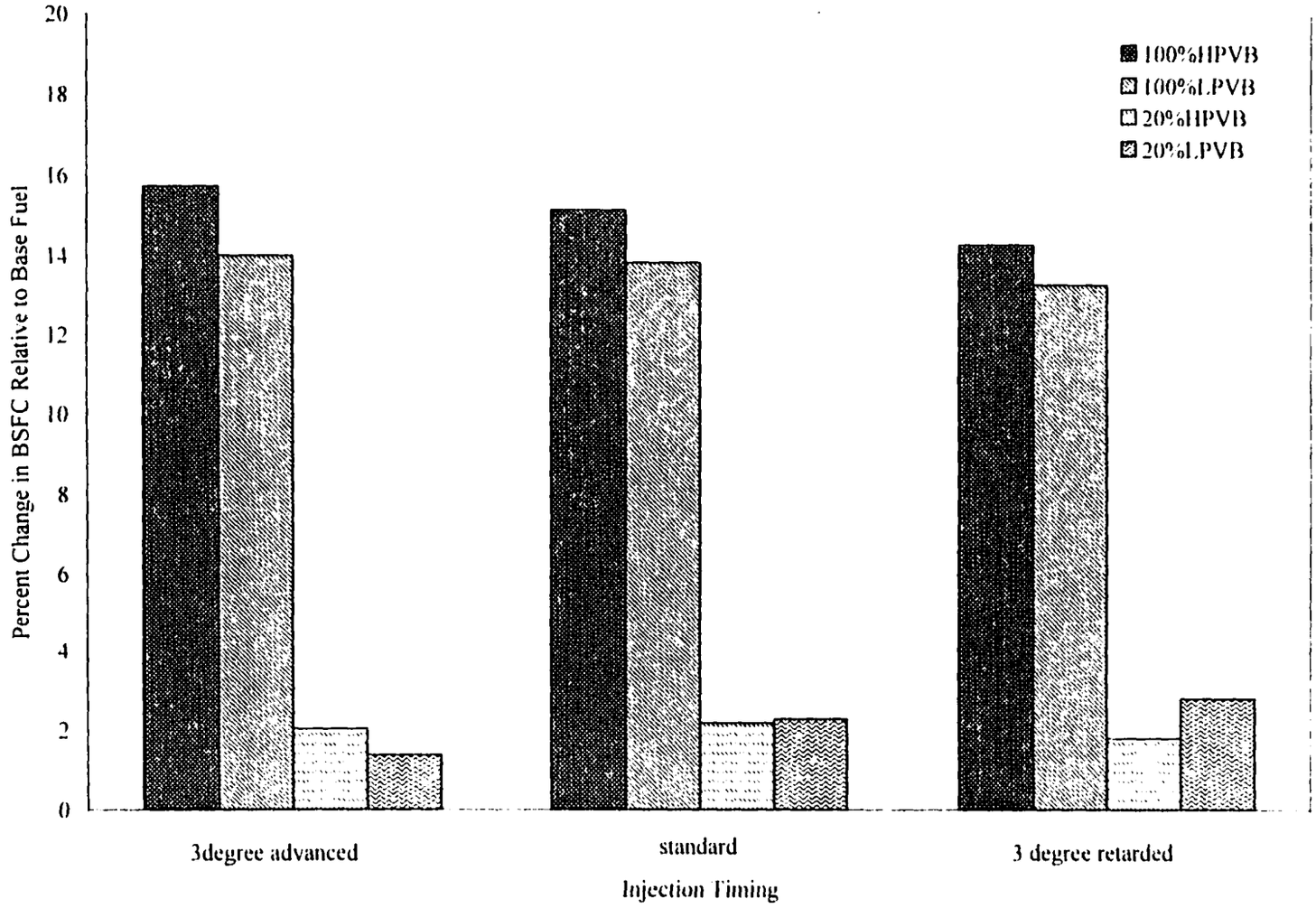

Figure 5.12 Percent change in BSFC at full-load engine condition

compared with No. 2 diesel fuel while the 100%LPV biodiesel has about a 14% increase. Thus, there was a 1.5% higher BSFC measured for the 100%HPV biodiesel than for the 100%LPB biodiesel and this was statistically significant. This also matches well with the 1.4% decrease in heating value observed by Thompson [74]. The 20% blend of HPV biodiesel and LPV biodiesel had a 2% and 1.4% increase in BSFC, respectively. For the standard injection timing, the 100%HPV and 100%LPV biodiesels had about 15.1% and 13.8% increases in BSFC, respectively, while the 20% blend of both HPV and LPV biodiesels had about 2.2% and 2.3% increases in BSFC, respectively. At the 3° retarded injection timing the 100%HPV and 100%LPV biodiesel had about 14.3% and 13.3% increases in BSFC while the 20% blends for HPV and LPV had 1.8% and 2.8% increase in BSFC, respectively. The 20% blends (20%HPV and 20%LPV) of biodiesel were found to be statistically different than the No 2 diesel, while the differences between the 20% blends (20%HPV and 20%LPV) were statistically the same. There was a 2.2% increase in BSFC found for the 3° advanced injection timing compared to the standard injection timing for the 100%HPV biodiesel while only a 0.6% decrease in BSFC was found for the 3° retarded injection timing. These results are similar to those of MacDonald et al. [77] who fueled a Caterpillar 3304 PCNA engine with low-sulfur diesel fuel and methyl-ester soybean oil. In their research they found about 13 to 14% increase in BSFC for neat methyl soyate.

Figure 5.13 shows the percent change in BSFC relative to the base fuel for 20% load. At all timings the 100%HPV and 100%LPV biodiesels have between 14% to 16% increase in BSFC while the 20% blends of both HPV and LPV biodiesel have between

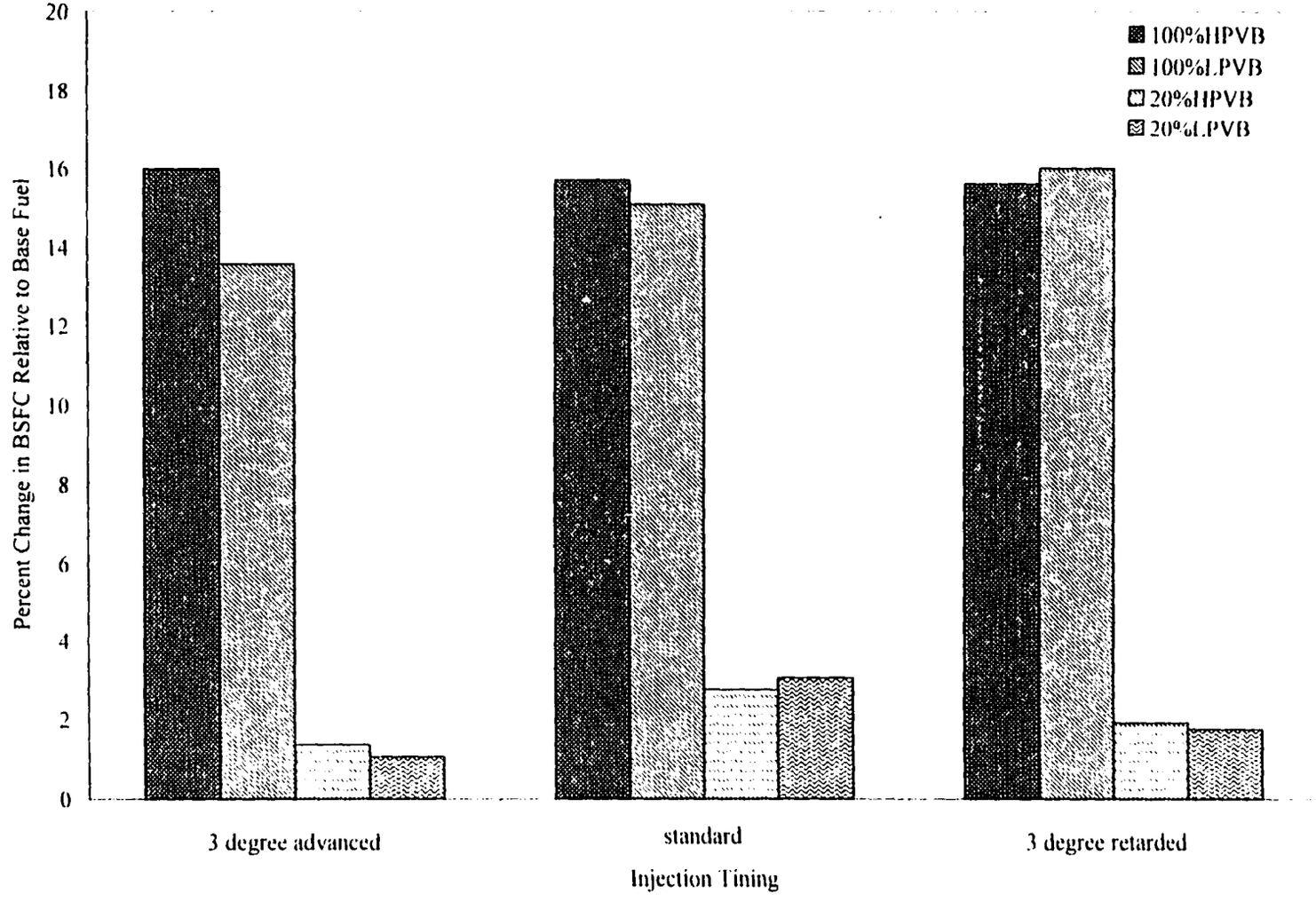

Figure 5.13 Percent change in BSFC at light-load engine condition

1% to 3% increases. For this low load engine condition, the advanced injection timing gives a 2.1% increase in BSFC compared with the standard injection timing while the 3° retarded injection timing has almost no effect on BSFC which is also confirmed by the statistical analysis. From the statistical analysis, it is clear that the difference between the BSFC for the 3° retarded injection timing and the standard injection timing is insignificant.

5.2.2 The effect of timing and fuel oxidation on diesel engine exhaust emissions

This section will discuss the diesel engine emissions for the five fuels (100%HPVB, 100%LPVB, 20%HPVB, 20%LPVB, and No. 2 diesel) at three injection timings. The injection timings were 3° advanced injection, standard injection, and 3° retarded injection. The engine emissions measured were carbon dioxide (CO_2), carbon monoxide (CO), unburned hydrocarbon (HC), oxides of nitrogen (NO_x) and the Bosch smoke number. All emissions were expressed on a brake specific (g/kW-hr) basis except for the Bosch smoke number. All points shown were the average of three data points and the error bars show the spread between the maximum and the minimum points among the three data points.

5.2.2.1 Carbon dioxide (CO_2) emissions

The analysis of variance (ANOVA) table for CO_2 emissions is shown in Table 5.4. The significant factors are shown by the symbol of star (*). Tukey's grouping is given in Appendix D. The emissions of CO_2 are direct products of the complete

Table 5.4 Analysis of variance (ANOVA) for $BSCO_2$

Source	DF	SS	Mean Square	F Value	Pr > F
MODEL	35	6594018.81	188400.45	2774.87	0.0001
BATCH	2	418.95	209.47	4.94	0.1693
AGE	2	280.39	140.19	3.31	0.2301
TIMING*	2	3154.12	1577.51	37.27	0.0261
WHOLE PLOT ERROR	2	84.75	42.38		
FUEL*	4	6511.66	1627.16	23.96	0.0001
LOAD*	1	6585284.95	6585284.95	96919.68	0.0001
FUEL×LOAD*	4	1185.04	296.26	4.36	0.0040
TIMING×FUEL	8	841.07	105.13	1.55	0.1630
TIMING×LOAD	2	14.10	7.05	0.10	0.9016
TIMING×FUEL×LOAD	8	434.86	54.36	0.80	0.6052
Error	54	3669.07	67.95		
Corrected Total	89	6601884.88			

R-Square = 0.999444
$BSCO_2$ Mean = 1001.72

combustion of the fuel so the $BSCO_2$ emissions are closely related to the BSFC. Generally, the higher the BSFC the higher the $BSCO_2$ emissions will be.

The brake specific carbon dioxide ($BSCO_2$) emissions for the five blends at three different timings are illustrated in Figure 5.14. The changes of the CO_2 emissions for the five different blends were very small as indicated by the narrow range of values given on the y-axis. The 100%HPV biodiesel shows the largest increase in CO_2 emissions for all three injection timings. It was seen from the previous section that the BSFC for 100%HPV biodiesel at all injection timings was significantly higher than all four of the other fuel blends. The increase of CO_2 emissions for 100%HPV biodiesel at all injection timings was logical because of the higher amount of fuel that was burned. Compared to the baseline fuel (No. 2 diesel) for 3° advanced injection, the 100%HPV biodiesel had about 2% higher CO_2 emissions while the 100%LPV biodiesel had only about 0.5%

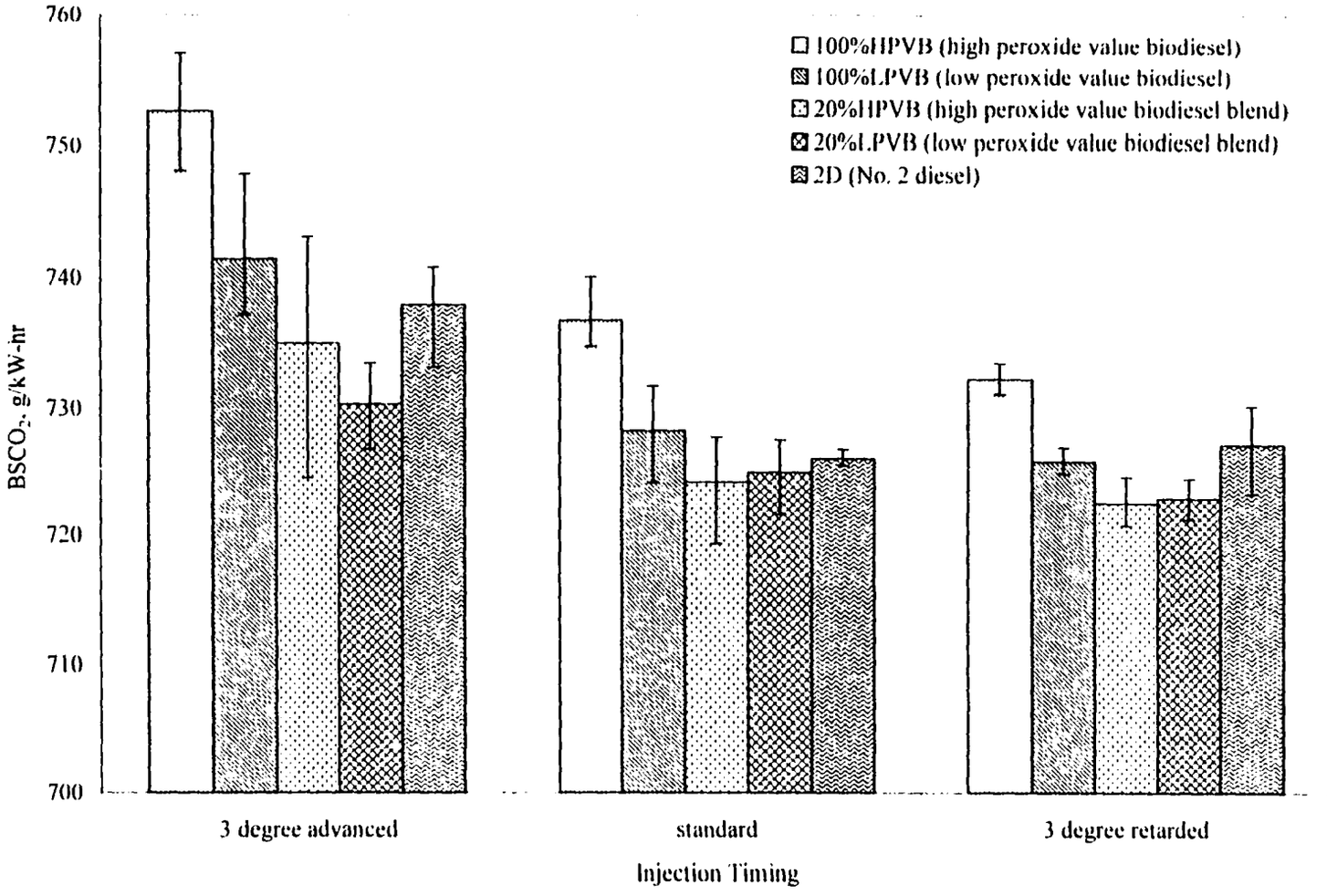

Figure 5.14 Brake specific CO_2 emissions at full-load engine condition

higher. At this injection timing the 100%HPV biodiesel had only about 1.5% higher CO_2 emissions than the 100%LPV biodiesel. The BSFC for the 100%HPV biodiesel at 3° advanced injection timing was also about 1.5% higher than the 100%LPV biodiesel. The larger amount of fuel produced higher CO_2 emissions. This explains why the CO_2 emissions were higher at this injection timing. At the standard and the 3° retarded injection timing, the 100%HPV biodiesel had about 1.2% and 0.9% higher CO_2 emissions compared to the 100%LPV biodiesel. At these injection timings the 100%HPV biodiesel also had a higher BSFC than the 100%LPV biodiesel and the base fuel. This higher BSFC justifies the higher CO_2 emissions. The 20% blends (20%HPV and 20%LPV) of biodiesel had less CO_2 emissions than the No. 2 diesel fuel for all injection timings, but the decrease was not statistically significant.

Relative to the standard injection timing the CO_2 emissions for all the fuel blends were higher for the 3° advanced injection timing. It was also seen in the statistical analysis that the effect of the 3° advanced injection timing on CO_2 emissions was statistically different than the standard and 3° retarded injection timings. The increase of CO_2 emissions for the 3° advanced injection timing compared to the standard injection timing was between 1.5% to 2.1% for all the fuel blends. This increase of CO_2 was due to the increase of fuel consumption.

At the light load engine condition, the $BSCO_2$ emissions were higher than for the full-load engine condition due to the higher BSFC at this engine condition. Figure 5.15 shows the $BSCO_2$ emissions for the three injection timing settings. In this figure the 100%HPV biodiesel shows the highest CO_2 emissions for all injection timings. The next

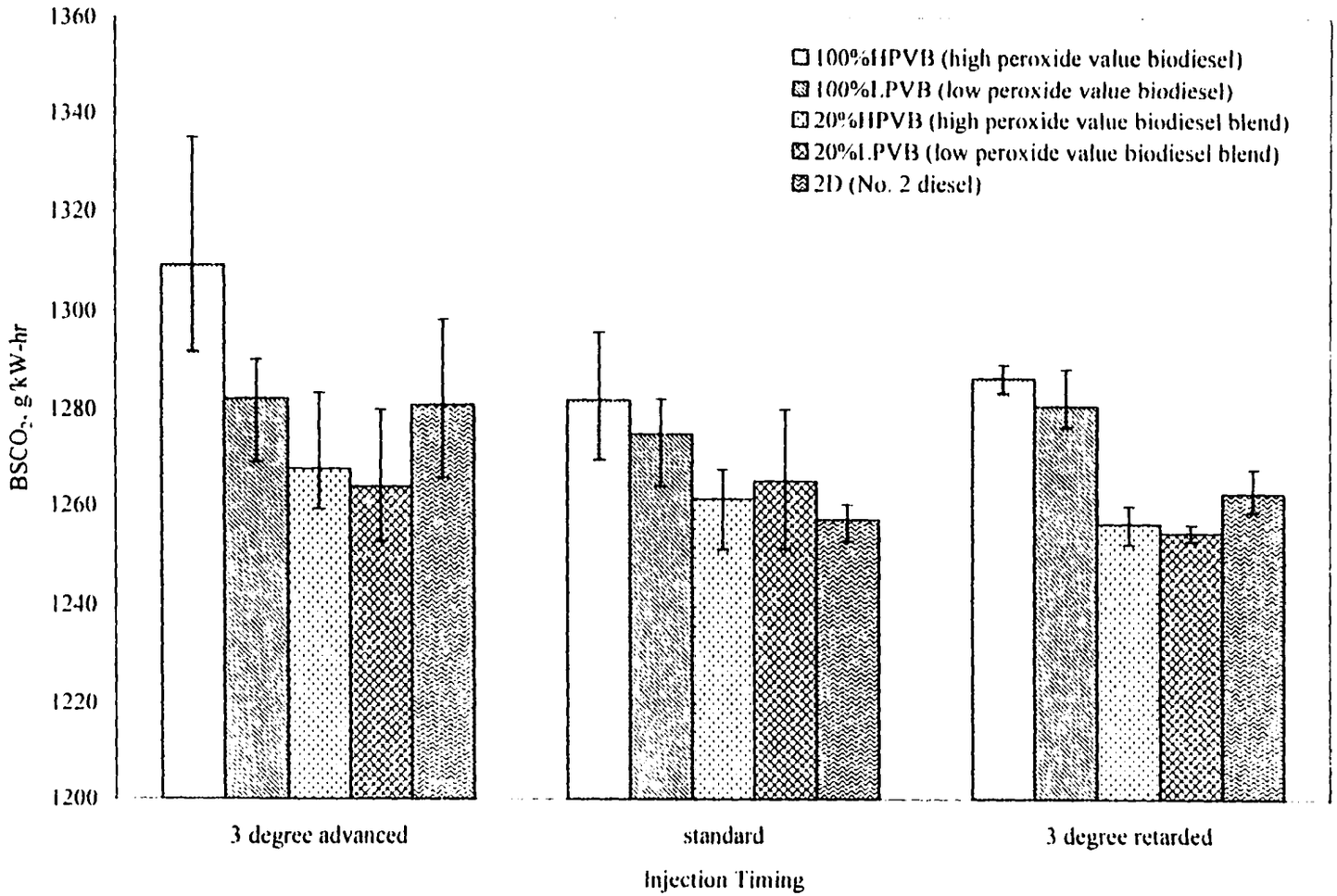

Figure 5.15 Brake specific CO_2 emissions at light-load engine condition

largest is the 100%LPV biodiesel. The CO_2 emissions for the 100%HPV biodiesel at 3° advanced, standard, and 3° retarded injection timings were increased by 2.22%, 1.97%, and 1.89%, respectively, relative to the base fuel, while the 100%LPV biodiesel increased by only 0.1%, 1.42% and 1.44%, respectively. Compared to 100%LPV biodiesel, the 100%HPV biodiesel had about 2.1% higher CO_2 emissions at 3° advanced injection timing. This increase of CO_2 emissions was related to the higher BSFC at this injection timing.

From the above discussion it can be stated that the CO_2 emissions track the BSFC very well and the oxidized biodiesel has higher CO_2 emissions than the non-oxidized biodiesel due to its higher fuel requirement.

5.2.2.2 Carbon monoxide (CO) emissions

The statistical analysis for CO emissions is shown in Table 5.5. From this ANOVA table it can be seen that the changes in CO emissions that resulted from the changes in injection timing, fuel, and load were statistically significant. From the Tukey's grouping (in Appendix D) it can be seen that the CO emission changes resulting from the 3° advanced timing are significantly different than the 3° retarded timing. But the difference between the CO emissions for the 3° advanced and standard timings are insignificant. Similarly, the difference between the standard and 3° retarded injection timings is not statistically significant either. It is important to note that the CO emissions for all five fuel blends are significantly different. These statistical statements will be supported by the numerical data for CO emissions as part of the discussion in this section.

Table 5.5 Analysis of variance (ANOVA) for BSCO

Source	DF	Type I SS	Mean Square	F Value	Pr > F
Model	39	1006.5952	25.7588	257.37	<.0001
BATCH	2	0.2107	0.1053	1.05	0.3548
AGE	2	0.0389	0.0194	0.19	0.8214
TIMING*	1	13.3354	13.3354	133.27	<.0001
WHOLE PLOT ERROR	2	0.4551	0.2275	2.27	0.1404
FUEL*	4	67.1332	16.7833	167.73	<.0001
LOAD*	1	867.0210	867.0210	8663.43	<.0001
FUEL×LOAD*	4	57.8517	14.4629	144.53	<.0001
TIMING×FUEL	8	1.6387	0.2048	2.05	0.0619
TIMING×LOAD*	2	4.5603	2.2801	22.78	<.0001
TIMING×FUEL×LOAD	8	1.3497	0.1687	1.69	0.1267
Error	54	6.0358	0.1117		
Corrected Total	99	1012.6310			

R-Square = 0.9940
BSCO Mean = 3.7169

Carbon monoxide is an intermediate product of hydrocarbon combustion. As the hydrocarbon fuel burns, it produces CO most of which oxidizes to CO_2. The brake specific CO emissions are shown in Figure 5.16. At the full load engine condition, the emissions of CO for the four biodiesel blends were less than for the base fuel (No. 2 diesel). It is important to note that the oxidized biodiesel had about 15% less CO emissions than the unoxidized biodiesel at the standard injection timing. The difference in CO emissions for the oxidized and non-oxidized biodiesel was statistically significant. This significant CO emissions reduction caused by oxidized biodiesel will be discussed in a later section. It can be seen from the Tukey's grouping table that differences between all the fuel blends were statistically different. The highest CO emissions for all of the injection timings were found for the baseline fuel, while the highly oxidized biodiesel (100%HPV) fuel had the lowest.

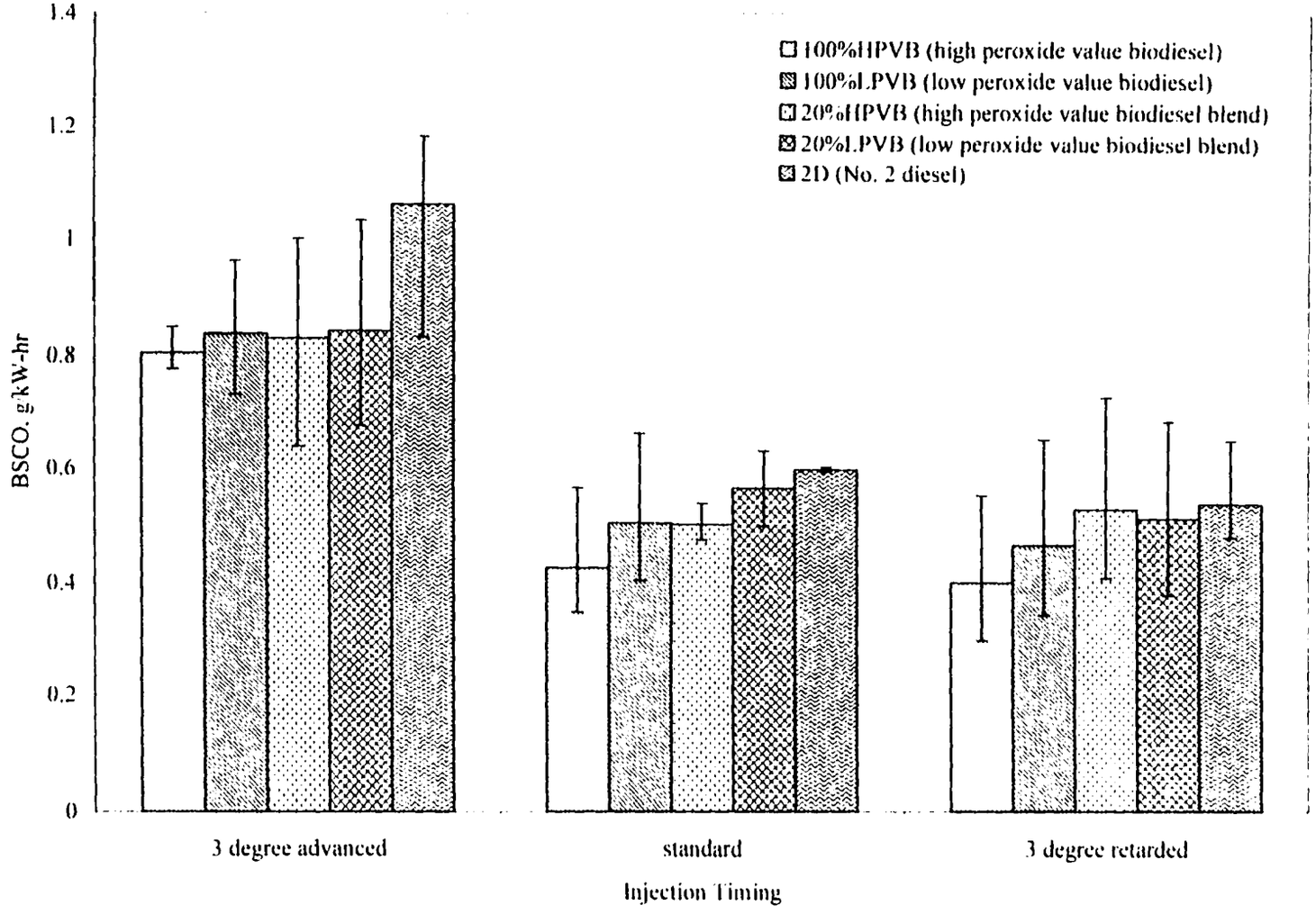

Figure 5.16 Brake specific CO emissions at full-load engine condition

Compared to the base fuel (No. 2 diesel), the CO emissions for highly oxidized (100%HPV) biodiesel were reduced over 24% for all injection timings. Relative to the base fuel, the 3° advanced, standard, and 3° retarded injection timings reduced CO emissions by 24.1%, 28.6%, and 25.3%, respectively. The unoxidized (100%LPV) biodiesel for the 3° advanced, standard, and 3° retarded injection timings reduced CO emissions by only 21.1%, 15.7%, and 13.3%, respectively. The CO emissions for the 20% blends of HPV and LPV biodiesel at the 3° advanced injection timing were reduced by 21.8% and 20.57% which were close to the 100% LPV biodiesel. Also, the 20%HPV biodiesel at the standard injection timing had 16.1% CO emissions reduction while the 3° retarded injection timing had only a 1.7% reduction. The 20% blend of LPV biodiesel at standard injection timing had a 5.5% reduction in CO and at 3° retarded injection timing had a 4.8% CO emissions reduction. It was found that the high peroxide (100%HPV) biodiesel had lower CO emissions than the low peroxide value (100%LPV) biodiesel. This reduction depends upon the injection timings that will be discussed in the later section. At the standard and 3° retarded injection timings the reduction of CO emissions were 15.3% and 13.8%, respectively. Chang et al. [76] also found that biodiesel blends lowered CO emissions. In their research, they found that a fuel consisting of 40% methyl palmitate, 10% methyl stearate, and 50% diesel fuel reduced CO emissions by 24%.

The advanced injection timing had much higher CO emissions for all fuel blends while the retarded injection timing had lower CO emissions than the standard injection timing. It was found that at 3° advanced injection timing for highly oxidized (100%HPV) biodiesel, the CO emissions increased by about 88.5% compared to the standard injection

timing while at 3° retarded injection timing the CO emissions were reduced by only 5.9%. Unoxidized (100%LPV) biodiesel and the 20% blend of HPV biodiesel at 3° advanced injection timing had close to 66% higher CO emissions than the standard injection timing. For the base fuel, 3° advanced injection timing increased the CO emissions by 77.2%, while the 3° retarded injection timing reduced the CO emissions by 10% compared to the standard injection. Compared to the 3° advanced injection timing, 3° retarded injection timing had about a 50% reduction in CO emissions.

The light-load (20% load) CO emissions are shown in Figure 5.17. The brake specific CO emissions were higher for the light-load condition than at full load. Similar to the full load condition, the light load condition had lower CO emissions for the highly oxidized biodiesel (100%HPV) than for the base fuel at all injection timings.

It can be seen in the figure that the CO emissions increased as the injection timing advanced and this was true for all five tested fuels. The highest CO emissions improvement was found for the oxidized biodiesel (100%HPV) which was between 49% to 56% less than diesel fuel regardless of injection timing. The unoxidized (100%LPV) biodiesel had within 39%-42% reduction for the 3° advanced and standard injection timings while the 3° retarded injection timing had about a 33.2% reduction. The 20% blends of HPV and LPV biodiesel also had significantly reduced CO emissions. This CO reduction was between 19% and 32% for the three injection timings.

At the light load engine condition, the difference in the CO emissions for 3° advanced injection timing compared to the standard injection timing was not statistically significant, but it was found that the 3° advanced injection timing had higher CO

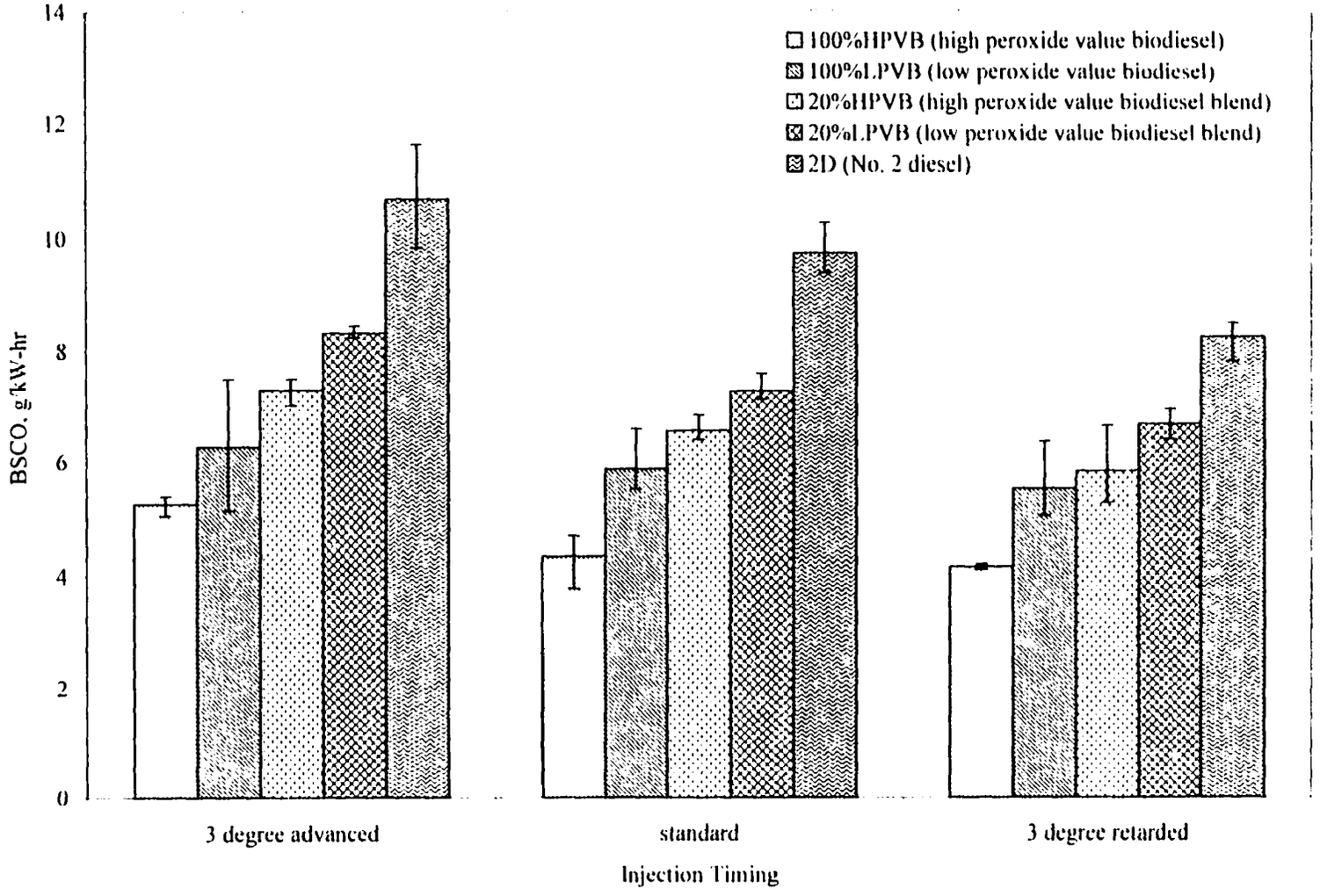

Figure 5.17 Brake specific CO emissions at light-load engine condition

emissions then the 3° retarded injection timing which was found to be statistically significant.

From the above discussions it can be concluded that all neat biodiesels and biodiesel blends produced lower CO emissions for all injection timings. Regardless of injection timing and load, the neat oxidized biodiesel reduced the CO emissions between 24% and 55% compared with diesel fuel. The oxidized biodiesel also produced less CO emissions than the unoxidized biodiesel. It reduced CO emissions in the range of 3.8% to 26.2% regardless of injection timing and load. The advanced injection timing produced higher CO emissions than the retarded injection timing. At the full load engine condition for the 3° advanced injection timing, the reduction in CO emissions was in the range of 48.9% to 88.4% for any blends compared to standard injection timing. The CO emissions were higher at the light load engine condition than at the full load engine condition. Compared to neat non-oxidized biodiesel, the neat oxidized biodiesel at this light load engine condition produced 16.1% to 24.6% less CO emissions.

5.2.2.3 Unburned hydrocarbon (HC) emissions

The changes in HC emissions that resulted from the change in injection timing, fuel, and load were statistically significant. The significance levels for these parameters are shown in Table 5.6. The Tukey's grouping table shown in Appendix D, also identifies the effect of changes in injection timing on the HC emissions. Further, the effect of oxidized biodiesel on the HC emissions can be identified from this table. With the help of the ANOVA table and the Tukey's grouping table, the effect of injection timing and

Table 5.6 Analysis of variance (ANOVA) for BSHC

Source	DF	Type I SS	Mean Square	F Value	Pr > F
Model	35	5.9469	0.1699	171.11	<.0001
BATCH	2	0.0075	0.0037	3.81	0.0269
AGE	2	0.0022	0.0011	1.13	0.3291
TIMING*	2	0.0397	0.0199	20.06	<.0001
WHOLE PLOT ERROR	2	0.0041	0.0020		
FUEL*	4	0.6636	0.1674	168.60	<.0001
LOAD*	1	4.6917	4.6917	4724.87	<.0001
FUEL×LOAD*	4	0.371	0.0929	93.56	<.0001
TIMING×FUEL	8	0.0129	0.0016	1.63	0.1375
TIMING×LOAD*	2	0.0815	0.0407	41.09	<.0001
TIMING×FUEL×LOAD	8	0.0055	0.0006	0.70	0.6921
Error	84	0.0536	0.0009		
Corrected Total	119	6.0005			

R-Square=0.991064
BSHC Mean=0.31397

oxidized biodiesel blends will be discussed in this section. In the same manner as the CO emissions, the HC emissions are affected by the injection timing, and the oxidized biodiesel was found to significantly reduce HC emissions compared with unoxidized biodiesel.

The HC emissions for all five fuel blends are shown in Figure 5.18 for the three injection timings. At the full load condition, the HC emissions for all the biodiesel fuels were less than for the base fuel (No. 2 diesel). It is important to note that like the CO emissions, the oxidized biodiesel (100%HPV) had less HC emissions than the unoxidized biodiesel (100%LPV). This decrease in HC emissions was also proven statistically significant as shown in the Tukey's grouping table in Appendix D. The highest HC emissions for all the injection timings were found for the baseline fuel, while the highly oxidized neat biodiesel (100%HPV) fuel had the lowest. Both 100%HPV and 100%LPV

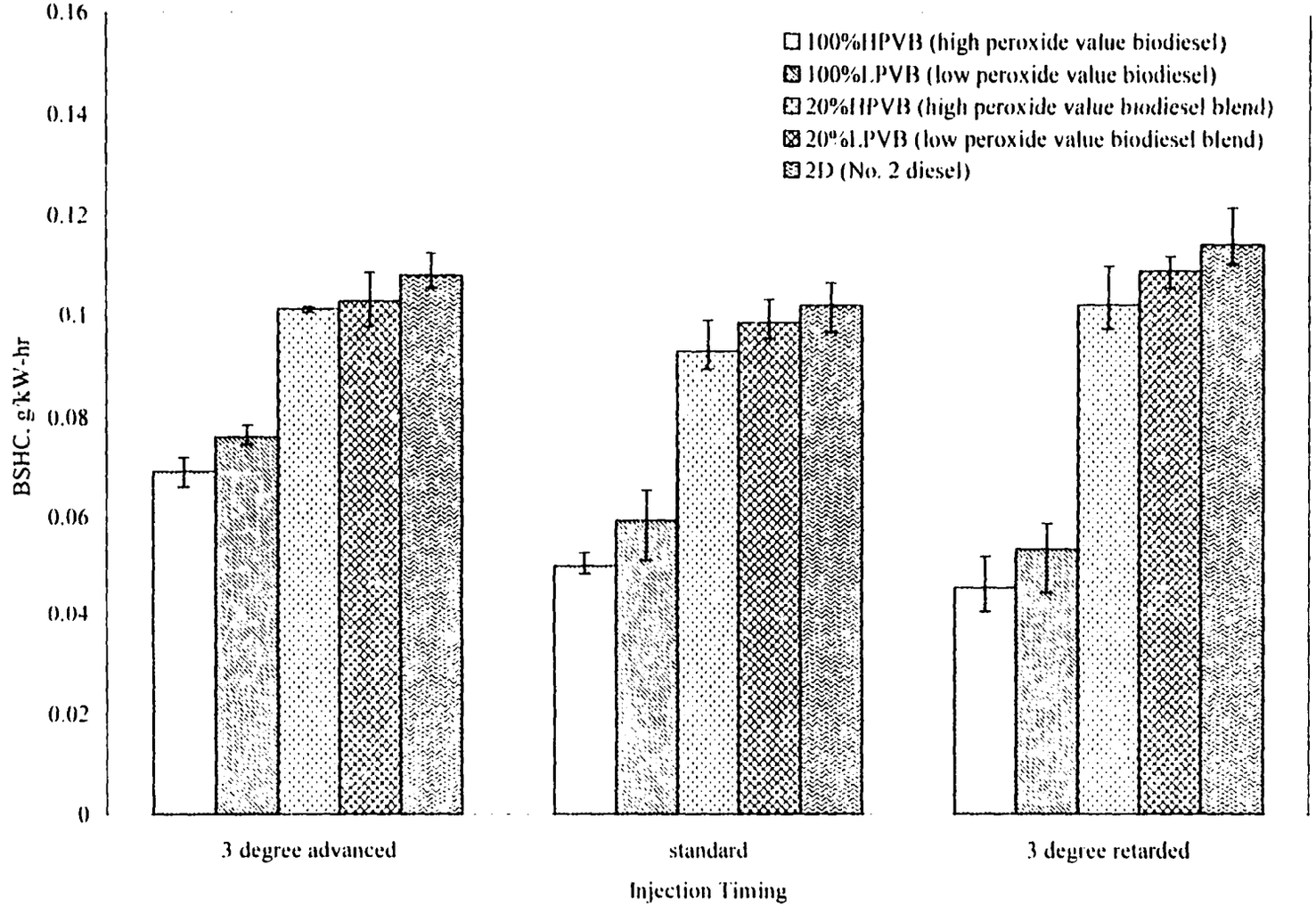

Figure 5.18 Brake specific HC emissions at full-load engine condition

biodiesel fuels showed a reduction in HC emissions compared to the base fuel, but the reduction for the 100%HPV biodiesel was significantly higher than for the 100%LPV biodiesel.

Compared to the base fuel, the HC emissions for the highly oxidized (100%HPV) biodiesel were reduced by between 36% and 60% regardless of injection timing. Relative to the base fuel, the 3° retarded injection timing had the highest reduction in HC emissions which was 60.1%. Unoxidized (100%LPV) biodiesel reduced the HC emissions by 53.2%. So it is clear that the oxidized biodiesel reduced HC emissions. This reduction in HC emissions for oxidized biodiesel was also found to be statistically significant. For the 3° retarded injection timing the 100%HPV biodiesel reduced the HC emissions by 14.8% compared to the 100%LPV biodiesel. At the standard injection timing, the oxidized biodiesel (100%HPV) reduced the HC emissions by 15.7% compared to the unoxidized biodiesel (100%LPV).

The 20% blends (20%HPV and 20%LPV) also reduced HC emissions compared to the base fuel (No. 2 diesel). The reduction of HC emissions for the 20%HPV biodiesel was higher than for the 20%LPV biodiesel. Compared to the 20%LPV biodiesel, the 20%HPV biodiesel had about 6% less HC emissions at the standard injection timing. This HC emissions reduction was also found for the blends of vegetable oil ester and diesel fuel tested by Chang et al. [76]. Rickeard et al. [78] also mentioned HC emissions reductions for the bio-fuels.

The brake specific HC emissions for the light-load engine condition are shown in Figure 5.19. The HC emissions were higher at the light-load engine condition than at the

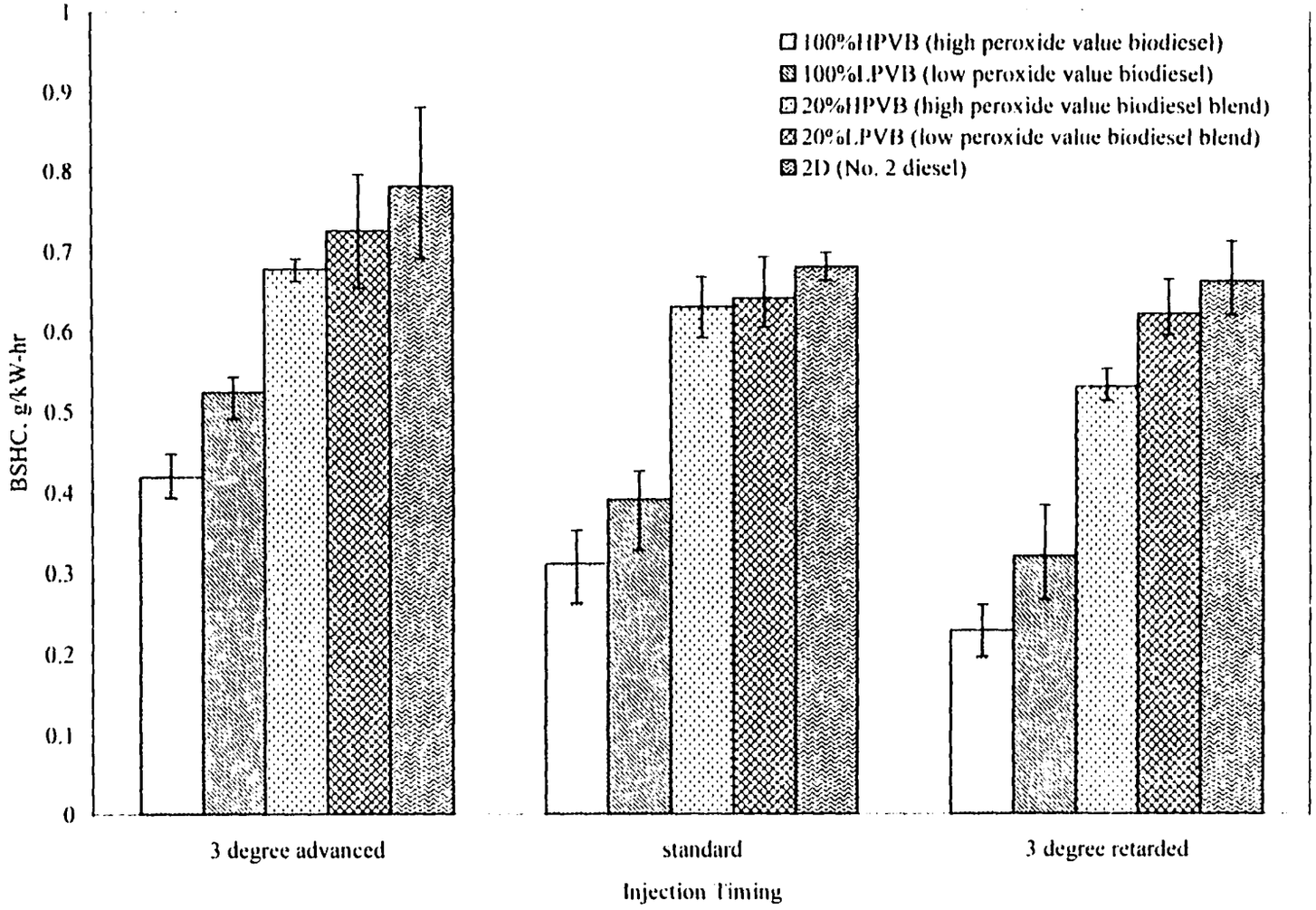

Figure 5.19 Brake specific HC emissions at light-load engine condition

full load engine condition by approximately a factor of 10. At the light load engine condition, the oxidized biodiesel (100%HPV) significantly reduced the HC emissions compared to the unoxidized biodiesel (100%LPV). This reduction in HC emissions was between 20% and 28.5% regardless of the injection timing. It was found from the figure that the HC emissions were increased as the injection timing advanced and this was true for all five tested fuel blends. Compared to the base fuel, the highest HC emissions improvement was found for the oxidized biodiesel (100%HPV) which was between 46% and 65% regardless of the injection timing. The next largest improvement in the HC emissions was for the unoxidized (100%LPV) biodiesel. This blend had between 32% and 52% reductions in HC emissions for all injection timings. The 20% blends (20%HPV and 20%LPV) also reduced the HC emissions, however, the 20%HPV biodiesel reduced HC emissions more than the 20%LPV biodiesel.

The injection timing also has an effect on the HC emissions. The advanced injection timing had higher HC emissions than the retarded injection timing. This change in HC emissions resulted from the change in injection timing and was statistically significant. It had been found that at the 3^{o} advanced injection timing, the oxidized biodiesel (100%HPV) increased HC emissions by about 38.5% compared to the standard injection timing while at the 3^{o} retarded injection timing the HC emissions were reduced by 8.8% compared to the standard injection timing. Compared to the 3^{o} advanced injection timing, the 3^{o} retarded injection timing had about 34% less HC emissions for the oxidized biodiesel. At the light-load engine condition, the advanced injection timing

also increased the HC emissions while the retarded injection timing significantly reduced HC emissions.

5.2.2.4 Oxides of Nitrogen (NO_x) emissions

Nitric oxide (NO) and nitrogen dioxide (NO_2) are usually combined together as NO_x emissions. The nitric oxide (NO) is the dominant part of the oxides of nitrogen produced inside the engine cylinder. The oxidation of molecular nitrogen is the principle source of NO emissions. At the full load engine condition, the brake specific NO_x emissions are shown in Figure 5.20. The NO_x emissions for biodiesel were higher than for the base fuel. The reason is that the biodiesel fuel contains significant oxygen. The fuel oxygen causes the areas of the cylinder that would ordinarily be rich to be leaner. This fuel oxygen may provide the additional oxygen needed to oxidize the nitrogen. The NO_x emissions for the oxidized biodiesel were not significantly different than unoxidized biodiesel.

The fuel blends have significant effect on NO_x emissions as shown in Table 5.7. The Tukey's grouping table in Appendix D compares the effect of fuel blends on the NO_x emissions. The NO_x emissions of the 20% blends were not significantly different than the base fuel (No. 2 diesel).

The neat oxidized biodiesel (100%HPV) at the standard injection timing had about 13% higher NO_x emissions than the No. 2 diesel fuel while the 100%LPV biodiesel had about 13.6% higher. The 20% blends (20%HPV and 20%LPV) had slightly higher NO_x emissions compared to the No. 2 diesel fuel although, as noted earlier, the difference

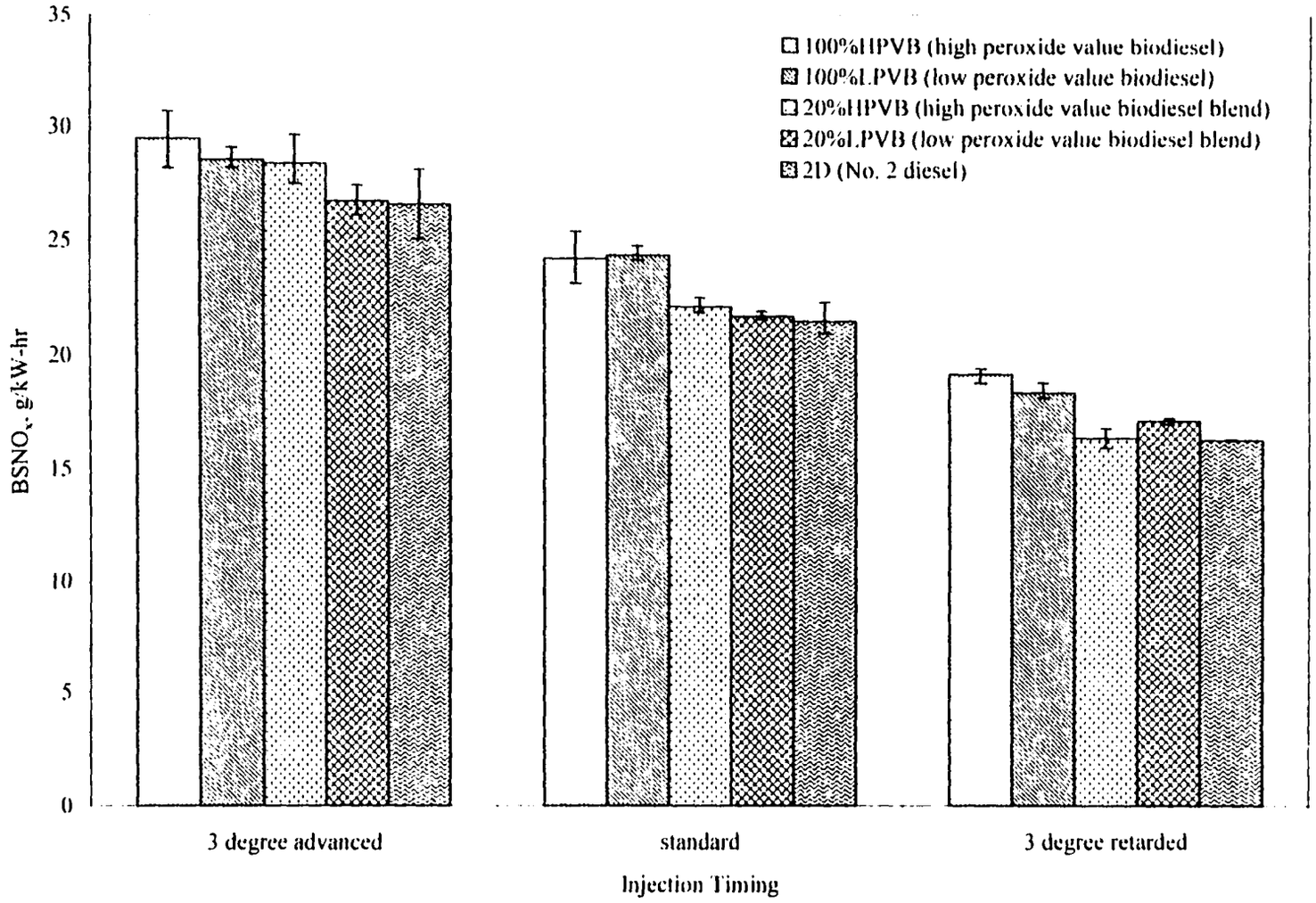

Figure 5.20 Brake specific NO_x emissions at full-load

was not statistically significant. The 3° advanced and 3° retarded injection timings increased NO_x emissions by 11% and 18%, respectively. Unoxidized, neat biodiesel (100%LPV) at the 3° advanced and 3° retarded injection timings had increased NO_x emissions by 7.5% and 12.9%, respectively.

Table 5.7 Analysis of variance (ANOVA) for $BSNO_x$

Source	DF	Type I SS	Mean Square	F Value	Pr > F
Model	15	2112.1191	60.3471	99.84	<.0001
BATCH	2	3.0464	1.5232	2.52	0.0821
AGE	2	2.3687	1.1843	1.96	0.1503
TIMING*	2	1719.0623	859.5311	1863.74	<.0001
WHOLE PLOT ERROR	2	0.9223	0.4611		
FUEL*	4	35.4813	8.8703	14.67	<.0001
LOAD*	1	298.4404	298.4404	493.73	<.0001
FUEL×LOAD*	4	32.0415	8.0103	13.25	<.0001
TIMING×FUEL*	8	16.9550	2.1193	3.51	0.0029
TIMING×LOAD	2	1.0514	0.5257	0.87	0.4249
TIMING×FUEL×LOAD	8	5.7795	0.7224	1.20	0.3194
Error	34	32.6412	0.6044		
Corrected Total	59	2144.7903			

Dependent Variable: $BSNO_x$
R-Square=0.984781
$BSNO_x$ Mean=10.8724

The light-load (20% load) NO_x emissions are shown in Figure 5.21. The $BSNO_x$ emissions were lower at the light-load condition than at full load. Similar to the full-load engine condition, at the light load engine condition the oxidized biodiesel (100%HPV) had no significant effect on the NO_x emissions compared to the unoxidized biodiesel (100%LPV). At the 3° advanced injection timing, the high and low oxidized biodiesel (100%) both had about 5.7% increase in NO_x emissions compared to the base fuel. All of

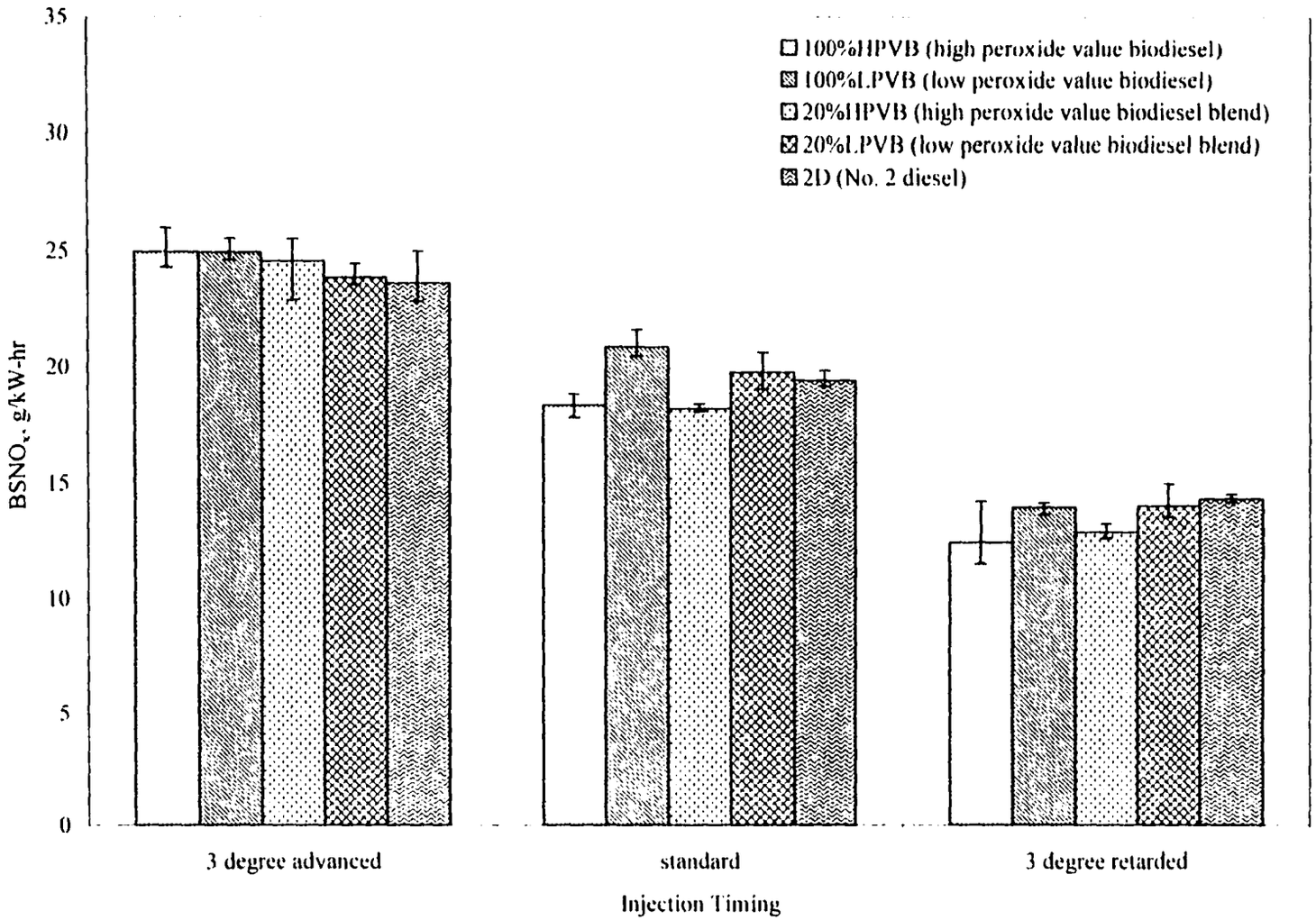

Figure 5.21 Brake specific NO_x emissions at light-load

the fuels increased the NO_x emissions at the 3° advanced injection timing but the standard and 3° retarded injection timing showed inconsistent results.

At both the full and light load engine conditions the injection timing had a significant effect on the NO_x emissions. The Tukey's grouping table in Appendix D also supports this statement. The NO_x emissions increased as the injection was advanced. For the full load engine condition, it was found that at the 3° advanced injection timing for the oxidized (100%HPV) biodiesel, the NO_x emissions increased by about 21.9% compared to the standard injection timing, while at the 3° retarded injection timing the NO_x emissions were reduced by 20.9%. Compared to the standard injection timing, the 3° advanced injection timing for unoxidized (100%LPV) biodiesel had 17.4% higher NO_x emissions, while the 3° retarded injection timing had a 24.6% reduction in NO_x emissions. The 20% blend of HPV biodiesel at the 3° advanced injection timing had 28.9% higher NO_x emissions than the standard injection timing while the 3° retarded injection timing reduced NO_x emissions by 25.9%. For the base fuel, the 3° advanced injection timing increased NO_x emissions by 24% while the 3° retarded timing reduced NO_x by 24.2% compared to the standard injection timing.

At the light load engine condition, the NO_x emissions increased at the advanced injection timing while at the retarded injection timing the NO_x emissions were reduced. A linear relation was found between NO_x emissions and injection timing. Feldman et al. [79] fueled a Yanmar 3TN75E-S, 3-cylinder, normally aspirated, direct injection diesel engine with vegetable oil ester and a No. 2 diesel fuel. They found that retarded injection reduces the NO_x and the particulate emissions. Mittelbach and Tritthart [80] tested

methyl esters of used frying oil and found lower CO and HC emissions and smoke level but increased NO_x emissions compared to No. 2 diesel fuel. Rickeard et al. [78] also mentioned that the NO_x emissions increased for the bio-fuels. These results support the findings of this project.

From the above discussion it can be concluded that the neat biodiesels produced slightly higher NO_x emissions than the base fuel (No. 2 diesel) at all three injection timings. Statistically, the difference between the neat oxidized biodiesel and the neat non-oxidized biodiesel did not produce significant differences in NO_x emissions. A linear relation was found between the injection timing and the NO_x emissions. The 3^o retarded injection timing gave at least 20.9% reduction in NO_x emissions compared with the standard injection timing. The light-load engine condition had more reduction in NO_x emissions than the full load engine condition.

5.2.2.5 Smoke Number (SN)

The statistical analysis given in Table 5.8 and Appendix D showed that the change in smoke number that resulted from the change in the fuel blend, injection timing, and load, were statistically significant. The smoke number at 3^o retarded injection timing was significantly different from that of standard injection timing while the difference between standard and 3^o advanced injection timings was not statistically significant. Even though the smoke number for the highly oxidized biodiesel (100%HPV) was lower than for the unoxidized biodiesel at full load, the difference was not statistically significant. Similarly, the smoke number for the 20% blends of HPV and LPV biodiesels were not

significantly different from each other. The smoke number for the base fuel had a statistically significant difference compared with the other four fuels. All three groups, the neat biodiesels (100%HPV, 100%LPV), the 20% blends (20%HPV, 20%LPV), and the base fuel were significantly different. The minimum significant difference in the smoke number was 0.05 for the fuel blends. At the full load condition, the smoke number for all the biodiesel fuels was significantly lower than for the base fuel (No. 2 diesel). The lowest smoke number was found for the oxidized biodiesel (100%HPV). Compared to the base fuel, the unoxidized biodiesel (100%LPV) had a 56.9% reduction in smoke number at the standard injection timing. However, the oxidized biodiesel (100%HPV) had even more reduction in smoke number. At the standard injection timing, it was found

Table 5.8 Analysis of variance (ANOVA) for Smoke Number

Source	DF	Type I SS	Mean Square	F Value	Pr > F
Model	35	30.6600	0.8760	283.36	0.0001
BATCH	2	0.0050	0.0025	0.81	0.7646
AGE	2	0.0140	0.0070	2.26	0.1393
TIMING*	2	3.9732	1.9866	642.63	0.0001
WHOLE PLOT ERROR	2	0.0163	0.0081		
FUEL*	4	2.0173	0.5043	163.14	0.0001
LOAD*	1	20.2113	20.2113	6537.76	0.0001
FUEL×LOAD*	4	2.4449	0.6112	197.72	0.0001
TIMING×FUEL*	8	0.0707	0.0088	2.86	0.0100
TIMING×LOAD*	2	1.7952	0.8976	290.36	0.0001
TIMING×FUEL×LOAD*	8	0.1116	0.0139	4.52	0.0003
Error	54	0.1669	0.0030		
Corrected Total	89	30.8269			

R-Square=0.9945
Smoke Number Mean=0.6090

that the oxidized biodiesel (100%HPV) had a 14% lower smoke number than the unoxidized biodiesel.

The smoke numbers for all five fuels are shown in Figure 5.22 for the three injection timings. The highest smoke number at all injection timings was found for the baseline fuel, while the highly oxidized biodiesel (100%HPV) fuel had the lowest. All fuel blends showed an increase in smoke number as the injection timing was retarded.

Compared to the base fuel, the smoke number for the highly oxidized (100%HPV) biodiesel was reduced by 59.4% at the 3° advanced injection timing and by 62.9% at the standard injection timing. Relative to the base fuel, the 3° retarded injection timing reduced the smoke number by 46.3%. Compared to the base fuel (No. 2 diesel), the unoxidized (100%LPV) biodiesel reduced the smoke number by 58.3% at the 3° advanced injection timing and by 56.9% at standard injection timing. This unoxidized biodiesel at 3° retarded injection timing reduced the smoke number by 35.4% compared to the base fuel. The smoke number reduction for the 20% blends of HPV and LPV biodiesel was between 8% and 22% at all injection timings. Schumacher et al. [75] found a large reduction in smoke number when using biodiesel. In their research, a Dodge pickup was fueled with methyl ester of soybean oil. The reduction was about 86% for 100% methyl ester of soybean oil.

As stated earlier, the advanced injection timing reduced the smoke number. Compared to the standard injection timing, the 3° advanced injection timing reduced the smoke number between 17% and 29% regardless of the fuel. However, the opposite result was found for the 3° retarded injection timing. At this injection timing, the smoke

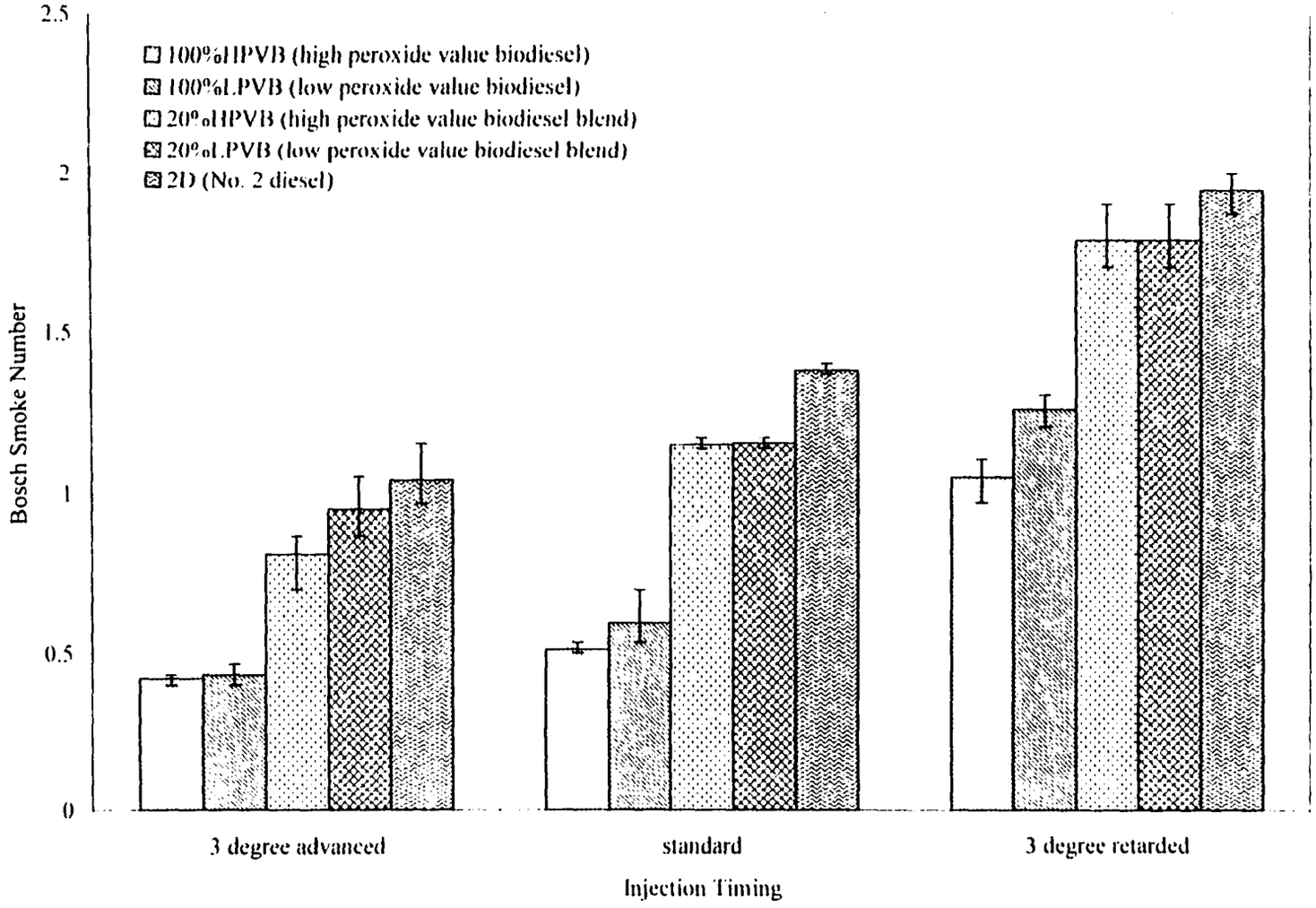

Figure 5.22 Bosch smoke number at full-load

number increased over 100% for both neat biodiesel fuels (100%HPV, 100%LPV) while the 20% blends (20%HPV, 20%LPV) showed increases of about 55% compared with the standard timing. For the base fuel, the 3° advanced injection timing reduced the smoke number by 24.6% while the 3° retarded injection timing increased the smoke number by 41.1% compared to the standard injection timing. Feldman et al. [79] investigated fuel injector timing and pressure optimization on a DI diesel engine for operation on biodiesel. In their research it was also found that the smoke number reduced at advanced injection.

The light-load (20% load) smoke numbers are shown in Figure 5.23. Since the smoke numbers were so small for this load the error bands are large. Any attempts to draw conclusions were not considered to be worthwhile.

5.2.2.6 Summary of emissions results

Figures 5.24 through 5.26 show the percent change in emissions compared to the base diesel fuel for the 3° advanced, standard, and 3° retarded injection timings at the full-load engine condition. This is the same data presented earlier but in a summarized form. All of the emissions are shown on the y-axis, and the percent change in emissions relative to the base fuel is shown on the x-axis. A reduction in the CO and HC emissions, and the smoke number were observed for all fuel blends (100%HPV, 100%LPV, 20%HPV, and 20%LPV) at all injection timings. The maximum reduction in these emissions was found for the oxidized biodiesel. However, an increase in the NO_x emissions was found for all fuel blends at all injection timings. Regardless of the

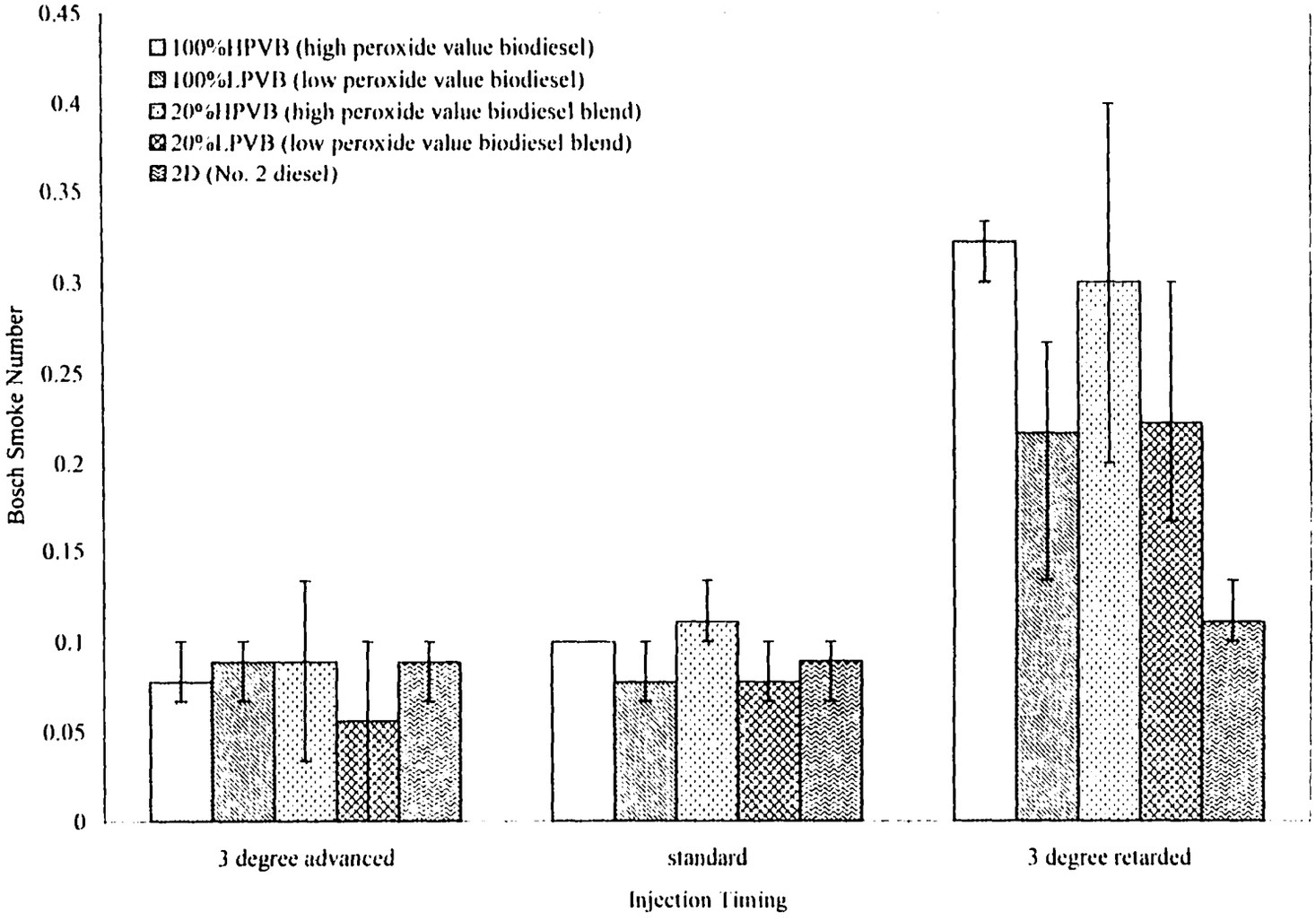

Figure 5.23 Bosch smoke number at light-load

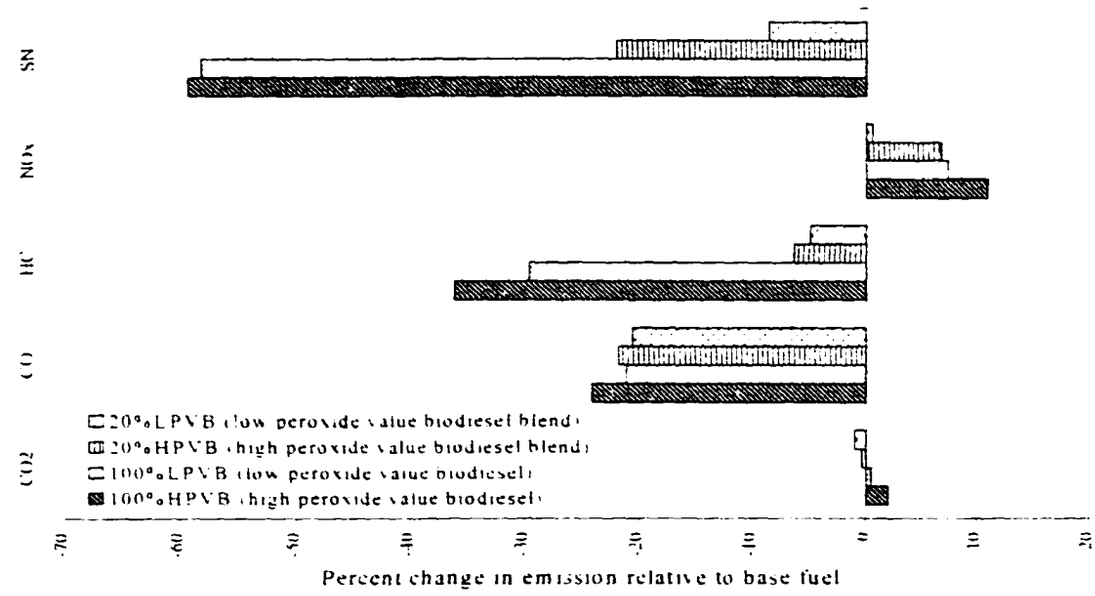

Figure 5.24 Percent change in emissions for 3° advanced injection timing at full-load engine condition

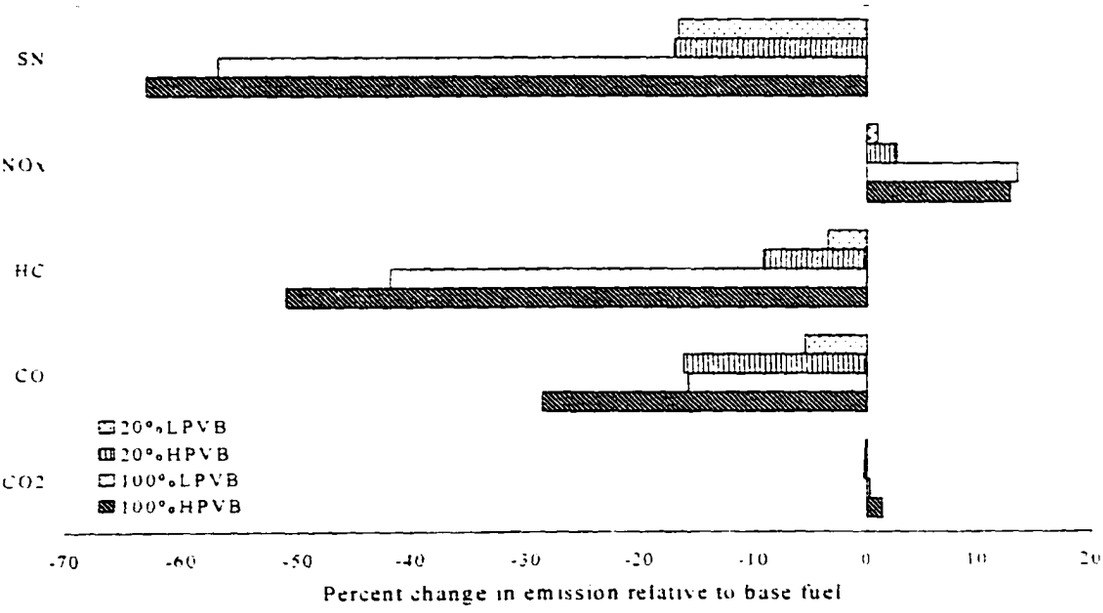

Figure 5. 25 Percent change in emissions for standard injection timing at full-load engine condition

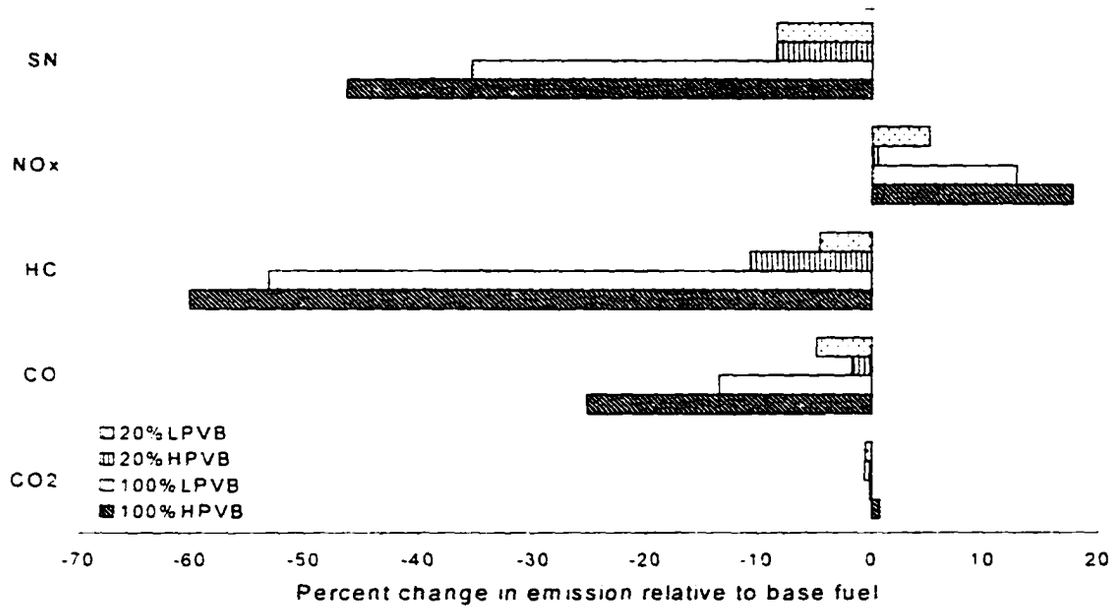

Figure 5.26 Percent change in emissions for 3° retarded injection timing at full-load engine condition

injection timings and the fuel blends, the smoke number, the CO emissions and HC emissions were reduced in the range of 8% to 63%, 2% to 29%, and 3% to 60%, respectively, while the NO_x emissions were increased in the range of 0.5% to 18%. Regardless of the injection timing, the oxidized neat biodiesel reduced the CO and HC emissions in the range of 4% to 15% and 9% to 16%, respectively, compared to unoxidized neat biodiesel. The emissions of CO_2 showed mixed results.

Figures 5.27 and 5.28 show the percent change in emissions at the full load engine condition for the 3° advanced and 3° retarded injection timings compared with standard timing. A reduction in CO emissions was observed for the 3° retarded injection timing. Compared to the 3° advanced injection timing, the standard injection timing reduced CO and HC emissions in the range of 33% to 47% and 4% to 28%, respectively, regardless of

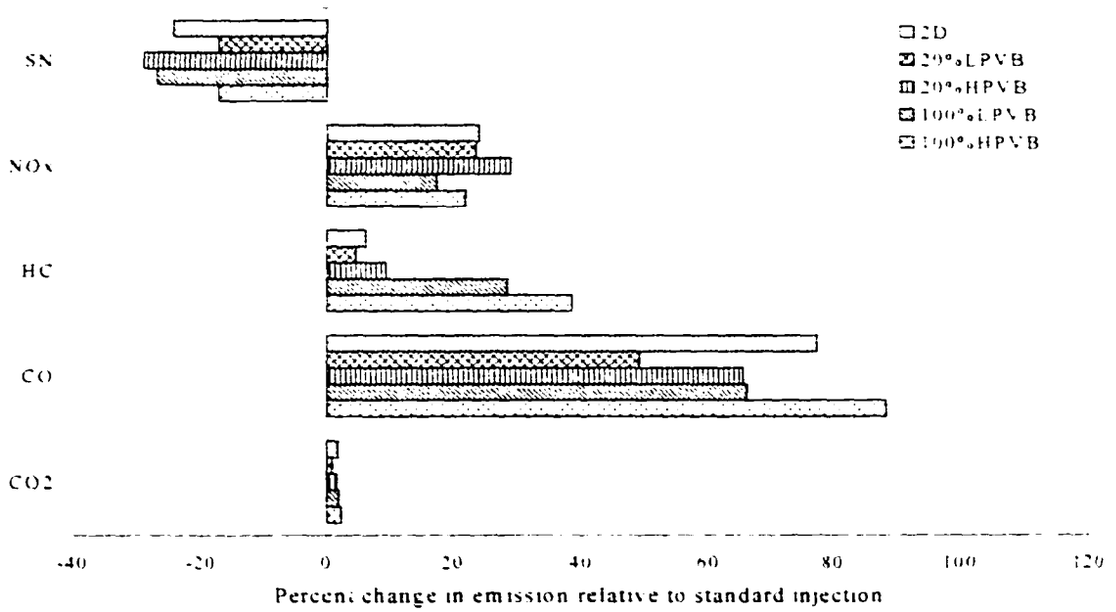

Figure 5.27 Percent change in emissions for 3° advanced injection timing (full-load)

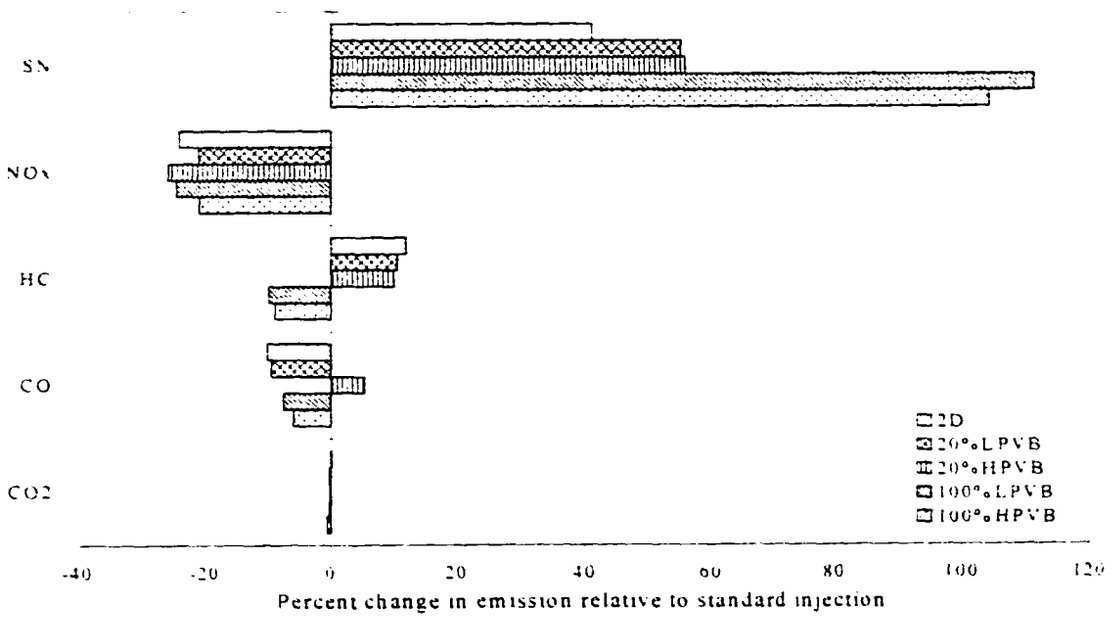

Figure 5.28 Percent change in emissions for 3° retarded injection timing (full-load)

fuels. The effect of fuel injection timing on the NO_x emissions is significant. A reduction on NO_x emissions in the range of 21% to 26% was observed for the 3° retarded injection timing while an increase in NO_x emissions in the range of 17% to 29% was observed for the 3° advanced injection timing. Smoke number behaved in an opposite manner to the NO_x emissions. At the 3° retarded injection timing, the smoke number were increased in the range of 41% to 112% while at the 3° advanced injection timing the smoke number were reduced in the range of 17% to 30% for the five fuels tested.

Figures 5.29, 5.30, and 5.31 show the percent change in emissions at the light-load engine condition for 3° advanced, standard, and 3° retarded injection timings, respectively. In these figures all emissions comparisons were made relative to the base fuel (No. 2 diesel). A reduction in CO and HC emissions were observed regardless of injection timing and fuel. These CO and HC reductions were in the range of 10% to 56% and 6% to 66%, respectively. The oxidized neat biodiesel reduced the CO and HC emissions more than unoxidized biodiesel in the range of 16% to 25% and 20% to 29%, respectively, over the range of injection timing studied. An increase in NO_x emissions was found for the 3° advanced injection timing for all fuel blends. However, a reduction in NO_x emissions was found for the 3° retarded injection timing for all fuel blends.

Figures 5.32 and 5.33 show the percent change in emissions for the 3° advanced and 3° retarded injection timings relative to the standard injection timing. It can be concluded that all of the emissions increase at the 3° advanced injection timing while all the emissions except CO_2 decrease at the 3° retarded injection timing. At the 3° advanced injection timing, the CO, HC, and NO_x emissions for all five fuels were increased in the

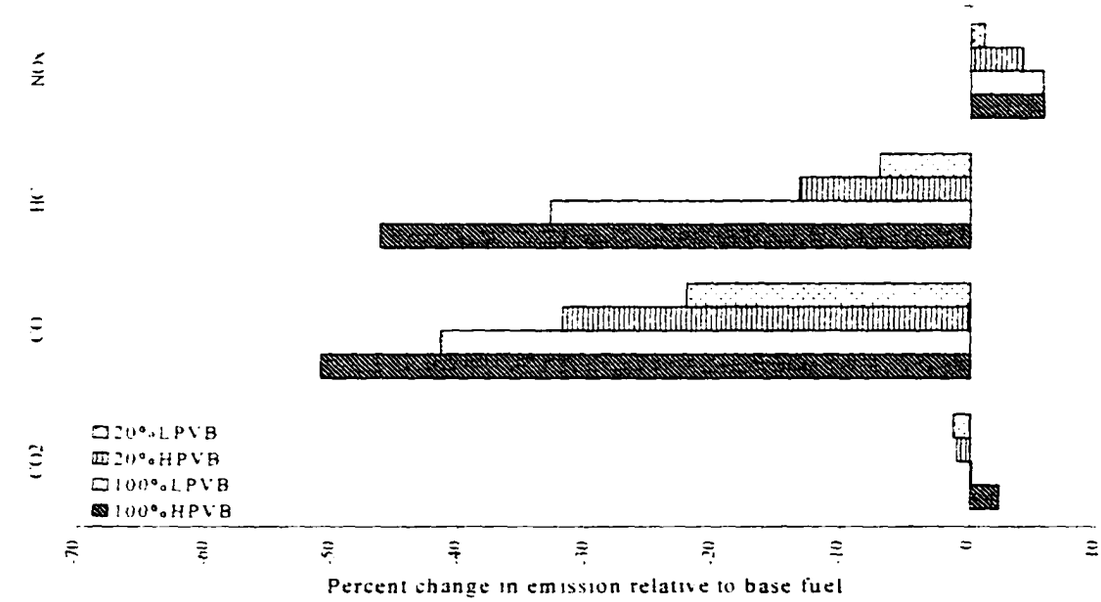

Figure 5.29 Percent change in emissions for 3° advanced injection timing at light-load engine condition

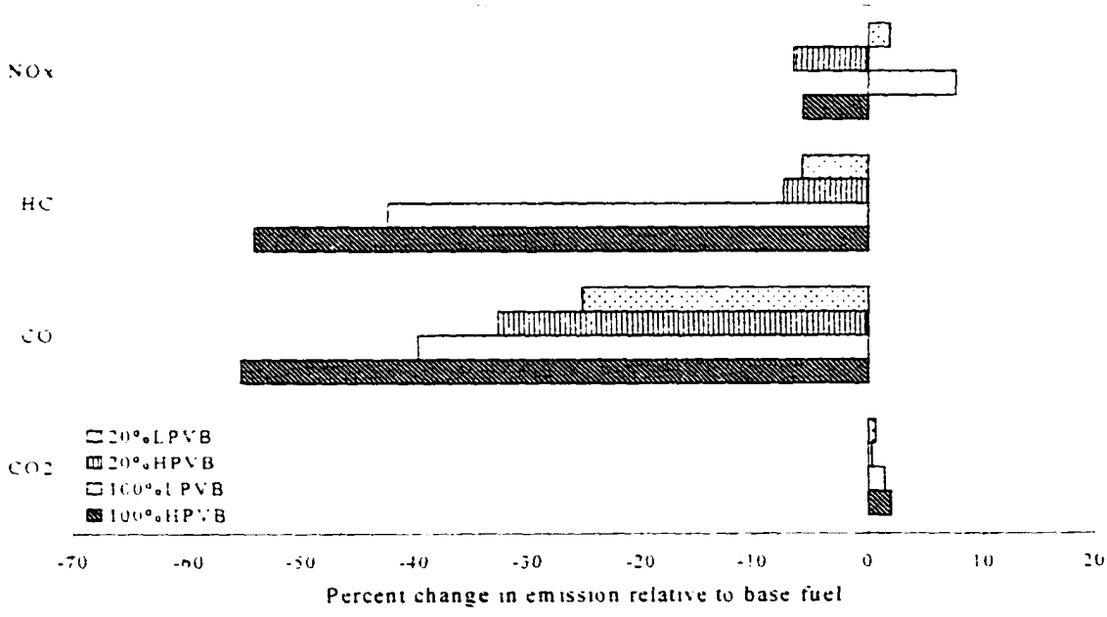

Figure 5.30 Percent change in emissions for standard injection timing at light-load engine condition

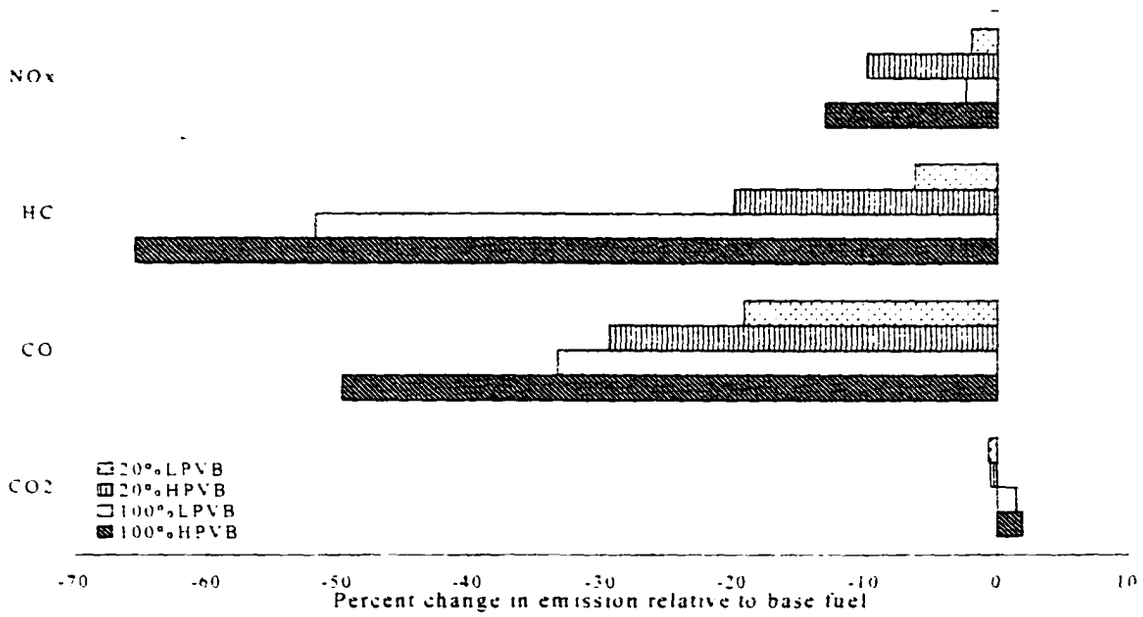

Figure 5.31 Percent change in emissions for 3° retarded injection timing at light load engine condition

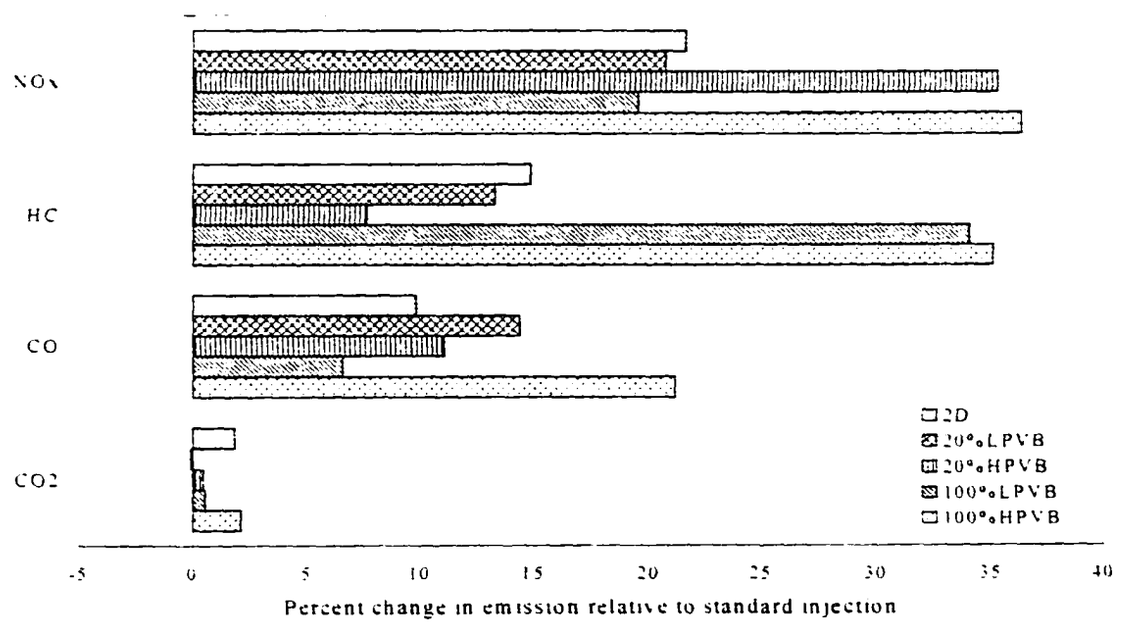

Figure 5.32 Percent change in emissions for 3° advanced injection timing (light-load)

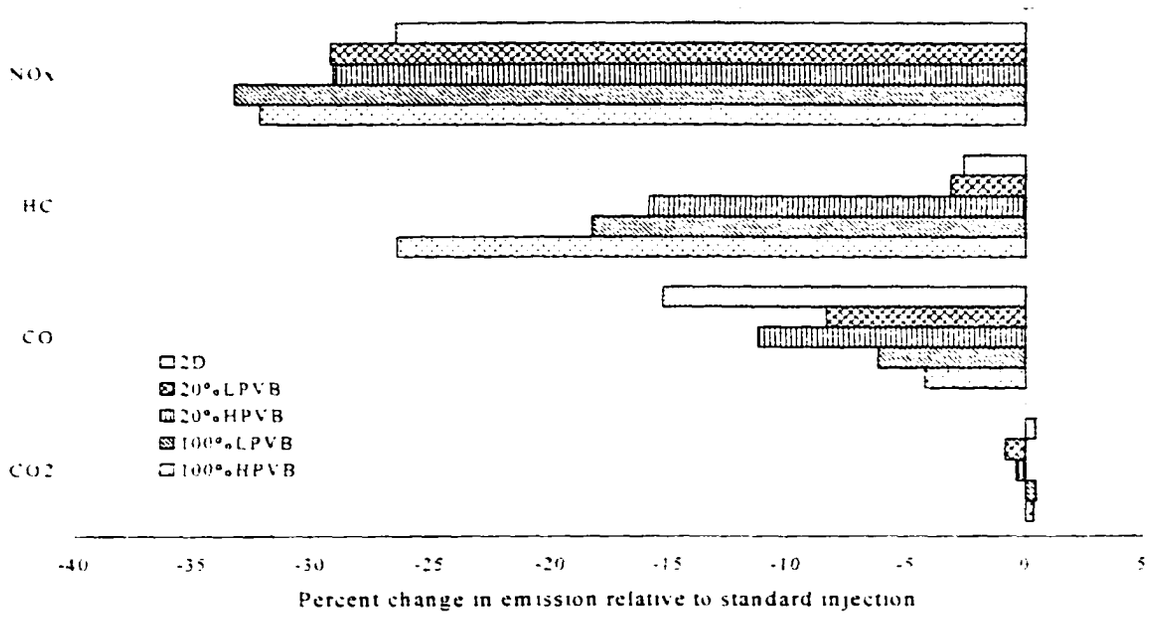

Figure 5.33 Percent change in emission for 3° retarded injection timing (light-load)

range of 6% to 21%, 7% to 35%, and 19% to 36% respectively. However, at the 3° retarded injection timing, the CO, HC, and NO_x emissions for the five fuels were decreased in the range of 4% to 15%, 3% to 26%, and 26% to 33% respectively. All of this data was discussed in detail in the previous sections.

5.3 Combustion Characteristics

In this section, a comparison of the injection pressure data for the different fuels and operating conditions will be presented first. Then, a comparison of the combustion characteristics will be presented in the second section. Finally, the effect of injection timing and fuel oxidation on the ignition delay will be presented.

5.3.1 Comparison of the start of fuel injection

Three different fuel injection pump settings were used for this study. They have been designated 3° retarded, standard, 3° advanced. The actual start of fuel injection will obviously be affected by this pump setting but it can also be influenced by changes in fuel properties such as the bulk modulus and speed of sound. The results of the statistical analysis for the start of fuel injection are shown in Table 5.9. It can be stated from this table that the change in the start of fuel injection that resulted from the change in the parameters, fuel batch, age of fuel, injection timing, fuel blends, load, and the interaction between fuel and load, timing and fuel, timing and load were all statistically significant. From the Tukey's grouping table shown in Appendix D, it can be stated that the effect of the different oxidized fuel batches on the start of fuel injection was statistically

Table 5.9 Analysis of variance (ANOVA) for start of fuel injection

Source	DF	Type I SS	Mean Square	F Value	Pr > F
Model	35	916.9045	26.1972	117.35	0.0001
BATCH*	2	3.4468	1.7234	633.35	0.0016
AGE*	2	4.7022	2.3511	864.03	0.0012
TIMING*	2	604.3450	302.1725	99999.99	0.0001
WHOLE PLOT ERROR	2	0.0054	0.0027		
FUEL*	4	37.0313	9.2578	41.44	0.0001
LOAD*	1	249.0342	249.0342	1114.62	0.0001
FUEL×LOAD*	4	7.3776	1.8444	8.26	0.0001
TIMING×FUEL*	8	7.2592	0.9074	4.06	0.0008
TIMING×LOAD*	2	2.1029	1.0514	4.71	0.0131
TIMING×FUEL×LOAD	8	1.5995	0.1999	0.89	0.5273
Error	54	12.0649	0.0234		
Corrected Total	89	928.9695			

R-Square = 0.987013
Start of fuel injection mean = 14.6861

significant. Three batches of fuel were oxidized for the entire test. Each batch of oxidized fuel lasted for three days of testing. The first, second and the third tests were day 1, day 2, and day3, respectively. The day 1, day 2, and day 3 oxidized biodiesels were about 24 hours, 72 hours, and 120 hours old, respectively, which were considered the ages of the oxidized biodiesel. The peroxide value (PV) of biodiesel changes with time and this is probably the reason the effect of the fuel age (24 hours, 72 hours, and 120 hours) on the start of fuel injection was statistically significant. All three injection timings' effect on the start of fuel injection were significantly different as would be expected. However, the differences between the fuels for the start of fuel injection were not all statistically significant. Neat biodiesel's effect on the start of fuel injection was significantly different than the other three fuels (the 20% blends and No. 2 diesel), but the difference between the neat biodiesels (100%HPV and 100%LPV) themselves were not significantly different. Similarly, the effect of the 20% blends (20%HPV, 20%LPV) and the No. 2 diesel fuel on the start of fuel injection were not significantly different from each other. The start of fuel injection is important because the fuel injected early will have more time to burn completely while the fuel injected late will have less time. The effect of changes in fuel injection timing on the start of combustion will be confounded by the effects of the different fuel cetane numbers. The cetane number has an effect on the time delay between when the fuel is injected and when it starts to burn. The higher the cetane number, the better the ignition quality of the fuel, and the faster the fuel will start to burn.

The injection line pressure at standard timing and the full load engine condition for all five tested fuels is shown in Figure 5.34. The start of fuel injection for

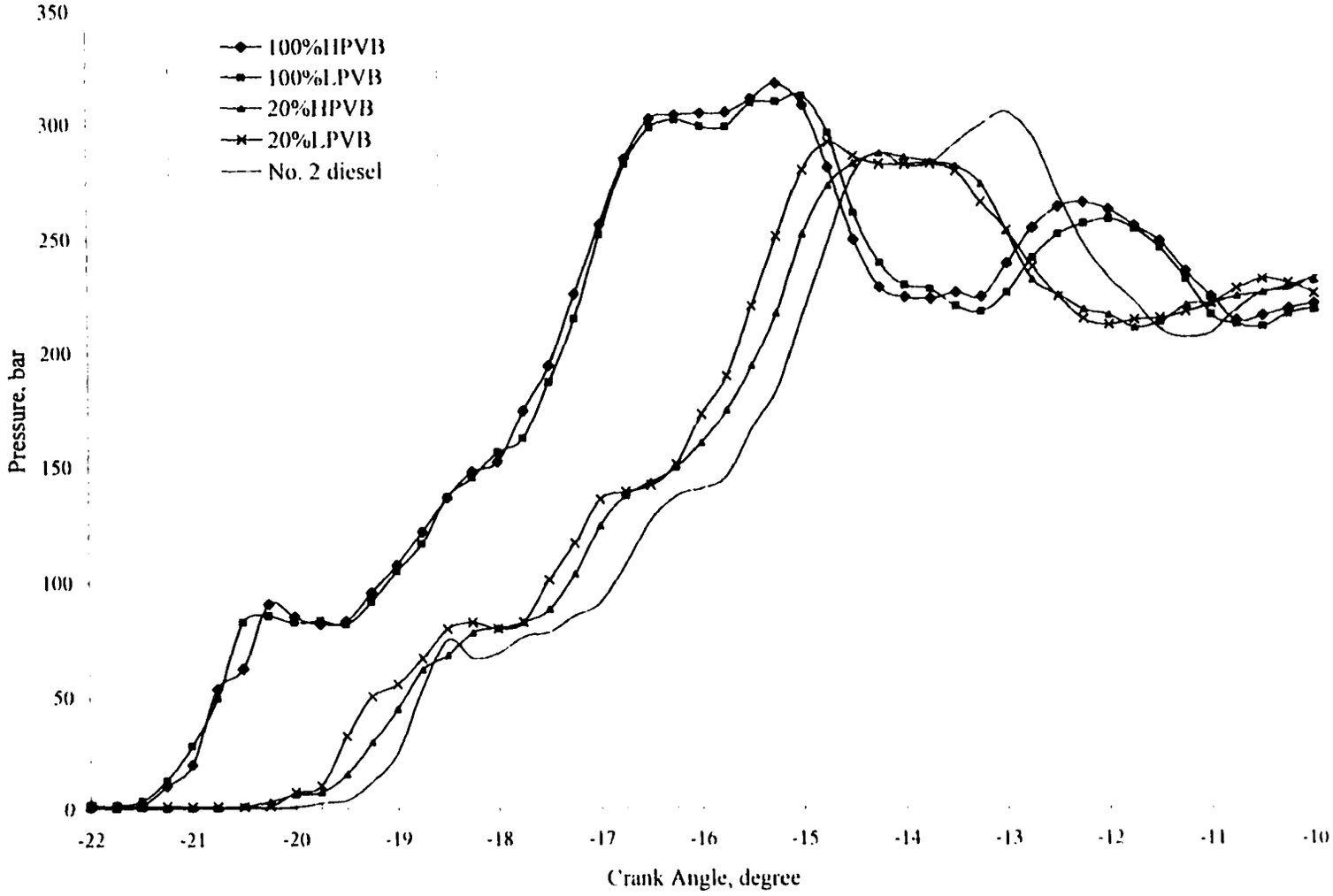

Figure 5.34 Injection line pressure for standard injection at full-load engine condition

100%HPVB, 100%LPVB, 20%HPV, 20%LPVB, and No. 2 diesel fuel were 17.4°, 17.3°, 15.4°, 15.6°, and 15.1° BTDC, respectively. The definition of the start of injection used in this study was the time when the injection line pressure had reached 207 bar. An injector nozzle tester tested three similar fuel injectors and the needle opening pressure for all the injectors was about 207 bar. This pressure was considered the start of fuel injection. The injector will open at a lower pressure than the peak injection pressure. The pressure in the injection line had the large amplitude pressure waves. These pressure waves may not be the characteristic of the actual injection pressure.

The 100%HPV and 100%LPV biodiesel fuel both injected about 2.3° earlier than the base fuel (No.2 diesel) and the blends (20%HPVB and 20%LPVB). All three blends (20%HPV, 20%LPV, and No. 2 diesel) had almost the same start of fuel injection. The peak injection line pressure for the 100% biodiesels was about 310 bars while the 20% blends and the base fuel had slightly lower peak injection pressures.

Figure 5.35 shows the injection line pressures at the light-load engine condition for all five tested fuels. In this case the 100% biodiesels still show a more advanced injection timing than the No. 2 diesel and the 20% blends. The 100%HPV biodiesel injected about 2.0° before the base fuel while the 100%LPV biodiesel injected about 1.2° before the base fuel. The 20% blends and the base fuel show almost the same injection timing. The peak injection pressures for the fuels were all about 293 bars.

Figures 5.36 and 5.37 show the start of fuel injection into the cylinder for all three injection timings (3° advanced, standard, and 3° retarded) at the full and light load engine conditions. Each bar on these figures is the average of three days of data. The error bands

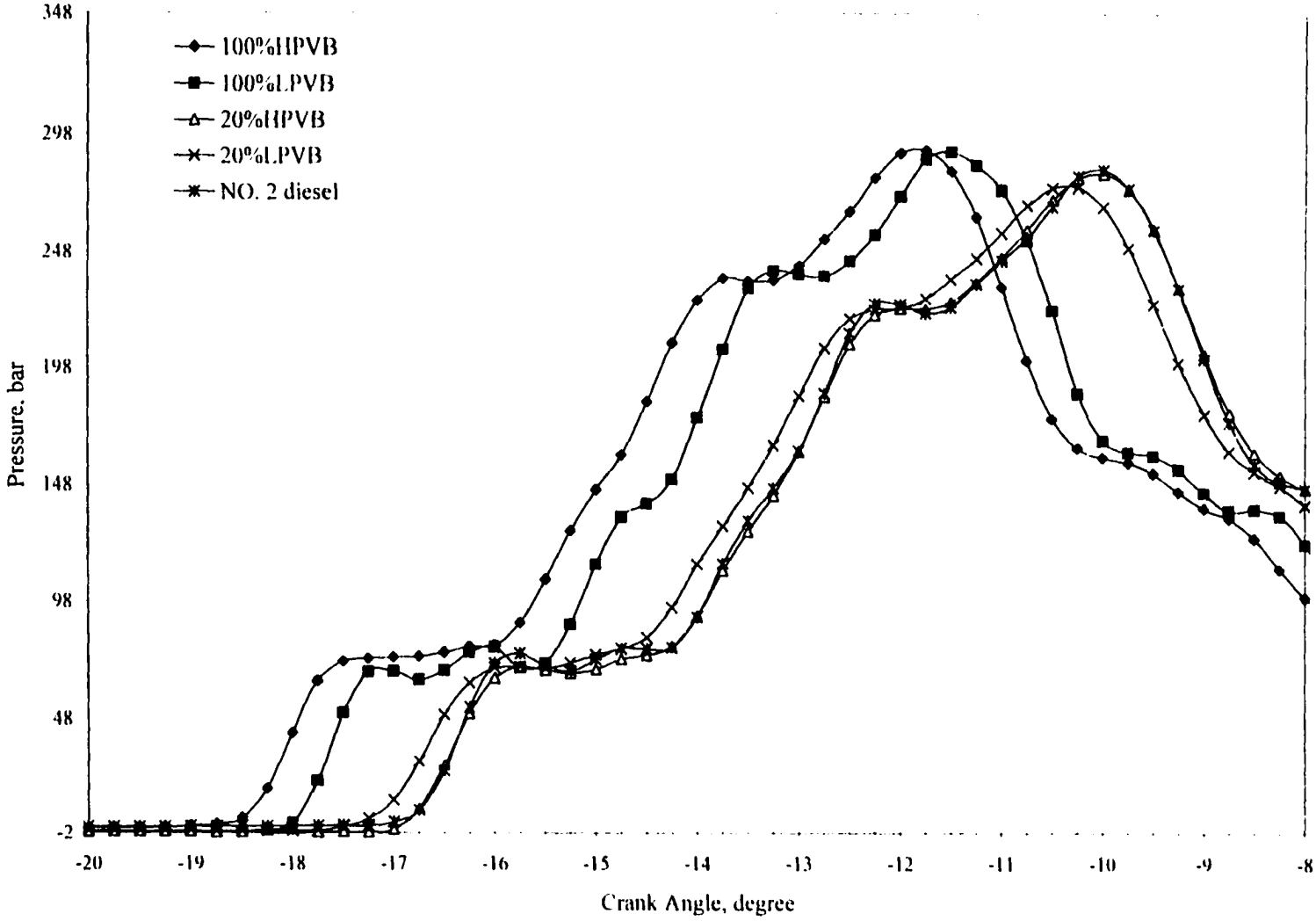

Figure 5.35 Injection line pressure for standard injection at light-load engine condition

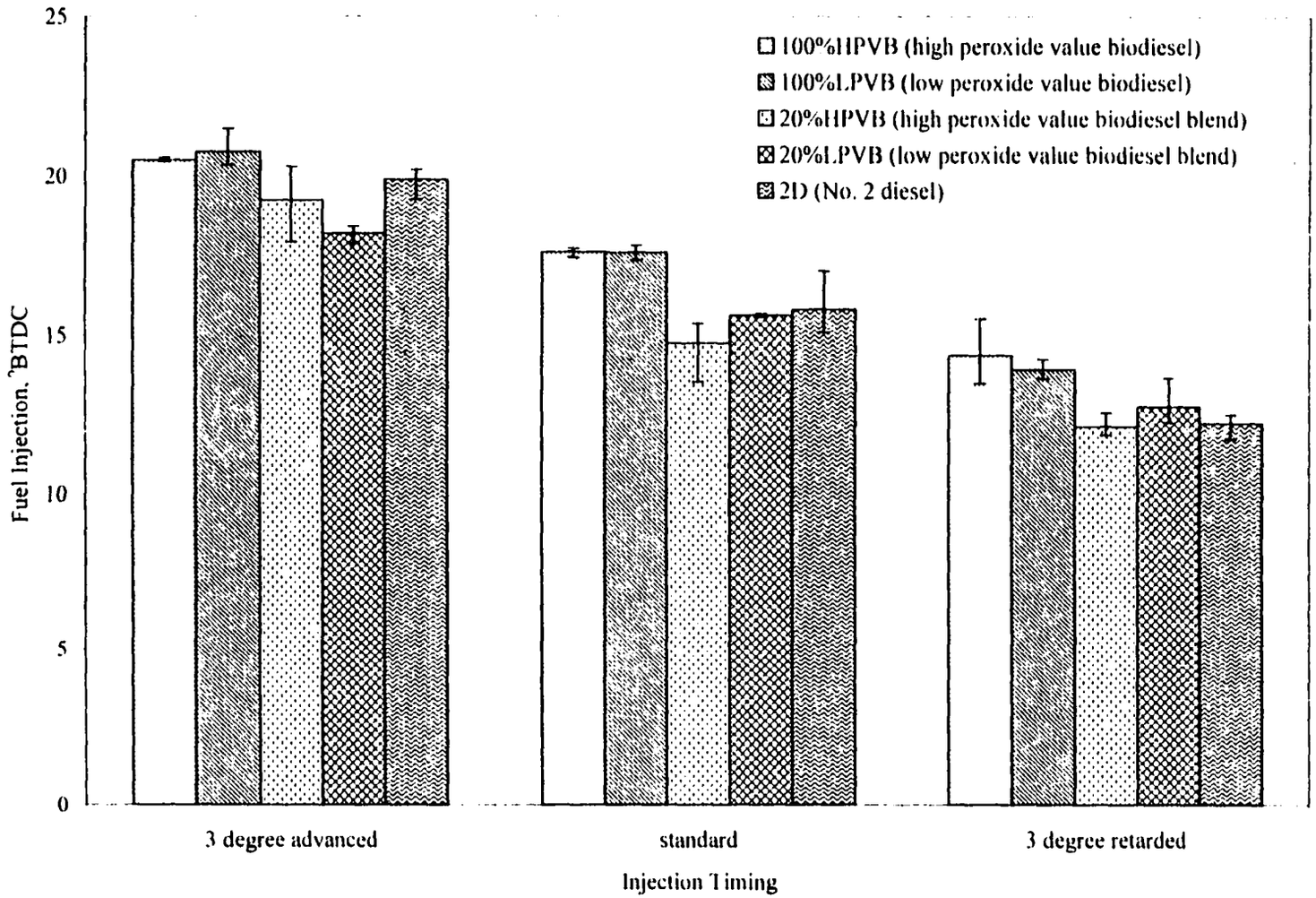

Figure 5.36 Fuel injection at full-load engine condition

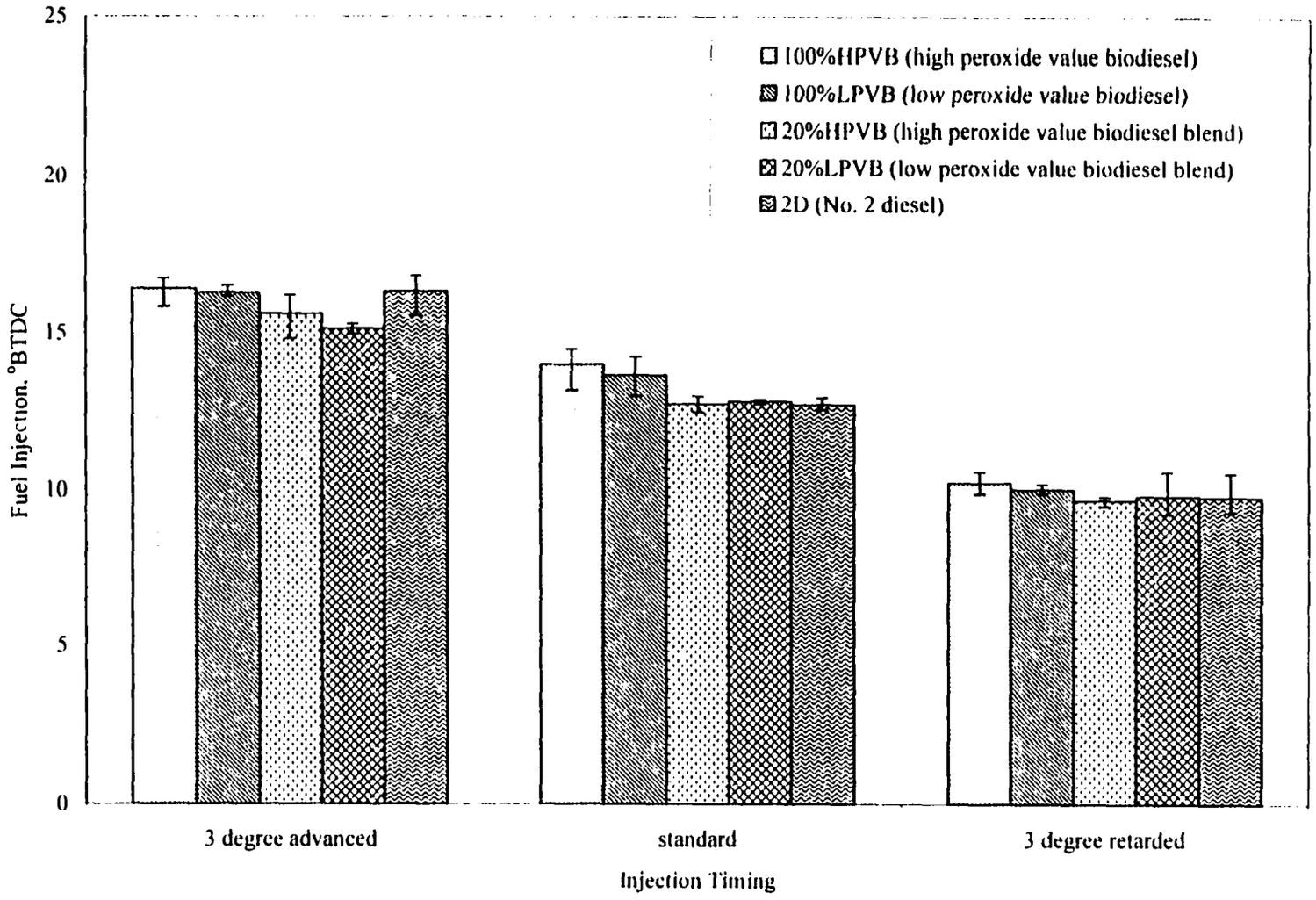

Figure 5.37 Fuel injection at light-load engine condition

show the extent of maximum and minimum value of the three. The injection timings were set every day and were confirmed using the data acquisition system. In the injection line pressure for some days, there were some unexplained anomalies. For example, at the full load engine condition on day 2 (3° advanced injection timing) the start of fuel injection for No. 2 diesel fuel was about 2° more advanced than the blends while it should be close or somewhat retarded from the blends.

5.3.2 Comparison of the start of combustion times and fuel burning rates

Table 5.10 shows the statistical results of the analysis of variance for the start of combustion. The definition of the start of combustion used in this study was the time when the slope of the heat release rate determined from the cylinder pressure data started

Table 5.10 Analysis of variance (ANOVA) for start of combustion

Source	DF	Type I SS	Mean Square	F Value	Pr > F
Model	35	1203.2036	34.3772	209.87	0.0001
BATCH*	2	4.1946	2.0973	34.76	0.0280
AGE*	3	3.5060	1.1687	29.06	0.0333
TIMING*	2	413.0006	206.5003	3422.66	0.0003
WHOLE PLOT ERROR	2	0.1206	0.0603		
FUEL*	4	159.4206	39.8551	243.31	0.0001
LOAD*	1	613.0890	613.0890	3742.86	0.0001
FUEL×LOAD*	4	2.4682	0.6170	3.77	0.0090
TIMING×FUEL*	8	5.3026	0.6628	4.05	0.0006
TIMING×LOAD	2	0.6020	0.3010	1.84	0.1690
TIMING×FUEL×LOAD	8	1.4991	0.1873	1.14	0.3499
Error	54	8.8453	0.1638		
Corrected Total	89	1212.0490			

R-Square= 0.992702
Start of combustion mean=7.40333

to rise rapidly. The significant factors that affect the start of combustion are fuel batch, age, injection timing, load, fuel, the interaction between fuel and load, and the interaction between timing and fuel. From the Tukey table in Appendix D, fuel batch one is significantly different from fuel batch two, but batch one and batch three, and batch two and batch three are not significantly different from each other. Like batch, age level 1 and age level 2 are significantly different. The time elapsed after oxidizing the biodiesel was defined as the age of the fuel. Age level 1 is one day old oxidized biodiesel and age level 2 is 3 day old oxidized biodiesel. The effect of all injection timings on the start of combustion was significantly different. Also, all fuels except for the base fuel and the 20%LPV biodiesel were shown to have starts of combustion that were statistically different.

Figures 5.38 and 5.39 show the heat release profiles for No. 2 diesel and 100%HPV biodiesel, respectively, for the three different injection timings. As the injection timing was retarded, a decreasing amount of the combustion takes place during the premixed portion of the combustion, and there is a corresponding increase in the diffusion phase. The premixed portion of the heat release curve is the spike that occurs shortly after ignition. This phenomenon was true for both No. 2 diesel fuel and the 100%HPV biodiesel. However, the peak premixed fuel burning rate for the No. 2 diesel fuel was higher than for the 100%HPV biodiesel. The No. 2 diesel fuel has a lower cetane number than the oxidized biodiesel [24]. For low cetane fuels with longer ignition delays, a larger fraction of the fuel is injected before ignition occurs, which results in very rapid burning rates once combustion starts. These rapid burning rates give high rates of

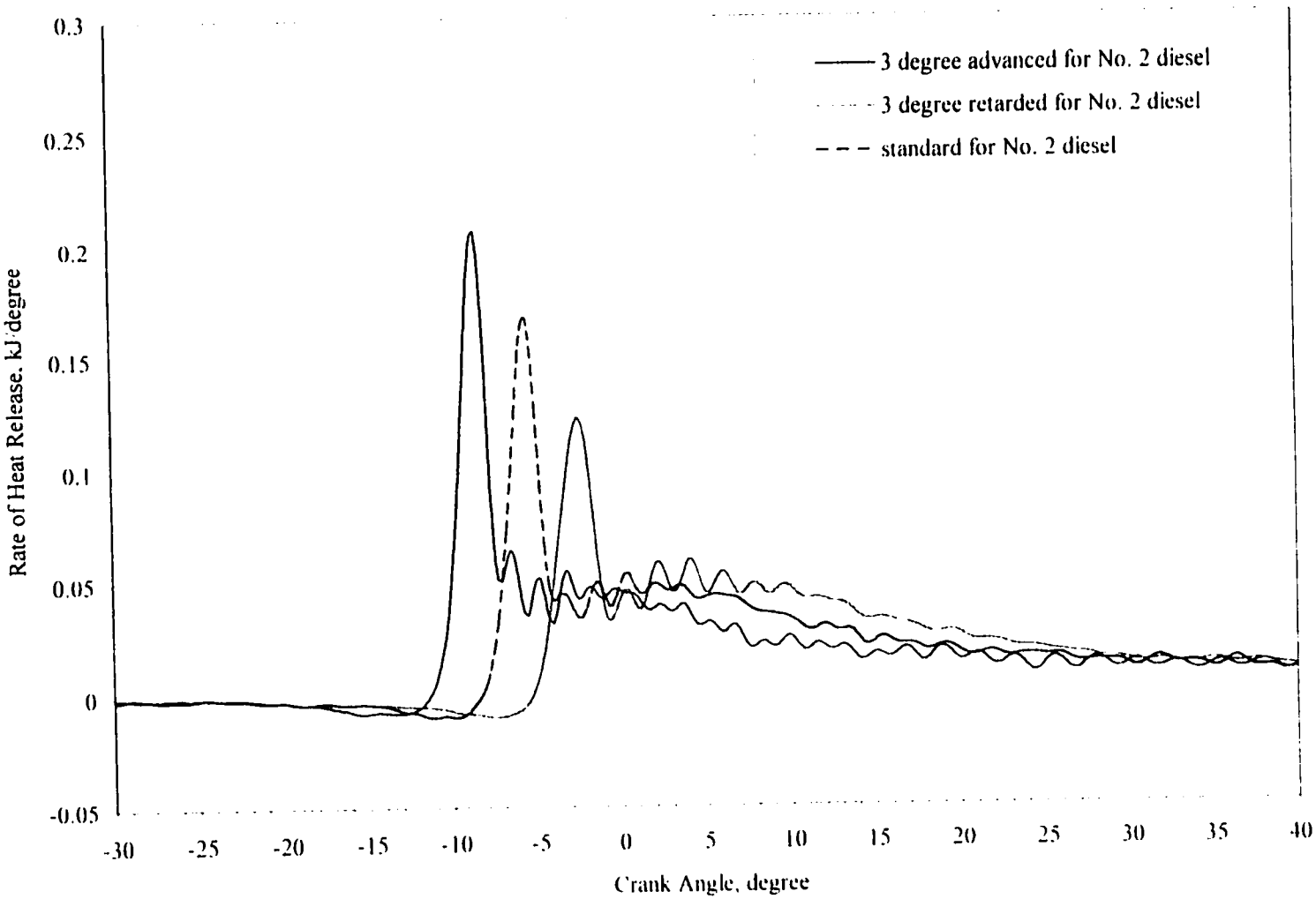

Figure 5.38 Heat release profiles for No. 2 diesel fuel at full-load engine condition

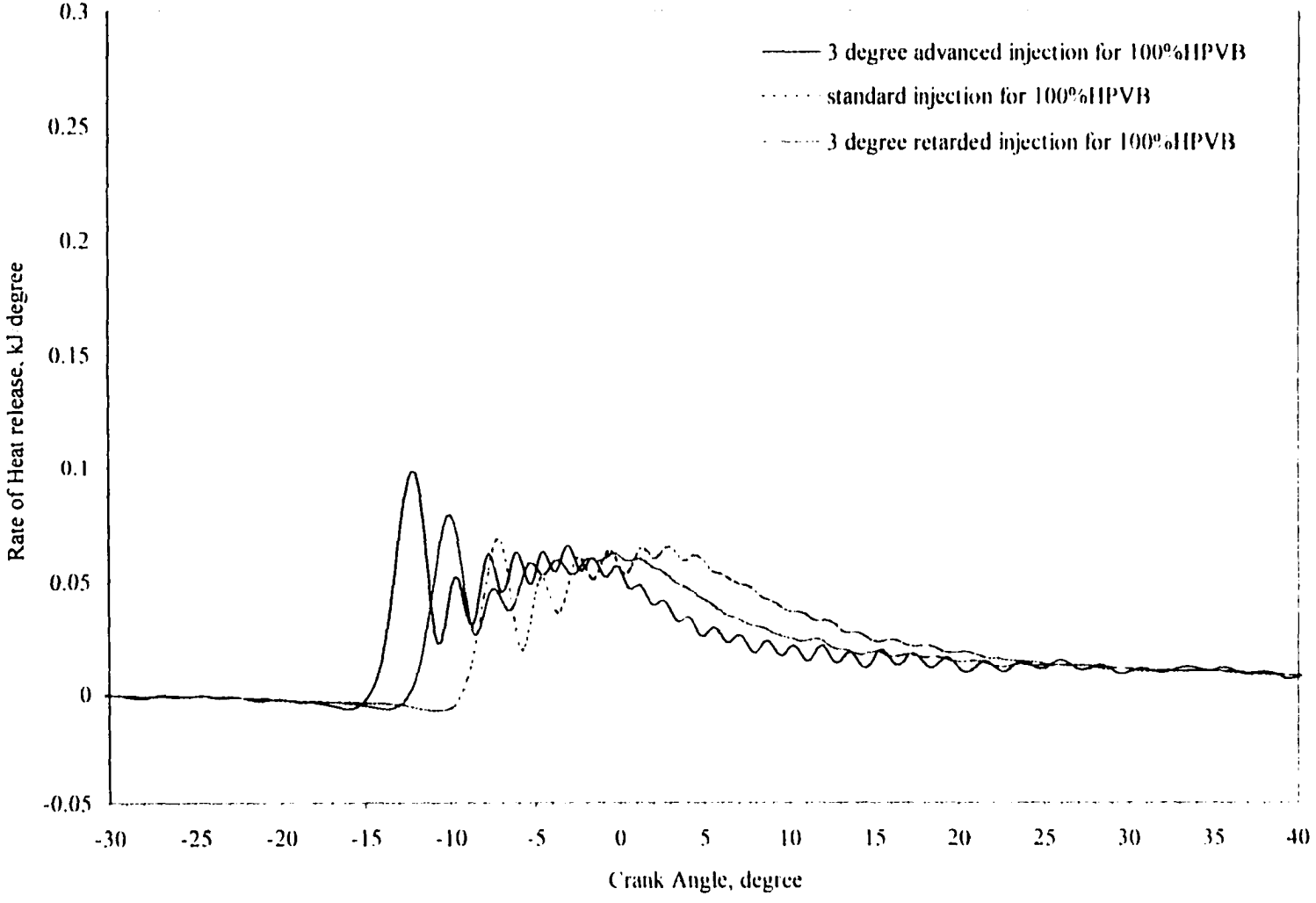

Figure 5.39 Heat release profiles for 100%HPV biodiesel at full-load engine condition

pressure rise and high peak pressure. An almost identical result was found by Ali [83] and Scholl et al. [1].

Figure 5.40 shows the heat release profiles at standard timing for all five fuels. The 100%HPV biodiesel showed the most advanced start of combustion of the 5 fuels. The next most advanced start of combustion was found for the 100%LPV biodiesel. The 20% blends and No. 2 diesel fuel show almost no difference in the start of combustion. Compared to the base fuel, the oxidized 100%HPB biodiesel had about 3.3° earlier start of combustion at the standard timing, while 100%LPV biodiesel had only 2.3° earlier start of combustion.

Figures 5.41 and 5.42 show the start of combustion at three different timings for the full and light load engine conditions. The start of combustion advanced for the 100%HPV biodiesel compared to No. 2 diesel fuel. The 100%LPV biodiesel also advanced the start of combustion but the other fuels (the 20% blends and No. 2 diesel) showed mixed results at the full load engine condition. At the light–load engine condition, the start of combustion occurred later than at the full-load engine condition. The 100%HPV biodiesel at this load showed the most advanced start of combustion while the No. 2 diesel fuel showed the most retarded.

5.3.3 The effect of timing and fuel oxidation on ignition delay

The analysis of variance (ANOVA) table for ignition delay is shown in Table 5.11. The significant factors that affect the ignition delay are injection timing, fuel, load, the interaction between fuel and load, and timing and load. All injection timings have a

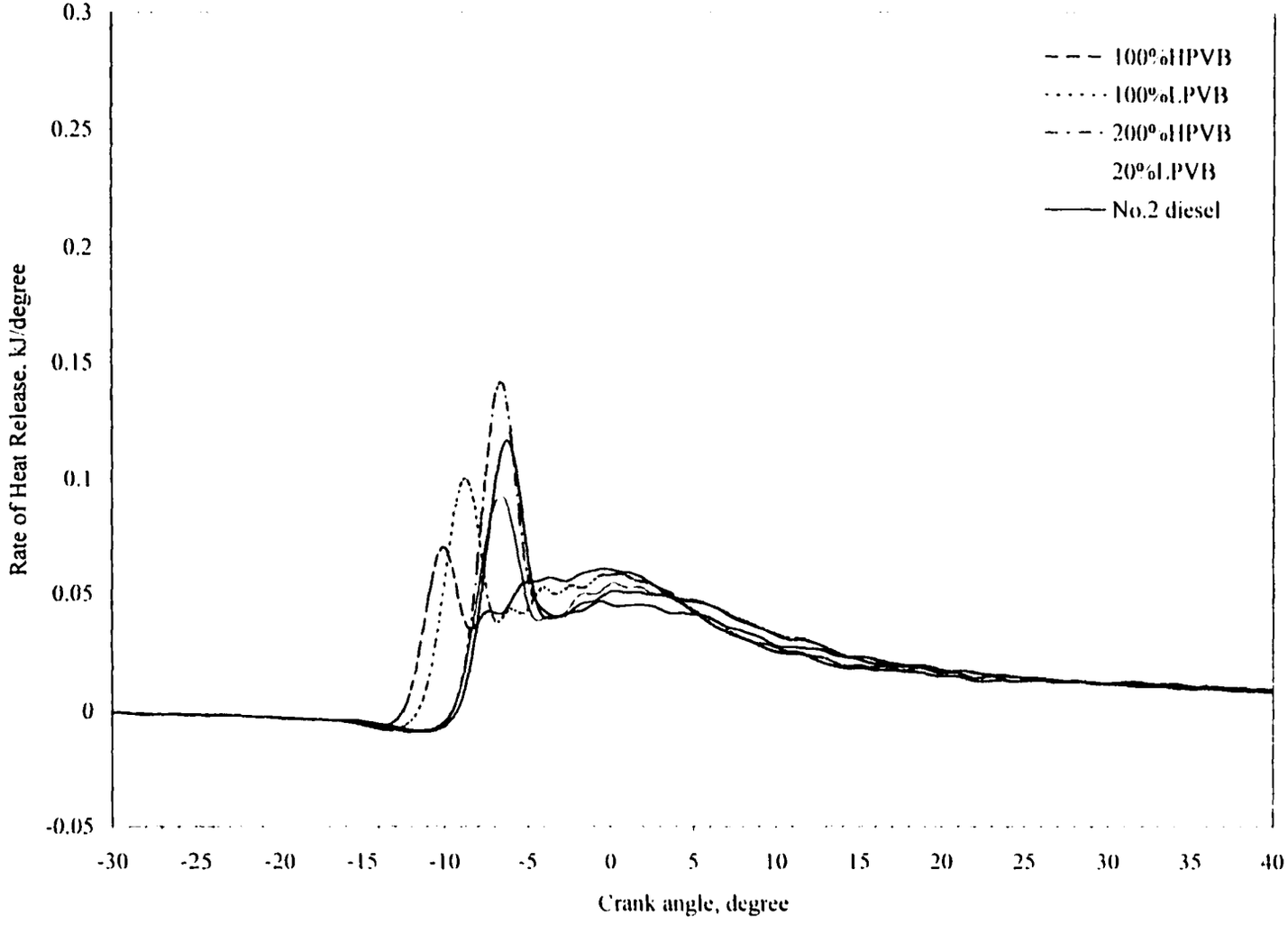

Figure 5.40 Heat release profiles at standard injection timing at full-load engine condition

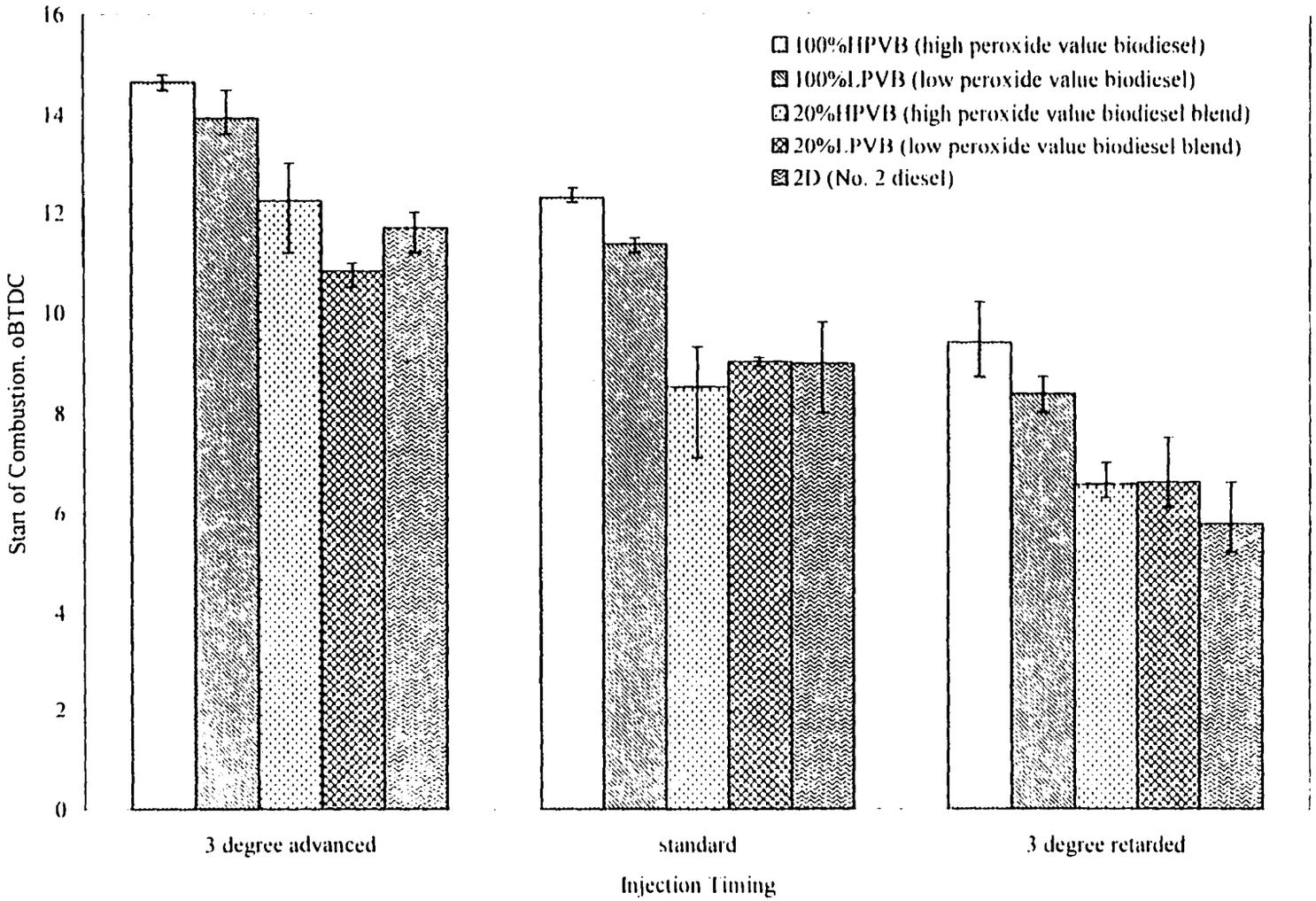

Figure 5.41 Start of combustion at full-load engine condition

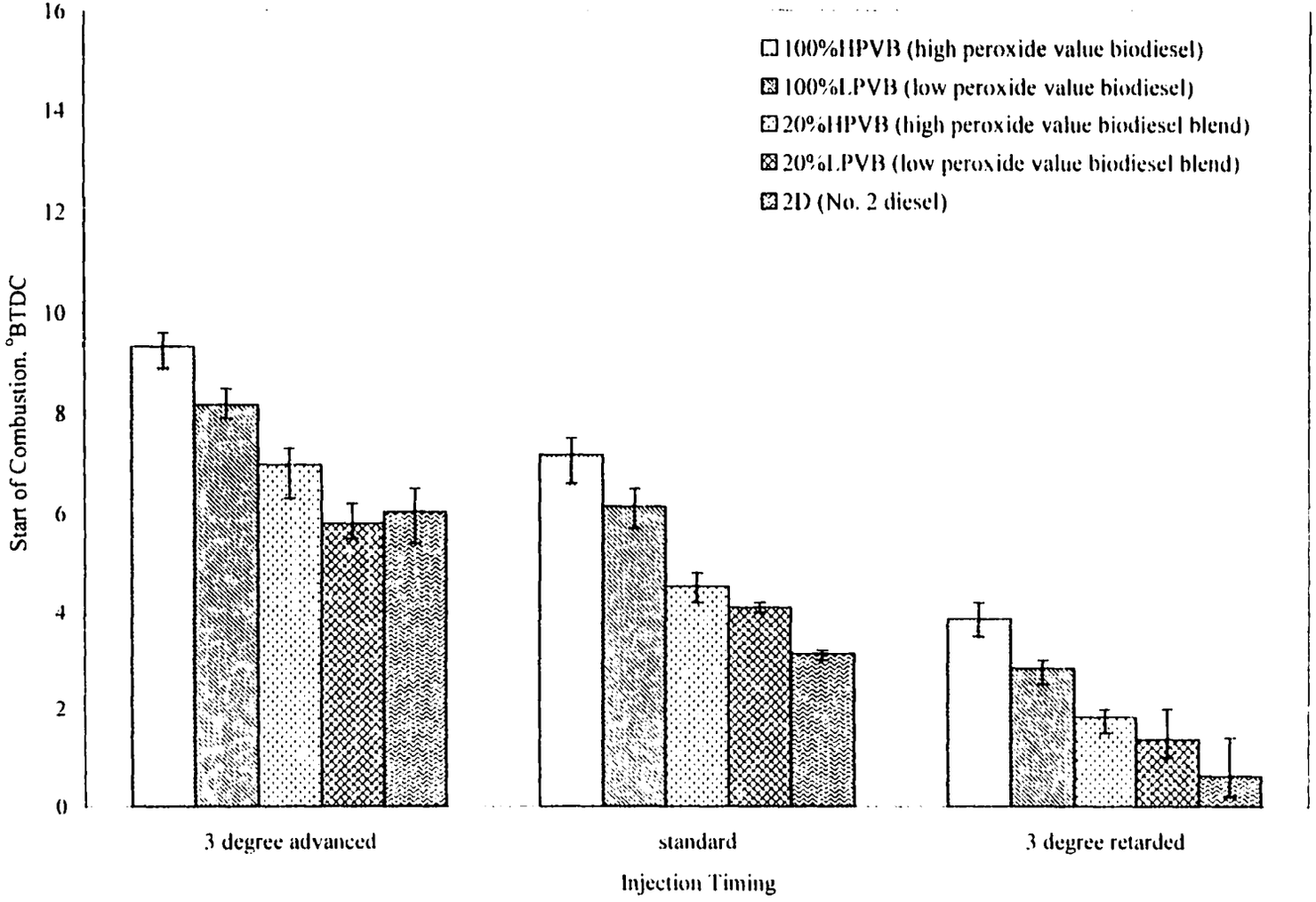

Figure 5.42 Start of combustion at light-load engine condition

significant effect on ignition delay. Also, all fuels have ignition delays that are significantly different from each other.

The ignition delay is the time between the start of injection and the start of combustion. The fuel injection data were taken immediately after the cylinder pressure data and were the average of fifty cycles. Both injection and cylinder pressures were taken every quarter of a degree of crank-shaft rotation and then the injection pressures were plotted to identify the injection timing. The start of combustion was identified from the change in slope of the heat-release rate, determined from cylinder pressure data using the techniques described in the previous chapter. The ignition delay is the time interval between the start of injection and the start of combustion.

Table 5.11 Analysis of variance (ANOVA) for ignition delay

Source	DF	Type I SS	Mean Square	F Value	Pr > F
Model	38	162.8721	4.6449	46.99	0.0001
BATCH	2	0.2392	0.1196	1.64	0.3792
AGE	2	0.1766	0.0883	1.21	0.4626
TIMING*	2	18.5229	9.2614	126.[illegible]	0.0079
WHOLE PLOT ERROR	2	0.1461	0.0730		
FUEL*	4	56.7050	14.1762	143.41	0.0001
LOAD*	1	80.6370	80.6370	815.72	0.0001
FUEL×LOAD*	4	4.2815	1.0703	10.83	0.0001
TIMING×FUEL	8	0.9004	0.1125	1.14	0.3532
TIMING×LOAD*	2	0.6648	0.3324	3.36	0.0421
TIMING×FUEL×LOAD	8	0.2982	0.0372	0.38	0.9282
Error	54	5.3380	0.0988		
Corrected Total	89	167.9102			

R-Square = 0.968209
Ignition delay mean = 7.28278

Figure 5.43 shows the ignition delay for the five fuels at the three injection timings. The delay was significantly different for the neat biodiesel and the blends. It can be seen from the figure that the oxidized biodiesel (100%HPV) had the shortest ignition delay of the four fuels. At the standard timing, the 100%HPV biodiesel had a 1.5° shorter ignition delay than the base fuel while the delay for the 100%LPV biodiesel was only about 0.6° shorter. This is probably because of the higher cetane number of the 100%HPV biodiesel compared with the 100%LPV biodiesel. Higher cetane number fuels give shorter ignition delays [69].

Advanced injection timing increased the ignition delay. For the earlier injection, the initial air temperature and pressure are lower so the delay will be increased. Neat oxidized biodiesel at the 3° retarded injection timing had a 0.9° shorter ignition delay than the 3° advanced injection timing.

Both physical and chemical processes take place during the ignition delay period. The effects of changes in the physical and chemical properties of fuels on the delay period have been studied by Glavincevske [70] and it was found that the chemical characteristics of the fuel are much more important. The ignition quality of the fuel, defined by its cetane number, has the greatest effect on the delay. The cetane number has been shown to increase as the biodiesel oxidizes [24]. Fuel viscosity has been found to have no effect on the ignition delay [81]. The cetane number of commercial diesel fuel is normally in the range of 40 to 46, while the cetane number of soybean-based biodiesel is between 46 and 55. The cetane number of biodiesel depends on the level of oxidation of the fuel. The cetane number of oxidized soybean-based biodiesel with a peroxide value

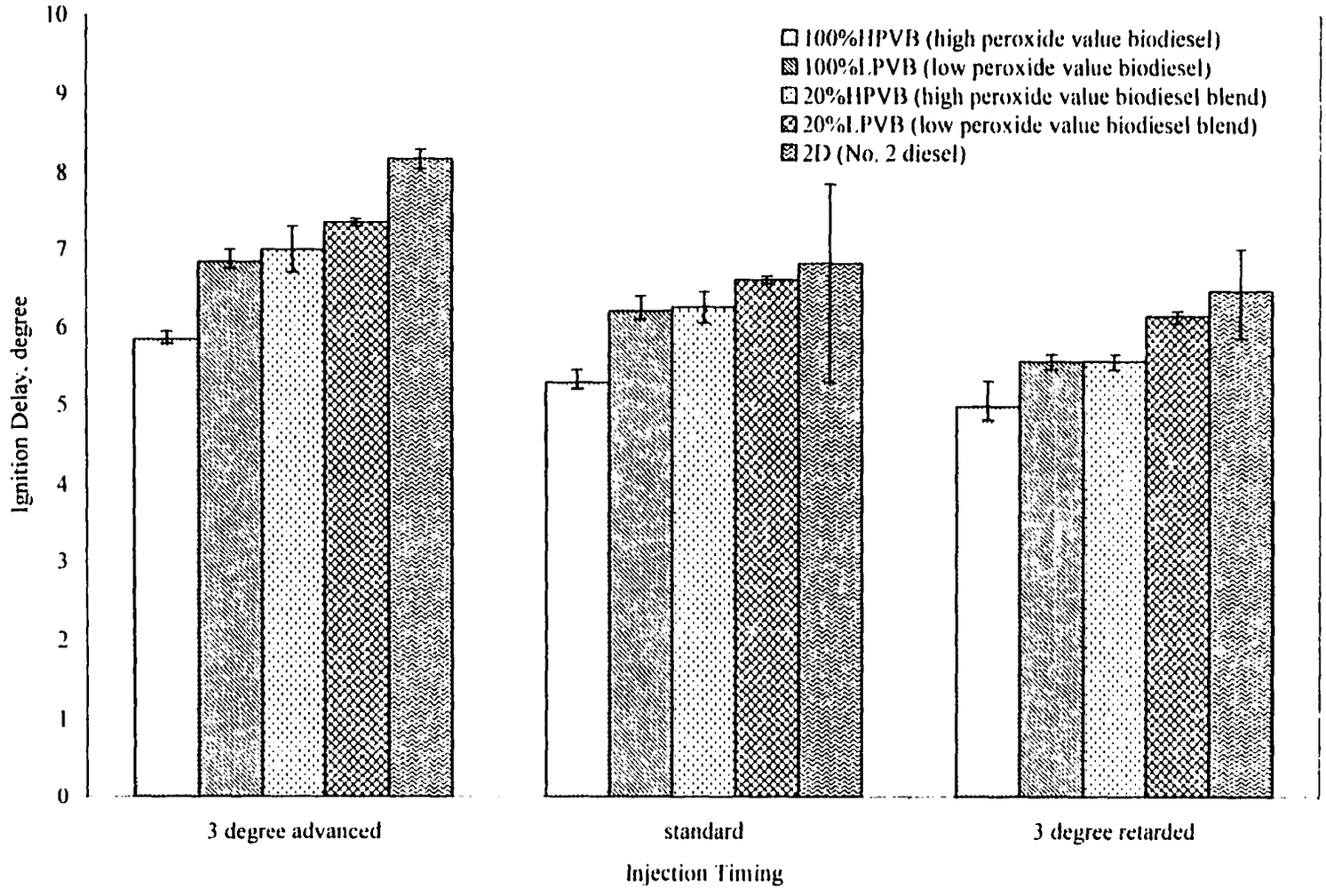

Figure 5.43 Ignition delay at full-load engine condition

81 is about 54.6 [24]. Even non-oxidized biodiesel has a higher cetane number than No. 2 diesel fuel and that is why the non-oxidized (100%) biodiesel has less ignition delay than the No. 2 diesel fuel.

Figure 5.44 shows the average of three days of data for each blend at all timings. The retarded injection timing has the lowest delay and the advanced injection timing has the highest. This was true for both 100% and 20% loads and for the diesel baseline. The 20% load had a longer ignition delay than 100% load. Wong et al. [81] found that the delay increases approximately linearly with decreasing load for direct injection diesel engines. The injection timing for the retarded timing was about 11° while for the advanced timing it was about 18°. A similar result was found by Lyn [62]. He found that at normal injection conditions the minimum delay occurs with the start of injection at about 10° to 15° BTDC. The calculated ignition delay is probably slightly off because of the start of injection was determined from the fuel line pressure which may be somewhat different than the actual needle lift.

5.4 Discussion of Observed Trends

In this section the effect of ignition delay, start of injection, and start of combustion on engine emissions will be discussed. The first two sections will discuss the effect of ignition delay on the HC and CO emissions. The next two sections will discuss the effect of the start of injection and the start of combustion on the NO_x emissions and the effect of the start of fuel injection on the smoke number. Finally, the tradeoff between NO_x emissions and smoke number, and CO and HC emissions will be discussed.

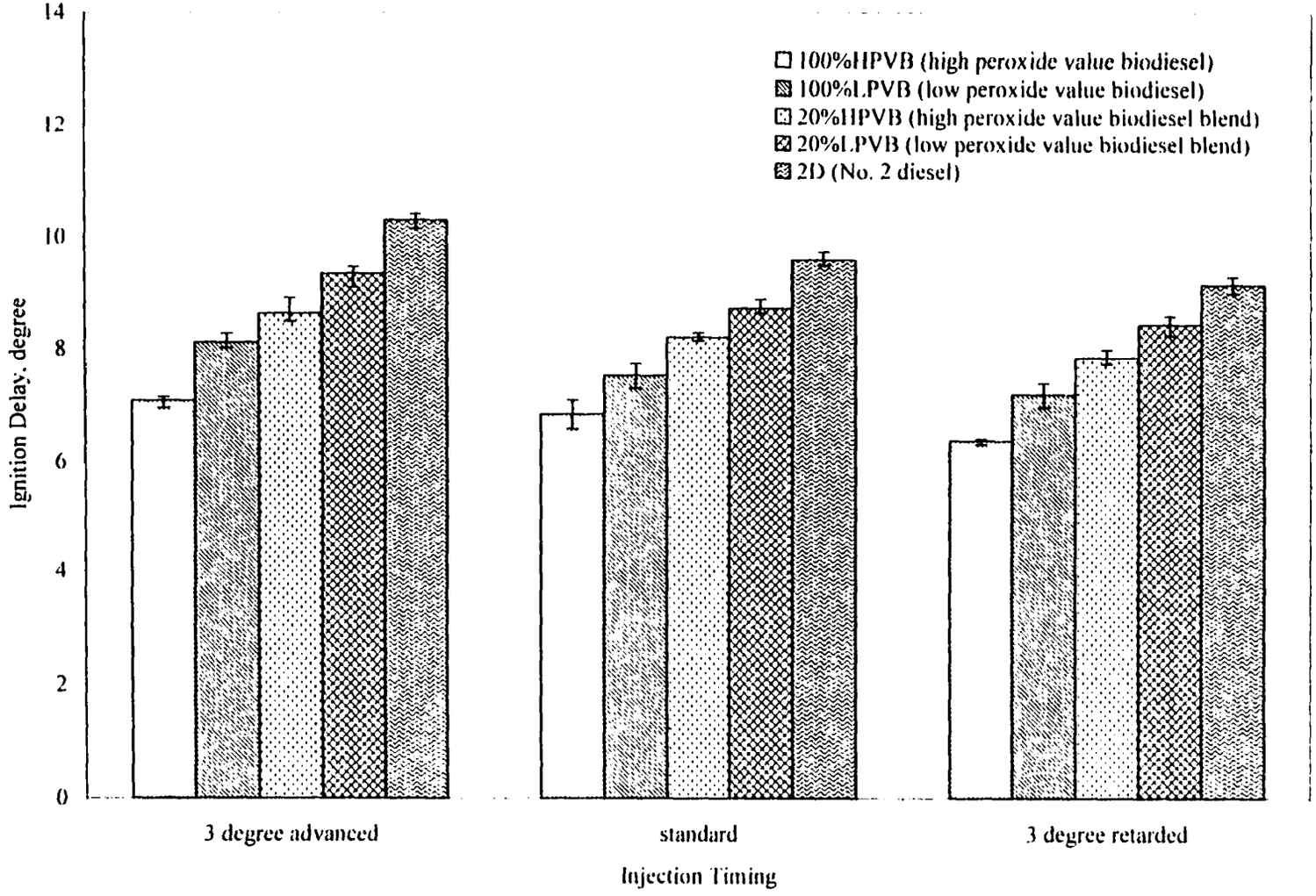

Figure 5.44 Ignition delay at light-load engine condition

5.4.1 Effect of ignition delay on HC emissions

There are two identified sources of unburned hydrocarbon (HC) emissions in diesel engines. One is in regions where excessive dilution with air prevents the combustion because the fuel-air mixture is past the lean combustion limit. The magnitude of the unburned HC from over-lean regions will be related to the amount of fuel injected during the ignition delay period, before combustion starts. The second source is the fuel that vaporizes from the nozzle sac volume during the later stage of combustion and during the exhaust stroke. Caton et al. [82] found that as the delay period increases beyond a certain value (11°), the HC emissions increase at an increasing rate.

The HC emission data were plotted for all the fuels and all injection timings against the ignition delay. Figures 5.45 and 5.46 show the correlation between HC emissions and the ignition delay for the full load and light load operating conditions. The HC emissions decrease as the ignition delay gets shorter. The neat biodiesels have a shorter ignition delay which results in less HC emissions while the No. 2 diesel fuel has higher HC emissions because of its longer ignition delay. The lower points on the figures represent the neat biodiesel while the upper points represent the No. 2 diesel fuel. The intermediate points represent the blends. The linear relationship is clearly more pronounced for the light load engine condition and this may be because of its higher HC emissions. The light load HC emissions are about six times higher than at full load. This due to the greater likelihood of overmixing due to the higher air/fuel ratio at low load. These HC emissions for all fuels and for all injection timings fall on one line. This indicates that the difference in HC emissions is related to the ignition delay and may not

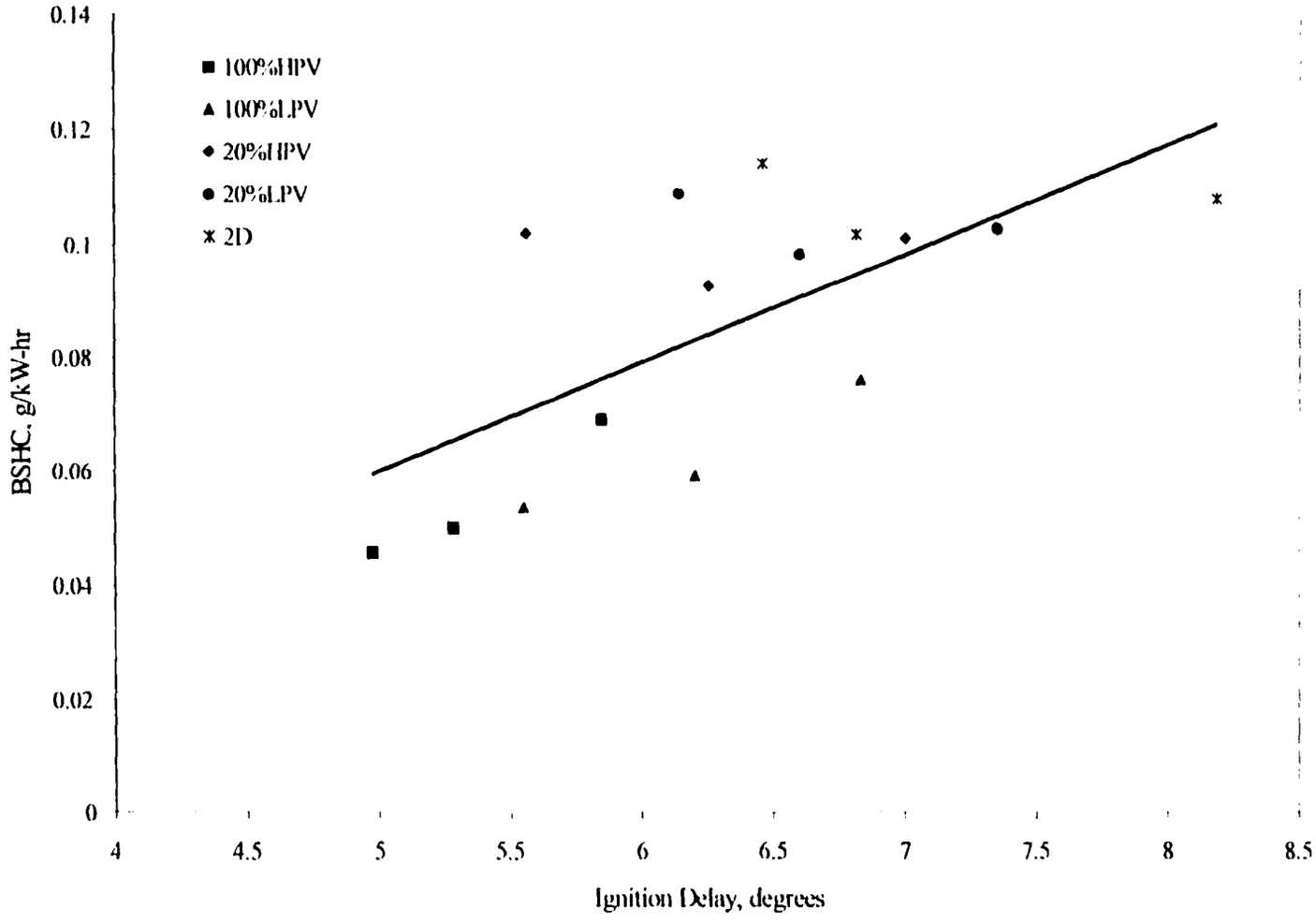

Figure 5.45 BSHC emissions as a function of ignition delay at full-load engine condition

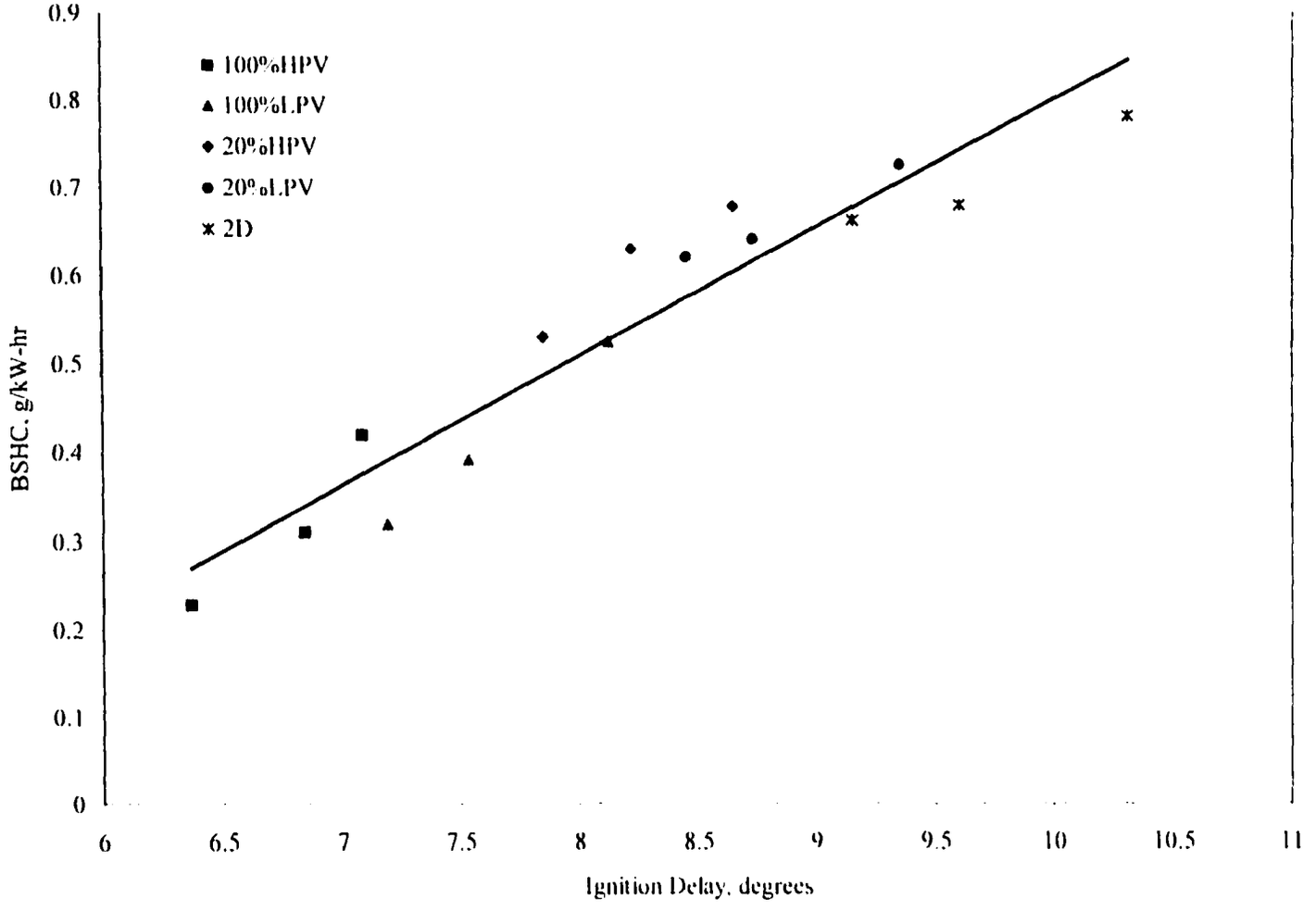

Figure 5.46 BSHC emissions as a function of ignition delay at light-load engine condition

be dependent on other fuel properties such as volatility. At the light load engine condition the HC emissions are higher because there is less fuel and more chance for overmixing. The effect of the longer ignition delay is to allow more time for overmixing which results in higher HC emissions.

5.4.2 Effect of ignition delay on CO emissions

Carbon monoxide is a natural intermediate product of hydrocarbon combustion. As the burned gas temperature falls due to expansion, the CO oxidation process slows and may freeze the CO concentration at a level higher than its equilibrium concentration. Figures 5.47 and 5.48 show the ignition delay vs. CO emissions curves at the full-load and light-load engine conditions, respectively. The CO emissions data were plotted for all fuels and all injection timings against the ignition delay. The CO emissions decrease as the ignition delay becomes shorter for both loads. The relation between CO emissions and the ignition delay are almost linear. This is most clearly shown for the light-load engine condition when the BSCO levels are about 10 times larger than at full load. The shorter ignition delay data points represent the neat biodiesels while the longer delay points represent No. 2 diesel fuel. The intermediate points are the blends. The CO emissions for all fuels and for all timings fall on one line particularly at light load. This indicates that the change in CO emissions may be related to the ignition delay.

Under the fuel-lean conditions of a diesel engine, incomplete HC oxidation can result in an increase in CO levels. The CO is a product of partial combustion. The HC in the overmixed regions oxidizes very slowly and they tend to produce more products of

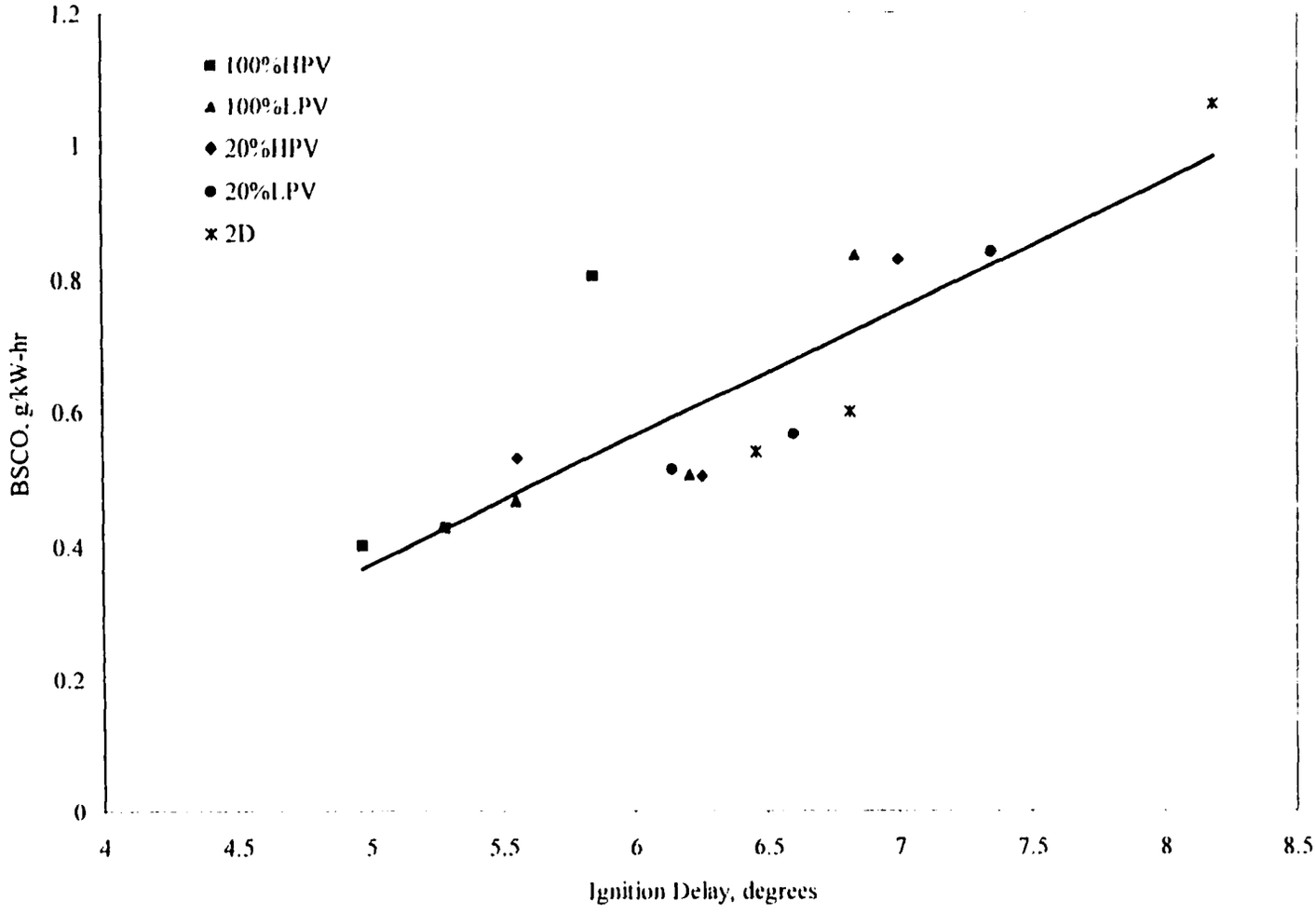

Figure 5.47 BSCO emissions as a function of ignition delay at full-load engine condition

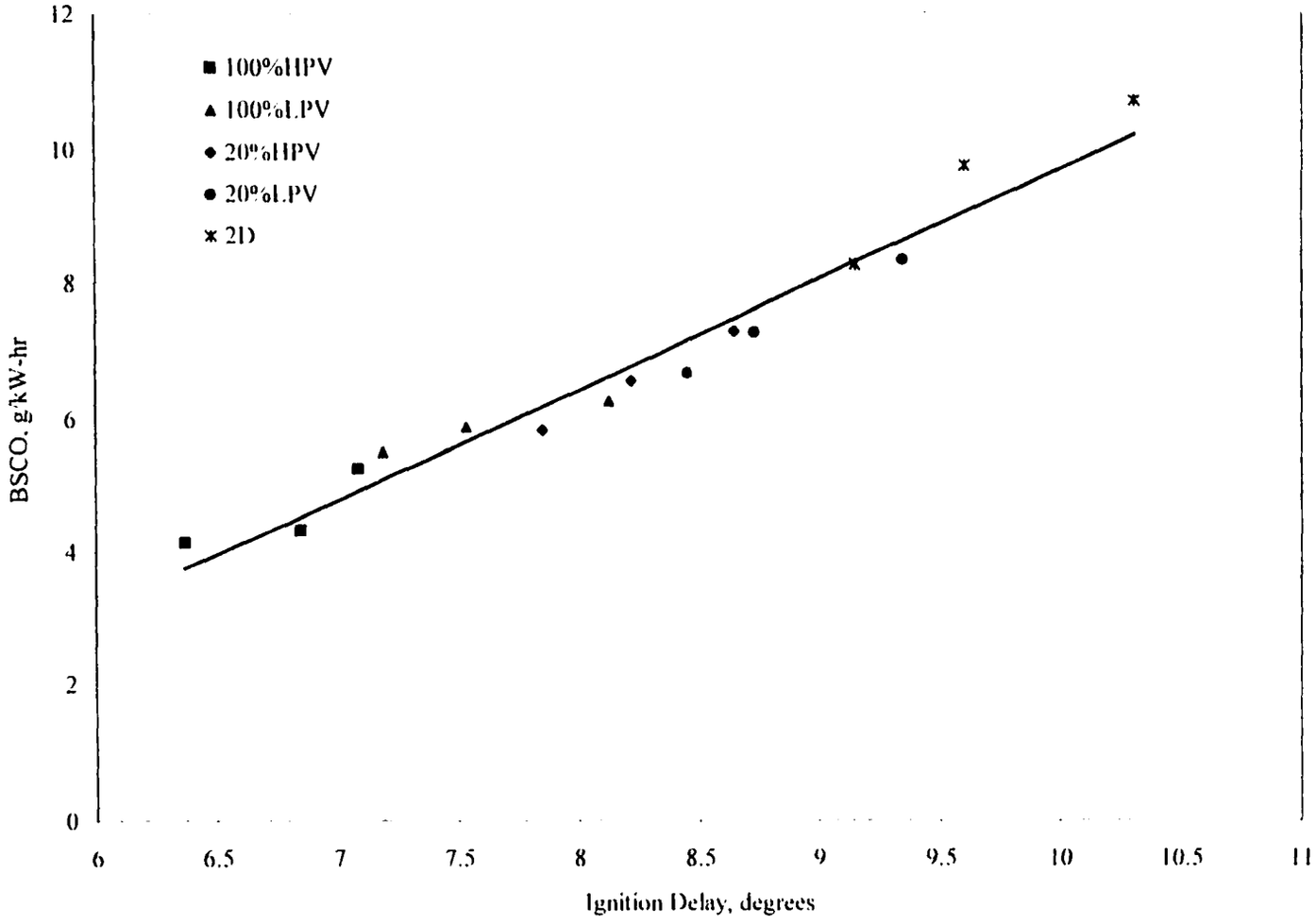

Figure 5.48 BSCO emissions as a function of ignition delay at light-load engine condition

incomplete combustion. More CO emissions will be produced if at the beginning more HC is present. Thus, one reason for the lower CO emissions at shorter ignition delays is the lesser amount of HC emissions. Another reason for the lower CO emissions could be that the oxidation of CO to CO_2 reaction proceeds to completion. Springer et al. [84] stated that the oxidation of CO to CO_2 reaction would be incomplete if there is a lack of oxidant, low average gas temperature in the engine cylinder, or a short residence time. The short residence time means there is less time available for the reaction. The biodiesel has a higher cetane number which results in a shorter ignition delay which in turn allows more time for the reaction to proceed from CO to CO_2. This process of oxidation allows the biodiesel to have less CO emissions. Figures 5.49 shows the relation between HC and CO emissions. The CO emissions increase as the HC emissions increase.

5.4.3 Effect of the start of fuel injection and the start of combustion on NO_x emissions

Generally, NO_x emissions form in the high temperature regions of the combustion chamber. This emission generally increases under conditions of high temperature and lean operation where O_2 is present. Springer et al. [84] mentioned that an increase in the local temperature and the O_2 concentration within the fuel spray envelope helps to increase the NO_x emissions from diesel engine combustion. Due to the oxygen contained in the biodiesel, more O_2 is available in the reaction zone during combustion and this could cause the NO_x emissions to rise.

Many researchers have shown that neat biodiesel produces higher NO_x emissions

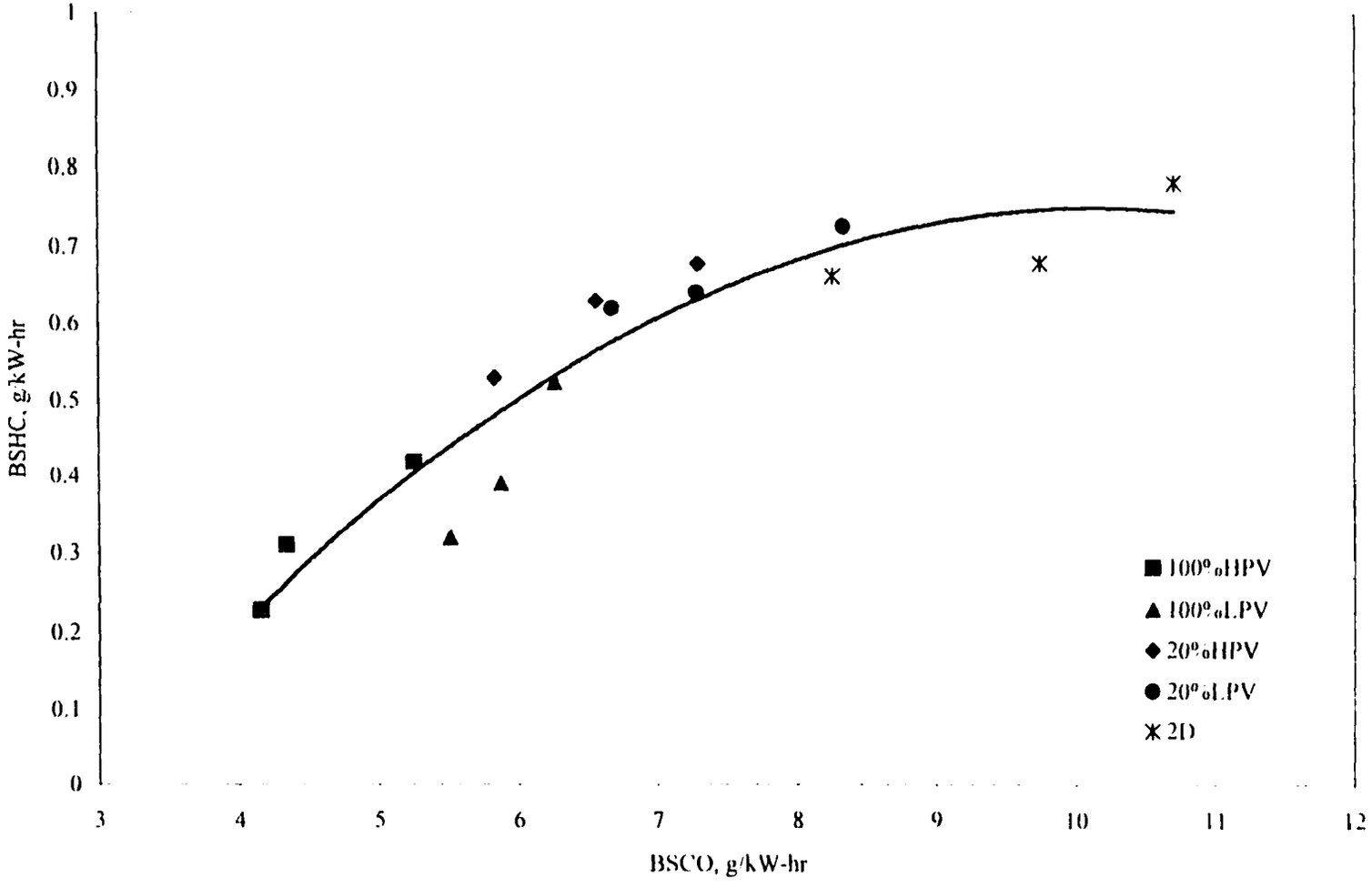

Figure 5.49 BSHC vs. BSCO emissions curve at light-load engine condition

than No. 2 diesel fuel. The biodiesel fuel chemistry was suspected to be the reason for the higher NO_x emissions. But in this study it was found that the biodiesel fuel chemistry may not be the reason of the higher NO_x emissions. The NO_x emissions at three different pump timings for the full and light load engine conditions are shown in Figures 5.50 and 5.51. It is clear from these figures that the pump timings (injection timing at the pump) and the fuels have an effect on the NO_x emissions. The NO_x emissions appear to be linearly related to the fuel injection timing with a separate line for each fuel. The neat oxidized biodiesel showed the highest NO_x emissions of any pump timing at the full load engine condition while No. 2 diesel fuel showed the lowest. This is the same result that many other researchers have observed [1, 78-80, 83].

It is important to realize that the pump timing was not the actual fuel injection timing. Because biodiesel properties are different from diesel fuel, the actual fuel injection timing for biodiesel is different than for diesel fuel. The actual injection timing for the biodiesel was not only different than the diesel fuel but also different from the pump timing which was set using diesel fuel. The biodiesel fuel is less compressible than diesel fuel, so the pressure waves can propagate faster in the biodiesel than in diesel fuel. This is one of the reasons for the advanced actual injection timing of biodiesel compared with diesel fuel. This advanced injection may contribute to the additional NO_x emissions for the biodiesel while the biodiesel itself may not be the reason for the higher NO_x emissions. To investigate this effect, the NO_x emissions were plotted against the actual injection timing for all fuels and all pump timings as shown in Figure 5.52. Both the full and light load data showed the same trend. The NO_x emissions for all fuels and all pump

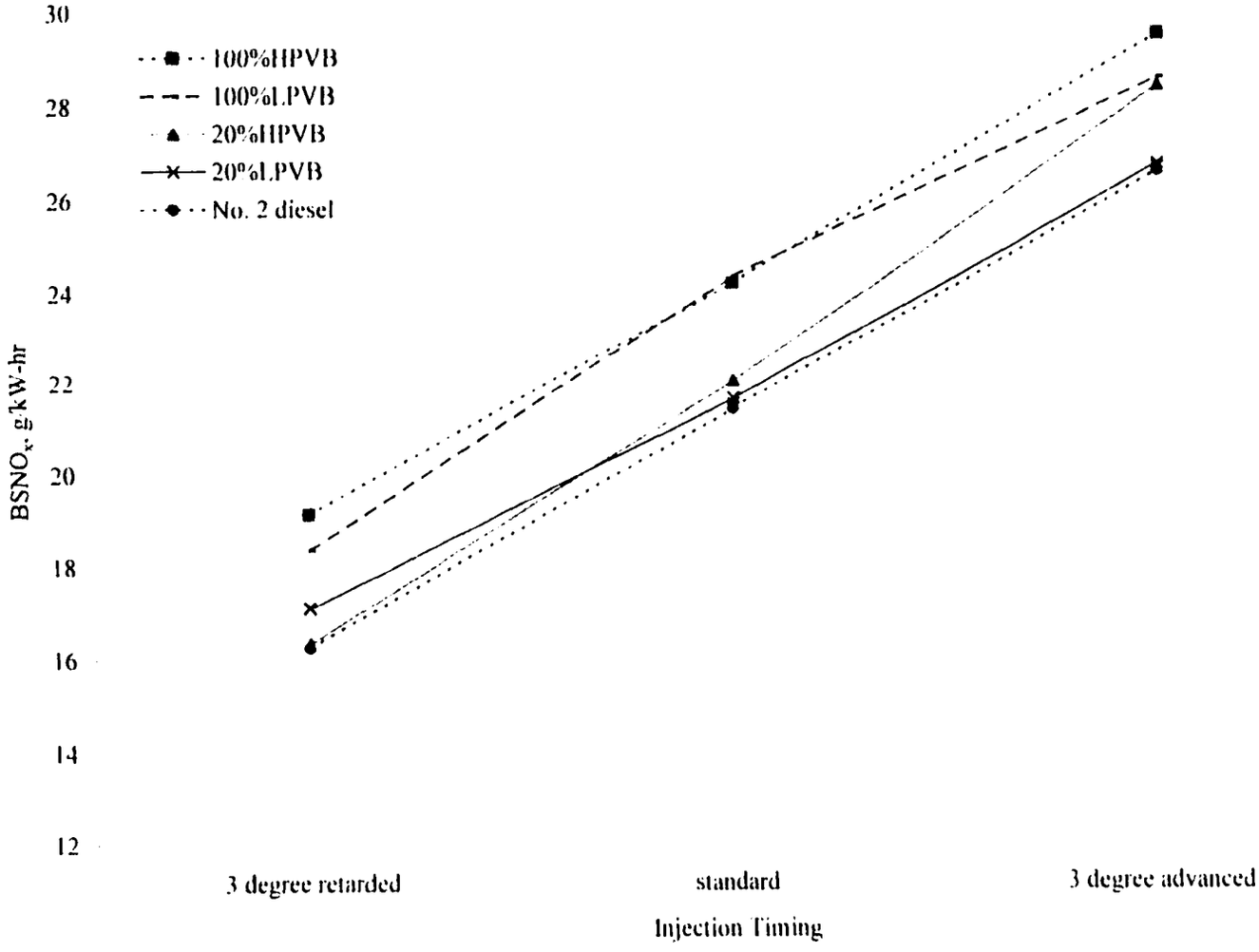

Figure 5.50 Brake specific NO_x emissions vs. pump timing (full-load)

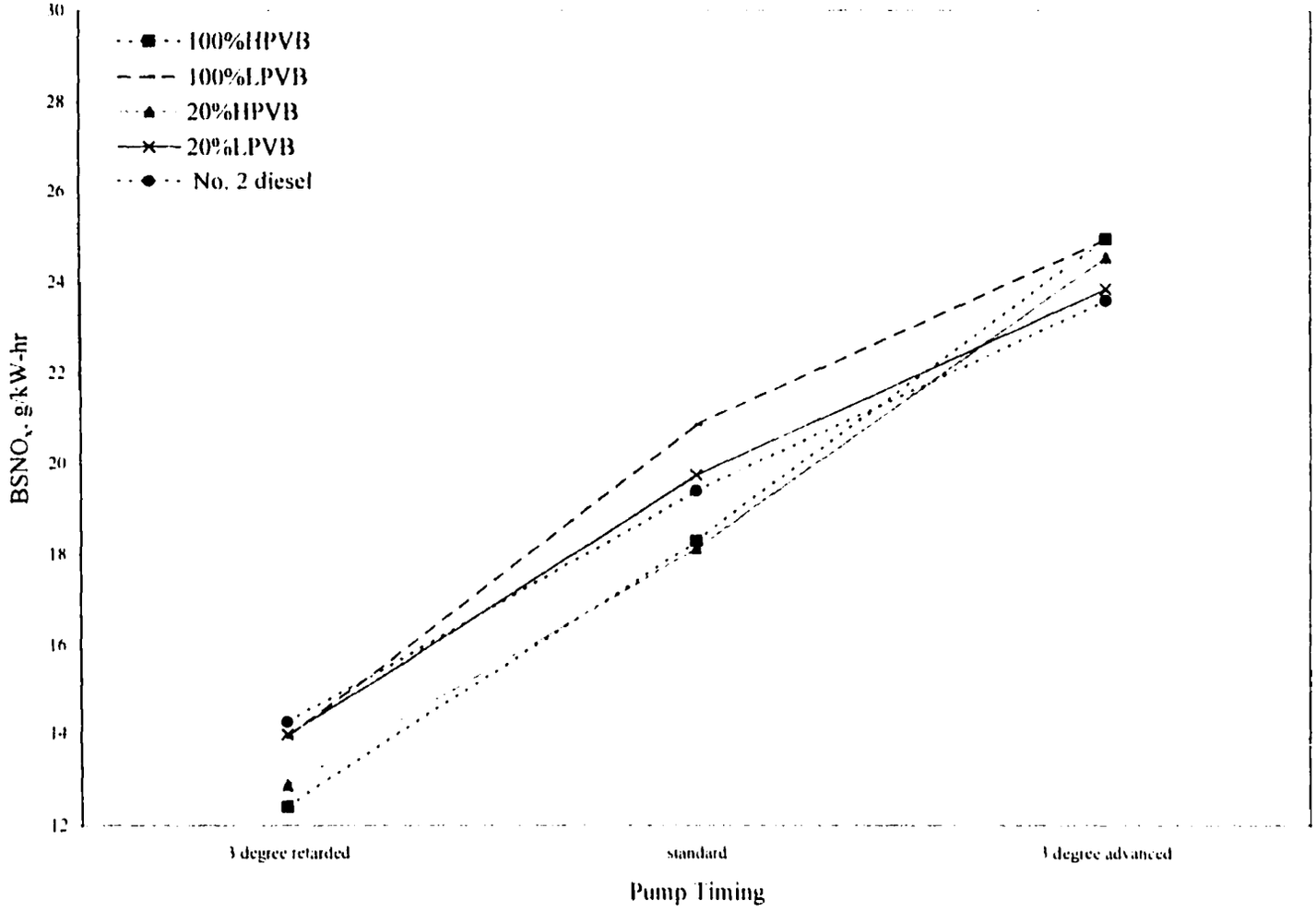

Figure 5.51 Brake specific NO_x emissions vs. pump timing (light-load)

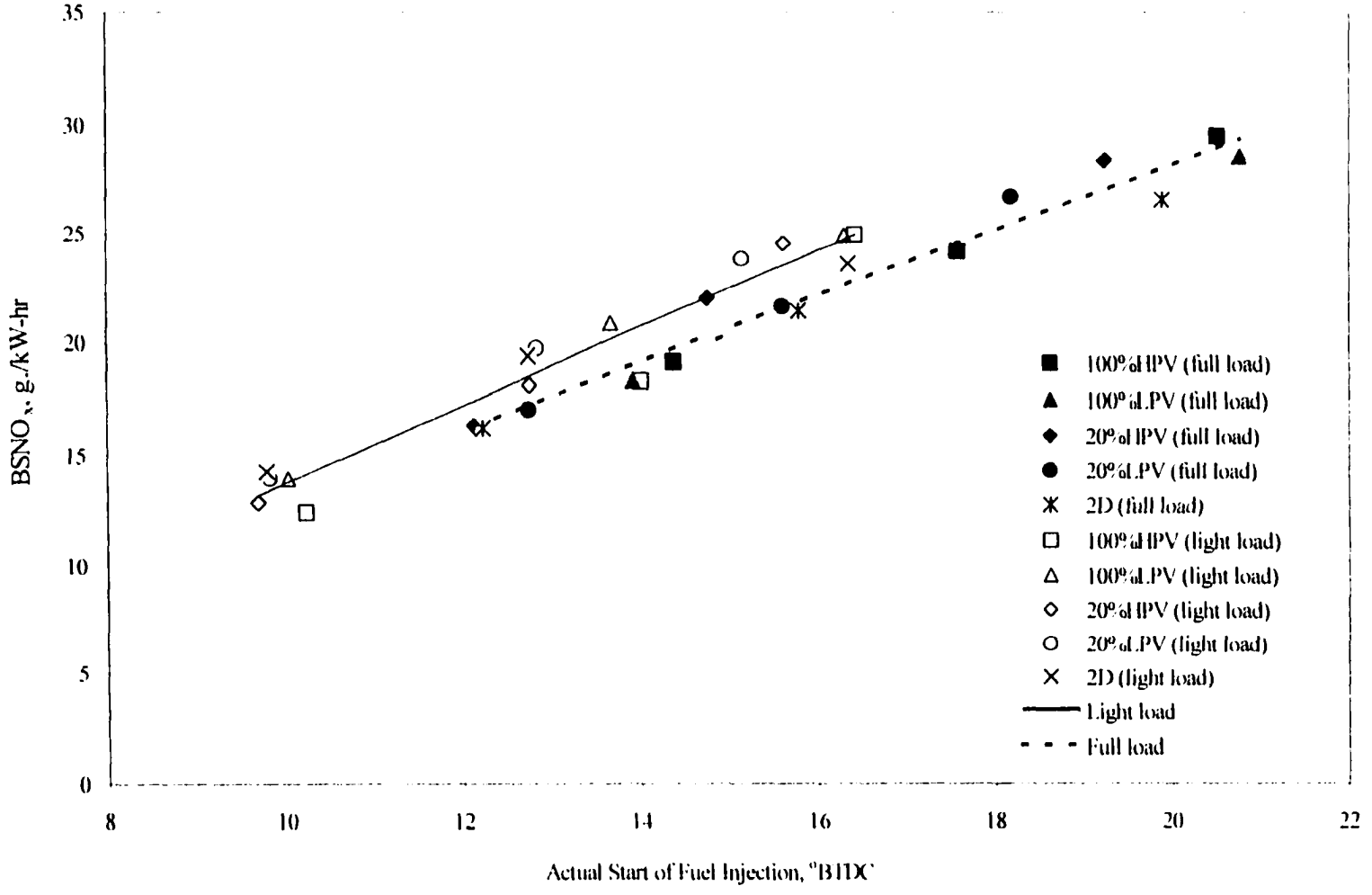

Figure 5.52 BSNO$_x$ emissions as a function of start of fuel injection

timings fall on one line when plotted against the actual start of injection. This indicates that the difference in NO_x emissions can be explained by variations in the start of actual fuel injection and not because of the fuel.

It would make better sense if the NO_x emissions and the actual start of combustion timing for all fuels and all pump timings fell on one line since the combustion is the process that actually produces the NO_x. This would also incorporate differences in the ignition delay periods between biodiesel and diesel fuel that are based on differences in the cetane number. The start of combustion for the neat oxidized biodiesel was seen to be more advanced than the diesel fuel. The reason was the cetane number for the neat oxidized biodiesel was higher than for the diesel fuel. The ignition delay period for the higher cetane number fuel is shorter than for the lower cetane number fuel, so the higher cetane number fuel will ignite earlier than the lower cetane number fuel. Another reason for the advanced combustion timing of the neat oxidized biodiesel was the early start of fuel injection. These two reasons caused the advanced combustion for the neat oxidized biodiesel and this advanced combustion can give higher NO_x emissions. Figures 5.53 and 5.54 show the NO_x emissions vs. the start of combustion timing for full and light load. When the NO_x data are plotted vs. the start of combustion, differences between the fuels emerge again. However, on these plots the lines corresponding to neat biodiesel are below those for No. 2 diesel fuel and the 20% blends. This means that for the same start of combustion timing, the 100% biodiesel fuels actually produced less NO_x than diesel fuel. This result is unexpected and has not been reported by other researchers. However, the author is not aware of any other comparisons

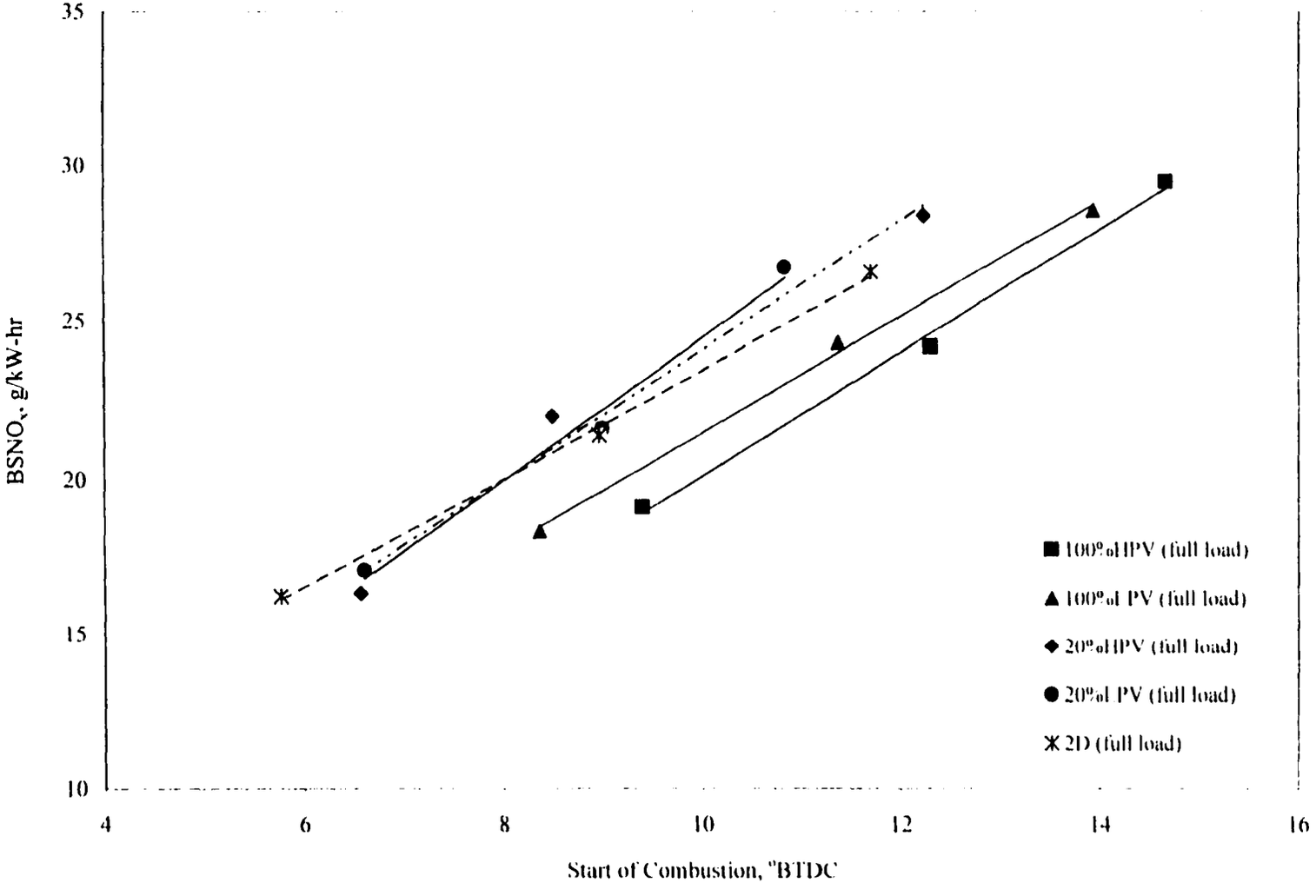

Figure 5.53 BSNO$_x$ emissions as a function of start of combustion at full-load engine condition

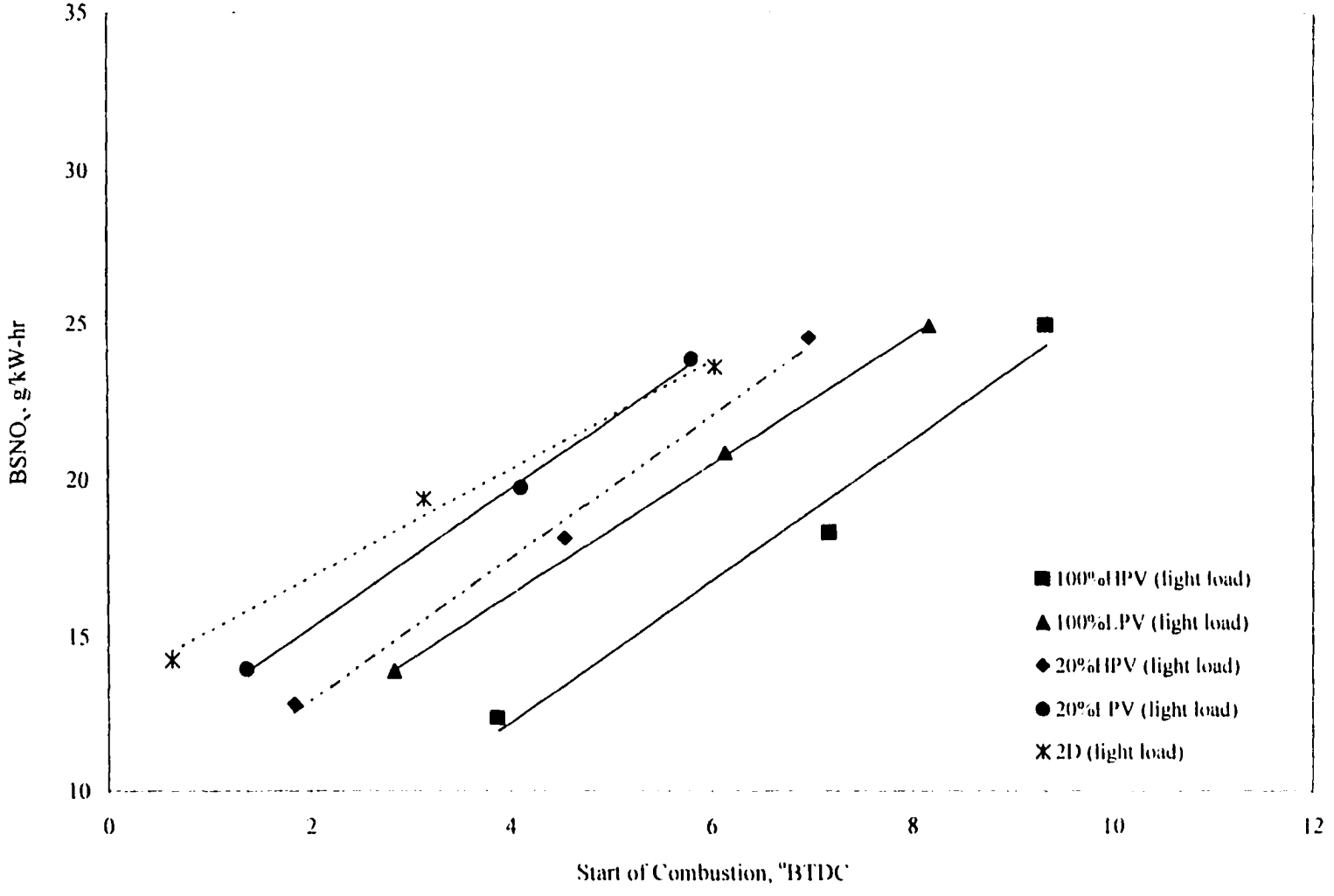

Figure 5.54 BSNO$_x$ emissions as a function of start of combustion at light-load engine condition

that have been made on this basis.

5.4.4 Effect of the start of fuel injection on smoke number

Diesel particulates are combustion generated carbonaceous material (soot) on which organic compounds have been adsorbed. Incomplete combustion of fuel hydrocarbons contributes to this component of the particulate material. Some of the particulate material is also produced from the lubricating oil. The engine exhaust system and the particulate collection system control the composition of the particulate material. Depending on the temperature, the particulates may change their characteristics. At temperatures below 500 °C, the particles become coated with condensed high molecular weight organic compounds. These condensed organic compounds are unburned hydrocarbons, oxygenated hydrocarbons, and polynuclear aromatic hydrocarbons. Inorganic species such as sulfur dioxide, nitrogen dioxide, and sulfuric acid are also the part of the condensed material.

The main concern of particulate measurement techniques is to determine the amount of particulate being emitted to the atmosphere. The particulates are normally obtained on a mass basis. The simplest technique uses a smoke meter which characterizes only the solid carbon portion of the particulate. This smoke meter measures the relative reflectance of a particulate sample collected on filter paper. It does not measure the mass directly. The smoke meter used in this experiment was a Bosch photoelectric densiometer which gave a number from 0 to 10 in units of Bosch Smoke Number. Bosch smoke number 0 corresponds to an absolutely white filter paper, while smoke number 10

corresponds to an absolutely dark filter paper which absorbs all the light.

Figure 5.55 shows the relationship between the start of fuel injection and the smoke number. The neat biodiesel advanced the start of fuel injection to occur earlier than for No. 2 diesel fuel. The neat biodiesel showed a lower smoke number while the No. 2 diesel fuel showed a higher smoke number. Azmi Bin Yahya [85] fueled a 4239D four cylinder inline John Deere tractor engine with soybean-based biodiesel. He found a significant reduction in the smoke number. In his experiment, soybean-based biodiesel reduced the smoke number by 81% to 85% compared to the base diesel fuel. Feldman et al. [79] also found that the advanced injection timing reduced the smoke level.

5.4.5 Tradeoff between NO_x emissions vs. smoke emissions

Figure 5.56 shows the tradeoff relationship between the NO_x emissions and the smoke number. This is a standard trade-off curve used by engine designers. Usually, anything that decreases NO_x increases the smoke and vice-versa. In this figure smoke is plotted versus NO_x for three injection timings (3° advanced, standard, and 3° retarded), and five fuel blends. The engine speed was maintained constant at 1400 rpm. The figure indicates that for this diesel engine, the smoke-nitric oxide tradeoff for biodiesel is lower than for the No. 2 diesel fuel. The smoke-nitric oxide tradeoff curve for No. 2 diesel fuel is in the upper right of the diagram while the oxidized neat biodiesel tradeoff curve is the lower left of the diagram. This means the oxidized neat biodiesel shows a better tradeoff than No. 2 diesel fuel. The neat non-oxidized and the 20% blends tradeoff curves are in between the oxidized neat biodiesel and the No. 2 diesel fuel.

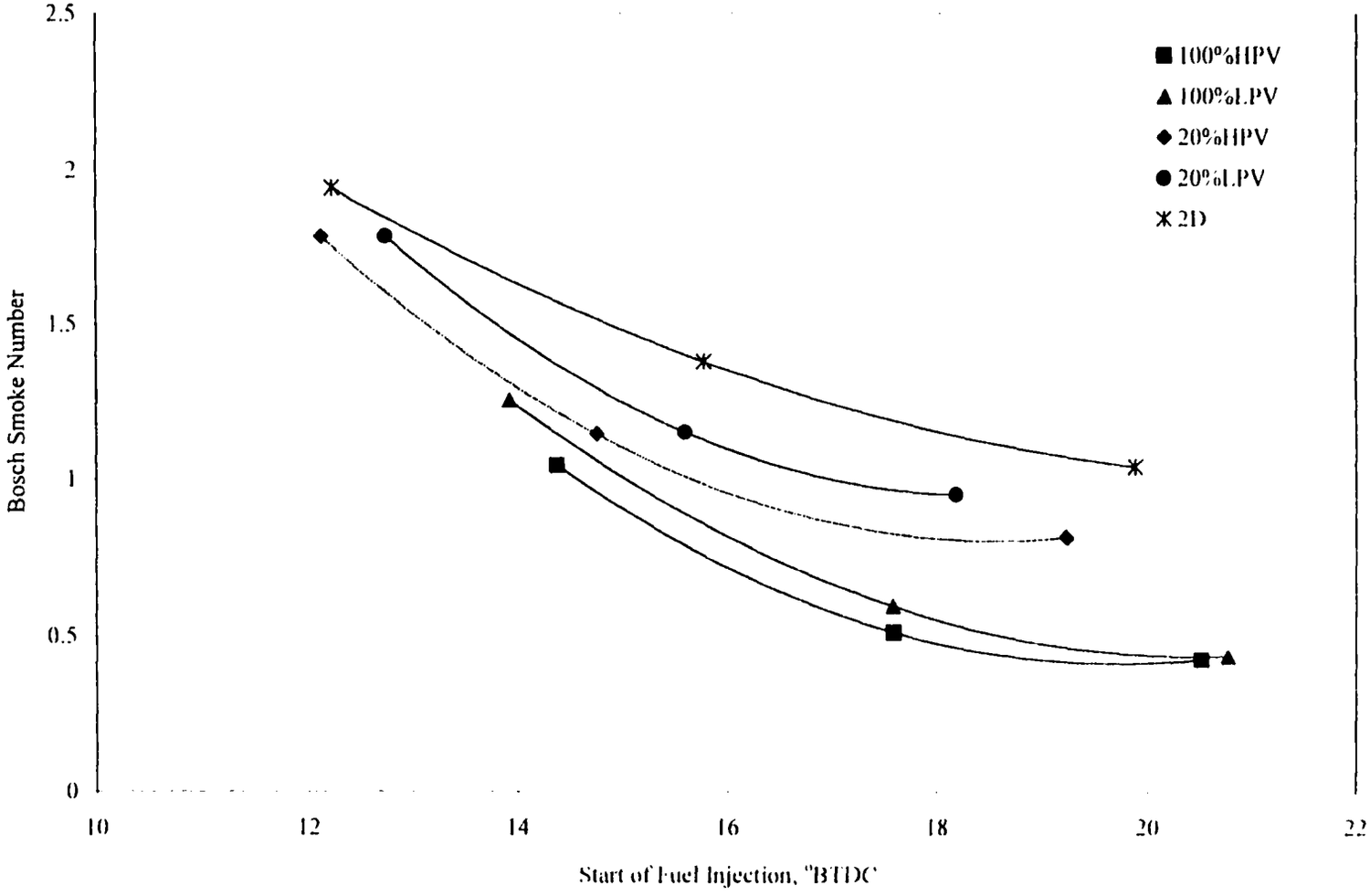

Figure 5.55 Smoke number as a function of start of fuel injection (full-load)

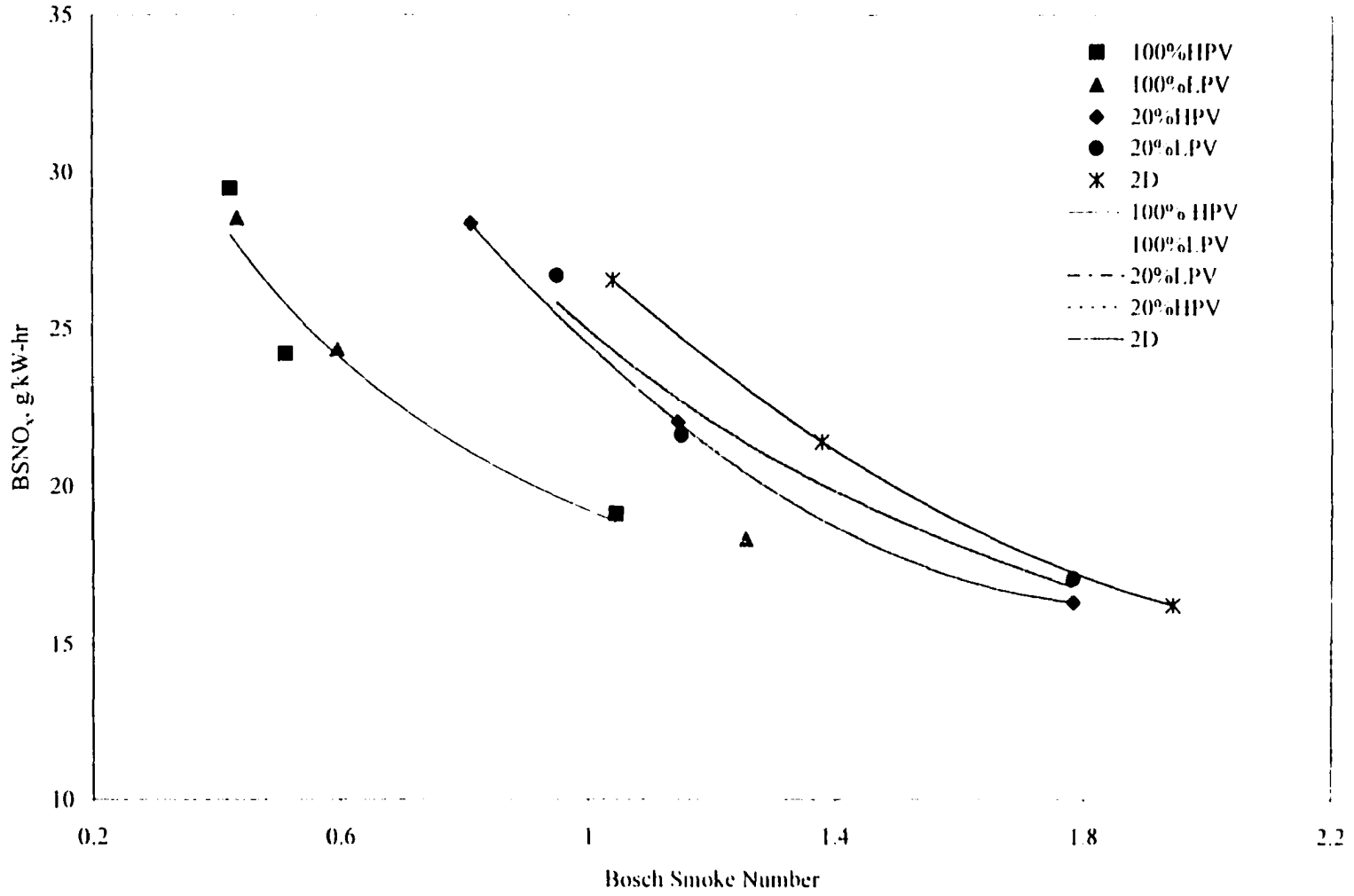

Figure 5.56 BSNO$_x$ vs. smoke number curve at full load engine condition

6. CONCLUSIONS

The objectives of this project were to understand the changes that occur in the fuel when it oxidizes, establish a connection between the ASTM fuel stability tests and the AOCS tests, evaluate the impact of oxidized fuel on engine performance and exhaust emissions, and compare the calculated fuel burning rate for oxidized biodiesel with the burning rate for unoxidized fuel and a baseline diesel fuel.

During the course of the project it was found that the standard ASTM procedure for characterizing the oxidative stability of diesel fuel (ASTM D2274) was not appropriate for biodiesel. The original expectation that the primary obstacle to using oxidized biodiesel in an engine would be fuel filter plugging was also found to be incorrect. Long term testing with biodiesel that had been oxidized well beyond what should be encountered in practice showed no instances of fuel filter plugging. Earlier work by other researchers had indicated that fuel filter plugging might be a problem. Now it is suspected that fuel filter plugging is caused by interactions between biodiesel and the fuel additives in the diesel fuel. Since these two aspects gave results that were different from what was expected, the chemical analysis portion of the project focused on understanding the changes that occur in the fuel when it oxidizes.

The purpose of this conclusion section is to summarize the experimental results as they relate to the objectives and then to make recommendations for future research.

6.1 Conclusions

1. It was expected that the fuel filters would plug as the vegetable oil esters oxidized but none of the blends (20%, 50%, or 100% biodiesel with No. 2 diesel fuel) were able to plug the filters even after many hours of operation.
2. The ASTM D2274 method was found to be inappropriate for measuring gum and filterable insoluble for biodiesel fuel because the washing fluid (isooctane) was not able to wash all the biodiesel from the filters. Also, it was found that the gum material collected on both the top (sample) and bottom filters which prevented the bottom filter from being used as a blank.
3. The maximum peroxide value that could be reached for any blend was between 300 and 400 meq. O_2/kg. Generally, the peroxide value rose to a maximum level of 300-400 meq. O_2/kg and then dropped off. Fuel with a high initial peroxide value oxidized faster than lower peroxide value fuel. The oxidation of the biodiesel occurred more rapidly at higher temperatures.
4. The initial rate of increase of the acid value was higher until the point where the peroxide value dropped off, then the rate of increase of the acid value was lower. A linear relation was found between the acid value and viscosity. The viscosity increased with time for all blends of biodiesel and diesel fuel. The induction period varied with different blend levels. The shortest one was evaluated for pure biodiesel and the longest one was evaluated at the 20% blend level.
5. The engine performance of the neat biodiesels and their blends was similar to that of No. 2 diesel fuel with nearly the same thermal efficiency, and slightly higher fuel

consumption.

6. Both of the neat biodiesel fuels increased the CO_2 emissions. Neat oxidized biodiesel increases the CO_2 emissions more than neat unoxidized biodiesel. CO_2 emissions increased with advanced injection timing. The higher CO_2 emissions were directly related to the BSFC. The higher the BSFC, the higher the CO_2 emissions.
7. The neat biodiesels and the biodiesel blends produced lower CO emissions for all injection timings. The oxidized biodiesel produced even more reduction in CO emissions than the unoxidized biodiesel. Regardless of the injection timing, the neat oxidized biodiesel reduced the CO emissions between 24% to 28.6% compared with diesel fuel. It also reduced the CO emissions as much as 15.3% compared to the neat unoxidized biodiesel at the full load engine condition. The injection timing has a significant effect on the CO emissions. The retarded injection timing produced 50% less CO emissions than the advanced injection. All neat biodiesels and biodiesel blends produced lower emissions of unburned hydrocarbon with a maximum reduction of 51% for the neat oxidized biodiesel at standard injection timing. The neat oxidized biodiesel produced 15.8% lower HC emissions than the neat unoxidized biodiesel at standard injection timing. The retarded injection produced about 34% less HC emissions than the advanced injection timing for neat oxidized biodiesel.
8. The neat biodiesels produced slightly higher NO_x emissions than the base fuel (No. 2 diesel). Statistically, the difference between the base fuel and the blends did not produce significant differences in NO_x emissions. Also, the effect of fuel oxidation on the NO_x emissions was found to be insignificant but the injection timing did have a

significant effect on the NO_x emissions. The 3° retarded injection timing gave at least a 20.9% reduction in NO_x emissions at the full load engine condition compared with the standard injection timing. The light-load engine condition had even more reduction in NO_x emissions.

9. The Bosch Smoke Number was significantly reduced when the diesel engine was fueled with neat biodiesel and blends with diesel fuel. The highest reduction was found for neat oxidized biodiesel at the standard injection timing, which was 62.9%. The neat oxidized biodiesel produced about 14% lower smoke number than the neat unoxidized biodiesel but this level was not statistically significant. Injection timing had a significant effect on smoke number. The advanced injection timing gave a lower smoke number than the retarded injection. The 3° advanced timing had over 59.6% lower smoke number than the 3° retarded injection timing for the neat biodiesels.
10. The fuel injection timing advanced for neat biodiesel compared with diesel fuel at the same injection pump settings. The neat biodiesels advanced fuel injection timing about 2.3° compared with diesel fuel. All neat biodiesels and their blends experienced the same combustion stages as the base fuel. The neat non-oxidized biodiesel advanced the start of combustion by about 2.3° and the neat oxidized biodiesel advanced the start of combustion by 3.3° compared with diesel fuel.
11. All neat biodiesel and its blends experienced a shorter ignition delay than diesel fuel. The neat oxidized biodiesel had a 0.9° shorter ignition delay than the neat non-oxidized biodiesel at standard timing. Retarded injection timing reduced the ignition

delay for all fuels.

12. Shorter ignition delay reduced CO and HC emissions. The ignition delay was almost linearly correlated to CO and HC emissions. A common linear relationship was found between the start of fuel injection and the NO_x and smoke emissions. When the NO_x was plotted against the start of combustion timing, there were differences between the fuels. However, at the same start of combustion, the neat biodiesel fuels were found to produce less NO_x than the No. 2 diesel fuel. Late injection timing reduced the NO_x emissions but increased the smoke number.

6.2 Recommendations for Future Work

In this section, several suggestions are made based on the experience gained during the experiment. If implemented, these suggestions will provide additional information about the effect of oxidized biodiesel on exhaust emissions.

1. A better mechanism to set the fuel injection timing is needed. A Lab view program that could control injection timing at the time of experiment would be helpful. This would ensure constant injection timing for all fuels (oxidized, unoxidized, and base fuel). This technique would also provide the additional information needed to confirm the injection timing effect on emissions.
2. Additional loads and different engine speeds would provide better supporting information on the effect of oxidation on emissions. Also, different blends of biodiesel and the diesel fuel would provide the information that can determine which is the best blend for lowest emissions.

3. Other oxygen-containing fuels should be added with oxidized and unoxidized biodiesel, and diesel fuel to determine which oxygenate produced the most desirable result. Suggested oxygenates are di-alcohols and ethers. Di-alcohols contain two oxygen atoms like esters.
4. Durability testing for the oxidized biodiesel would provide the information whether the oxidized biodiesel has any effect on engine.

APPENDIX A. AOCS OFFICIAL METHOD CD 3A-63 FOR ACID VALUE TEST [41]

The acid value is the number of milligrams of potassium hydroxide (KOH) necessary to neutralize the free acids in 1 gram of sample. This method is applicable to crude and refined animal, vegetable, and marine fats and oils, and various products derived from them. The necessary apparatus, reagents, test procedure, and the calculations for the acid value test are explained below.

Apparatus:

1. Erlenmeyer flasks, 250 ml.
2. Burette, 50 ml.

Reagents:

1. Potassium hydroxide (KOH), 0.1 N and 0.01N in water.
2. Solvent mixture contains of equal parts by volume isopropyl alcohol and toluene
3. Phenolphthalein indicator solution, 1.0% in isopropyl alcohol.

Procedure:

1. Add 0.8 ml phenolphthalein indicator solution to 50 ml of solvent mixture (1:1 isopropyl alcohol - toluene) and neutralize with alkali (0.01N KOH) to a faint but permanent pink color. The amount of alkali (0.01N KOH) used to neutralize the solvent mixture is the blank (B).
2. Determine the sample size from Table A.1 by comparing the expected acid value. Higher acid value needs less amount of sample and lower acid value needs a large amount of sample.

Table A.1. Sample size for the test

Acid value	Wt. Of sample (gm)
0 to 1	20
1 to 4	10
4 to 15	2.5
15 to 75	0.5
75 and over	0.1

3. Weigh the specified amount of sample from Table A.1 into an Erlenmeyer flask.
3. Add 50 ml of solvent mixture (1:1 isopropyl alcohol - toluene). Be sure that the sample is completely dissolved. Warming may be necessary in some cases.
5. Shake the sample vigorously while titrating with standard alkali (0.1N or 0.01N KOH depending upon the level of acid value in the sample) to the first permanent pink color of the same intensity as that of the neutralized solvent. The color must persist for 30 seconds. The amount of standard alkali used in this step is A, where A is defined below.

Calculation:

The acid value, mg KOH/g of sample = (A-B) * N * 56.1/W

where:

A= ml of standard alkali (0.1N or 0.01N KOH) used in the titration

B= ml of standard alkali (0.1N or 0.01N KOH) used in the titrating the blank

N= normality of the standard alkali (0.1 or 0.01N KOH)

W= grams of sample

APPENDIX B. AOCS OFFICIAL METHOD CD 8-53 FOR PEROXIDE VALUE TEST [42]

The peroxide value is a number that indicates the level of peroxides in a fat or oil that has developed as a result of oxidation. Peroxides are considered intermediates in the lipid oxidation reaction scheme. This method determines all peroxides, in terms of milliequivalents of peroxide per 1000 grams of sample, which oxidize potassium iodide (KI). This method is applicable to all normal fats and oils. The necessary apparatus, reagents, test procedure, and the calculations for the peroxide value test are explained below.

Apparatus:

1. Pipet, 0.5 ml.
2. Erlenmeyer flasks, 250 ml.
3. Burette, 50 ml.

Reagents:

1. Acetic acid- chloroform solution, 3:2 (volume basis).
2. Potassium iodide (KI) solution, saturated, prepared each day is preferred by dissolving an excess of KI in recently boiled distilled water. Make sure that the solution of KI remains saturated during use, as indicated by the presence of undissolved KI crystals in the solution.
3. Sodium thiosulfate solution 0.1N, prepared by dissolving 24.9 g of sodium thiosulfate in distilled water and diluting to 1 liter.

4. Starch indicator solution is used to test the sensitivity. This solution is prepared by making a paste with 1g of starch and a small amount of cold distilled water. Add this paste, while stirring, to 200 ml of boiling distilled water and boil for a few seconds. Immediately remove from the heat and cool. Store the solution in the refrigerator and use within 2 to 3 weeks.

Procedure:

1. Weigh 5.0 g of sample into a 250 ml flask. Add 30 ml of 3:2 acetic acid-chloroform solution. Shake to dissolve the sample. Add 0.5 ml of saturated KI solution.
2. Allow the solution to stand with occasional shaking for 1 minute and then add 30 ml of distilled water.
3. Titrate with 0.1 N or 0.01N sodium thiosulfate. Continue titration until the yellow color almost disappears. Add about 0.5 ml of starch indicator solution. Continue titration until the blue color just disappears.
4. Conduct a blank determination of the reagents daily. The blank can be determined by using the same above three steps without the 5.0 g sample. The blank titration must not exceed 0.1 ml of the 0.1 N sodium thiosulfate solution.

Calculations:

Peroxide Value (milliequivalents peroxide/1000 g sample)= (A-B) * N * 1000 / W

where: A= ml of standard alkali used in the titration

B= titration of blank, ml

N= normality of the standard alkali

W= grams of sample

APPENDIX C. CALIBRATIONS OF PRESSURE TRANSDUCERS

Two pressure transducers were used in this experiment. One of them was a Kistler model 6061B pressure transducer. and the other was a Kistler model 6230M1 pressure transducer. The Kistler model 6061B pressure transducer was calibrated with a dead-weight tester. The factory calibration was used for the 6230M1 pressure transducer. The specifications of these pressure transducers are shown in Table C.1.

Table C.1 Specifications of pressure transducers

Type	Range	Linearity	Application
Kistler 6061B	0-250 bar	± 0.2 (full scale)	Cylinder pressure
Kistler6230M1	0-250 bar		Injection pressure

The Kistler model 6061B pressure transducer was calibrated before it was installed in one of the engine cylinders. The calibration procedure was to load and unload the known weights on the dead weight tester plate. From the pressure transducer. the output signal was amplified by a PCB Model 462A charge amplifier as a voltage. A computer with a Lab-View program was used to record the voltage. A linear regression analysis was performed to fit a straight line to the collected pressure data. The linear equation used to calculate the pressure for the Kistler model 6061B is as follows:

$$P = A_o + A_1 \times V \; : \quad R^2 = 1$$

Where P = Cylinder pressure in bar:

V = voltage output from the pressure transducer in volt

A_o and A_1 = linear regression coefficients

A_1= 16.384 bar/V

A_o= 0.0939 bar

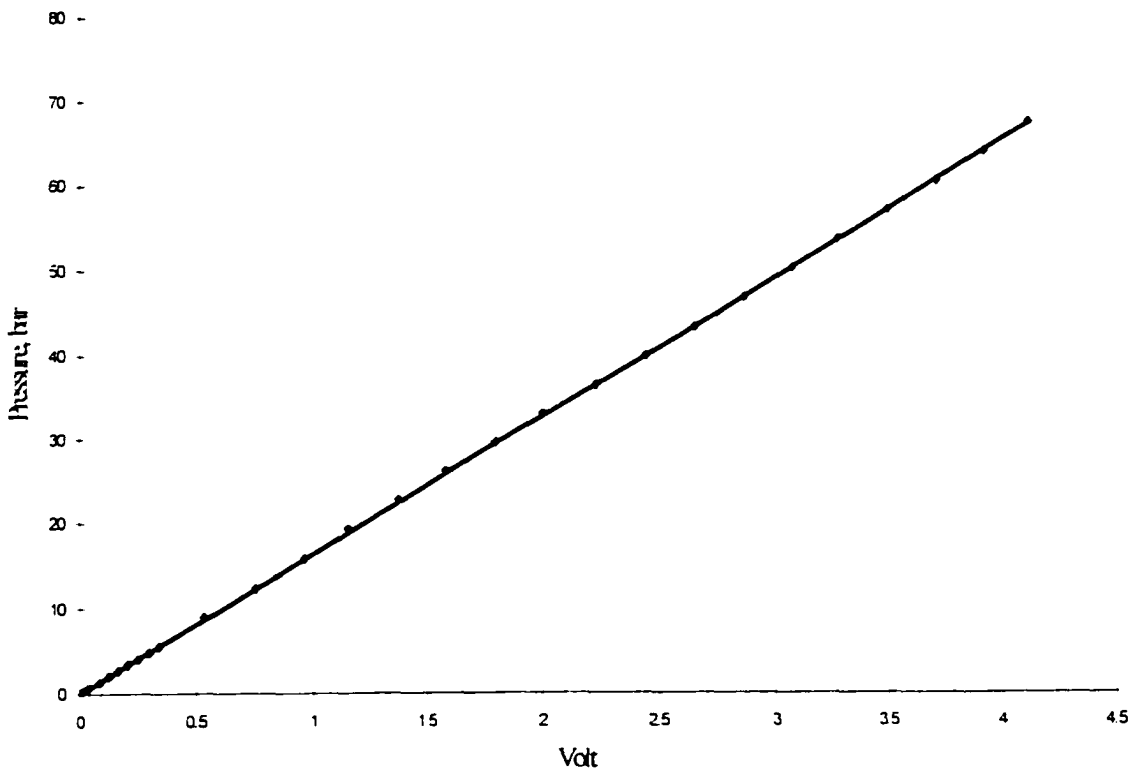

Figure C.1 Calibration of the Kistler model 6061B pressure transducer

The factory calibration was used for the model 6230M1 pressure transducer. This pressure transducer was installed in the fuel injection line. The sensitivity of this pressure transducer was 1.755 pC/bar. The charge amplifier sensitivity was 100 pC/volt. Combining these two sensitivities, the pressure transducer sensitivity was calculated in terms of pressure (bar). This calculated pressure transducer sensitivity was 56.98 bar/volt.

APPENDIX D. TUKEY'S GROUPING

This section contains the results of the calculations to produce a table known as Tukey's grouping. The same letter in the Tukey grouping column means there is no significant difference.

Table D.1 Tukey's Studentized Range (HSD) Test for variable: BSFC

Effect of Timing

Tukey Grouping	Mean	N	TIMING
A	335.3754	30	3deg_advanced
B	331.5928	30	3deg_retarded
B			
B	331.3316	30	Standard

Minimum Significant Difference= 2.7547

Effect of Fuel

Tukey Grouping	Mean	N	FUEL
A	359.8831	18	100%HPV
B	356.6013	18	100%LPV
C	317.9084	18	20%LPV
C			
C	317.8479	18	80%HPV
D	311.5921	18	DD

Minimum Significant Difference= 2.7641

Effect of Load

Tukey Grouping	Mean	N	LOAD
A	422.6494	45	80%
B	242.8848	45	100%

Minimum Significant Difference= 1.242

Table D.2 Tukey's Studentized Range (HSD) Test for variable: $BSCO_2$

Effect of Timing

Tukey Grouping	Mean	N	TIMING
A	1011.090	30	3deg_advanced
B	998.029	30	Standard
B			
B	997.053	30	3deg_retarded

Minimum Significant Difference= 9.9010

Effect of Fuel

Tukey Grouping	Mean	N	FUEL
A	1016.476	18	10%HPV
B	1005.641	18	10% LPV
B			
C B	998.669	18	CD
C			
C	994.460	18	20%HPV
C			
C	993.636	18	20 LPV

Minimum Significant Difference= 7.7841

Effect of Load

Tukey Grouping	Mean	N	LOAD
A	1172.220	45	20%
B	731.221	45	100%

Minimum Significant Difference= 3.4841

Table D.3 Tukey's Studentized Range (HSD) Test for variable: BSCO

Effect of Timing

Tukey Grouping		Mean	N	TIMING
	A	4.2214	31	3deg_advanced
	A			
B	A	3.6433	31	Standard
B				
B		3.2967	31	3deg_retarded

Minimum Significant Difference= 0.7286

Effect of Fuel

Tukey Grouping	Mean	N	FUEL
A	3.1464	18	CD
B	4.0427	18	20%LPV
C	3.5888	18	20%HPV
D	3.2422	18	100%LPV
E	2.8626	18	100%HPV

Minimum Significant Difference= 0.3145

Effect of Load

Tukey Grouping	Mean	N	LOAD
A	4.80279	45	20%
B	2.63109	45	100%

Minimum Significant Difference= 0.1413

Table D.4 Tukey's Studentized Range (HSD) Test for variable: BSHC

Effect of Timing

Tukey Grouping	Mean	N	TIMING
A	1.35933	30	3deg_advanced
A			
B A	1.33519	30	Standard
B			
B	1.27921	31	3deg_retarded

Minimum Significant Difference= 0.0694

Effect of Fuel

Tukey Grouping	Mean	N	FUEL
A	1.41742	18	CD
A			
B A	1.38262	18	20%LPV
B			
B	1.35533	18	20%HPV
C	1.23703	18	100 LPV
D	1.18697	18	100%HPV

Minimum Significant Difference= 0.0296

Effect of Load

Tukey Grouping	Mean	N	LOAD
A	1.341191	45	20%
B	1.283547	45	100%

Minimum Significant Difference= 0.0133

Table D.5 Tukey's Studentized Range (HSD) Test for variable: BSNOx

Effect of Timing

Tukey Grouping	Mean	N	TIMING
A	22.1886	31	3deg_advanced
B	21.1131	31	Standard
C	19.4856	31	3deg_retarded

Minimum Significant Difference= 1.0319

Effect of Fuel

Tukey Grouping	Mean	N	FUEL
A	21.8219	18	100 LPV
A			
A	21.4136	14	100 HPV
B	21.4999	19	20%LPV
B			
B	20.3806	18	20%HPV
B			
B	20.2448	18	22

Minimum Significant Difference= 1.7514

Effect of Load

Tukey Grouping	Mean	N	LOAD
A	22.6934	46	100%
B	19.0514	46	22

Minimum Significant Difference= 1.0286

Table D.6 Tukey's Studentized Range (HSD) Test for variable: Smoke Number

Effect of Timing

Tukey Grouping	Mean	N	TIMING
A	[illegible]	[illegible]	[illegible]
B	[illegible]	[illegible]	Standard
B			
B	[illegible]	[illegible]	[illegible]

Minimum Significant Difference= [illegible]

Effect of Fuel

Tukey Grouping	Mean	N	FUEL
A	[illegible]	[illegible]	[illegible]
B	[illegible]	[illegible]	[illegible]
B	[illegible]	[illegible]	[illegible]
C	[illegible]	[illegible]	[illegible]
C	[illegible]	[illegible]	[illegible]

Minimum Significant Difference= [illegible]

Effect of Load

Tukey Grouping	Mean	N	LOAD
A	[illegible]	[illegible]	[illegible]
B	[illegible]	[illegible]	[illegible]

Minimum Significant Difference= [illegible]

Table D.7 Tukey's Studentized Range (HSD) Test for variable: Start of Injection

Effect of Fuel Batch

Tukey Grouping	Mean	N	BATCH
A	14.92733	30	2
B	14.68300	30	3
C	14.44900	30	1

Minimum Significant Difference= 0.0793

Effect of Fuel Age

Tukey Grouping	Mean	N	AGE
A	14.96133	30	1
B	14.69533	30	3
C	14.40167	30	2

Minimum Significant Difference= 0.0793

Effect of Timing

Tukey Grouping	Mean	N	TIMING
A	17.83867	30	3deg_advanced
B	14.72800	30	Standard
C	11.49167	30	3deg_retarded

Minimum Significant Difference= 0.0793

Effect of Fuel

Tukey Grouping	Mean	N	FUEL
A	15.5217	18	100 HPV
A			
A	15.3722	18	100 LPV
B	14.4572	18	20
B			
B	14.0533	18	20 LPV
B			
B	14.0261	18	20 HPV

Minimum Significant Difference= 0.4446

Table D.8 Tukey's Studentized Range (HSD) Test for variable: Start of Combustion

Effect of Fuel Batch

Tukey Grouping	Mean	N	BATCH
A	7.69667	30	2
A			
B A	7.33000	30	3
B			
B	7.14333	30	1

Minimum Significant Difference= 0.3736

Effect of Fuel Age

Tukey Grouping	Mean	N	AGE
A	7.66000	30	1
A			
B A	7.37000	30	3
B			
B	7.18000	30	2

Minimum Significant Difference= 0.3736

Effect of Timing

Tukey Grouping	Mean	N	TIMING
A	9.46667	30	3deg_advanced
B	7.32000	30	Standard
C	4.70333	30	3deg_retarded

Minimum Significant Difference= 0.3736

Effect of Fuel

Tukey Grouping	Mean	N	FUEL
A	9.4556	18	100%HPV
B	8.4667	18	100%LPV
C	6.7722	18	20%HPV
C	6.2833	18	20%LPV
C			
C	6.0389	18	2D

Minimum Significant Difference= 0.3807

Table D.8 (continued)

Effect of Load

Tukey Grouping	Mean	N	LOAD
A	[illegible]	45	[illegible]
B	[illegible]	45	[illegible]

Minimum Significant Difference= [illegible]

Table D.9 Tukey's Studentized Range (HSD) Test for variable: Ignition Delay

Effect of Fuel Batch

Tukey Grouping	Mean	N	BATCH
A	7.38301	31	3
A			
A	7.26467	30	1
A			
A	7.23047	31	2

Minimum Significant Difference= 0.4111

Effect of Fuel Age

Tukey Grouping	Mean	N	AGE
A	7.30533	30	3
A			
A	7.30133	31	1
A			
A	7.28167	30	2

Minimum Significant Difference= 0.4111

Effect of Timing

Tukey Grouping	Mean	N	TIMING
A	7.37200	30	3deg_advanced
B	7.30800	30	Standard
C	7.26833	31	3deg_retarded

Minimum Significant Difference= 0.4111

Effect of Fuel

Tukey Grouping	Mean	N	FUEL
A	8.4183	18	CD
B	7.7700	18	20%LPV
C	7.2533	18	20%HPV
D	6.9056	18	100%LPV
E	6.0661	18	100%HPV

Minimum Significant Difference= 0.2958

Table D.9 (continued)

Effect of Load

Tukey Grouping	Mean	N	LOAD
A	8.22933	45	20%
B	6.33622	45	100%

Minimum Significant Difference= 0.1329

APPENDIX E. TEST DATA

This section presents the raw data collected for this study.

Table E.1 Raw data at standard timing (day 1)

Fuel	NO. 2 diesel	NO. 2 diesel	100%LPV	100%LPV	20%HPV	20%HPV	100%HPV	100%HPV	20%LPV	20%LPV
Date	4/25/98	4/25/98	4/25/98	4/25/98	4/25/98	4/25/98	4/25/98	4/25/98	4/25/98	4/25/98
Engine speed (rpm)	1400	1400	1400	1400	1400	1400	1400	1400	1400	1400
% of rated load	100	20	20	100	100	20	20	100	100	20
Brake torque (ft lbf)	190	38	38	190	190	38	38	190	190	38
Fuel weight (g)	285	246	114	807	1013	302	231	1311	1597	604
Time (min)	2	5	2	5	7	6	4	8	11	12
Ambient air temp (°F)	70	70	70	70	70	70	70	70	21	21
P_{atm} (mmHg)	733	733	733	733	733	733	733	733	733	733
Temperature (°F)										
1 Inlet air temp	68	70	69	70	70	68	69	69	70	69
3 Inlet manifold temp	115	83	92	117	117	84	82	114	118	85
4 Fuel temp	40	40	40	40	40	40	40	40	40	40
6 Cooling water inlet temp	160	117	18	160	159	121	118	160	159	122
7 Cooling water outlet temp	176	161	162	177	174	155	154	177	174	155
8 Exhaust manifold temp										
9 Exhaust temp shielded	835	390	38	836	838	396	386	832	844	393
10 Thermocouple shield	137	102	104	134	134	103	103	138	137	101
11 Exhaust temp unshield	846	401	408	847	851	407	397	844	212	404
12 Oil temp	214	185	186	214	212	183	181	213	212	184
13 Building cooling water inlet	51	50	51	51	51	50	50	51	51	51
14 Building cooling water outlet	93	70	70	92	93	71	70	92	92	72
Coolant Count/10 sec	130.5			134 3	144			132 7	139 6	
Pressure:										
Pressure diff of EE (in H_2O)	1 96	1 85	1 83	1 98	1 97	1 91	1 9	1 96	2	1 9
Boost pressure (psi)	3	0 5	0 5	3	3	0 5	0 5	3	3	0 5
Oil pressure (psi)	51	55	55	50	51	55	55	50	51	55
Exhaust pressure (psi)	3 2	1 9	2	3 3	3 3	2	2	3 2	3 2	1 9
Relative humidity	33	34	33	33	34	33	33	40	42	43
Emissions $BSCO_2$ (g/kW-hr)	725 529	1252 492	1278 852	724 234	719 314	1250 930	1295 679	735 340	721 638	1250 930
BSCO (g/kW-hr)	0 598	9 392	5 506	0 445	0 476	6 401	3 775	0 367	0 566	7 120
BSHC (g/kW-hr)	0 103	0 677	0 426	0 065	0 089	0 630	0 317	0 053	0 095	0 624
$BSNO_x$ (g/KW-hr)	22 228	19 141	21 620	24 748	22 448	18 348	17 751	24 121	21 821	19 633
BSNO (g/kW-hr)	20 689	14 807	16 292	23 155	20 993	14 695	14 322	22 258	20 225	15 469
BSO_2 (g/kW-hr)	632 224	4652 841	4555 558	623 427	629 033	4605 017	4692 789	634 660	624 818	4613 794
Smoke Number (Bosch)	1 400	0 100	0 067	0 550	1 133	0 100	0 100	0 500	1 150	0 100
BSFC (g/kW-hr)	226 389	390 818	452 777	256 415	229 906	399 821	458 735	260 347	230 649	399 821
File Names Cylinder Pressure	d12dfc	d12dlc	d1bllc	d1blfc	1bhptfc	1bhptlc	1bhphlc	1bhphfc	1blptfc	1blptlc
Injection Pressure	d12dfi1	d12dli1	d1blli1	d1blfi1	1bhptfi1	1bhptli1	1bhphli1	1bhphfi1	1blptfi1	1blptli1
Emissions (Nox)	d12dfnox	d12dlnox	d1bllnox	d1blfnox	1bhptfnx	1bhptlnx	1bhphlnx	1bhphfnx	1blptfnx	1blptlnx
Emission (NO)	d12dfno	d12dlno	d1bllno	d1blfno	1bhptfn	1bhptln	1bhphln	1bhphfn	1blptfn	1blptln

Table E.2 Raw data at 3° advanced timing (day 2)

Fuel	No. 2 diesel	No. 2 diesel	20%LPV	20%LPV	100%HPV	100%HPV	20%HPV	20%HPV	100%LPV	100%LPV
Date	4/28/98	4/28/98	4/28/98	4/28/98	4/28/98	4/28/98	4/28/98	4/28/98	4/28/98	4/28/98
Engine speed (rpm)	1400	1400	1400	1400	1400	1400	1400	1400	1400	1400
% of rated load	20	100	100	20	100	20	100	20	100	20
Brake torque (ft.lb$_f$)	38	190	190	38	190	38	190	38	190	38
Fuel weight (g)	348	1296	1316	618	1167	580	1895	659	1150	509
Time (min)	7	9	9	12	7	10	13	13	7	9
Ambient air temp (°F)	69 8	69 8	69 8	69 8	69 8	69 8	69 8	69 8	69 8	69 8
Patm (mmHg)	733	733	733	733	733	733	733	733	733	733
Temperature (°F)										
1 Inlet air temp	69	69	68	67	70	69	68	69	68	68
3 Inlet manifold temp	82	113	116	83	118	86	116	84	115	85
4 Fuel temp	40	40	40	40	40	40	40	40	40	40
6 Cooling water inlet temp	123	162	163	125	164	125	162	125	165	127
7 Cooling water outlet temp	156	178	176	156	178	156	176	155	179	156
8 Exhaust manifold temp										
9 Exhaust temp shielded	385	841	840	388	839	393	835	390	838	391
10 Thermocouple shield	96	129	129	102	135	102	137	100	136	103
11 Exhaust temp unshieled	396	852	854	399	850	403	847	402	849	402
12 Oil temp	182	214	213	183	216	184	213	182	216	184
13 Building cooling water inlet	59	60	60	59	60	59	60	58	60	59
14 Building cooling water outlet	72	88	89	72	90	72	90	71	90	73
Coolant count/ 10 sec	33 9	147 6	167 9		157 3	35 4	163 5	34	164 1	36 6
Pressure:										
Pressure diff of LFE (in H_2O)	1 85	1 97	2	1 9	1 99	1 84	1 99	1 86	1 97	1 87
Boost pressure (psi)	0 5	3	3	0 5	3	0 5	3	0 5	3	0 5
Oil pressure (psi)	55	50	51	55	50	55	51	55	50	55
Exhaust gass pressure (psi)	1 8	3 2	3 2	1 8	3 2	1 8	1 8	2	2 8	1 7
Relative humidity	31	29	36	40	37	37	40	39	39	38
Emissions: BSCO$_2$ (g/kW-hr)	1265 584	733 166	726 810	1279 925	748 080	1301 288	724 558	1259 852	737 183	1268 880
BSCO (g/kW-hr)	9 838	0 831	0 675	8 292	0 778	5 308	0 639	7 022	0 732	5 138
BSHC (g/kW-hr)	0 690	0 105	0 098	0 654	0 066	0 416	0 102	0 662	0 075	0 538
BSNO$_x$ (g/kW-hr)	23 023	28 102	27 420	23 514	28 175	24 606	27 497	22 868	28 175	24 606
BSNO (g/kW-hr)	20 447	26 727	25 986	20 397	26 627	21 230	25 982	20 009	26 627	21 230
BSO$_2$ (g/kW-hr)	4594 834	625 522	627 686	4661 413	637 346	4628 413	627 512	4596 198	632 456	4565 859
Smoke Number (Bosch)	0 100	1 150	1 050	0 100	0 433	0 100	0 867	0 133	0 467	0 100
BSFC (g/kW-hr)	394 903	228 772	232 302	409 088	264 858	460 721	231 582	402 672	260 999	449 247
File Names Cylinder Pressure	a22dlc	a22dfc	a2lptlc	a2lptlc	a2hphflc	a2hphlc	a2hptflc	a2hptlc	a2lphflc	a2lphlc
Injection Pressure	a22dli	a22dfi	a2lptfi	a2lpthi	a2hphfli	a2hphli	a2hptfi	a2hpthi	a2lphfi	a2lphli
Emissions (NO$_x$)	a22dlnx	a22dfnx	a2lptlnx	a2lptlnx	a2hphflnx	a2hphlnx	a2hptflnx	a2hptlnx	a2lphflnx	a2lphlnx
Emission (NO)	a22dlnx	a22dfn	a2lptflnx	a2lptlnx	a2hphflnx	a2hphlnx	a2hptflnx	a2hptlnx	a2lphflnx	a2lphlnx

Table E.3 Raw data at 3^0 retarded timing (day 3)

Fuel		No 2 diesel	No 2 diesel	20%HPV	20%HPV	100%LPV	100%LPV	100%HPV	100%HPV	20%LPV	20%LPV
Date		4/30/98	4/30/98	4/30/98	4/30/98	4/30/98	4/30/98	4/30/98	4/30/98	4/30/98	4/30/98
Engine speed (rpm)		1400	1400	1400	1400	1400	1400	1400	1400	1400	1400
% of rated load		100	20	100	20	20	100	100	20	100	20
Brake torque (ft lb$_f$)		190	38	190	38	38	190	190	38	190	38
Fuel weight (g)		2273	791	3197	1062	1665	3720	3753	1204	1324	1413
Time (min)		16	16	22	21	29	23	23	21	9	28
Ambient air temp (°F)		69 8	69 8	69 8	69 8	69 8	69 8	69 8	69 8	69 8	69 8
Patm (mmHg)		733	733	733	733	733	733	733	733	733	733
Temperature (°F)											
1 Inlet air temp		67	67	69	68	67	68	68	68	68	68
3 Inlet manifold temp		114	82	118	84	83	115	119	87	120	90
4 Fuel temp		40	40	40	40	40	40	40	40	40	40
6 Cooling water inlet temp		159	119	159	118	118	160	160	121	158	120
7 Cooling water outlet temp		176	153	176	154	155	176	177	154	175	154
9 Exhaust temp shielded		853	392	852	395	397	833	834	398	854	396
10 Thermocouple shield		127	98	138	96	98	126	128	100	128	99
11 Exhaust temp unshielded		867	403	868	407	408	847	846	409	869	408
12 Oil temperature		210	180	211	180	180	212	213	182	211	182
13 Building cooling water inlet		59	58	57	59	59	60	60	59	60	59
14 Building cooling water outlet		85	70	83	70	70	86	87	71	86	71
Coolant count/ 10 sec		124 6	28 6	123 9			127 3	132 2	31 6	130 9	30 4
Pressure diff of EFE (in H_2O)		1 99	1 88	1 99	1 9	1 9	1 99	1 99	1 9	1 99	1 92
Boost pressure (psi)		3 2	0 5	3 2	0 5	0 5	3	3	0 5	3 2	0 5
Oil pressure (psi)		51	55	51	55	55	51	51	55	51	55
Exhaust gass pressure (psi)		3 3	2	3 3	2	2	3 2	3 2	2	3 3	2
Relative humidity		46	46	42	44	44	43	43	46	47	45
Emissions	BSCO$_2$ (g/kW-hr)	723 301	1258 538	722 316	1256 847	1288 136	725 756	732 194	1286 331	721 228	1254 185
	BSCO (g/kW-hr)	0 483	8 496	0 410	5 573	5 035	0 346	0 301	4 105	0 380	6 690
	BSHC (g/kW-hr)	0 110	0 655	0 110	0 524	0 265	0 057	0 040	0 195	0 112	0 594
	BSNO$_x$ (g/kW-hr)	16 232	14 131	16 342	13 217	13 593	18 098	18 762	14 176	17 192	14 889
	BSNO (g/kW-hr)	15 516	9 462	15 607	9 526	9 861	17 212	17 802	10 039	16 285	10 080
	BSO$_2$ (g/kW-hr)	640 238	4694 997	635 050	4644 387	4668 659	648 148	647 344	4664 362	639 037	4655 284
Smoke Number (Bosch)		1 967	0 100	1 750	0 200	0.250	1 200	1 100	0 333	1 750	0 200
BSFC (g/kW-hr)		225 693	392 705	230 866	401 712	456 064	256 954	259 233	455 425	233 714	400 861
File Names	Cylinder Pressure	r32dfc	r32dlc	r3hptfc	r3hptlc	r3lphlc	r3lphfc1	r3hphfc	r3hphlc	r3lptfc	r3lptlc
	Injection Pressure	r32dfi	r32dli	r3hptfi	r3hptli	r3lphli	r3lphfi	r3hphfi	r3hphli	r3lptfi	r3lptli
	Emissions (NO$_x$)	r32dfnx	r32dlnx	r3hptfnx	r3hptlnx	r3lphlnx	r3lphfnx	r3hphfnx	r3hphlnx	r3lptfnx	r3lptlnx
	Emission (NO)	r32dfn	r32dln	r3hptfn	r3hptln	r3lphln	r3lphfn	r3hphfn	r3hphln	r3lptfn	r3lptln

Table E.4 Raw data at 3° retarded timing (day 4)

Fuel	No 2 diesel	No 2 diesel	100%HPV	100%HPV	20%LPV	20%LPV	20%HPV	20%HPV	100%LPV	100%LPV
Date	5/6/98	5/6/98	5/6/98	5/6/98	5/6/98	5/6/98	5/6/98	5/6/98	5/6/98	5/6/98
Engine speed (rpm)	1400	1400	1400	1400	1400	1400	1400	1400	1400	1400
% of rated load	100	20	100	20	20	100	100	20	20	100
Brake torque (ft lbf)	190	38	190	38	38	190	190	38	38	190
Fuel weight (g)	1287	498	1955	632	657	583	1312	659	1024	2100
Time (min)	9	10	12	11	13	4	9	13	18	13
Ambient air temp (°F)	71 6	71 6	71 6	71 6	70 7	71 6	71 6	71 6	71 6	71 6
Patm (mmHg)	733	733	733	733	733	733	733	733	733	733
Temperature (°F)									70	
1 Inlet air temp	69	69	69	69	69	72	70	69	70	117
3 Inlet manifold temp	117	84	118	86	86	123	118	86	86	40
4 Fuel temp	40	40	40	40	40	40	40	40	40	156
6 Cooling water inlet temp	157	118	158	119	117	156	154	117	117	175
7 Cooling water outlet temp	173	153	176	153	153	175	171	153	154	835
9 Exhaust temp shielded	849	394	832	399	393	854	851	395	397	136
10 Thermocouple shield	141	113	136	108	105	134	133	103	102	849
11 Exhaust temp unshieled	860	403	845	409	404	867	866	407	408	211
12 Oil temperature	210	180	212	181	179	211	209	181	180	56
13 Building cooling water inlet	57	56	57	57	57	56	57	56	56	86
14 Building cooling water outlet	86	71	86	71	71	84	86	71	71	113 4
Coolant count/ 10 sec	138	30 1	121 1	30 1	28 3	113 5	123	28 2	25 6	1 99
Pressure diff of EFE (in H_2O)	1 99	1 91	1 99	1 94	1 95	1 99	1 99	1 91	1 95	3
Boost pressure (psi)	3	0 5	3	0 5	0 5	3	3	0 5	0 5	51
Oil pressure (psi)	52	55	55 5	55	55	51	51	55	55	3 3
Exhaust gass pressure (psi)	3 2	2	3 3	1 8	2	3 3	3 4	1 9	1 9	46
Relative humidity	22	26	39	43	45	44	44	45	45	
Emissions $BSCO_2$ (g/kW-hr)	728 07437	1267 7659	731 03963	1289 0501	1256 0282	724 46251	724 60058	1259 8517	1276 3591	724 85535
BSCO (g/kW-hr)	0 4802851	7 8096035	0 3520033	4 1964929	6 4005593	0 470194	0 4481035	5 2597523	5 1312311	0 4023038
BSHC (g/kW-hr)	0 110787	0 7108044	0 0440539	0 2297962	0 6636457	0 1094388	0 0971149	0 551341	0 3091238	0 0444716
$BSNO_x$ (g/kW-hr)	16 282978	14 442604	19 378626	11 470205	13 482501	17 109917	16 758761	12 589992	14 045516	18 15005
BSNO (g/kW-hr)	16 360075	11 412793	18 171001	7 6433268	9 744498	16 288949	16 065223	8 4029847	10 347403	17 421623
BSO_2 (g/kW-hr)	637 40306	4666 5495	639 90746	4595 8931	4597 0466	628 68526	632 87771	4658 523	4662 3653	639 25882
Smoke Number (Bosch)	1 8667	0 1333	0 9667	0 3333	0 3	1 7	1 7	0 4	0 2667	1 3
BSFC (g/kW-hr)	227 18287	395 58416	258 82431	456 38771	401 45009	231 55177	231 5959	402 67216	451 89444	256 63476
File Names Cylinder Pressure	r42dfc	r42dlc	r4hphfc	r4hphlc	r4lptlc	r4lptfc	r4hptfc	r4hptlc	r4lphlc	r4lphfc
Injection Pressure	r42dfi	r42dli	r4hphfi	r4hphli	r4lptli	r4lptfi	r4hptfi	r4hptli	r4lphli	r4lphfi
Emissions (NO_x)	r42dfnx	r42dlnx	r4hphfnx	r4hphlnx	r4lptlnx	r4lptfnx	r4hptfnx	r4hptlnx	r4lphlnx	r4lphfnx
Emission (NO)	r42dfn	r42dln	r4hphfn	r4hphln	r4lptln	r4lptfn	r4hptfn	r4hptln	r4lphln	r4lphfn

Table E.5 Raw data at standard timing (day 5)

Fuel	No 2 diesel	No 2 diesel	20%HPV	20%HPV	100%HPV	100%HPV	100%LPV	100%LPV	20%LPV	20%LPV
Date	5/17/98	5/17/98	5/17/98	5/17/98	5/17/98	5/17/98	5/17/98	5/17/98	5/17/98	5/17/98
Engine speed (rpm)	1400	1400	1400	1400	1400	1400	1400	1400	1400	1400
% of rated load	100	20	20	100	100	20	20	100	20	100
Brake torque (ft lb)	190	38	38	190	190	38	38	190	38	190
Fuel weight (g)	2855	594	357	1757	1965	679	507	1137	356	1171
Time (min)	20	12	7	12	12	12	9	7	7	8
Ambient air temp (°F)	68	66	66	66	65	66	65	65	66	66
Patm (mmHg)	733	733	732	732	732	732	732	732	732	732
Temperature (°F)										
1 Inlet air temp	71	69	69	69	69	69	69	69	70	71
3 Inlet manifold temp	119	94	85	113	122	90	90	118	94	123
4 Fuel temp	40	40	40	40	40	40	40	40	40	40
6 Cooling water inlet temp	162	122	119	162	162	124	122	164	123	161
7 Cooling water outlet temp	175	154	161	177	176	155	154	177	154	176
8 Exhaust manifold temp				829						
9 Exhaust temp shielded	843	388	394	843	832	393	394	831	390	842
10 Thermocouple shield	139	114	105	134	145	114	116	147	114	147
11 Exhaust temp unshieled	844	393	399	841	831	398	398	829	395	841
12 Oil temp	212	181	184	212	214	183	180	212	182	212
13 Building cooling water inlet	54	53	54	54	54	53	53	53	53	53
14 Building cooling water outlet	89	73	72	88	90	74	74	89	74	89
Coolant count/ 10 sec	177 3	34 8	26 2	146 6	159 3	37 5	34 5	154 4	35 5	148 8
Pressure:										
Pressure diff of FFE (in H_2O)	1 96	1 8	1 81	1 97	1 9	1 8	1 79	1 92	1 72	1 9
Boost pressure (psi)	3	0 5	0 5	3	3	0 5	0 5	3	0 5	3
Oil pressure (psi)	55	55	54	50	50	54	54	50	55	50
Exhaust gass pressure (psi)	3 3	1 8	2	3 2	3 1	1 9	2	3 2	1 8	3 2
Relative humidity	52	57	58	57	58	59	59	58	58	58
Emissions: $BSCO_2$(g/kW-hr)	726 802	1260 129	1267 499	727 776	734 779	1269 504	1263 895	728 849	1263 948	727 569
BSCO(g/kW-hr)	0 603	10 272	6 431	0 491	0 349	4 526	5 515	0 405	7 128	0 499
BSHC(g/kW-hr)	0 096	0 697	0 667	0 090	0 049	0 352	0 418	0 061	0 692	0 097
$BSNO_x$(g/kW-hr)	20 883	19 213	18 011	21 804	23 082	18 369	20 447	24 112	20 604	21 505
BSNO(g/kW-hr)	19 639	15 057	14 806	19 989	21 959	15 147	16 070	22 764	15 652	19 799
BSO_2(g/kW-hr)	611 138	4556 063	4623 736	622 491	625 364	4556 304	4471 519	626 634	4590 412	618 156
Smoke Number (Bosch)	1 367	0 100	0 100	1 167	0 500	0 100	0 100	0 533	0 067	1 133
BSFC(g/kW-hr)	226 786	393 201	405 116	232 611	260 148	449 467	447 481	258 049	403 982	232 545
File Names Cylinder Pressure	5a2dfc	5b2dlc	5bhptlc	5bhptfc	5bhphfc	5bhphlc	5blphlc	5blphfc	5blptlc	5blptfc
Injection Pressure	5a2dfi	5b2dli	5bhptli	5bhptfi	5bhphfi	5bhphli	5blphli	5blphfi	5blptli	5blptfi
Emissions (NO_x)	5a2dfnx	5b2dlnx	5bhptlnx	5bhptfnx	5bhphfnx	5bhphlnx	5blphlnx	5blphfnx	5blptlnx	5blptfnx
Emissions (NO)	5a2dfn	5b2dln	5bhptln	5bhptfn	5bhphfn	5bhphln	5blphln	5blphfn	5blptln	5blptfn

Table E.6 Raw data at 3° advanced timing (day 6)

Fuel	No 2 diesel	No 2 diesel	20%alHPV	20%HPV	100%al PV	100%al PV	100%alHPV	100%alHPV	20%al PV	20%al PV
Date	5/21/98	5/21/98	5/21/98	5/21/98	5/21/98	5/21/98	5/21/98	5/21/98	5/21/98	5/21/98
Engine speed (rpm)	1400	1400	1400	1400	1400	1400	1400	1400	1400	1400
% of rated load	20	100	100	20	20	100	20	100	20	100
Brake torque (ft lb$_f$)	38	190	190	38	38	190	38	190	38	190
Fuel weight (g)	653	1455	1632	568	460	1500	806	2348	504	441
Time (min)	13	10	11	11	8	9	14	14	10	3
Ambient air temp (°F)	67	67	66	67	66	67	66	67	65	67
Patm (mmHg)	732	730	730	730	730	729	732	729	730	730
Temperature (°F)										
1 Inlet air temp	70	70	70	71	71	71	70	71	69	71
3 Inlet manifold temp	86	120	120	89	87	119	87	118	84	116
4 Fuel temp	40	40	40	40	40	40	40	40	40	40
6 Cooling water inlet temp	125	165	163	126	123	165	124	165	124	165
7 Cooling water outlet temp	156	178	177	156	156	179	155	179	156	178
9 Exhaust temp shielded	386	858	850	391	394	846	391	851	387	849
10 Thermocouple shield	117	140	135	105	104	133	104	136	103	136
11 Exhaust temp unshieled	391	856	849	397	398	854	394	849	393	849
12 Oil temperature	182	214	215	184	183	217	183	217	183	215
13 Building cooling water inlet	58	60	58	56	55	55	54	55	55	55
14 Building cooling water outlet	74	91	91	75	75	91	74	92	75	92
Coolant count/ 10 sec	368	1716	1721	371	342	1764	362	1793	36	1697
Pressure diff of EFF (in H_2O)	1 81	1 97	1 93	1 76	1 76	1 99	1 77	1 94	1 79	1 95
Boost pressure (psi)	0 5	3	3	0 5	0 5	3	0 5	3	0 5	3
Oil pressure (psi)	54	50	50	54	54	50	54	50	54	50
Exhaust gass pressure (psi)	1 9	3	3 2	1 9	1 9	3 2	1 9	3 2	1 8	3
Relative humidity	38	46	44	43	47	47	48	50	48	45
Emissions BSCO$_2$(g/kW-hr)	1278 732	740 803	737 454	1283 314	1290 070	747 867	1291 673	752 568	1252 587	730 676
BSCO(g/kW-hr)	10 639	1 166	0 849	7 504	6 149	0 816	5 054	0 789	8 460	0 817
BSHC(g/kW-hr)	0 770	0 106	0 101	0 691	0 543	0 079	0 448	0 069	0 795	0 102
BSNO$_x$(g/kW-hr)	24 955	26 558	28 004	25 270	25 524	29 074	24 297	29 593	23 586	26 627
BSNO(g/kW-hr)	21 199	26 452	26 690	16 803	21 706	27 569	21 333	27 006	18 954	25 125
BSO$_2$(g/kW-hr)	4613 736	610 612	613 566	4628 777	4584 850	616 049	4598 706	618 899	4552 678	612 664
Smoke Number (Bosch)	0 100	0 967	0 700	0 100	0 067	0 433	0 067	0 433	0 067	0 933
BSFC (g/kW-hr)	399 006	231 155	235 704	410 171	456 749	264 782	457 316	266 446	400 350	233 538
File Names Cylinder Pressure	62dlc1	62dlc	6hptlc	6hptlc	6lphlc	6lphtc	6hphlc	6hphtc	6lptlc	6lptlc
Injection Pressure	62dli	62dli	6hptli	6hptli	6lphli	6lphti	6hphli	6hphti	6lptli	6lptli
Emissions (NO$_x$)	62dlnx	62dlnx	6hptlnx	6hptlnx	6lphlnx	6lphlnx	6hphlnx	6hphlnx	6lptlnx	6lptlnx
Emissions (NO)	62dln	62dln	6hptln	6hptln	6lphln	6lphln	6hphln	6hphln	6lptln	6lptln

Table E.7 Raw data at 3° advanced timing (day 7)

Fuel		No. 2 diesel	No. 2 diesel	20%HPV	20%HPV	100%HPV	100%HPV	20%LPV	20%LPV	100%LPV	100%LPV
Date		5/28/98	5/28/98	5/28/98	5/28/98	5/28/98	5/28/98	5/28/98	5/28/98	5/28/98	5/28/98
Engine speed (rpm)		1400	1400	1400	1400	1400	1400	1400	1400	1400	1400
% of rated load		20	100	100	20	20	100	20	100	20	100
Brake torque (ft lb$_f$)		38	190	190	38	38	190	38	190	38	190
Fuel weight (g)		765	2325	2392	608	952	2193	1013	2066	746	1812
Time (min)		15	16	16	12	16	13	20	14	13	11
Ambient air temp (°F)		66	66	66	66	66	66	67	67	67	68
Patm (mmHg)		731	731	731	731	732	733	733	732	730	730
Temperature (°F)											
1	Inlet air temp	71	71	71	70	70	71	71	70	70	72
3	Inlet manifold temp	91	123	125	91	89	121	90	118	86	114
4	Fuel temp	40	40	40	40	40	40	40	40	40	40
6	Cooling water inlet temp	126	166	166	126	124	166	124	163	125	165
7	Cooling water outlet temp	155	178	178	155	156	178	155	177	156	179
9	Exhaust temp shielded	386	860	860	389	392	847	388	845	390	847
10	Thermocouple shield	104	148	145	111	109	138	109	141	105	143
11	Exhaust temp unshield	392	856	857	396	398	846	394	844	395	846
12	Oil temperature	182	217	217	183	183	217	183	215	183	216
13	Building cooling water inlet	57	59	58	56	55	55	55	55	65	63
14	Building cooling water outlet	75	93	93	76	76	93	76	93	78	92
Coolant count/ 10 sec		39 2	187 4	187 8	38 6	36 8	186 1	37	166 4	35 8	169 7
Pressure diff Of LFE (in H_2O)		1 81	1 94	1 94	1 79	1 77	1 95	1 81	1 95	1 73	1 94
Boost pressure (psi)		0 5	3	3	0 5	0 5	3	0 5	3	0 5	3
Oil pressure (psi)		54	50	50	54	54	50	54	50	54	50
Exhaust gass pressure (psi)		1 8	3 4	3 2	1 8	1 8	3 3	1 8	3 4	2	3 2
Relative humidity		58	57	56	57	57	57	58	59	61	59
Emissions	$BSCO_2$(g/kW-hr)	1298 314	739 848	743 102	1259 214	1334 942	756 956	1258 800	733 516	1287 481	739 164
	BSCO(g/kW-hr)	11 621	1 184	1 001	7 338	5 397	0 849	8 246	1 034	7 498	0 963
	BSHC(g/kW-hr)	0 880	0 113	0 102	0 680	0 393	0 072	0 728	0 109	0 490	0 075
	$BSNO_x$(g/kW-hr)	22 813	25 025	29 643	25 508	25 976	30 679	24 449	26 100	24 689	28 403
	BSNO(g/kW-hr)	21 465	22 762	27 454	20 529	23 307	28 811	18 566	24 227	19 279	26 358
	BSO_2(g/kW-hr)	4625 783	601 883	604 198	4511 985	4672 952	614 495	4513 319	611 778	4598 351	616 070
Smoke Number (Bosch)		0 067	1 000	0 867	0 033	0 067	0 400	0 000	0 867	0 100	0 400
BSFC (g/kW-hr)		405 116	230 857	237 509	402 468	472 636	268 000	402 336	234 445	455 832	261 701
File Names	Cylinder Pressure	72dlc	72dfc	7hptfc	hptlc	7hphlc	7hphfc1	7lptlc	7lptfc	7lphlc	7lphfc
	Injection Pressure	72dli	72dfi	7hptfi	hptli	7hphli	7hphfi	7lptli	7lptfi	7lphli	7lphfi
	Emissions (NO_x)	72dlnx	72dfnx	7hptfnx	hptlnx	7hphlnx	7hphfnx	7lptlnx	7lptfnx	7lphlnx	7lphfnx
	Emissions (NO)	72dln	72dfn	7hptfn	hptln	7hphln	7hphfn	7lptln	7lptfn	7lphln	7lphfn

Table E.8 Raw data at 3° retarded timing (day 8)

Fuel	No. 2 diesel	No. 2 diesel	20%HPV	20%HPV	100%LPV	100%LPV	100%HPV	100%HPV	20%LPV	20%LPV
Date	5/29/98	5/29/98	5/29/98	5/29/98	5/29/98	5/29/98	5/29/98	5/29/98	5/29/98	5/29/98
Engine speed (rpm)	1400	1400	1400	1400	1400	1400	1400	1400	1400	1400
% of rated load	100	20	20	100	20	100	20	100	100	20
Brake torque (ft lb)	190	38	38	190	38	190	38	190	190	38
Fuel weight (g)	2151	743	403	188	641	1620	572	1798	2065	756
Time (min)	15	15	8	13	11	10	10	11	14	15
Ambient air temp (°F)	68	69	68	68	69	69	69	66	66	66
Patm (mmHg)	732	733	732	732	731	731	730	730	728	728
Temperature (°F)										
1 Inlet air temp	69	70	69	69	70	70	70	70	70	70
3 Inlet manifold temp	127	91	89	115	89	119	89	121	124	92
4 Fuel temp	40	40	40	40	40	40	40	40	40	40
6 Cooling water inlet temp	160	121	117	161	122	161	121	161	159	122
7 Cooling water outlet temp	175	154	160	176	156	177	155	176	173	155
9 Exhaust temp shielded	858	395	394	849	397	838	399	840	856	394
10 Thermocouple shield	154	118	110	143	108	147	109	140	142	109
11 Exhaust temp unshieled	858	401	400	850	403	839	403	840	861	399
12 Oil temperature	211	182	183	211	182	212	181	212	210	182
13 Building cooling water inlet	63	65	63	64	65	66	65	64	63	64
14 Building cooling water outlet	91	76	74	92	77	93	77	93	93	78
Coolant count/ 10 sec	138 5	32 7	24	136 2	32 7	143 8	32 3	142 1	151 9	33 6
Pressure diff of EFF (in H_2O)	1 99	1 82	1 8	1 95	1 8	1 98	1 79	1 95	1 99	1 82
Boost pressure (psi)	3	0 5	0 5	3	0 5	3	0 5	3	3	0 5
Oil pressure (psi)	50	54	54	55	54	50	54	50	50	54
Exhaust gass pressure (psi)	3 2	2	2	3 2	2	3 3	2	3 2	3 2	3
Relative humidity	60	61	62	61	61	61	61	60	60	60
Emissions $BSCO_2$(g/kW-hr)	730 111	1260 977	1251 966	720 735	1277 407	726 926	1283 339	733 453	723 161	1252 587
BSCO(g/kW-hr)	0 651	8 455	6 645	0 729	6 365	0 652	4 156	0 554	0 686	6 936
BSHC(g/kW-hr)	0 121	0 619	0 512	0 099	0 383	0 059	0 259	0 052	0 105	0 602
$BSNO_x$(g/kW-hr)	16 200	14 214	12 774	15 892	14 119	18 772	11 592	19 261	16 939	13 564
BSNO(g/kW-hr)	15 372	9 641	9 291	14 474	10 140	17 402	11 592	18 091	16 020	9 482
BSO2(g/kW-hr)	631 182	4563 353	4579 261	633 385	4700 556	641 176	4641 027	646 116	639 479	4652 011
Smoke Number (Bosch)	2 000	0 100	0 300	1 900	0 133	1 267	0 300	1 067	1 900	0 167
BSFC (g/kW-hr)	227 818	393 466	400 152	230 360	462 887	257 368	454 366	259 679	234 332	400 350
File Names Cylinder Pressure	82dfc	82dlc	8hptlc	8hptfc	8lphlc	8lphfc1	8hphlc	8hphfc	8lptfc	8lptlc
Injection Pressure	82dfi1	82dli	8hptli	8hptfi	8lphli	8lphfi	8hphli	8hphfi	8lptfi	8lptli
Emissions (NO_x)	82dfnx	82dlnx	8hptlnx	8hptfnx	8lphlnx	8lphfnx	8hphlnx	8hphfnx	8lptfnx	8lptlnx
Emission (NO)	82dfn	82dln	8hptln	8hptfn	8lphln	8lphfn	8hphln	8hphfn	8lptfn	8lptln

Table E.9 Raw data at standard timing (day 9)

Fuel	No. 2 diesel	No. 2 diesel	20%HPV	20%HPV	20%LPV	20%LPV	100%HPV	100%HPV	100%LPV	100%LPV
Date	6/1/98	6/1/98	6/1/98	6/1/98	6/1/98	6/1/98	6/1/98	6/1/98	6/1/98	6/1/98
Engine speed (rpm)	1400	1400	1400	1400	1400	1400	1400	1400	1400	1400
% of rated load	100	20	20	100	20	100	100	20	20	100
Brake torque (ft lb)	190	38	38	190	38	190	190	38	38	190
Fuel weight (g)	998	791	560	1420	618	1460	2639	913	800	2120
Time (min)	7	16	11	10	12	10	16	16	14	13
Ambient air temp (°F)	66	65	65	65	66	65	65	66	65	65
Patm (mmHg)	722	723	723	724	723	723	723	723	724	725
Temperature (°F)										
1 Inlet air temp	70	70	69	70	69	70	69	70	69	69
3 Inlet manifold temp	121	89	87	117	89	119	119	89	86	117
4 Fuel temp	40	40	40	40	40	40	40	40	40	40
6 Cooling water inlet temp	161	122	121	161	122	161	160	123	122	162
7 Cooling water outlet temp	176	155	155	176	156	177	176	156	156	177
8 Exhaust manifold temp										
9 Exhaust temp shielded	854	391	396	841	393	847	838	395	394	840
10 Thermocouple shield	138	105	108	140	96	135	135	103	100	134
11 Exhaust temp unshieled	854	396	402	839	397	846	838	401	399	839
12 Oil temp	213	182	181	213	183	213	214	184	182	215
13 Building cooling water inlet	62	62	61	62	65	65	63	63	63	63
14 Building cooling water outlet	91	76	75	92	78	93	93	77	77	93
Coolant count/ 10 sec	145 7	33 4	31 9	145 3	32 4	142 8	141 6	33 6	32 3	146 6
Pressure										
Pressure diff of FFE (in H_2O)	1.95	1 75	1 8	1 97	1 84	1 96	1 95	1 75	1 81	1 93
Boost pressure (psi)	3	0 5	0 05	3	0 5	3	3	0 5	0 5	3
Oil pressure (psi)	50	54	54	50	54	50	50	54	54	50
Exhaust pressure (psi)	3 2	1 8	1 8	3 2	1 8	3 2	3 2	2	2	3
Relative humidity	51	51	50	50	51	51	51	53	53	51
Emissions BSCO$_2$(g/kW-hr)	725 892	1258 538	1265 239	725 705	1279 925	725 705	740 108	1280 254	1282 057	731 759
BSCO(g/kW-hr)	0 594	9 557	6 844	0 539	7 596	0 632	0 566	4 705	6 598	0 663
BSHC(g/kW-hr)	0 107	0 662	0 591	0 099	0 604	0 103	0 048	0 262	0 327	0 051
BSNOx(g/kW-hr)	21 136	19 827	18 060	21 818	19 006	21 557	25 369	18 791	20 512	24 126
BSNO(g/kW-hr)	20 365	15 174	14 374	19 983	14 569	19 797	23 425	15 059	16 127	23 142
BSO$_2$(g/kW-hr)	604 736	4560 778	4526 697	609 266	4643 756	616 227	624 739	4556 729	4545 592	616 074
Smoke number (Bosch)	1 367	0 067	0 133	1 133	0 067	1 167	0 533	0 100	0 067	0 700
BSFC(g/kW-hr)	226 502	392 705	404 394	231 949	409 088	231 949	262 035	453 274	453 912	259 079
File Name Cylinder Pressure	92dfc	92dlc	9hptlc	9hptfc	9lptlc	9lptfc	9hphfc	9hphlc	9lphlc	9lphfc
Injection Pressure	92dfi	92dli	9hptli	9hptfi	9lptli	9lptfi	9hphfi	9hphli	9lphlc	9lphfi
Emission (NO$_x$)	92dfnx	92dlnx	9hptlnx	9hptfnx	9lptlnx	9lptfnx	9hphfnx	9hphlnx	9lphlc	9lphfnx
NO emission (NO)	92dfn	92dln	9hptln	9hptfn	9lptln	9lptfn	9hphfn	9hphln	9lphlc	9lphfn

Table E.10 Combustion characteristics at standard timing

% load	Fuel	Start of Injection (°BTDC)				Start of Combustion (°BTDC)				Ignition Delay (degree)			
		Day 1	Day 5	Day 9	Average	Day 1	Day 5	Day 9	Average	Day 1	Day 5	Day 9	Average
100	100%HPV	17.65	17.40	17.70	17.58	12.20	12.20	12.50	12.30	5.45	5.20	5.20	5.28
100	100%LPV	17.61	17.30	17.80	17.57	11.50	11.20	11.40	11.37	6.11	6.10	6.40	6.20
100	20%HPV	15.36	15.35	13.55	14.75	9.10	9.30	7.10	8.50	6.26	6.05	6.45	6.25
100	20%LPV	15.55	15.60	15.65	15.60	9.00	9.00	9.00	9.00	6.55	6.60	6.65	6.60
100	2D	16.96	15.08	15.30	15.78	9.10	9.80	8.00	8.97	7.86	5.28	7.30	6.81
20	100%HPV	13.18	14.50	14.35	14.01	5.60	7.40	7.50	7.17	6.58	7.10	6.85	6.84
20	100%LPV	13.00	13.75	14.25	13.67	5.70	6.20	6.50	6.13	7.30	7.55	7.75	7.53
20	20%HPV	12.75	12.50	13.00	12.75	4.60	4.20	4.80	4.53	8.15	8.30	8.20	8.22
20	20%LPV	12.85	12.75	12.90	12.83	4.20	4.10	4.00	4.10	8.65	8.65	8.90	8.73
20	2D	12.70	12.55	12.95	12.73	3.20	3.00	3.20	3.13	9.50	9.55	9.75	9.60

Table E.11 Combustion characteristics at 3° advanced timing

% load	Fuel	Start of Injection (°BTDC)				Start of Combustion (°BTDC)				Ignition Delay (degree)			
		Day 2	Day 6	Day 7	average	Day 2	Day 6	Day 7	average	Day 2	Day 6	Day 7	average
100	100%HPV	20.45	20.59	20.50	20.51	14.50	14.80	14.70	14.67	5.95	5.79	5.80	5.85
100	100%LPV	20.45	21.50	20.35	20.77	13.70	14.50	13.60	13.93	6.75	7.00	6.75	6.83
100	20%HPV	17.90	19.50	20.30	19.23	11.20	12.50	13.00	12.23	6.70	7.00	7.30	7.00
100	20%LPV	17.85	18.30	18.40	18.18	10.50	11.00	11.00	10.83	7.35	7.30	7.40	7.35
100	2D	19.25	20.20	20.20	19.88	11.20	11.90	12.00	11.70	8.05	8.30	8.20	8.18
20	100%HPV	15.85	16.65	16.75	16.42	8.90	9.50	9.60	9.33	6.95	7.15	7.15	7.08
20	100%LPV	16.18	16.52	16.17	16.29	7.90	8.50	8.10	8.17	8.28	8.02	8.07	8.12
20	20%HPV	14.82	15.80	16.22	15.61	6.30	7.30	7.30	6.97	8.52	8.50	8.92	8.65
20	20%LPV	14.97	15.17	15.30	15.15	5.50	5.70	6.20	5.80	9.47	9.47	9.10	9.35
20	2D	15.55	16.62	16.85	16.34	5.40	6.20	6.50	6.03	10.15	10.42	10.35	10.31

Table E.12 Combustion characteristics at 3° retarded timing

% load	Fuel	Start of Injection (°BTDC)				Start of Combustion (°BTDC)				Ignition Delay (degree)			
		Day 3	Day 4	Day 8	average	Day 3	Day 4	Day 8	average	Day 3	Day 4	Day 8	average
100	100%HPV	14.12	15.50	13.50	14.37	9.30	10.20	8.70	9.40	4.82	5.30	4.80	4.97
100	100%LPV	13.85	14.25	13.65	13.92	8.40	8.70	8.00	8.37	5.45	5.55	5.65	5.55
100	20%HPV	11.85	12.57	11.95	12.12	6.40	7.00	6.30	6.57	5.45	5.57	5.65	5.56
100	20%LPV	12.25	13.67	12.30	12.74	6.20	7.50	6.10	6.60	6.05	6.17	6.20	6.14
100	2D	11.72	12.45	12.50	12.22	5.20	6.60	5.50	5.77	6.52	5.85	7.00	6.46
20	100%HPV	10.20	10.60	9.90	10.23	3.90	4.20	3.50	3.87	6.30	6.40	6.40	6.37
20	100%LPV	9.97	10.20	9.90	10.02	3.00	3.00	2.50	2.83	6.97	7.20	7.40	7.19
20	20%HPV	9.50	9.80	9.75	9.68	1.50	2.00	2.00	1.83	8.00	7.80	7.75	7.85
20	20%LPV	9.60	10.60	9.25	9.82	1.10	2.00	1.00	1.37	8.50	8.60	8.25	8.45
20	2D	9.50	10.55	9.30	9.78	0.20	1.40	0.30	0.63	9.30	9.15	9.00	9.15

REFERENCES

1. Scholl, K.W., Sorenson, S.C. Combustion of Soybean Oil Methyl Ester in a Direct Injection Diesel Engine. SAE paper 930934, 1993.

2. Wagner, L.E., Clark, S.J., Schrock, M.D. Effects of Soybean Oil Esters on the Performance, Lubrication Oil, and Water of Diesel Engines. SAE paper 841385, 1984.

3. Ryan III, T.W., Dodge, L.G., and Callahan, T.J. The Effects of Vegetable Oil Properties on Injection and Combustion in Two Different Diesel Engines. JAOCS, Vol. 61(10), p1610, 1984.

4. Goering, C.E., Schwab, A.W., Dangherty, M.J., Pryde, E.H. and Heakin, A.J. Fuel Properties of Eleven Vegetable Oils. Transactions of the ASAE Vol. 25(6): November, 1982.

5. Bagby, M.O., Freedman, B. and Schwab, A.W. Seed Oils for Diesel Fuels: Source and Properties. ASAE Technical Paper No. 87-1583, ASAE, Chicago, 1987, pp. 1-16.

6. Knothe, G., Bagby, M.O., Ryan III, T.W., Callahan, T.J., and Wheeler, H.G. Vegetable Oils as Alternative Diesel Fuels: Degradation of Pure Triglycerides During the Precombustion Phase in a Reactor Simulating a Diesel Engine. SAE paper 920194, 1992, pp37-63.

7. Engelman, H.W., Guerther, D.A., and Silver, T.W. Vegetable Oil as a Diesel Fuel. ASME, July, 1978, Presented at the Energy Technology Conf. & Exhibition. Houston, Texas, Nov. 5-9, 1978.

8. Hawkins, C.S., Fuls, J., and Hugo, F.J.C. Engine Durability Tests with Sunflower Oil in an Indirect Injection Diesel Engine. ASAE paper 831357, 1983, pp1-4.

9. Baker, Q.A. Alternative Fuels for Medium-Speed Diesel Engines (AFFMSDE), Southwest Research Institute, October 26-29, 1981.

10. Sims, R.E.H. Tallow Esters as an Alternative Diesel Fuel. ASAE Trans., Vol. 28(3), May-June, 1985, pp716-721.

11. Anon. The Biological Liquid Fuels Alternative Technology Status and Engineering Considerations. America Society of Agricultural Engineering, St. Joseph, MI, 36, 1981.

12. Korus, R.A., Mousetis, T.L. and Lloyd, L. Polymerization of Vegetable Oils. Vegetable Oils Fuels Proceedings of the Int. Conf. on Plant and Vegetable Oils as Fuels. ASAE 482, Fargo, ND, 1982.

13. Lague, C.M., Lo, K.V., and Slaley, L.M. Waste Vegetable Oil as a Diesel Fuel Extender. Canadian Agricultural Engineering, Vol. 30(1), 1988, pp 27-32.

14. Perkins, L.A. and Peterson, C.L. Durability, and Auld, D.L. Testing of Transesterfied Winter Rape Oil (Brassica Napus L.) as Fuel in Small Bore, Multi-Cylinder, DI, CI Engines. SAE paper 911764, 1991.

15. Pestes, N.M. and Stanislao, J. Piston Ring Deposits when Using Vegetable Oil as a Fuel. Journal of Testing and Evaluation, Vol. 12, No. 2, March 1984, pp 61-68.

16. Clark, S.J., Wagner, L., Schrock, M.D. and Piennaar, P.G. Methyl and Ethyl Soybean Esters as Renewable Fuels for Diesel Engines. JAOCS, Vol. 61, No. 10, Oct. 1984, pp 1632-1638.

17. Vellguth, G. Performance of Vegetable Oils and Their Monoesters as Fuels for Diesel Engines. SAE paper 831358, 1983.

18. Zhang, Q., Feldman, M. and Peterson, C.L. Diesel Engine Durability when Fueled with Methyl Ester of Winter Rapeseed Oil. ASAE paper 881562, 1988

19. Kusy, P.F. Transesterification of Vegetable Oils for Fuels. Vegetable Oils Fuels Proceedings of the Int. Conf. on Plant and Vegetable Oils as Fuels. ASAE 482, Fargo, ND, 1982.

20. McCormick, R.L., Ross, J.D. and Graboski, M.S. Effect of Several Oxygenates on Regulated Emissions from Heavy-Duty Diesel Engines. Environmental Science & Technology, Vol. 31, No. 4, 1997, pp. 1140-1150.

21. Chang, Y.Z.D., Van Gerpen, J.H., Lee, I., Johnson, L.A., Hammond, E.G. and Marley, S.J. Fuel Properties and Emissions of Soybean Oil Esters as Diesel Fuel. JAOCS, vol. 73, No. 11, 1996, pp. 1549-1555.

22. Last, J.R., Kruger, M.K. and Durnholz, M. Emissions and Performance Characteristics of a 4-stroke, Direct Injection Diesel Engine Fueled with Blends of Biodiesel and Low Sulfur Diesel Fuel. SAE paper 950054, 1995.

23. Schumacher, L.G., Borgelt, S.C., Hires, W.G., Spurling, C., Humphrey, J.K., and Fink, J. Fueling Diesel Engines with Esterified Soybean Oil. ASAE paper MC93-101, 1993.

24. Van Gerpen, J.H., Hammond, E.G., Liangping, Y. and Monyem, A. Determining the Influence of Contaminants on Biodiesel Properties. SAE paper 971685, 1997.

25. Peterson, C.L. Vegetable Oil as a Diesel Fuel: Status and Research Priorities. Transactions of the ASAE vol. 29(5): September-October, 1986, pp. 1413-1422.

26. Mazed, M.A., Summers, J.D. and Batchelder, D.G. Peanut, Soybean and Cottonseed Oil as Diesel Fuels. Transactions of the ASAE Vol. 28(5), 1985, pp1375-1377.

27. Ziejewski, M. and Kaufman, K.R. Vegetable Oils as a Potential Alternate Fuel in Direct Injection Diesel Engines. SAE paper 831357, 1983.

28. Ishii, Y. and Takeuchi, R. Vegetable Oils and Their Effect on Farm Engine Performance. Transactions of the ASAE Vol. 30(1), 1987, pp2-6.

29. Ziejewski, M. and Pratt, G.L. Comparative Analysis of the Long-Term Performance of a Diesel Engine on Vegetable Oil Based Alternative Fuels. SAE paper 860301, 1986.

30. Graboski, M.S., and McCormic, R.L. Combustion of Fat and Vegetable Oil Derived Fuels in Diesel Engines. Prog. Energy Combust. Sci., Vol 24, 1998, pp125-164.

31. Dorn, P., Mourao, A.M., and Herbstman, S. The Properties and Performance of Modern Automotive Fuels. ASAE paper 861178, 1986, pp51-67.

32. Sapuan, S.M., Masjuki, H.H., and Azlan, A. The Use of Palm Oil as Diesel Fuel Substitute. Proc. Instn. Mech. Engrs., Vol 210, A04994, I. Mech. E , 1996, pp47-53.

33. Hemmerlein, N., Korte, V. and Richter, H. Performance, Exhaust Emissions and Durability of Modern Diesel Engines Running on Rapeseed Oil, SAE paper 910848, 1991.

34. Humke, A.L. and Barsic, N.J. Performance and Emissions Characteristics of a Naturally Aspirated Diesel Engine with Vegetable Oil Fuels- (part 2), SAE paper 810955, 1981.

35. Nitske, W.R. and Wilson, C.M., Rudolf Diesel: Pioneer of the Age of Power, 1st ed., University of Oklahome Press, Norman, 1965.

36. Ryan II, T.W., and Bagby, M.O. Identification of Chemical Changes Occurring During the Transient Injection of Selected Vegetable Oils. SAE paper 930933, 1993, pp201-210.

37. Schlick, M.L., Hanna, M.A., and Schinstock, J.L. Soybean and Sunflower Oil Performance in a Diesel Engine. Transactions of the ASAE, Vol. 31(5), Sept., 1988.

38. Blackburn, J.H., Pinchin, R., Nobre, J.I.T., Crichton, B.A.L., abd Cruse, H.W. Performance of Lubricating Oils in Vegetable Oil Ester-Fueled Diesel Engines. SAE paper 831355, 1983, pp1-9.

39. Stauffer, E.C. Fats and Oils, American Association of Cereal Chemists, Inc. 1996.

40. Standard Test Method for Oxidation Stability of Distillate Fuel Oil (Accelerated Method). American Society of Testing Materials (ASTM) D 2274-94, Designation: 388/90, pp776-780

41. Official Test Method Cd 3a-63 for Acid Value. American Oil Chemists Society (AOCS).

42. Official Test Method Cd 8-53 for Peroxide Value. American Oil Chemists Society (AOCS).

43. The Oil Stability Index (OSI) method Cd 12b-92, American Oil Chemists Society (AOCS).

44. DuPlessis, M.L., De Villiers, J.B.M. and Van Der Walt, W.H. Stability Studies on Methyl and Ethyl Fatty Acid Esters of Sunflower seed Oil, JAOCS, vol. 62, No. 4, April 1985, pp 748-752.

45. Schmidt, K.J. The Effect of Fatty Acid Composition on Emissions from Biodiesel-Fueled Diesel Engines. M.S. Thesis, Iowa State University, 1995.

46. Geyer, M.S., Jacobus, M.J., and Lestz, S.S. Comparison of Diesel Engine Performance and Emissions from Neat and Transesterfied Vegetable Oils, Transactions of the ASAE Vol. 27, No.2, 1984

47. Graboski, S.M., Ross, J.D. and McCormick, R.L. Transient Emissions from No. 2 Diesel and Biodiesel Blends in a DDC Series 60 Engine. SAE paper 961166, 1996, pp. 55-62.

48. Alfuso, S., Auriemma, M., Police, G. and Prati, M.V. The Effect of Methyl Ester of Rapeseed Oil on Combustion and Emissions of DI Diesel Engine, SAE paper 932801, Oct. 1993.

49. Liotta, J.F.,Jr. and Daniel, M.M. The Effect of Oxygenated Fuels on Emissions from a Modern Heavy-Duty Diesel Engine. SAE paper 932734, 1993.

50. Liotta, J.F.Jr. A Peroxide Based Cetane Improvement Additive with Favorable Fuel Blending Properties. SAE paper 932767, 1993, pp149-161.

51. Ott, L.R. An Introduction to Statistical Methods and Data Analysis. Marion Merrell Dow, Inc., Belmont, California, 1993.

52. Neter, J., Kutner, M.H., Nachtsheim, C.J., and Wasserman, W. Applied Linear Statistical Models. The McGraw-Hill Companies, Inc., 1996.

53. SAE Handbook. Society of Automotive Engineers, Inc. Warrendale, 1993, pp25.04-25.05.

54. Standard Method for Determining Relative Humidity by Wet and Dry-Bulb Psychrometer. ASTM E337-72, American Society for Testing and and Materials.

55. Keenan, J.H., Keyes, F.G., Hill, P.G. and Moore, J.G. Steam Tables: Thermodynamic Properties of Water Including Vapor, Liquid, and Solid Phase. John Wiley & Sons, Inc. New York, 1978.

56. Lancaster, D. R., Krieger, R. B., and Lienesch, J. H. Measurement and Analysis of Engine Pressure Data. SAE paper 750026, 1975.

57. Tadakazu, S., Takayuki, S., Takeshi, M., and Keizo, S. Low Emission Combustion Influences Duribility of Fuel Injection Pipe Line and Treatment of the Pipe. SAE paper, 871614, 1987.

58. Henein, N.A., and Bolt, J.A. Ignition Delay in Diesel Engines. SAE paper 670007, 1967.

59. Van Gerpen, J.H. The Effects of Air Swirl and Fuel Injection System Parameters on Diesel Combustion. PhD thesis, University of Wisconsin- Madison, 1984.

60. Krieger, R.B., and Borman, G.L. The Computation of Applied Heat Release for Internal Combustion Engines. ASME paper 66-WA/DGP-4, 1966.

61. Watson, N., Pilley, A.D, and Marzouk, M. A Combustion Correlation for Diesel Engine Simulation. SAE paper 800029, 1980.

62. Lyn, W.T. Study of Burning Rate and Nature of Combustion in Diesel Engines. In Proceedings of Ninth International Symposium on Combustion. The Combustion Institute, 1962, pp1069-1082.

63. Kort. R.T., Mansouri. S.H., Heywood. J.B., and Ekchian. J.A. Divided-Chamber Diesel Engines Part II: Experimental Validation of a Predictive Cycly-Simulation and Heat Release Analysis. SAE paper 820274. SAE Trans. Vol. 91. 1982.

64. Olikara. C., and Borman. G.L. A Computer Program for Calculating Properties of Equilibrium Combustion Products with same Application to I.C. Engines. SAE paper 750468.

65. Heywood. J.B. Internal Combustion Engine Fundamentals. McGraw-Hill. Inc. U.S.A., 1988.

66. Cheng. W., and Gentry. R. Effect on Charge Non-Uniformity on Diesel Heat Release Analysis. SAE paper 861568. 1986.

67. Gatowski. J.A., Balles. E.N., Chun. K.M., Nelson. F.E., Ekchian. J.A., and Heywood. J.B. Heat Release Analysis of Engine Pressure Data. SAE paper 841359. SAE Trans., Vol. 93. 1984.

68. Austen A.E.W., and Lyn, W.T. Relation Between Fuel Injection and Heat Release in a Direct-Injection Engine and the Nature of the Combustion Process. Proc. Instn. Mech. Engr. (No. 1). 25. November 8. 1960.

69. Andree. A., and Pachernegg. S.J. Ignition Conditions in Diesel Engines. SAE paper 690253. SAE Trans., Vol. 78. 1969.

70. Galvincevski. B., Gulder. O.L., and Gardner. L. Cetane Number Estimation of Diesel Fuels from Carbon Type Structural Composition. SAE paper 841341. 1984.

71. Miyashita. K., and Takagi. T. Autoxidation Rates of Various Esters of Safflower Oil and Linoleic Acid. JAOCS. Vol. 65. No. 7, July. 1988. pp1156-1158.

72. Takagi. T., Mitsuno. Y., and Masumura. M. Lipids 13:147. 1978.

73. Gan. L.H., Ooi. K.S., Gan. L.M., and Goh, S.H. Effects of Epoxidation on the Thermal Oxidative Stabilities of Fatty Acid Esters Derived from Palm Olein. JAOCS. Vol. 72. No. 4, 1995. pp439-442.

74. Thompson. C.J., Peterson, L.C., Reece. L.D., and Beck, M.S. Two Years Storage Study with Methyl and Ethyl Esters of Rapeseed. Liquid Fuels and Industrial Products from Renewable Resources - Proceedings of the Third Liquid Fuels Conference. Nashville. Tenn., Sept. 15-17. 1996.

75. Schumacher, L.G., Hires, W.G., and Borgelt, S.C. Fueling a Diesel Engine with Methyl-Ester Soybean Oil. Liquid Fuels from Renewable Resources-Proceedings of an Alternative Energy Conference, Ed. By John Cundiff, ASAE, 14-15 December, 1992, Nashville, TN., pp124-131.

76. Chang, Y.Z.D. and Van Gerpen, J.H. Fuel Properties and Engine Performance for Biodiesel Prepared from Modified Feedstocks. SAE paper 971684, 1997, pp153-172.

77. McDonald, J.F., Purcell, D.L., McClure, B.T., and Kittelson, D.B. Emissions Characteristics of Soy Methyl Ester Fuels in an IDI Compression Ignition Engine. SAE paper 950400, 1995.

78. Rickeard, D.J., and Thompson, N.D. A Review of the Potential for Bio-Fuels as Transportation Fuels. SAE paper 932778, 1993, pp109-125.

79. Feldman, M.E., Peterson, C.L. Fuel Injection Timing and Pressure Optimization on a DI Diesel Engine for Operation on Biodiesel. Liquid fuels from renewable resources. Proceedings of an Alternative Energy Conference 14-15 December, 1992, Nashville by ASAE pp111-123, 1992.

80. Mittelbach, M., and Trillhart, P. Diesel Fuel Derived from Vegetable Oils. III. Emission Tests Using Methyl Esters of Used Frying Oil. JAOCS, Vol. 65, No. 7, July 1988, 001185-1187.

81. Wong, C.L., and Steere, D.E. The Effect of Diesel Fuel Properties and Engine Operating Conditions on Ignition Delay. SAE paper 821231, SAE Trans. Vol. 91, 1982.

82. Caton, J.A., Haywood, J.B., and Mendillo, J. V. Hydrocarbon Oxidation in a Spark Ignition Engine Exhaust Port. Combust. Sci. Technol., Vol. 37, No. 3 & 4, 1984, pp153-169.

83. Ali, Y. Beef Tallow as a Biodiesel Fuel. PhD thesis, University of Nebraska, Lincoln, Nebraska, May, 1995.

84. Springer, G.S. and Patterson, D. J. Engine Emissions: Pollutant Formation and Measurement. Plenum Press, New York, 1972.

85. Yahya, B.A. Performance Characteristics of a Direct Injection Diesel Engine Operating on Methyl Soyoil and Methyl Tallow Esters. PhD. Thesis, Iowa State University, 1988.

86. Chan, H.W.S. Autoxidation of Unsaturated Lipids. Academic press, 1987, pp6

ACKNOWLEDGMENTS

I would like to express my sincerest appreciation to my major professor, Dr. Jon H. Van Gerpen, for his guidance, assistance, and encouragement throughout this research. My appreciation is also extended to my committee members, Dr. Howard N. Shapiro, Dr. Ron M. Nelson, Dr. Ambar K. Mitra, Dr. Stephen J. Marley, and Dr. Graeme Quick.

I would like to thank my office mates Mustafa Canakci, Seref Soylu, Mustafa E. Tat, Fazil Senel, and David Yu Zhang Chang for lots of good company and conversation. Also I would like to thank Xiao-Hu Liu, Shah Rashid, Ferdaus Hossain, and Forhad Hossain for their help.

I wish to thank the technical staff of the Mechanical Engineering Department at Iowa State University: James Dautremont, Robert Hap Steed and Gaylord Scandrell for their technical support and assistance.

Finally, I want to thank Sofia Khatun Jabber, Enamul Haque Talukder, Rehana Akhtar Talukder, Mamunur Rashid Talukder, Aminul Islam, Arifa Islam, and others who have directly or indirectly helped me in completing my graduate studies at Iowa State.

IMAGE EVALUATION
TEST TARGET (QA-3)

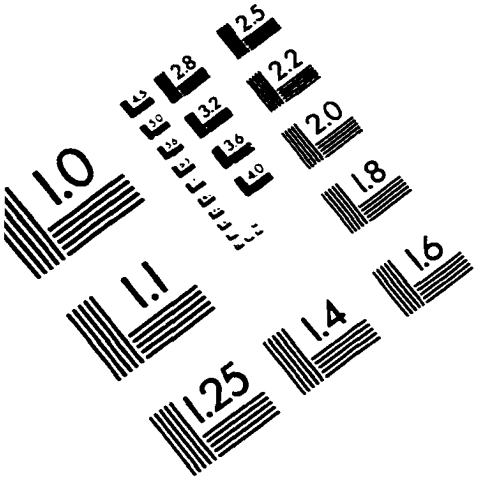

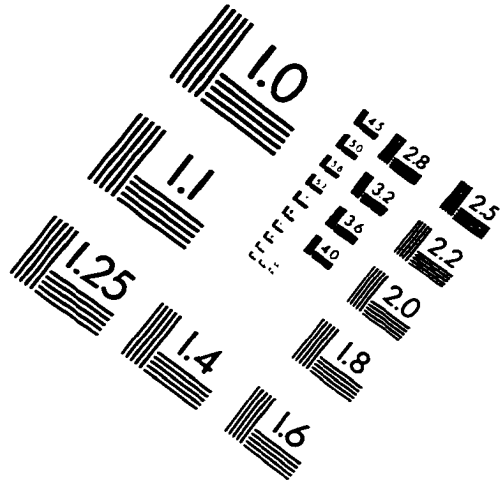

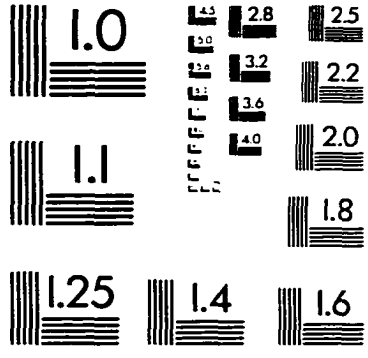

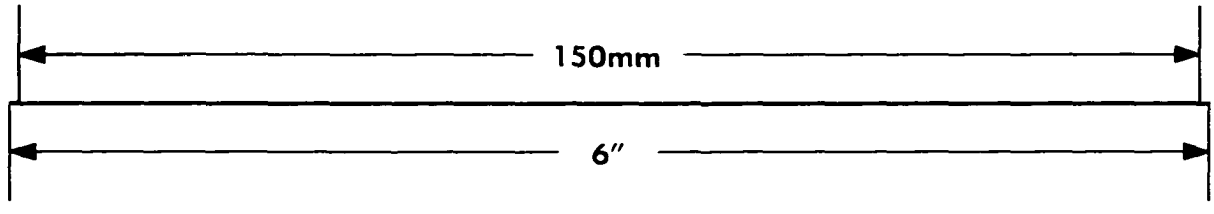

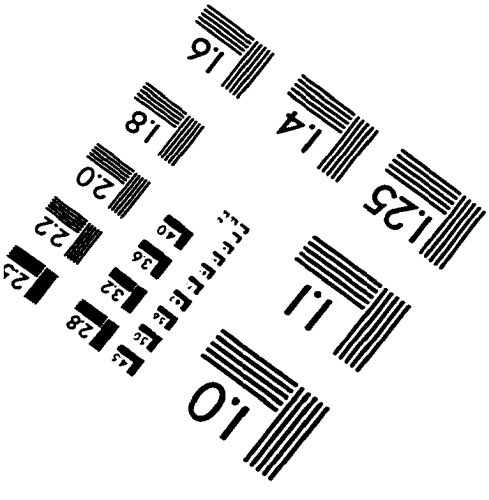

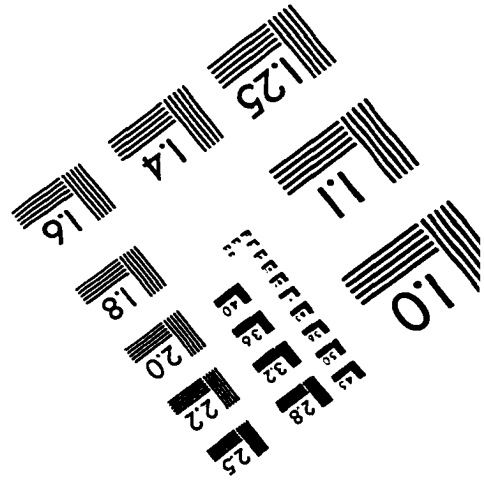

APPLIED IMAGE . Inc
1653 East Main Street
Rochester, NY 14609 USA
Phone: 716/482-0300
Fax: 716/288-5989